An investigation into the cytotoxicity of *cis,cis*-triaminocyclohexane derivatives

Luisa Ciano

PhD

University of York
Department of Chemistry

September 2013

Abstract

N,*N*',*N*''-Tris(2-pyridylmethyl)-*cis*,*cis*-1,3,5-triaminocyclohexane, tachpyr, has been studied for several years for its potential application in cancer therapy. Several studies have been carried out to understand the mechanism of action of this molecule and Planalp and co-workers have reported evidence to support the hypothesis that iron chelation, followed by iron deprivation in cells, are a likely reason for cytotoxicity.

We have investigated the properties of tachpyr with the aim of improving cytotoxicity and gaining a deeper understanding of its mechanism of action. A series of tach-based ligands were synthesised with the purpose of modifying the general structure of tachpyr and evaluating the pharmacophores necessary for activity.

The biological evaluation of the mechanism of action involved various techniques, such as dichroism and X-ray crystallography, and the anti-proliferative activity of all tri-amine compounds was evaluated with *in vitro* tests against tumour cells. A series of experiments to monitor the effect of increasingly higher concentrations of Fe on the toxicity of tachpyr against tumour cell lines were performed. These results disagree with those previously reported in the literature and show that the cytotoxicity of tachpyr is independent of the concentration of Fe (up to 400 μM), which is inconsistent with the proposed mechanism of action.

A different cellular target was investigated. Binding experiments with DNA showed an interaction with tachpyr and co-crystallisation with a short DNA oligonucleotide produced crystals suitable for X-ray diffraction. Analysis of structure activity relationships gave insights on the essential features of these molecules to retain anti-proliferative activity. The data obtained and presented in this thesis suggest a completely new potential mechanism of action for this class of compounds.

Table of contents

Figures, Tables and Equations

Accompanying material

A compact disk with CIF files from single crystal X-ray diffraction is attached at the back of this thesis.

Compound*	**File name**
Tachprl **[4b]**	phw1114
Salimtach **[6a]**	phw1101
5-Me-salimtach **[9a]**	phw1113
Saltach **[6b]**	phw1117
5-Cl-saltach **[7b]**	phw1115
5-Me-saltach **[9b]**	phw1118
4-NMe_2-tachimben **[11a]**	phw1301
4-CF_3-tachimben **[15a]**	phw1308
Co(II)-tachimpyr **[18]Cl_2**	phw1303
Co(II)-tachpyr **[19]$CoCl_4$**	phw1106_twin1_hklf4
Ru-dimer	phw1120
Ru(II)-tachpyr **[20]Cl_2**	phw1202

Table A: CIF files provided with the CD. *Solvent molecules omitted from the structural formula.

Acknowledgements

This thesis would have not been possible without the help and support of several people during these past four years. I feel blessed for the number of amazing people that have accompanied me during this journey and saying thank you to all of them in the appropriate way would make these acknowledgments as long as one of the chapters, therefore I will try to be brief.

First of all, I would like to thank my supervisors, Prof Paul Walton and Dr Jason Lynam, the University of York, the Wild Fund and my parents for giving me the possibility to undertake this PhD. Paul and Jason, you have been amazing supervisors, providing guidance and support throughout these years, especially when I needed it the most. Not only have you taught me lots of chemistry, but you have also given me a great role model I will always look at of what a good supervisor should be: positive, supportive and (sometimes over-)enthusiastic. And for all of this I will always be grateful. A special thanks goes also to my parents, not only for the financial support, but mainly for the unconditioned love they have always showed me. I know it has not been easy for you guys either, so this thesis is also for you. Vi voglio bene. Thanks to my brother Antonio as well, who did not contribute to this PhD, but always showed his support. And to my grandparents, too.

A big thanks goes to the members of the technical staff at the University of York. Naser, thanks for all the help in the lab; Adrian, Rob and Natalie for the crystallography service and for spending so much time introducing me to the wonderful world of small molecule crystallography; Heather and Pedro for the NMR; Graeme for CHN analysis; and Karl and Ed for the MS service. Apologies for some crazy experiment I came up with. Thanks also to the technical support in YSBL: Sally, Simon, Maria and Shirley. In particular, I would like to thank Shirley for her time, patience and help over the last 18 months with setting up crystallisation for what was a very ambitious idea. It worked out fine and I am sure the outcome would have been very different without Shirley's help! Also for the DNA crystallography, I would like to thank Johan, Sam and in particular Eleanor for the endless hours spent solving and refining my structure. Apologies for all the headaches it caused.

An enormous thank you goes to all my friends, I definitely would not have gotten to this point without you! First of all, thanks to the people in the E002 office for making the last year of my life so enjoyable. You are a crazy bunch, I am sure you all know that already! Thanks to: the "espresso lovers" Barby, Chiara, Jess, Rob T. and Tom (+ Lucy and Dan), for providing much needed coffee breaks, especially during thesis writing; Rob T. also for lending me his cat every now and then; the lobe-friends Danielle, Nat, Nathan and Rob M., for feeding me with so many amazing cakes; Sindhu and Rob S., who contributed in making the office such a great working environment! Thanks to the "lunch break" people: Dave, Linda, Lizzie and Richard among the ones I have not cited yet. Lunch is always good, but with your company it was even better! A great thank you to the past and present members of the PHW and JML groups and the guys from the AKDK group, in particular Aimee, for teaching me most of the things I know about cell cultures and Schlenk techniques; Abeda, Maria and Steve for being amazing friends and so supportive when I was going through a very hard time; also, Emma and Becky. Thanks to other friends from York, in particular Will, Kat and Dan S., and all my friends back home, especially my "almost sisters" Cinzia and Antonella.

Some people deserve special acknowledgements. Thanks to: Dan "3rd supervisor" Raines, for countless hours of chemistry discussions, IT support and great friendship. It is a great pleasure to be your friend. Natalie, who made sure I was surviving the thesis writing process and tried her best to teach me to be on time...sorry, still quite a lot of work there! Karin, the wisest person I have ever met, who was a great housemate and an even better friend since the day we moved in together. And finally, Lucy "starfish" Milner, the only one that can beat me for craziness, a beautiful person and a great friend. I definitely would have not made it without you!

A special thanks to the Mumba and Marriott' families, for always making me feel welcome and showing so much faith in me. And finally, a super thank you to my amazing fiancée. Andy, you have been by my side for all these years, laughing with me and wiping my tears, we shared every moment of this journey, and I can only say thank you for always being with me and making me so happy.

Declaration

The research presented in this thesis is, to the best of my knowledge, original and my own, except for the following:

- ESI-MS experiments were carried out by Mr Karl Heaton or Miss Helen Robinson;
- X-ray crystallography was performed by, or with the assistance of, Dr Adrian Whitwood, Dr Robert Thatcher or Miss Natalie Pridmore;
- Elemental analyses were carried out by Dr Graeme McAllister;
- Several synthetic procedures for the synthesis of compounds **[11a-b]** were tested by Miss Emily Wallace under my supervision as part of her BSc project;
- The study of the complexation between compound **[3b]** and ruthenium was carried out by Mr Oliver Brown under my supervision as part of his BSc project;
- All circular and linear dichroism, ethidium bromide displacement and agarose gel experiments were performed in collaboration with Prof Michael J. Hannon in his laboratories at the School of Chemistry, University of Birmingham;
- X-ray crystallography of DNA was performed by, or with the help of, Mrs Shirley Roberts for crystallisation set up, Dr Johan Turkenburg and Mr Sam Hurt for data collection, Dr Johan Turkenburg and Prof Eleanor Dodson for structure solution and refinement.

Luisa Ciano

Chapter 1

Introduction

1. Introduction

1.1 Cancer: statistics, genesis and characteristics

Cancer is one of the leading causes of death worldwide, accounting for about 14% of all deaths, due to any cause, across the planet in 2008.[1-2] Lung, liver, breast, colon and stomach cancers are responsible for most of the deaths due to cancer, which sum up to about 7.6 million people in the world in 2008.[2] It has been estimated that by 2030 there will be about 22.2 million new cases of cancer diagnosed annually in the world, which will cause about 13.1 million deaths.[1]

More than 320,000 people were diagnosed with cancer in the UK in 2010, with breast and prostate cancer being the most common in females and males, respectively,[3] while over 1.6 million new cases have been estimated to occur in the United States in 2013.[4]

Cancer, more precisely defined as neoplasia, is characterised by the loss of regulating mechanisms of cell cycle and replication, which results in the uncontrolled growth of cells.[5] Cancer includes over 200 different types of diseases, which can be divided into benign, if the tumour is not invasive and localised to a specific tissue, or malignant, if it is prone to aggressively invade the organ in which it was first developed and/or diffuse to organs different from the primary site of proliferation, giving rise to metastases.[5] Cancer is caused by genetic mutations that occur in cells during the life due to the action of mutagens, carcinogens and radiations.[6-9] Natural mutations can also occur during cell division, typically at the rate of 10^{-5} mutations per gene per replication.[10] Considering the number of divisions which take place in the human body during a lifetime, which were estimated to be in the order of 10^{16} cell replications, it is clear that one single mutation is not enough to develop cancer, but several different changes need to occur in a cell to have the development of a tumour.[11-12] For this reason, cancer is more often found in older people, with three out of five cases diagnosed to the over 65 in the UK,[3] due to the accumulation of several mutations which interfere with the normal cell growth.

The mutations which occur in cancerous cells lead to several differences in the biological pathways when compared to normal cells. The main characteristic of cancer is the limitless replication of the cells, which is due to several mechanisms that can be summarised in the activation of oncogenes and the suppression of growth-control mechanisms and apoptosis.[13] Cancer cells often express over-induction of cell-growth signals, such as growth and mitogenic factors, which deregulate the progression through the cell cycle.[13] Due to the progressive decrease of checkpoints on the cell division, several control and repair mechanisms of the DNA replication are lost, increasing the chances to have mutations during the replication.[14-15] On the other hand, down regulation of feedback mechanisms of cell-growth control, as, for instance, cell contact inhibition, can similarly produce abnormal proliferation of the cells.[13, 16] The life of non-cancerous cells is controlled by programmed cell death, apoptosis, which is triggered in response to physiological damage or malfunction of the cell. Cancer cells can overcome the apoptotic signals, and for this reason they are often referred to as immortal.[13, 17] As an example, the gene coding for the tumour suppressor protein p53 has been found mutated in nearly all kind of tumours, with rates that change from 10% to up to nearly 100%,[18] which shows how important the mutation of apoptotic signals is in cancer development. The immortalisation of the cells is also related to the presence of telomerases, enzymes involved in the maintenance of the length of the DNA.[19] Telomeres are structures found at the end of chromosomes, formed by repetition of short nucleotide sequences.[17] DNA replication causes a shortening of the telomeres which, after a certain number of cell divisions, leads to apoptosis. Telomerases are enzymes able to add oligonucleotide sequences on to the telomeres, preserving the length of the chromosome and immortalising the cells.[20]

Due to their continuous growth, cancer cells are in need for increased amount of oxygen and nutrients. For this reason, several cancers have the ability to promote angiogenesis, i.e. the development of new blood vessels.[21] However, the growth of these new vessels is usually chaotic and unstructured, which causes the appearance of hypoxic regions within the tumour, characterised by low oxygen levels.[22-23] Hypoxia is associated with more malignant forms of cancer and resistance to radio- and chemotherapies.[24] Cancer cells undergo a selection process during their development,

with the accumulation of genetic mutation being the selective criteria in the survival of unfavourable conditions (such as hypoxia) or external factors (such as chemotherapy).[25] The result of this process is the appearance of more resistant and aggressive mutant cells over time, which are more difficult to treat.[26]

1.2 Cancer therapy

Cancer therapy is based on chemotherapy, radiotherapy and surgery, and quite often combinations of these methods. Due to their genesis from normal cells, tumours are usually difficult to treat due to lack of selective targets.[5] For this reason, chemotherapy is often associated with severe adverse side effects, although a deeper understanding of cancer physiology and biochemistry is progressively leading to the development of therapeutic agents able to interact with cellular targets over-expressed in cancer cells.[5]

One of the main problems in cancer therapy is the insurgence of resistance to the chemotherapeutic agents. The resistance can be intrinsic or acquired, in relation to a lack of response to the drugs since the beginning of the therapy or its appearance after a certain time, respectively.[27] The mechanisms of resistance can be various, such as decreased uptake of the chemotherapeutic agent or alteration of metabolic pathways to overcome the effect of the drug.[27] For example, resistance to cisplatin can be due to several different mechanisms, such as changes in the uptake/efflux of the compound, expression of sulfur-containing molecules to deactivate the drug or increased ability to repair or by-pass the DNA damages caused by cisplatin.[28] Sometimes resistance is not restricted to one particular drug, but influences also compounds with different mechanisms of action and cellular targets. This phenomenon is known as multidrug resistance and it can affect significantly the outcome of the therapy.[29]

The anti-cancer agents currently used in therapy have different targets inside the cells, from DNA to enzyme to cellular signalling.[5] In the effort of improving activity and selectivity, the research of novel anti-cancer agents has involved thousands of people, with over £500 million invested in cancer research in 2010 in the UK.[30] A

comprehensive review of all anticancer compounds developed and reported in the literature is beyond the purpose of this introduction, but a few examples are presented herein.

It should be noted that some confusion is present in the literature on the definition of anti-cancer compounds. Compounds able to kill cells should be defined as "cytotoxic", even if the cells frequently chosen for these tests are immortalised cell lines. Unless the compounds have proven to have at least some degree of selectivity for cancer cells over non-cancerous cells then they can be described as anti-cancer. The compounds described in this thesis are therefore defined as cytotoxic unless their selectivity has been tested.

1.2.1 Anti-cancer compounds not targeting DNA

Among the compounds acting on enzymes, methotrexate and 5-fluorouracil (**Figure 1.1**) are two of the most used in chemotherapy.

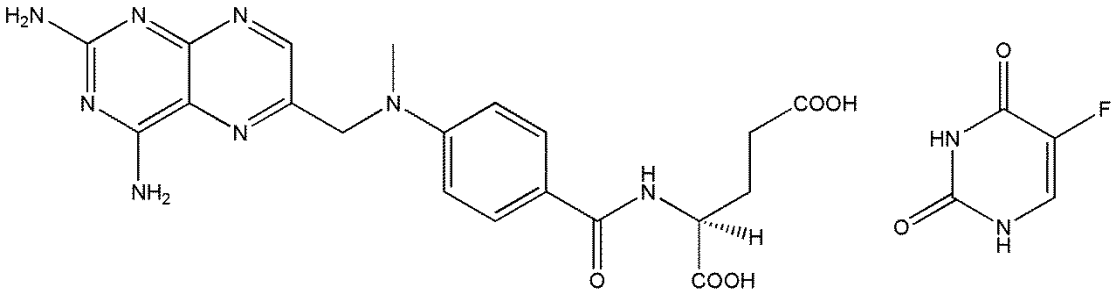

Figure 1.1: Structures of methotrexate (left) and 5-fluorouracil (right).

Methotrexate inhibits the synthesis of DNA nucleotides, consequently slowing down cell division.[31-32] Similarly, the suicide binder 5-fluorouracil is able to stop the synthesis of thymidine through the formation of a covalent bond with the thymidylate synthetase.[33]

The mechanism of action of methotrexate was studied for several years, in order to gain a better understanding of its cellular targets and so improve the activity of the compound. Following the initial discovery of Osborn *et al.* that methotrexate was able

to inhibit the action of the dihydrofolate reductase,[34] several other studies were carried out to elucidate further details about the effect of the molecule on cells. Borsa and Whitmore showed that the main cause of cell death due to methotrexate was the lack of thymidine, essential for the synthesis of new DNA.[32] The study showed that addition of thymidine to the culture medium was able to stop the cytotoxic activity of methotrexate, and it also highlighted some possible causes of resistance to this anti-cancer agent.[32] The crystal structures of folic acid bound to human dihydrofolate reductase[35] and of methotrexate in the active site of the enzyme[36] allowed to understand the nature of the interaction between the anti-cancer compound and its target. Several derivatives of methotrexate have then been synthesised,[37-38] although none of them has reached therapy so far.

Several anti-cancer compounds are based on natural hormones and are used against tumours whose growth is regulated by hormones.[39] One example is given by tamoxifen, shown in **Figure 1.2**, a synthetic agent widely used in the treatment of breast cancers which express estrogen receptors. This synthetic derivative is able to compete with estrogens for the binding to the receptor and hence inhibiting the hormone-induced cell growth.[5, 40]

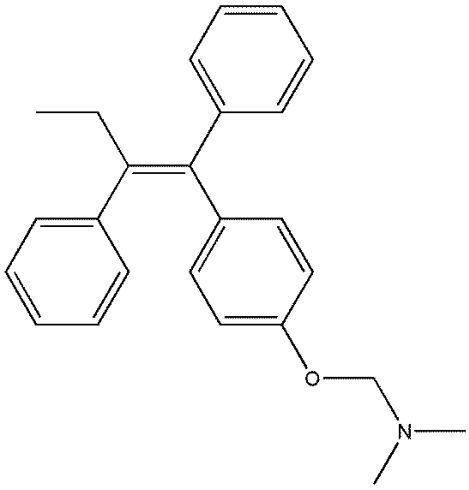

Figure 1.2: Structure of tamoxifen.

A number of tamoxifen derivatives are reported in the literature and are being developed to increase the cytotoxic activity of this compound.[41-42]

Several other cellular targets have been exploited for cancer therapy, and the research has led to many compounds used in therapy, such as inhibitor of tubulin polymerisation and depolymerisation,[43] protein kinase inhibitors[44-45] and antibodies and gene therapy agents,[46] just to name a few examples.

Increasing attention has been given in recent years to organometallic and coordination metal-based anti-cancer compounds, a discussion of which is presented in section **3.1**.

1.2.2 Anti-cancer compounds targeting DNA

Several anti-cancer compounds, both approved for therapy and still under development, have DNA as the target for their action. These compounds can be divided in three main categories: alkylating agents, intercalators and groove binders.

1.2.2.1 Alkylating agents

Alkylating agents are electrophilic molecules able to react with the nucleophilic sites present on DNA, typically guanine residues, to form a covalent bond which interferes with the replication of the genetic material.[47-48] Some alkylating agents can react twice with nucleophiles, and so have the ability to form cross-links in the DNA double helix. Due to the strong covalent nature of the bond, alkylating agents are usually very toxic and show severe side effect due to the lack of selectivity for cancer cells.[49-50] Furthermore, these compounds can themselves be mutagenic or carcinogenic because of the damage to the DNA.[51]

Nitrogen mustards are alkylating agents used in therapy since the 1940s and several compounds belonging to this class are currently used in cancer treatment.[5, 52] Chlormethine, shown in **Figure 1.3**, was the first molecule studied for its alkylating properties and its mechanism of action is reported below.[53] Nitrogen mustards can undergo an intramolecular reaction which liberates chloride and forms the highly reactive aziridinium ion. This compound can then react with the DNA to form a covalent bond with the nucleotides. The process can be repeated on the other

chloroethyl moiety, causing cross linkage of the DNA mainly between guanine residues and, hence, stopping the replication of the genetic material.[53-54]

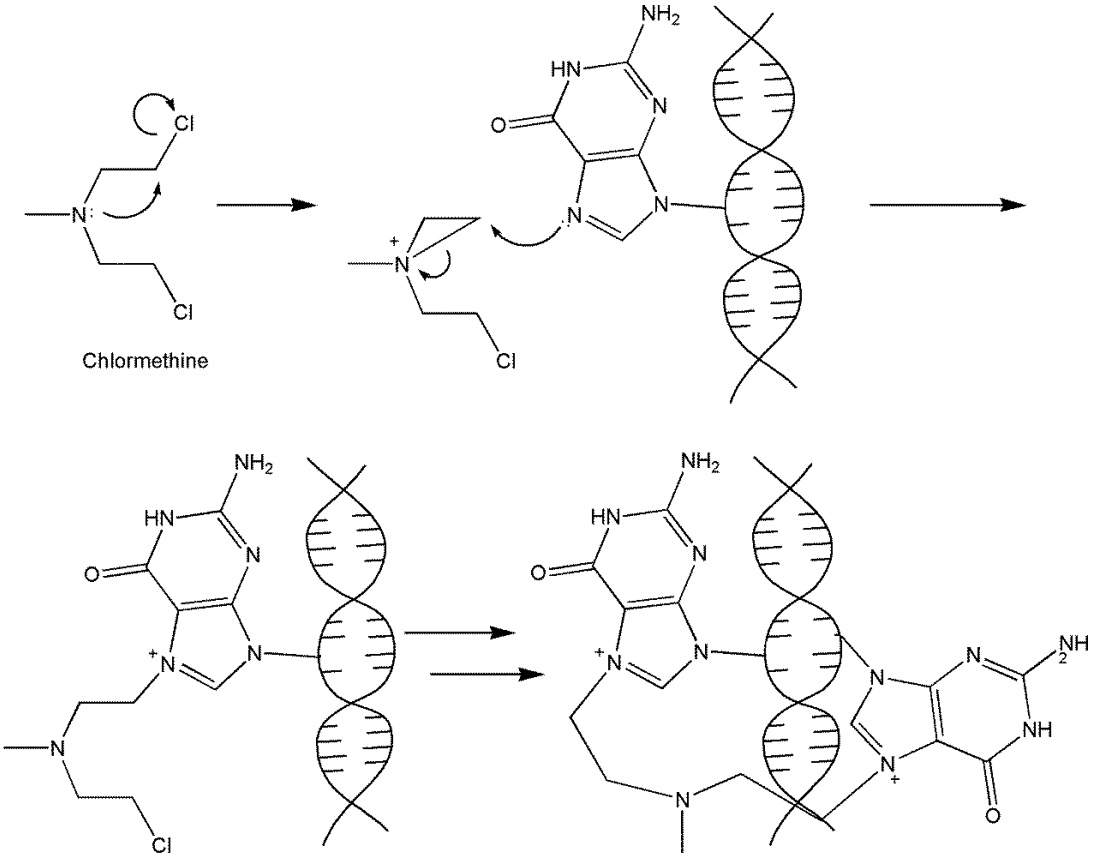

Figure 1.3: Scheme of the alkylation of DNA by the nitrogen mustard chlormethine.

Due to its high reactivity, chlormethine presented several problems when used in patients. To overcome toxicity and improve the selectivity, several nitrogen mustard derivatives have been synthesised and tested for activity. Among them, aryl substituted mustards, such as melphalan (L-phenylalanine mustard) and uracil mustard shown in **Figure 1.4**, were made to reduce the reactivity, and hopefully increase the selectivity, of the compound.

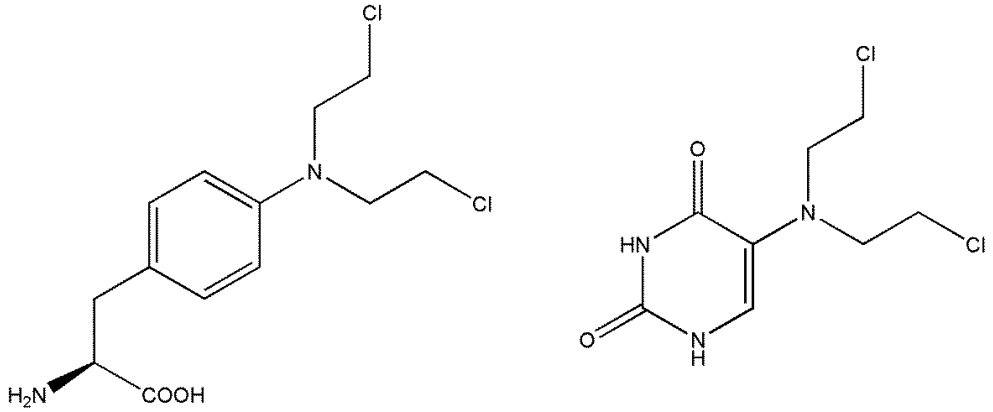

Figure 1.4: Structure of melphalan (left) and uracil mustard (right).

In the melphalan molecule, the lone pair of electrons on the nitrogen atom can interact with the aromatic system, inhibiting the formation of the aziridinium ion and, therefore, reducing the reactivity of the compound.[55] The phenylalanine moiety was added with the intention of adding a further site of interaction inside the cells. The compound could mimic the role played by phenylalanine in protein synthesis, hence alkylating ribosomes/enzymes and so stopping the protein synthesis.[55] Similarly, uracil mustard was made to improve the selectivity of the anti-cancer compound for tumour cells. Cancer cells have an increased need for nucleic acid precursor, which causes the accumulation of the uracil mustard in these cells.[54, 56]

An improvement in the use of nitrogen mustards was achieved with the introduction in to therapy of cyclophosphamide (**Figure 1.5**).[57]

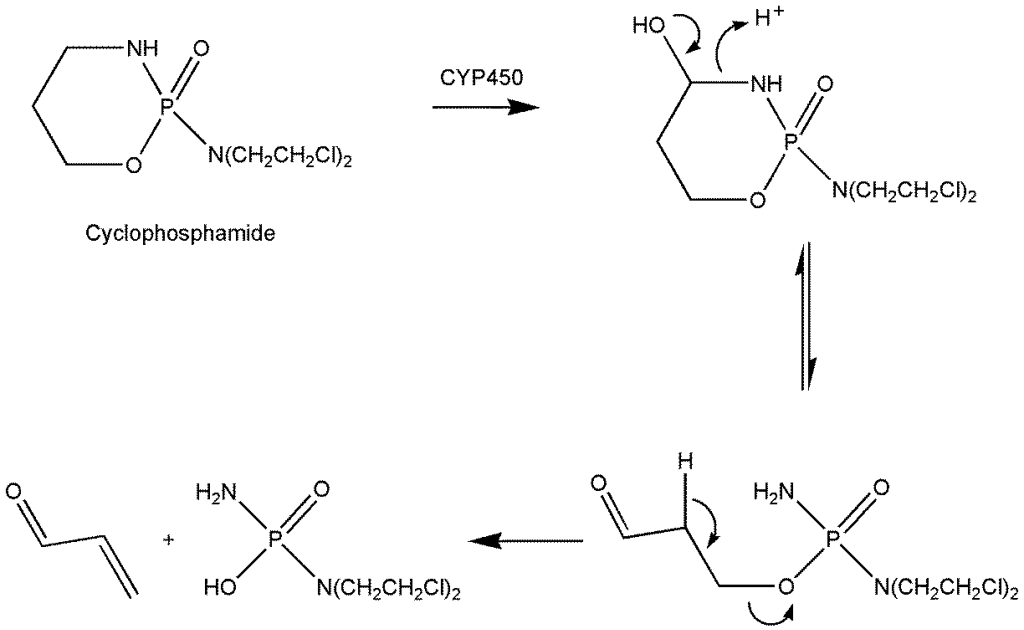

Figure 1.5: Scheme of the activation of cyclophosphamide to phosphoramide mustard.

Cyclophosphamide is a prodrug activated in the liver by an enzyme belonging to the cytochrome P450 family.[58] The cyclic compound is oxidised by the enzyme and the reaction causes the ring opening shown in **Figure 1.5**. The active compound can then be liberated and its alkylating function exploited.[57] Unfortunately the acrolein molecule liberated as a result of this rearrangement was shown to be the main cause of toxicity, limiting the use of cyclophosphamide.[59]

Alkylation of the DNA is also proposed to be the mechanism of action of compounds belonging to the class of nitrosoureas[60] and cisplatin and its derivatives (section **3.1**).

Although there are drawbacks for the use of alkylating agents, several compounds are currently used in cancer therapy and new molecules are developed in the continuous effort of producing new anti-cancer drugs with high selectivity and toxicity. Purine-based,[61] benzoic acid[62] and quinazoline[63] nitrogen mustard derivatives have been reported and showed promising activity against tumour cells.

1.2.2.2 Intercalators

DNA intercalators are molecules, typically planar and aromatic, able to insert between DNA base pairs causing distortion and lengthening of the double helix.[64] This

distortion is responsible for the inhibition of replication and transcription of the genetic material.[65-66]

Several intercalating agents are used, or are being developed, as fluorescent probes to study the structure and the interaction with the DNA.[67-69] Among them, ethidium bromide is widely used to study the interaction of other intercalators with DNA[70-71] (section **4.3.1**).

For cancer therapy, anthracyclines have been shown to possess good intercalating and anti-cancer activity and are used in therapy for different kind of tumours.[72] Although the mechanism of action has not been completely understood,[73-75] evidence shows that these compounds act as poisons of the enzyme topoisomerase II.[76]

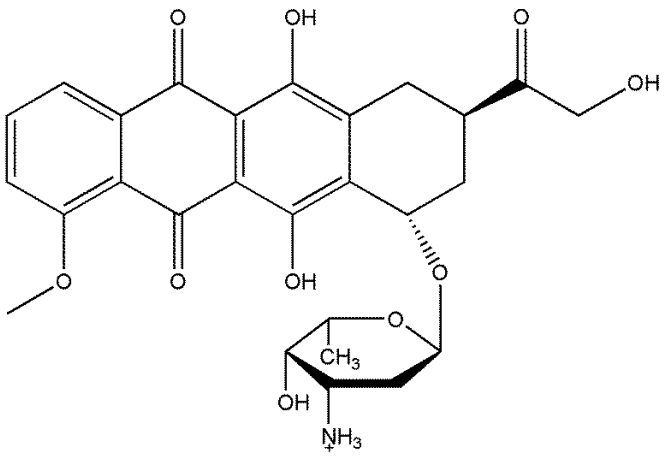

Figure 1.6: Structure of doxorubicin.

Topoisomerase II is an enzyme involved in DNA replication.[77] This enzyme is able to cleave the phosphate backbone of both DNA strands to unwind the structure and release the tension due to the replication process.[78] The enzyme binds to the phosphate through a tyrosine residue and causes a breakage in the phosphate chain. An intact double helix of DNA can then pass through the cut, and the topoisomerase can re-bind the phosphate backbone together, re-establishing the original structure of the DNA.[79] Doxorubicin (**Figure 1.6**) and the other anthracycline derivatives interfere with this step during replication, by stabilising the bond between the phosphate and tyrosine residue of topoisomerase.[80-81] As a consequence, DNA experiences a permanent break in the structure, which triggers apoptosis.[82-83] Due to the success of anthracyclines in

cancer therapy, new derivatives are currently under development[84-86] to improve selectivity against cancer cells and overcome some of the adverse side effects (cardiotoxicity and nephrotoxicity being the most relevant) shown by doxorubicin and it analogues.[87-89]

1.2.2.3 Groove binders

Another class of molecules able to interact with DNA is represented by the groove binders. In recent years these compounds have been the focus of attention due to the discovery of very active molecules which act as DNA binders. Groove binder compounds can either irreversibly bind to the DNA through covalent bonds or form a reversible interaction which inhibits DNA replication.[90] These compounds have been extensively reviewed in the past,[90-92] but some significant examples are reported herein.

Anthramycin and mitomycin (**Figure 1.7**) represent examples of binders able to form covalent bonds with the double helix of DNA.[93] Anthramycin and its derivatives undergo activation inside the body on the benzodiazepine ring and react preferentially with the exocyclic N-2 nitrogen of guanine residues.[94-95] Mitomycin shows very high sequence selectivity for C-G fragments[96-97] and the alkylation mechanism has to be preceded by activation of the molecule in the liver.[98]

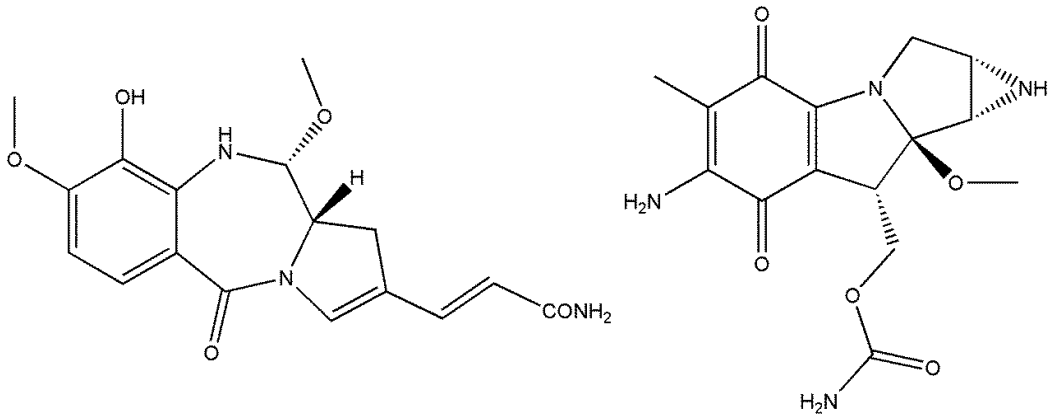

Figure 1.7: Structure of anthramycin (left) and mitomycin (right).

These compounds were found to be very active against several tumours, although they showed cardiotoxicity.[99]

Among molecules which act as non-covalent binders to DNA, distamycin, **Figure 1.8**, and its derivatives showed to be promising anti-cancer agents and specific binders to A-T DNA sequences.[100-101]

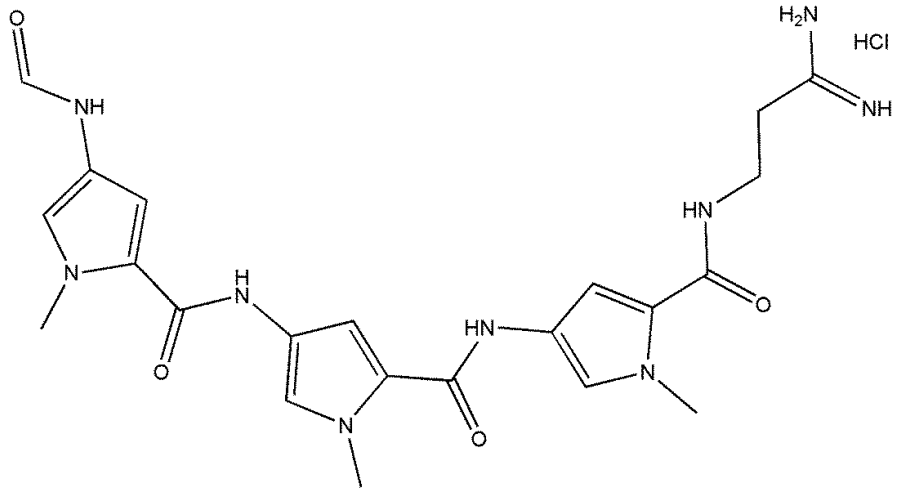

Figure 1.8: Structure of distamycin.

These compounds were shown to bind DNA without causing elongation or unwinding of the double helix and that the base pair selectivity was due to van der Waals interactions.[102-103] It has been suggested that A-T regions in the DNA have a smaller minor groove, which allows for tight binding of the molecule to the double helix.[104] Furthermore, Coll and co-workers proposed that the presence of the $-NH_2$ group of the guanine residues could cause steric hindrance for the binding.[104]

In order to improve the cytotoxicity of these compounds, some mixed groove binder/alkylating agents were synthesised. Among them, tallimustine, shown in **Figure 1.9**, possessed good activity against cancer cells *in vitro* and entered phase II clinical trials, but it proved mainly inactive *in vivo*.[105]

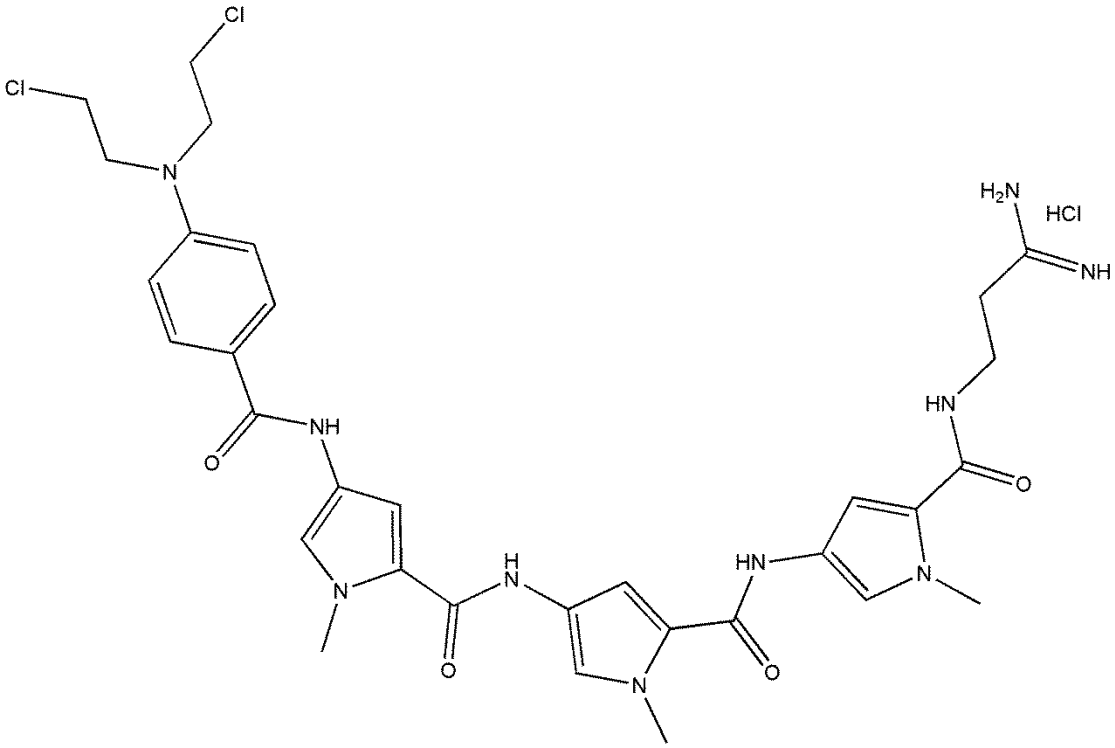

Figure 1.9: Structure of tallimustine.

From the structure it is clear how the distamycin moiety was modified through the addition of the nitrogen mustard. In contrast to the precursor chlormethine, tallimustine showed selectivity in the alkylating action for adenosine rather than guanine residues on the DNA.[106] The rate of alkylation was quite poor and it was hypothesised that the alkylation followed the groove binding event. The distamycin moiety would therefore drive the interaction towards A-T rich segments of the DNA, decreasing the possibility for the nitrogen mustard moiety to be an effective alkylating agent.[106]

Following the promising results shown by the minor groove binder presented above, several other derivatives have been described.[107-109] Yang and co-workers reported novel minor groove binders able to interfere with the action of RNA polymerase,[110] while Vidal *et al.* showed that the minor groove binder lurbinectedin was able to inhibit cell growth in cisplatin-resistant ovarian cells.[111]

1.2.3 Understanding the mechanism of action to target activity

A deeper understanding of the mechanism of action of compounds used in therapy can greatly contribute to the development of novel, more active and more selective compounds. The examples of this strategy in the history of pharmacology are various, both in cancer therapy and not. From a chemical perspective, the development of structure activity relationships (SARs) allows new target molecules to be identified, and information about the mode of action to be inferred. To highlight the importance of understanding how a candidate drug exploits its action, two selected examples are reported here.

1.2.3.1 Topoisomerase I inhibitors

Topoisomerase I is an enzyme which, similarly to topoisomerase II described in section **1.2.2.2**, is able to release the stress of supercoiled DNA.[112] In contrast to topoisomerase II, this enzyme breaks only one chain in the DNA to allow the relaxation of the DNA.[77] As for the inhibitors of topoisomerase II, several compounds are able to bind to the DNA/enzyme complex, inhibiting the re-ligation of the DNA backbone and leading to apoptosis.[113] Camptothecin and its derivatives, which are shown in **Figure 1.10**, are used in cancer therapy as inhibitors of topoisomerase I.[114] Although the mechanism of action of the compound was already understood, new insight on the interaction between the enzyme and its inhibitor emerged when the crystal structure of topoisomerase I and the camptothecin analogue topotecan was obtained.[115]

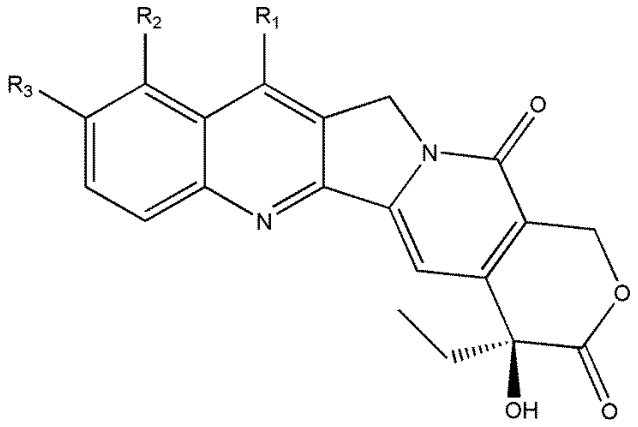

Camptothecin: $R^1 = R^2 = R^3 = H$

Topotecan: $R^1 = H$, $R^2 = CH_2NMe_2$, $R^3 = OH$

Irinotecan: $R^1 = Et$, $R^2 = H$, $R^3 =$ 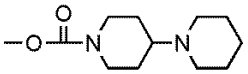

Figure 1.10: Structure of the topoisomerase I inhibitor camptothecin and its derivatives.

The crystal structure showed that topotecan is able to intercalate at the site of the DNA cleavage and that the compound is present inside the active site of the enzyme in both the closed lactone and the open carboxylate forms.[115] Furthermore, the crystal structure showed the steric availability around the binding pocket, which allows to have bulky R_1, R_2 and R_3 substituent,[115] confirming what had been previously reported by structural modifications and structure activity relationships.[116] The quinoline moiety is in fact oriented towards the major groove of the DNA, with plenty of space to accommodate rather large groups.[115]

As a result of these studies and thanks to a better understanding of the interaction with the target, several camptothecin derivatives have been synthesised[117] and two of them, topotecan and ironotecan, have been approved for cancer therapy.[118-119]

1.2.3.2 Thalidomide

A very different example of this approach is given by thalidomide, shown in **Figure 1.11**.

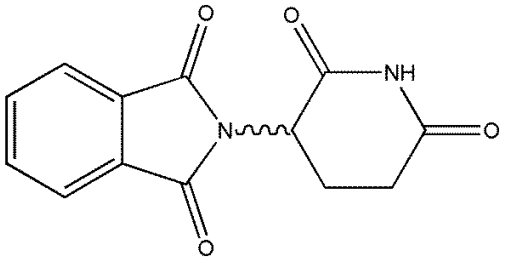

Figure 1.11: Structure of thalidomide.

Thalidomide is very well know for the phocomelia disaster during the 1960s.[120] The compound was on the market as a sedative and was widely used to relieve pregnant women from morning sickness.[121] Unfortunately, the compound proved to be a strong teratogen and caused deformities to over 10,000 babies worldwide.[122]

Several studies were carried out to understand the mechanism of action of this molecule and, as a result, the compound was approved for use against leprosy.[123] The activity seems to be related to the inhibition of the pro-inflammatory factor TNF-α.[123] Further studies focused on the elucidation of the cellular targets of the molecule and led to the discovery that thalidomide was able to inhibit angiogenesis.[124] This feature of the molecule was exploited for cancer therapy and the compound was approved for treatment of multiple myeloma.[125] Although the complete mechanism of action and all the cellular targets of thalidomide have yet to be fully elucidated, further studies on thalidomide have led to novel uses for this molecule and its derivatives.

These examples show, in different ways, the importance of the understanding of molecular targets and mechanism of action in the development of new therapeutic agents.

1.3 Tachpyr as a novel anti-cancer compound

As described in this introduction, although extensive effort has been applied to find effective ways to treat cancer, the need for new selective and potent anti-cancer compounds is still a priority.

Cis,cis-1,3,5-triaminocyclohexane (tach) has been used as a scaffold for several applications due to its ability to act as a tri-dentate ligand. Due to its structure, this compound can form an adamantane-like structure upon complexation with metals, as shown in **Figure 1.12**.

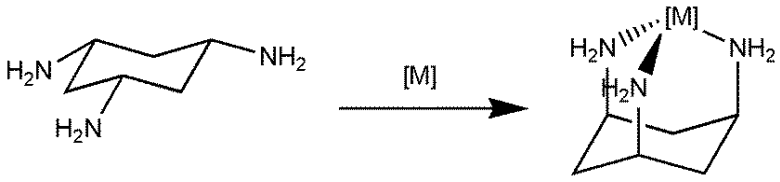

Figure 1.12: Change of conformation of tach upon complexation with metals.

Tach has been reported in the literature in the study of the complexation with different metals in complexes of general structure $[M(tach)_2]^{n+}$.[126-127] Alternatively, the amine nitrogen atoms can be used in the condensation with aldehydes to form Schiff base derivatives. The derivatives obtained have been used, mainly by Walton and co-workers, as small-molecule functional analogues of active sites of enzymes.[128-130]

Recently, Gamble *et al.* reported the use of *cis*-tach for the synthesis of ruthenium(II) complexes having the general structure shown in **Figure 1.13**.[131]

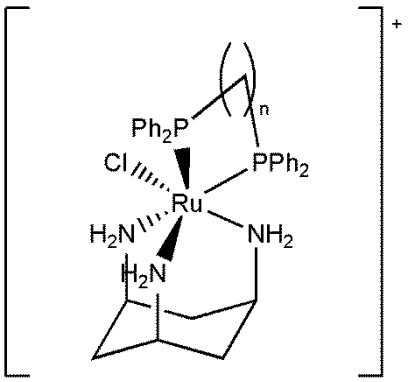

Figure 1.13: General structure of Ru(II)-tach complexes.

These complexes showed very high cytotoxicity against tumour cells, although their mechanism of action has not been clarified.[132]

Among the tach derivatives, in the last decade several studies have been conducted, mainly by Planalp's group, on *N,N',N''*-tris(2-pyridylmethyl)-*cis,cis*-1,3,5-

triaminocyclohexane (tachpyr), an organic molecule with promising anticancer activity.[133]

Tachpyr was shown to have cytotoxic activity against human and mouse bladder cancer cells lines with an IC_{50} value (inhibitory concentration which give 50% cell growth) of 4.6 ± 2.0 μM.[133] The mechanism of action is not completely understood, but Planalp and co-workers suggest a role in iron deprivation.[134] Tachpyr can bind strongly both Fe(II) and Fe(III), and complexation with Fe(III) causes the reduction of the metal to Fe(II).[135] When the ligand is not bound to a metal, it is in the all equatorial conformation, in which the N-substituents are occupying the energetically most favourable equatorial position of the cyclohexane ring. When a metal is bound, instead, the arms can flip and assume the all axial conformation (**Figure 1.14**). Binding with iron can promote oxidation of one, two or three of the amine bonds to C=N double bonds. A low-level oxidative stress, caused by the complex, was also suggested as one of the possible mechanisms of action of this compound.[136] (**Figure 1.14**)

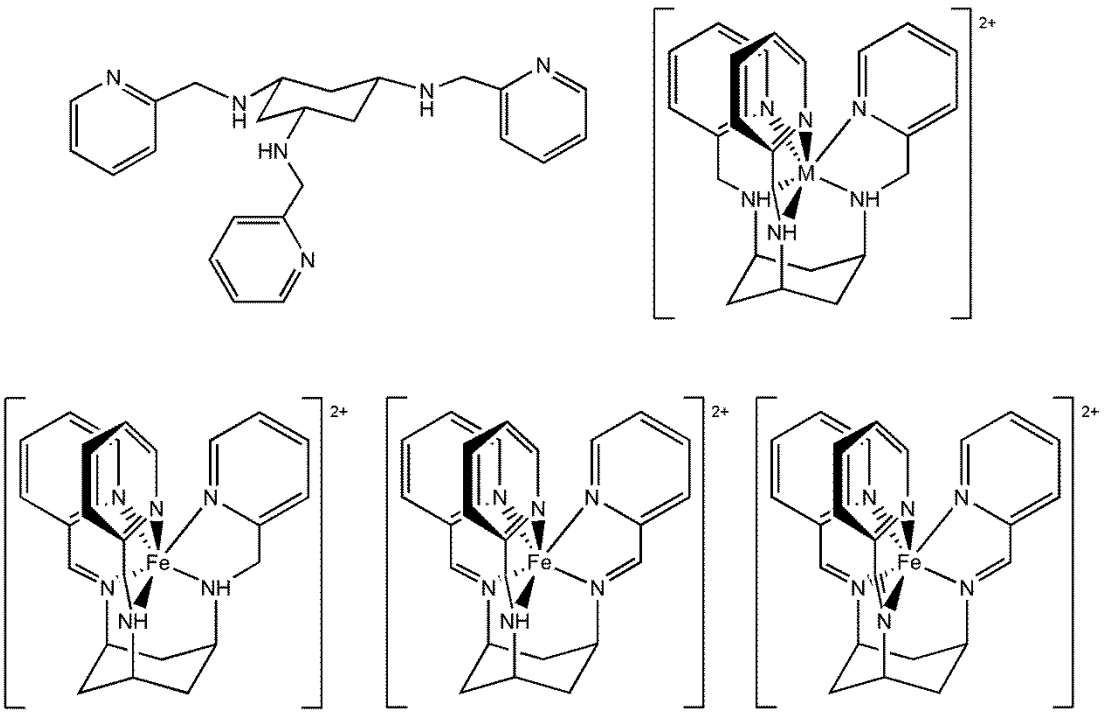

Figure 1.14: Change of conformation of tachpyr upon complexation with a metal (top) and scheme of iron binding and oxidation (bottom). Scheme modified from Zhao *et at*.[134]

The effects of tachpyr on tumour cells have been compared with those of desferoxamine (**Figure 1.15**), an iron chelator used in the treatment of acute intoxication by $FeSO_4$. Both compounds have a delay of 24 h before showing toxic effects on cells and they induce inhibition of ferritin synthesis.[133]

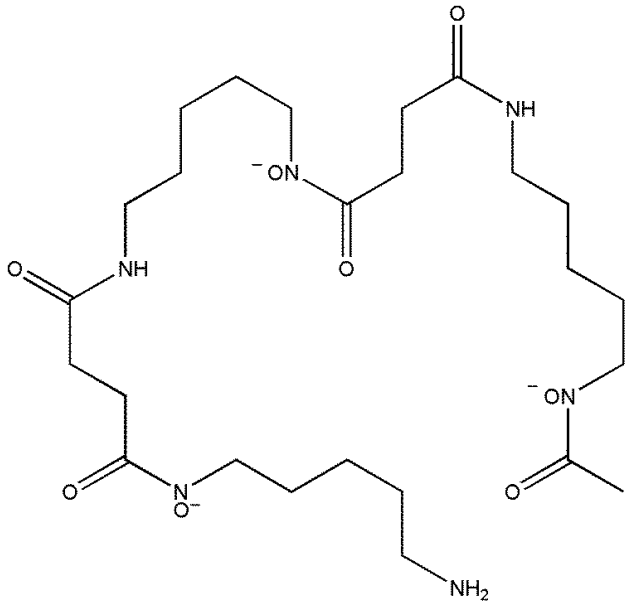

Figure 1.15: Structure of desferioxamine B.

To investigate further the mechanism of action, several metal complexes of tachpyr were tested on tumour cells: Fe(II)-, Zn(II)- and Cu(II)- complexes did not present any cytotoxic effect, while Ca(II)-, Mn(II)- and Mg(II)- complexes had the same activity profile as the free ligand.[133] Similarly, the N-Me and N-Et tachpyr ligands were found inactive.[133] The steric effect due to the alkyl groups on the amine nitrogen atoms upon complexation was considered responsible for the poor activity of these compounds. The N-alkylation of tachpyr causes a lengthening of the metal-nitrogen bonds upon complexation and makes the complex weaker, which might also provide a possible explanation of the poor activity of these compounds *in vitro*.[137] All these results seem to support the hypothesis of a chelation mechanism.

Tachpyr has also proved to activate caspases, enzymes involved in cell death, leading to apoptosis, whilst derivatives with alkylated tach nitrogen atoms did not show activation of this group of enzymes.[138]

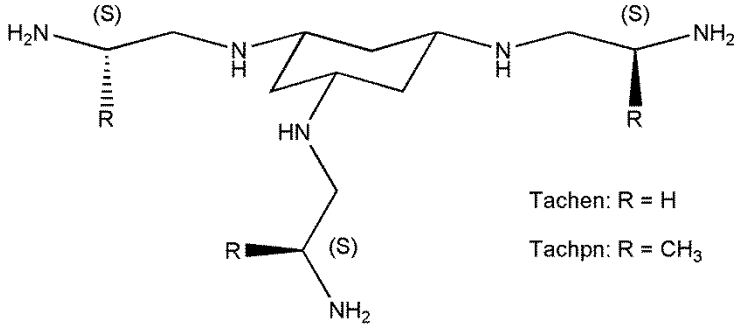

Figure 1.16: General structure of tach tris(ethylendiamine) derivatives.

Tris(ethylendiamine) derivatives, shown in **Figure 1.16**, were then synthesised and their cytotoxic and binding properties towards Ni(II), Cu(II) and Zn(II) studied. These compounds proved to be less cytotoxic than tachpyr, with IC_{50} values ranging between 8 and 200 μM.[139]

To gain information about the possible binding of tachpyr with metals present inside the cell, HPLC was performed on cell lysate both before and after treatment with tachpyr 50 μM for 16 h, with the intention of quantifying the amount of iron, zinc and their respective tachpyr complexes that could be observed.[134] The analysis showed tachpyr to be the most abundant product, followed by the zinc and iron complexes. The partially re-oxidised ligand could also be identified. From the quantitative analysis it was possible to calculate that, during the incubation period, tachpyr had bound approximately 9% of intracellular iron and 13% of zinc.[134] In the same study, Zhao *et al.* reported that pre-treatment of cells for 24 h with either zinc sulfate or iron sulfate at concentrations of 25 μM or 200 μM, respectively, stops completely the cytotoxic activity of tachpyr and synthesis of caspase enzymes, protecting cells from tachpyr-induced apoptosis.[134]

Further evidence of the importance of the binding properties of tachpyr was obtained through structural modification of the pyridine moiety, in particular methylating positions 3, 4, 5 or 6 of the aromatic ring.[140] A scheme of the methylation of the pyridine ring is shown in **Figure 1.17**.

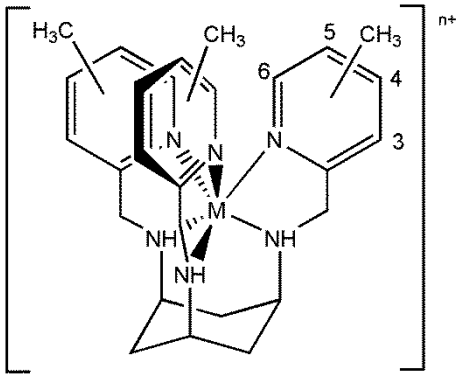

Figure 1.17: Representation of the methyl substituted tachpyr complexes.

It was reported by Childers *et al.* that 6-Me-tachpyr did not shown any cytotoxicity, which was rationalised by the presence of steric interactions which destabilise the metal complex or prevent its formation.[140] Also, 3-Me-tachpyr was found to have a shorter delay time than tachpyr in its cytotoxic activity,[140] possibly due to a difference in the kinetics of binding.

In order to test the hypothesis that a more flexible ligand could show better chelation properties than tachpyr, some tris-2-aminoethylamine (tren) compounds were synthesised (**Figure 1.18)**. Trenpyr was slightly less active than tachpyr, as was tren(5-Me)pyr, whilst trenpyr(C-Me), tren(3-Me)pyr and tren(4-Me)pyr presented approximately the same IC_{50} values as tachpyr, with the 3-Me derivative being the most active. The 6-Me derivative, instead, was found to be about 10 times less active than tachpyr.[141] The difference in activity might be due to a difference in the iron complex formed.

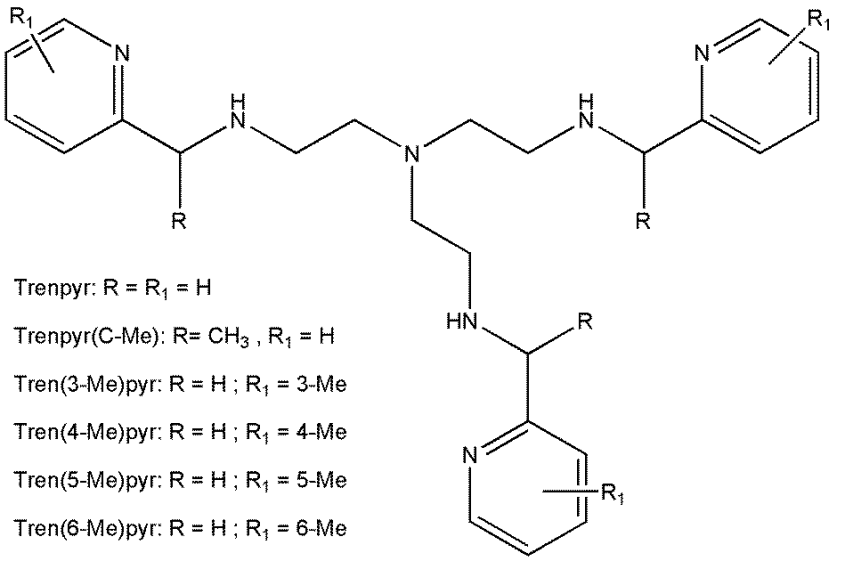

Figure 1.18: Structure of trenpyr derivatives.

A further variation on the general backbone of these compounds has been achieved with the tamepyr derivatives (**Figure 1.19**),[142] but no studies into cytotoxicity have been conducted on these compounds so far.

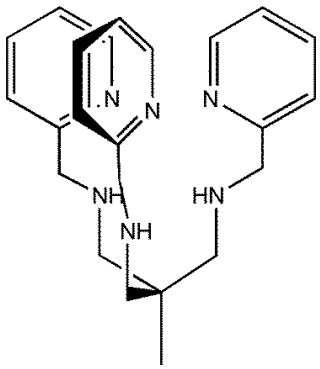

Figure 1.19: Structure of tamepyr.

Tachpyr has proved to be a promising compound with good cytotoxicity and it could be used as the precursor for the development of a new class of anti-cancer agents.

1.4 Aims of the project

Tachpyr showed good cytotoxic activity, and the original aim of the project was to exploit the properties of this compound to improve its cytotoxicity.

An additional aim of the project was to gain a deeper understanding of the possible mechanism of action of tachpyr and related tach-based compounds. The hypothesis-driven investigation of the structural characteristics of the compounds necessary to show cytotoxic activity is presented in this thesis.

The study focused on the synthesis of tach-based derivatives, with different groups as substituents on the amine nitrogen atoms. The synthetic procedures and example of characterisation of such molecules are described in **Chapter 2** .

Some metal complexes of tachpyr were also synthesised to study the binding properties of the free ligand and to evaluate the cytotoxicity of Co and Ru complexes of tachpyr in cancer cells (**Chapter 3**).

Finally, the biological evaluation of the cytotoxic activity of all the ligands was carried out, alongside the development of structure-activity relationships. An alternative hypothesis for the mechanism of action of tachpyr and other tach derivatives was developed and cellular targets and type of interaction were explored. These results are described in **Chapter 4**.

Chapter 2

Synthesis and characterisation of tach-based ligands

2. Synthesis and characterisation of tach-based ligands

2.1 Introduction

Schiff bases, obtained by the condensation of a primary amine with aldehydes or ketones, have been widely used in synthetic chemistry due to their facile synthesis and good stability in neutral or basic environments. Schiff bases are also indicated as aldimines or ketimines, depending on the precursor (i.e. aldehyde or ketone, respectively) used for the synthesis (**Figure 2.1**). These compounds have frequently been used in medicinal chemistry[143] and the literature can offer plenty of examples of potential applications, such as anticancer,[144-147] antibacterial,[148-150] antiviral,[151] anti-HIV,[152] anti-inflammatory,[153-154] etc. agents and as scaffolds for metal complexes with biological applications.[155-157] Some examples of Schiff bases developed for medicinal applications are shown in **Figure 2.1**.

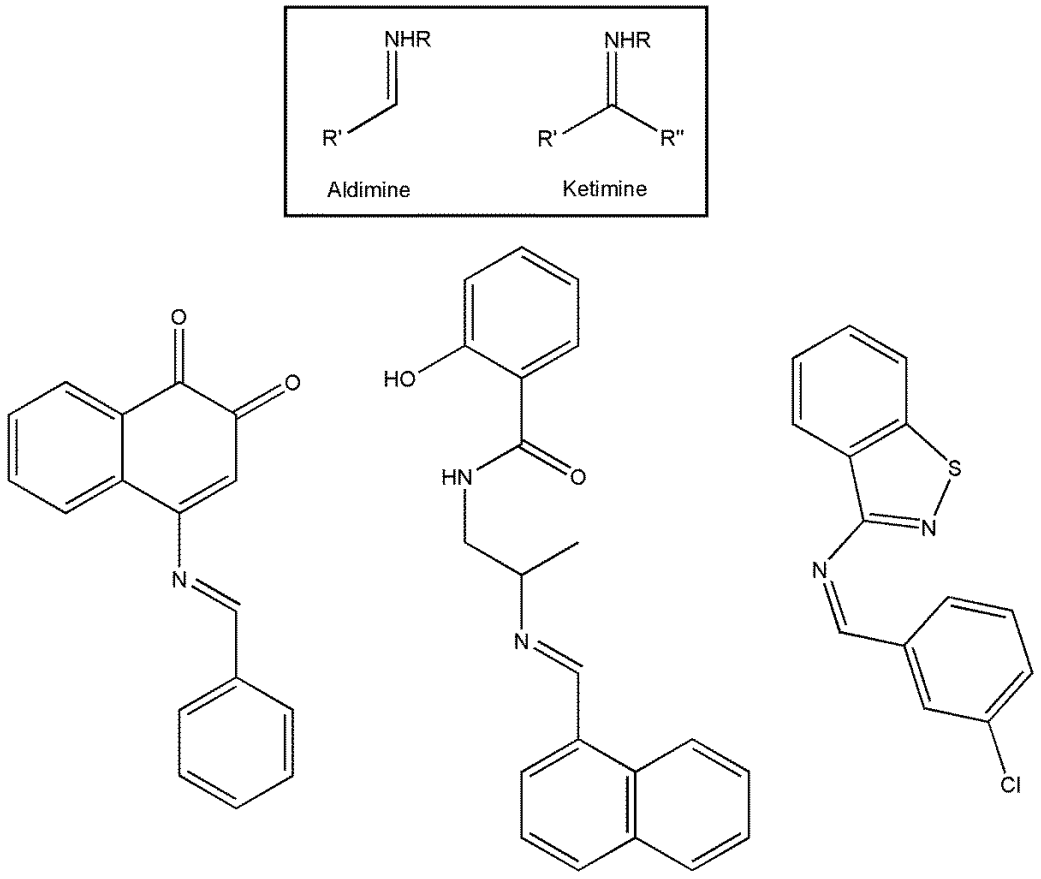

Figure 2.1: General structure of aldimines and ketimines (top) and some examples of Schiff bases studied for anticancer,[144] antibacterial[148] and antiviral activity[151] (bottom).

All the compounds presented in this thesis belong to the class of aldimines, for which the general mechanism of formation is shown in **Figure 2.2**. Ketimines were not explored because the final targets of the syntheses are the reduced compounds and ketimines would give rise to stereogenic centres upon reduction.

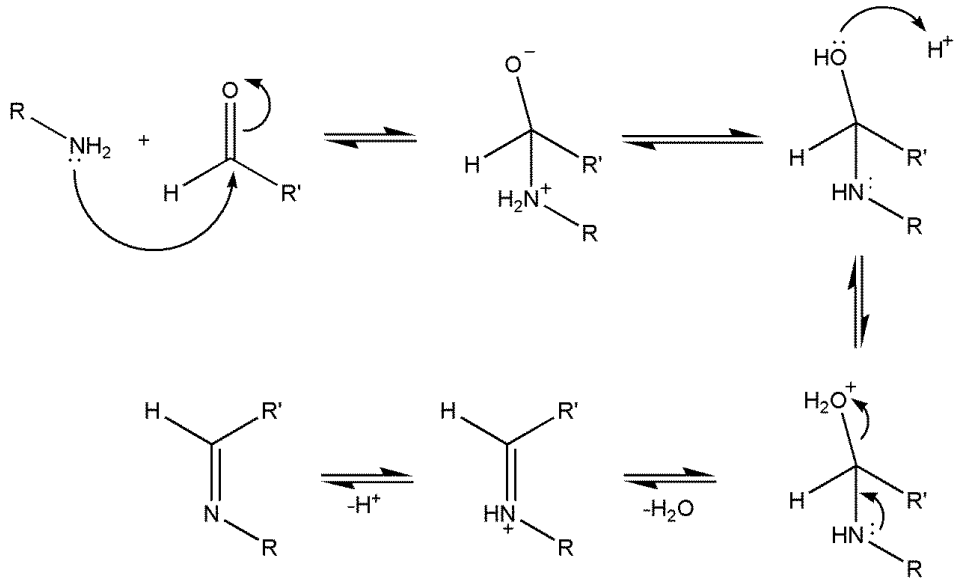

Figure 2.2: General mechanism of Schiff base formation.

The general mechanism of formation involves the nucleophilic attack by the amine to the electrophilic carbon of the carbonyl group, followed by proton transfer to re-establish a neutral charge. Protonation of the oxygen atom leads to the formation of the C-N double bond with elimination of water. Deprotonation of the imine nitrogen forms the final neutral Schiff base. Optimal conditions for Schiff base formation require mild acidic conditions (pH = 4.5)[158] to favour the elimination of water without causing the protonation of the amine, which would stop the nucleophilic attack to the carbonyl. The whole condensation is a reversible process: re-protonation of the imine nitrogen and addition of water can hydrolyse the imine back to the starting materials. For this reason, Schiff bases are usually unstable in strong acid. Elimination of water from the reaction mixture is typically a good strategy to successfully synthesise Schiff bases for two main reasons: if water is subtracted from the reaction, the equilibrium is pushed towards the product and, on the other hand, the reverse hydrolysis reaction is inhibited. The stability of the Schiff base is often dependent on the electronic properties of the carbonyl group used for the reaction. A very electrophilic carbonyl,

in fact, reacts readily with the nucleophilic amine, but the resulting imine bond is more susceptible to hydrolysis. On the other hand, a less electron poor imine carbon would disfavour a nucleophilic attack on the imine bond, but the condensation would be harder to achieve.

If, on one hand, synthesis of Schiff bases allows for the possibility of introducing almost endless chemical variations to molecules, on the other hand the imine bond has some major limitations, especially considering biological applications; above all, the low stability to acidic pH and the poor water solubility. To overcome these problems the imine can easily be reduced to an amine. Several advantages are obtained when Schiff bases are reduced: the corresponding amine compounds are more stable, more water soluble, more flexible (due to the lost of the rigid imine double bond), and a hydrogen bond donor is introduced in the molecule, which might contribute to interaction with biomolecules. All these characteristics can be of importance for biological application, therefore the reduced Schiff bases are the main focus of this thesis. Among the different reducing methods that can be used for the Schiff base reduction, sodium borohydride has proven to be a good reagent for this reaction.[159-160] Reduction with sodium borohydride provides a clean, relatively safe and facile reaction and, therefore, is the method of choice for the imine reductions described herein.

In this chapter the synthesis and characterisation of several Schiff bases is described, as well as their reduction to amines, with relative characterisation. The amines synthesised were tested for cytotoxic activity against cancer cells, as discussed in **Chapter 4**.

2.2 Nomenclature and numbering

For clarity all of the ligands presented in this thesis are named according to their relation to the starting materials. *Cis,cis*-1,3,5-triaminocyclohexane is identified as "tach" across the thesis. "Short names" and a numbering system have also been used.

All compounds synthesised from salicylaldehyde derivatives (section **2.5**) are named with respect to the parent aldehyde (e.g. as *cis,cis*-1,3,5-tris(5-chlorosalicylidenamino)cyclohexane rather than 2-hydroxy-5-chlorobenzyl-derivative). The short names for all of the ligands are given by the moieties which form that compound and a scheme of the nomenclature is shown in **Figure 2.3**. For example, "tachpyr" is the tri-amine made by the condensation of tach and pyridine-2-aldehyde, and subsequent reduction of the Schiff base. To indicate the Schiff base, the infix "-im-" is added to the name, so "tachimpyr" indicates the tri-imine formed by tach and pyridinaldehyde. Benzaldehyde derivatives are shortened as "ben", salicylaldehyde derivatives as "sal" and the cyclohexylaldehyde derivative as "cyc"; the heterocycles are "pyr", "prl" and "fur" for pyridine-, pyrrole- and furan- aldehydes, respectively. If a substituent is present on the aromatic rings, it is outlined in the short name (e.g. 4-Br-tachben).

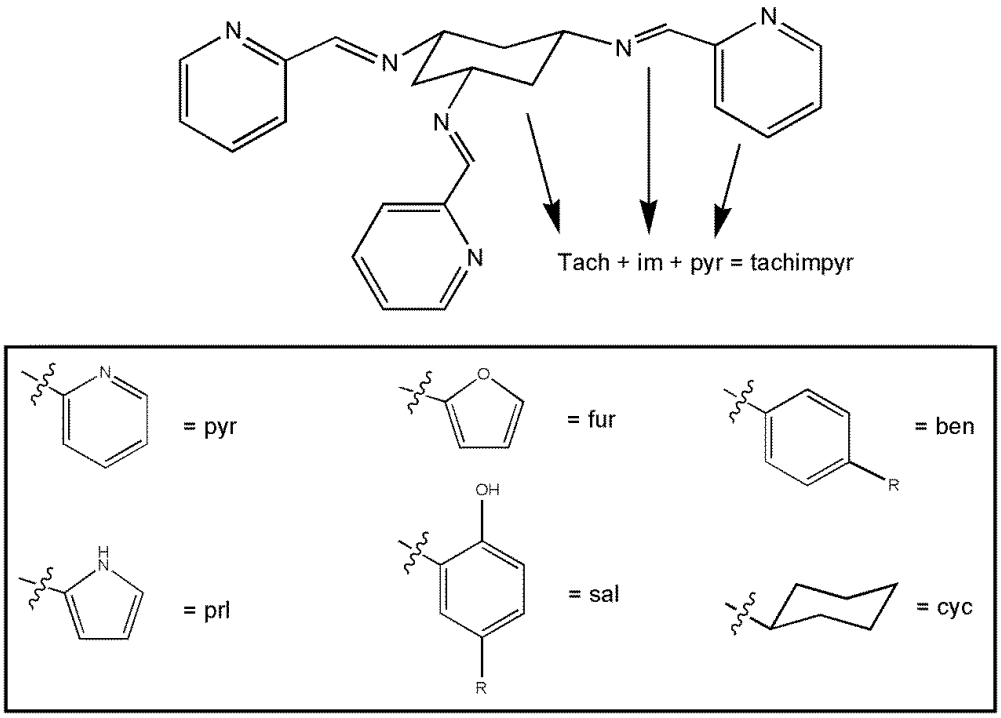

Figure 2.3: Diagram of the nomenclature scheme used.

The mono-N-substituted tach derivatives (section **2.7**) have the infix "mono", to highlight the mono-substitution of the tach amines. All compounds are identified by progressive numbers. Related Schiff base/amine pairs are labelled with the same number with the addition of "a" or "b", respectively, for a quick identification of the

oxidised or reduced ligand (e.g. tachimpyr is compound **[3a]** and tachpyr is **[3b]**). In the case of the mono-armed compounds (section **2.7**), which required a multi-step synthesis, the final compound is labelled with a number, whilst the intermediates are numbered as **[Compound no.-synthetic step no.]**.

All crystal structures presented in this thesis are numbered according to a common scheme, which is shown in **Figure 2.4**: the carbon atoms on the cyclohexane ring are always C(1)-C(6), the tach-nitrogen atoms are N(1)-N(3) and then the numbering proceeds to the arms, starting with C(7) bound to N(1) and continuing down the arm, then moving on to the arm bound to N(2) and finishing with the remaining arm bound to N(3).

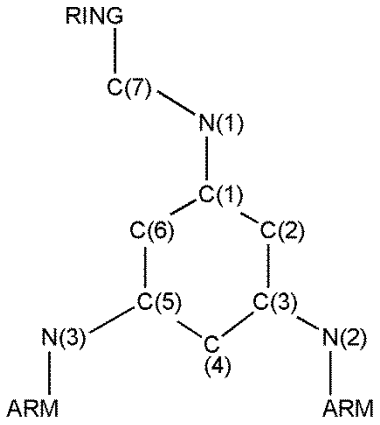

Figure 2.4: Example of numbering scheme for the crystal structures.

Tables with crystal information and details of structural refinement for all the crystal structures included in this thesis can be found in the **Appendix**.

2.3 Synthesis and characterisation of tach

The synthesis of *cis,cis*-1,3,5-triaminocyclohexane (tach) follows the well-established procedure reported in the literature[161] and outlined in **Figure 2.5**. Starting from the corresponding tricarboxylic acid, *cis,cis*-1,3,5-triaminocyclohexane was obtained through a Curtius rearrangement from the reaction of diphenyl phosphoryl azide (DPPA) and benzyl alcohol in the presence of triethylamine in benzene. The

benzylcarbamate derivative **[1]** was isolated by filtration as a cream coloured compound with a high degree of purity and in good yield (67%).

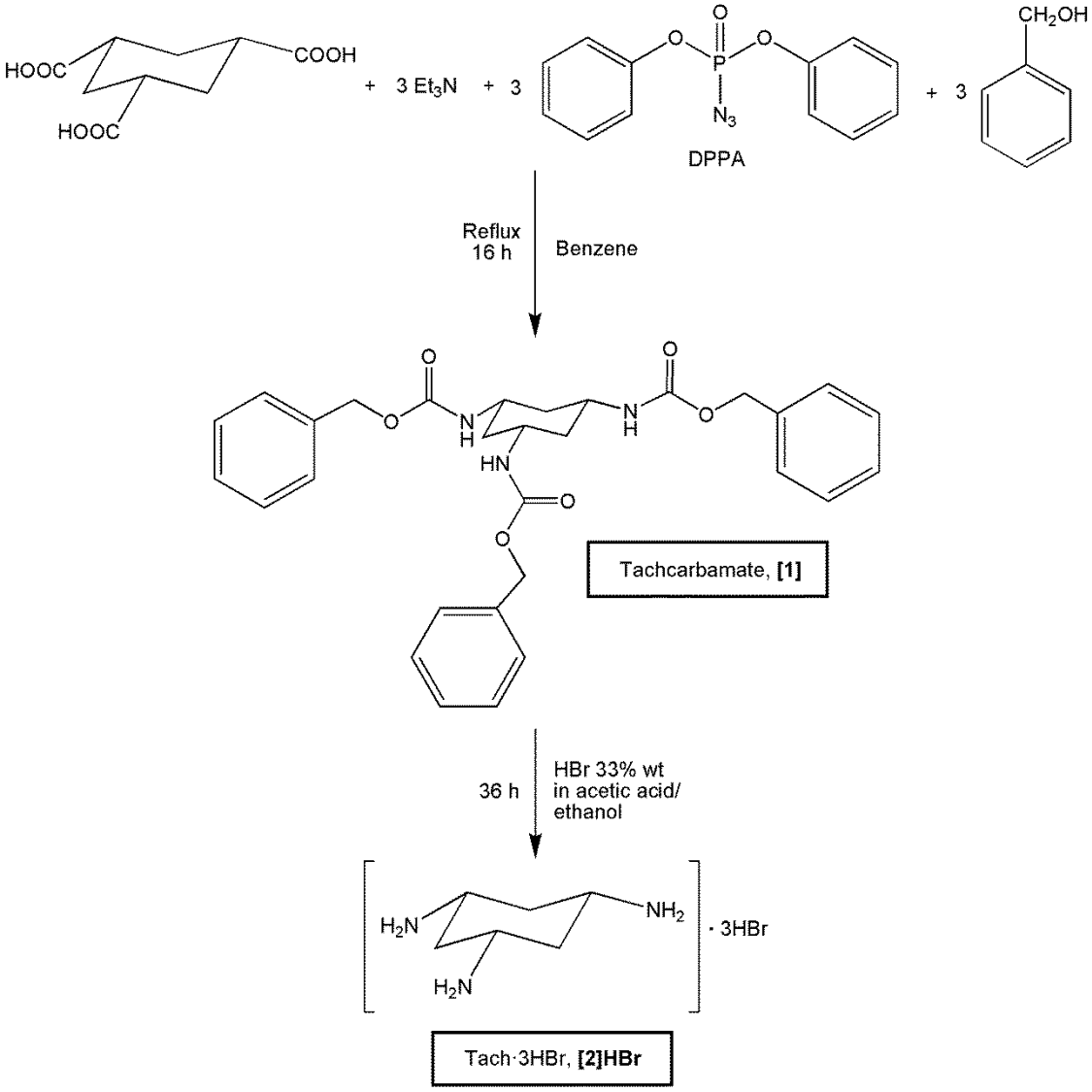

Figure 2.5: Synthetic scheme for tach·3HBr **[2]HBr**.[161]

The carbamate derivative **[1]** was then hydrolysed under strongly acidic conditions to give the desired compound in 91% yield as a hydrobromide salt (tach·3HBr, **[2]HBr**),[161] which can be used without further purification as a starting material for the preparation of the ligands described in the following sections. If the free amine was required instead of the HBr salt, compound **[2]HBr** was passed down an ion exchange column, sublimed and collected as a bright white solid.[128] A significant

change in the NMR chemical shifts is evident after the process, as shown in **Figure 2.6**.

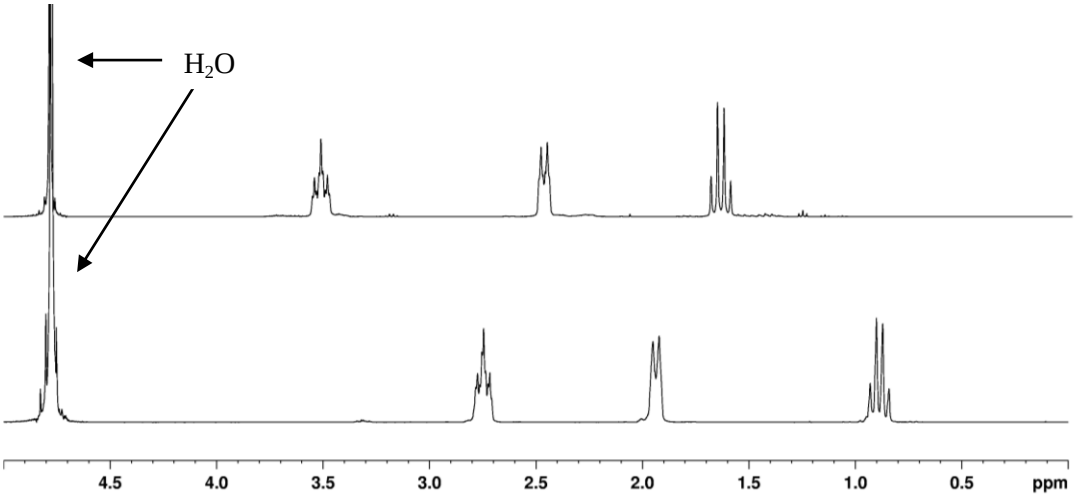

Figure 2.6: ^{1}H NMR spectra in D_2O of compounds **[2]HBr** (top) and free amine **[2]** after sublimation (bottom).

Figure 2.6 also shows the characteristic NMR signals of tach, which can be explained by an analysis of the structure.

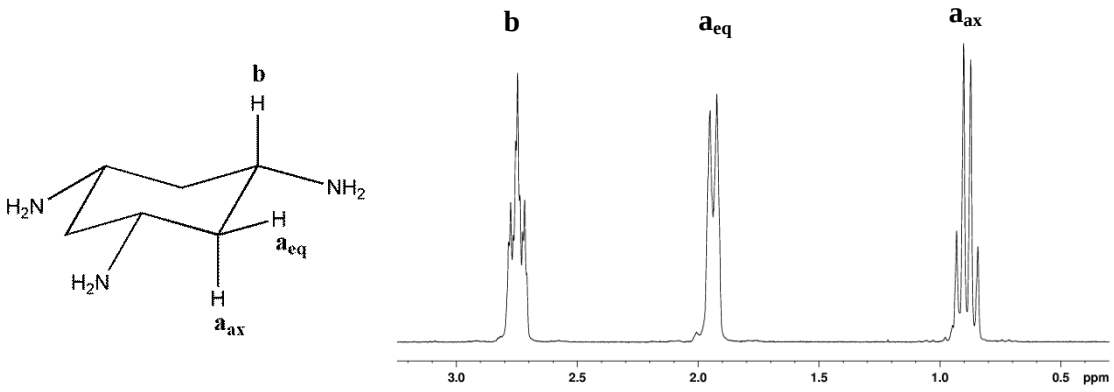

Figure 2.7: Structure of tach **[2]** (right) and its NMR spectrum in D_2O (left).

The tach molecule presents a C_3 rotation axis, so only non-equivalent protons are shown in **Figure 2.7**. Amine protons are usually not observed, presumably due to fast exchange with the solvent. Protons **b** are the most deshielded, at 2.75 ppm, due to the proximity of the electronegative nitrogen atoms. The splitting pattern for these protons is a triplet of triplets (**Figure 2.8**) due to the large coupling constant (ca. 12 Hz) with

the two equivalent axial protons $\mathbf{a_{ax}}$ and the small coupling (ca. 4 Hz) with the two equivalent equatorial protons $\mathbf{a_{eq}}$.

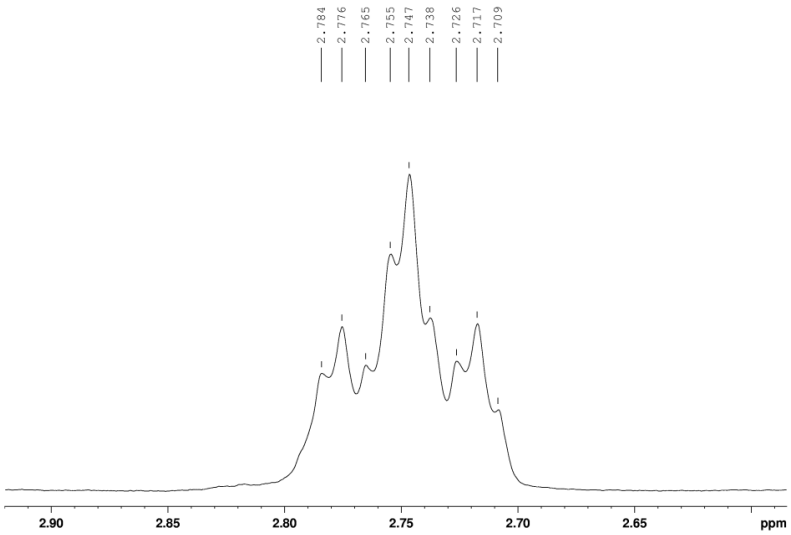

Figure 2.8: Detail of the NMR splitting of proton **b** in compound **[2].**

Geminal protons $\mathbf{a_{ax}}$ and $\mathbf{a_{eq}}$ appear as two different signals at 0.89 and 1.94 ppm, respectively. The equatorial protons $\mathbf{a_{eq}}$ appear as a broad doublet due to the large *J* geminal coupling (ca. 12 Hz) with protons $\mathbf{a_{ax}}$. Protons $\mathbf{a_{ax}}$, on the other hand, are affected by both axial-axial and geminal couplings, which coincidentally are very similar, therefore giving rise to a pseudo quartet signal. All the coupling constants observed fall in the range of values reported in the literature for cyclohexane systems (^2J = 12-20 Hz; $^3J_{ax\text{-}ax}$ = 10-13 Hz; $^3J_{ax\text{-}eq}$ = 2-5 Hz).[162] The NMR spectra also demonstrate, as expected, that the compound adopts the energetically favourable equatorial conformation when free in solution. The axial conformation, shown in **Figure 2.9**, would exhibit alternative NMR multiplicities due to different couplings between the tach protons.

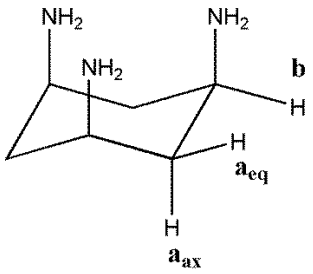

Figure 2.9: Structure of tach **[2]** in the axial conformation.

In the axial conformation, the coupling between protons **b** and $\mathbf{a_{ax}}$ would be smaller due to the change in the dihedral angle, resulting in a triplet with a $^{3}J_{\text{ax-eq}}$ coupling in the range of 2-5 Hz.[162] Furthermore, protons **b** would also show the $^{3}J_{\text{eq-eq}}$ coupling in the range of 2-5 Hz[162] with protons $\mathbf{a_{eq}}$. Protons $\mathbf{a_{eq}}$ and $\mathbf{a_{ax}}$ would display the large ^{2}J geminal coupling, which would give a doublet for both of them, and the small ^{3}J couplings with protons **b**. Therefore, as a result of the axial conformation, the ^{1}H NMR spectrum would show, in first approximation, a multiplet and two doublet with possibly some fine structure for protons **b**, $\mathbf{a_{ax}}$ and $\mathbf{a_{eq}}$, respectively. Such a splitting pattern was never observed in the ^{1}H NMR spectra of free tach in solution, thus confirming that the molecule is found in the equatorial conformation.

All of the ligands described in sections **2.4**-**2.6** present similar symmetry and NMR spectra for the tach moiety as seen in compound **[2]** described above.

2.4 Synthesis and characterisation of heterocyclic ligands

The investigation of tach-based compounds began from previously published literature, presented in **Chapter 1**. The motivation for the syntheses of these molecules was to investigate the effect of different heterocycles, when they were added as "arms" to tach, on the biological activity of these compounds against cancer cells. The hypotheses which led to the developments of all the derivatives described in this chapter are explained in more details in **Chapter 4**. The heterocyclic ligands were made following the reported procedures or by their modification.[161, 163]

2.4.1 Schiff bases

For the synthesis of the Schiff bases, three equivalents of sodium hydroxide were added to one equivalent of tach·3HBr, **[2]HBr**, in water to neutralise the HBr and form the free amine. Subsequent reaction with three equivalents of the appropriate aldehyde afforded the desired Schiff base in good yields. The general synthetic scheme is shown in **Figure 2.10**. The imine formation was carried out in toluene for

tachimpyr and tachimprl, in benzene for tachimfur; in both cases a Dean-Stark apparatus was used to remove water (both used to dissolve the starting material and generated during the condensation). This minimised the reverse hydrolysis reaction and improved the yields. Although none of the reagents was air sensitive, inert atmosphere was used during the reflux, generally improving the yield of compound **[3a]** from 34% to 68%.

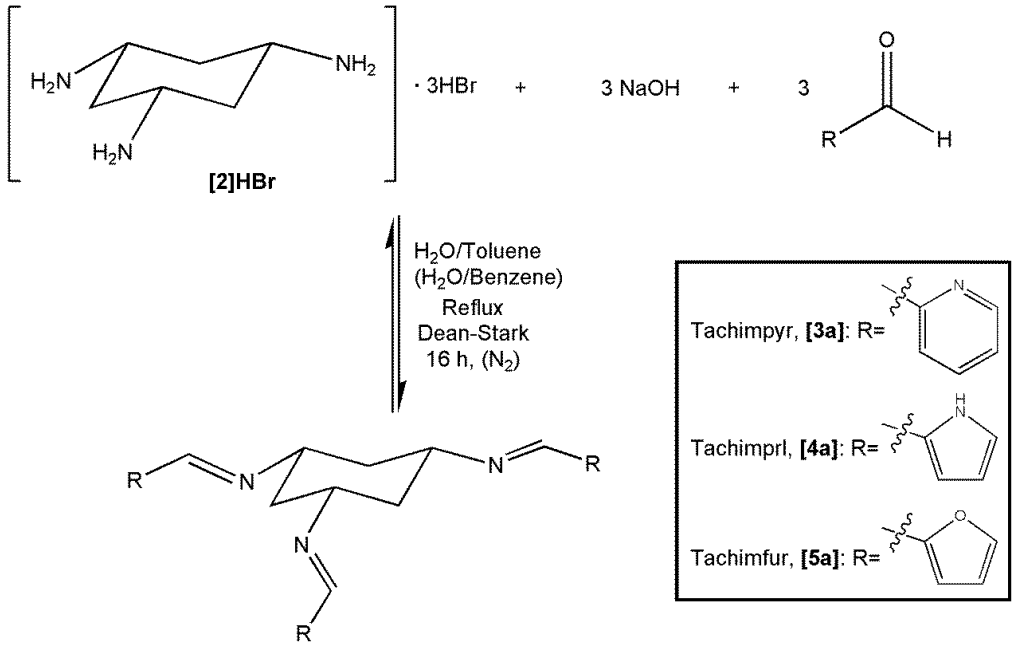

Figure 2.10: General synthetic scheme for tach-heterocycles.

To the best of our knowledge, the synthesis of the pyrrolyl derivative **[4a]** has not been reported before. To prepare this compound, the synthetic procedure used for **[3a]** was utilised. Tachimpyr and tachimprl were isolated by evaporation of the solvent and a subsequent wash with diethyl ether and pentane, and the compound typically used without further purification. For the furanyl derivative **[5a]**, two different synthetic methods were explored. The literature reported the synthesis of this compound in benzene,[163] but a safer synthesis was attempted using water and diethyl ether for a bi-layer reaction. Tach·3HBr and sodium hydroxide were dissolved in water, furfural was added as a solution in diethyl ether and the reaction was vigorously stirred under a N_2 atmosphere for 16 h. Both methods produced the desired compound, although the benzene reaction with Dean-Stark apparatus gave better yields (62% instead of 45%). Evaporation of the solvent gave the final product as a yellow oil. Compounds **[3a]**,

[4a] and **[5a]** were isolated in 68, 45 and 62% yields, respectively. The presence of the Schiff base was indicated by the appearance of a characteristic singlet signal in the ^{1}H NMR spectrum at low field, typically at 8.0-8.5 ppm in $CDCl_3$, with a relative integration of three and belonging to the N=C*H* protons. Similarly, a signal at 148-160 ppm in the ^{13}C NMR belonging to the imine carbon was diagnostic of the presence of the Schiff base.

2.4.1.1 Characterisation: selected example

A selected example is presented herein to illustrate how the compounds were analysed and the NMR signals assigned. The same general methods and techniques, mainly 1D- and 2D-NMR and mass spectrometry (MS), have been used for all other compounds described in the chapter. Particular examples are discussed in the appropriate sections and full characterisation data for the compounds made can be found in **Chapter 6**.

Tachimpyr **[3a]** is used as an example for the characterisation of the Schiff bases.

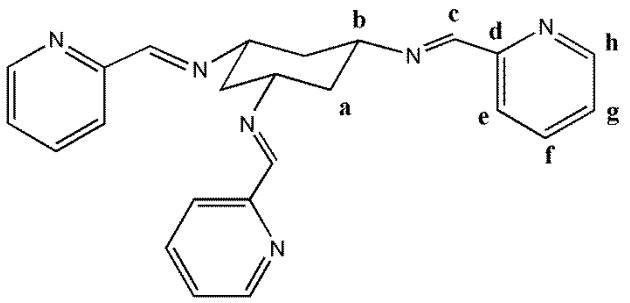

Figure 2.11: Tachimpyr **[3a]**.

The ^{1}H NMR spectrum of the compound, **Figure 2.12**, shows the characteristic splitting patterns of the tach moiety in the aliphatic region. The ligand has the same symmetry as compound **[2]**, so each signal has a relative integration of three protons. The aromatic region of the spectrum includes, among others, two very diagnostic signals: the strongly deshielded doublet of doublets belonging to protons **h** at 8.64 ppm, which falls at low field due to the proximity of the nitrogen atom, and the singlet of the imine protons **c** at 8.48 ppm. The presence of tach and imine signals, together with the correct integration of the protons, were usually a clear indication of the presence of the desired compound for all the Schiff bases described in this chapter.

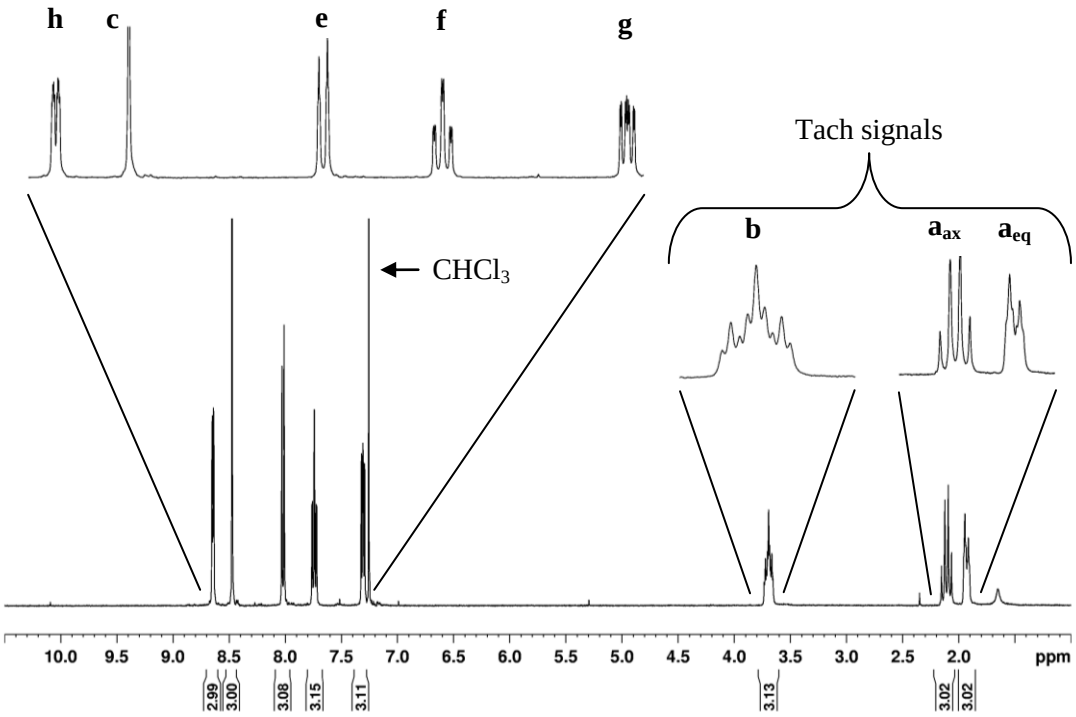

Figure 2.12: ^{1}H NMR spectrum of tachimpyr **[3a]** with relative integration of the signals, recorded in $CDCl_3$.

The doublet at 8.02 ppm was assigned to protons **e**, which are the only ones for which a doublet is expected due to the coupling to protons **f**. Protons **f** and **g** were assigned on the basis of 2D-NMR experiments, as discussed below.

^{13}C and Distortionless Enhancement by Polarisation Transfer (DEPT) 135 NMR experiments were used to characterise the carbon signals (**Figure 2.13**). DEPT 135 experiments give characteristic anti-phase signals for carbons bound to two protons and they highlight quaternary carbons, as they are observed in the ^{13}C spectrum, but not in the DEPT.

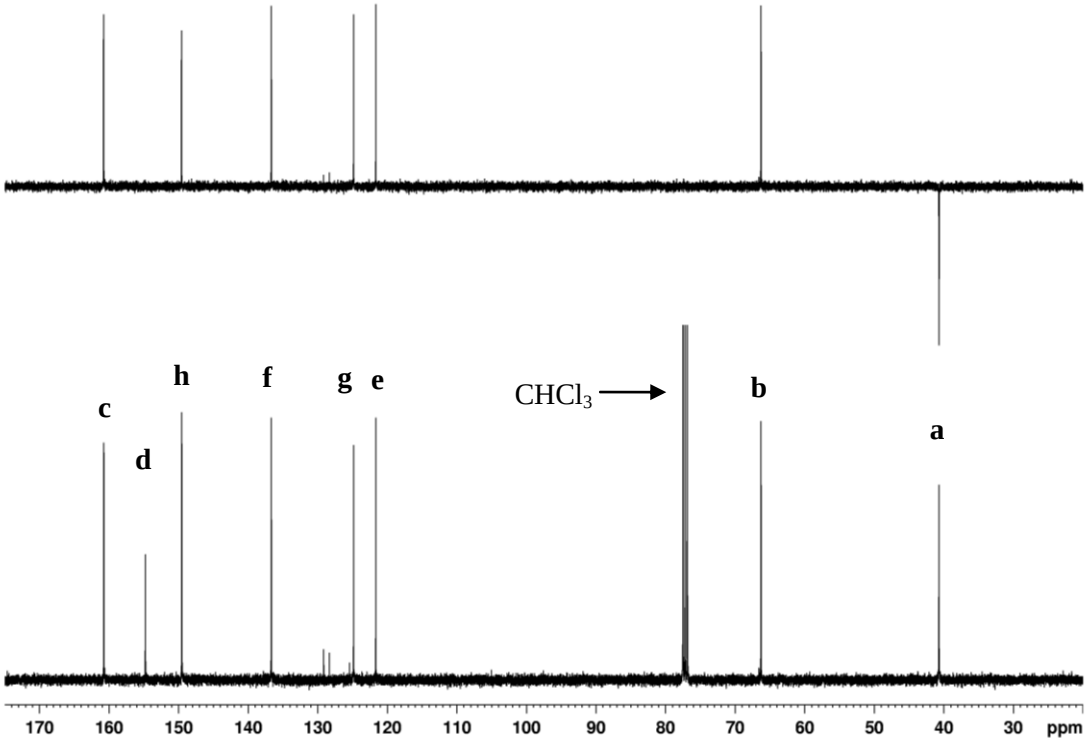

Figure 2.13: $^{13}C\{^{1}H\}$ (bottom) and DEPT 135 (top) NMR experiments for compound **[3a]**, recorded in $CDCl_3$. The small signals between 125 and 130 ppm belong to residual toluene from the reaction.

The aliphatic region of the ^{13}C NMR spectrum presents, as expected, two signals for the tach carbons. The most deshielded of the two (66.3 ppm) was assigned to carbons **b**, which are bound to the nitrogen atoms. The signal at 40.7 ppm was therefore assigned as the tach *C*H_2 carbons **a**, as confirmed by DEPT 135. Carbons **d** were also assigned on the basis of DEPT 135 spectrum to the signal at 154.8 ppm. The assignment of the remaining carbons required the use of 2D-NMR experiments, primarly ^{1}H-^{13}C Heteronuclear Single Quantum Correlation (HSQC) and Heteronuclear Multiple Bond Correlation (HMBC).

Figure 2.14 shows the aromatic region of the Correlation Spectroscopy (COSY) NMR of tachimpyr **[3a]**. Beginning from protons **h** and following the cross peaks in the spectrum it was possible to assign all the remaining pyridine protons in the molecule. Protons **h** show coupling with the multiplet at 7.31 ppm, indicating that this signal belongs to protons **g**. It is then possible to observe coupling between **g** and the triplet

at 7.74 ppm, which was assigned as protons **f**. Finally, protons **f** are coupled to the doublet at 8.02 ppm, belonging to protons **e**.

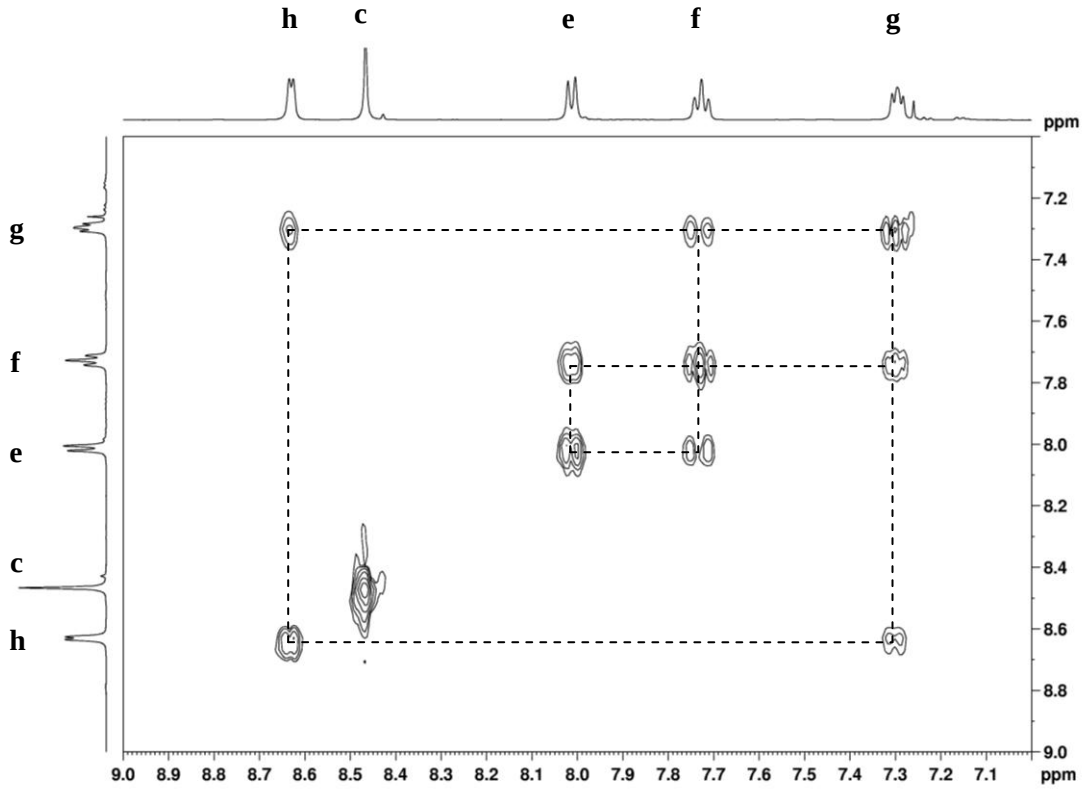

Figure 2.14: COSY NMR of tachimpyr **[3a]**, detail of the aromatic region, recorded in $CDCl_3$.

On the basis of the assignment, it is possible to explain the splitting pattern of the signals observed in **Figure 2.12**. Protons **h** appear as a doublet of doublets due to the coupling to both **g** (^3J = 4.8 Hz) and **f** (^4J = 1.2 Hz). Protons **g**, which are a doublet of doublets of doublets, have two different ^3J values for the coupling with protons **f** and **h** of 7.6 and 4.8 Hz respectively, which gives rise to a doublet of doublets. A small ^4J coupling constant of 1.2 Hz with protons **e** is also observed, which splits the signal into a further set of doublets. Protons **f**, a triplet of doublets in the ^{1}H spectrum, are coupled to protons **e** and **g** apparently with the same coupling constant, which therefore produces a triplet. The small ^4J coupling constant with protons **h** (1.2 Hz) splits the triplet into doublets, giving the fine structure observed in **Figure 2.12**. Interestingly, protons **e** do not show the splitting due to the coupling with **g**, appearing as a slightly broad doublet with a *J* coupling of 7.6 Hz with protons **f**.

Heteronuclear experiments allowed to complete and confirm the assignment of ^{1}H and ^{13}C spectra. HSQC is a ^{1}H-^{13}C heteronuclear 2D experiment which highlights the $^{1}J_{H\text{-}C}$ couplings, correlating the protons to the carbon which they are bound to.

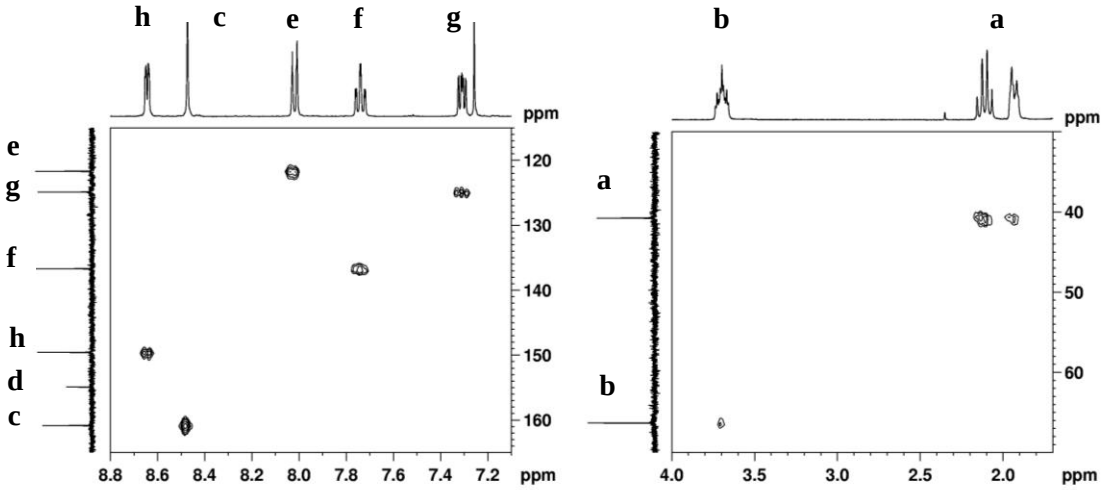

Figure 2.15: HSQC spectrum of tachimpyr **[3a]**, recorded in $CDCl_3$. Detail of the aromatic region (left); detail of tach signals (right).

Figure 2.15 shows the HSQC spectrum of tachimpyr, with details of the aromatic region, on the left, and the tach signals, on the right. The tach region confirms the ^{1}H and ^{13}C assignment, with the deshielded protons **b** bound to the most deshielded carbon and both the quartet and the doublet of protons **a** bound to the same carbon. In the aromatic region, the assignment of the proton signals done through COSY NMR permitted full assignment of the signals in the ^{13}C spectrum.

Similarly to HSQC, HMBC is a ^{1}H-^{13}C heteronuclear 2D experiment, but shows long range ^{1}H-^{13}C correlations, from ^{2}J to ^{4}J coupling, which are visualised as cross peaks in the spectrum.

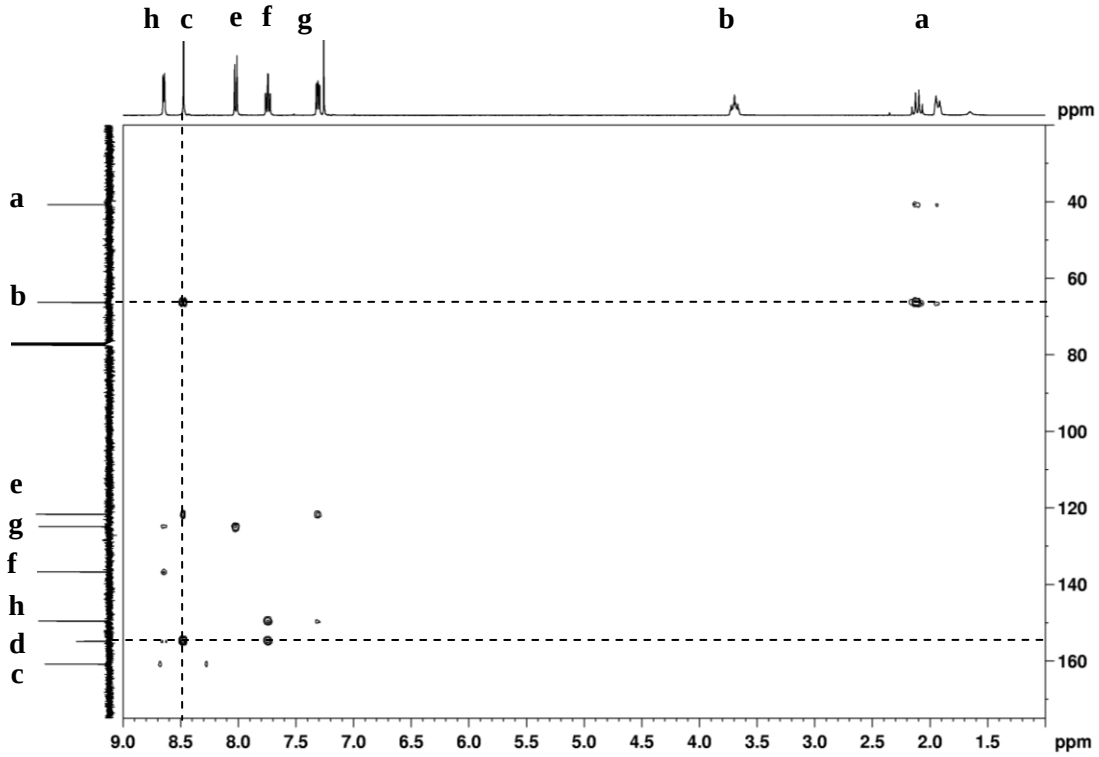

Figure 2.16: HMBC of tachimpyr **[3a]**, recorded in $CDCl_3$.

Figure 2.16 shows the HMBC spectrum of compound **[3a]**. In particular, coupling between the imine protons **c** and both the tach carbons **b** (^3J) and the quaternary carbons of the pyridine ring **d** (^2J) are observed, which confirms the assignment of the signals.

Compound **[3a]**, similar to compounds presented later in the chapter, showed selectivity for the tri-substituted compound in the Schiff base formation. No evidence of mono- or di-substitution was observed by NMR spectroscopy. Mono- or di-substitution would change the symmetry of the molecule, giving rise to a different NMR pattern, predominantly in the tach region. Mono-substitution and its consequences on the appearance of the NMR spectra are discussed further in section **2.7**.

Mass spectrometry generally showed the presence of mono- and di-armed derivatives for all of the compounds. **Figure 2.17** shows the MS of tachimpyr. The protonated molecule peak was observed in low abundance at *m/z* 397.2128, consistent with the

elemental composition of the molecule. The highest peak in the spectrum at *m/z* 308.1864 was assigned to the di-armed fragment. The mono- or di-armed species of the compounds were likely to have formed in the MS instrument rather than being impurities of the reaction, considering that no other evidence for them was observed and elemental analysis confirmed the purity of the compounds made.

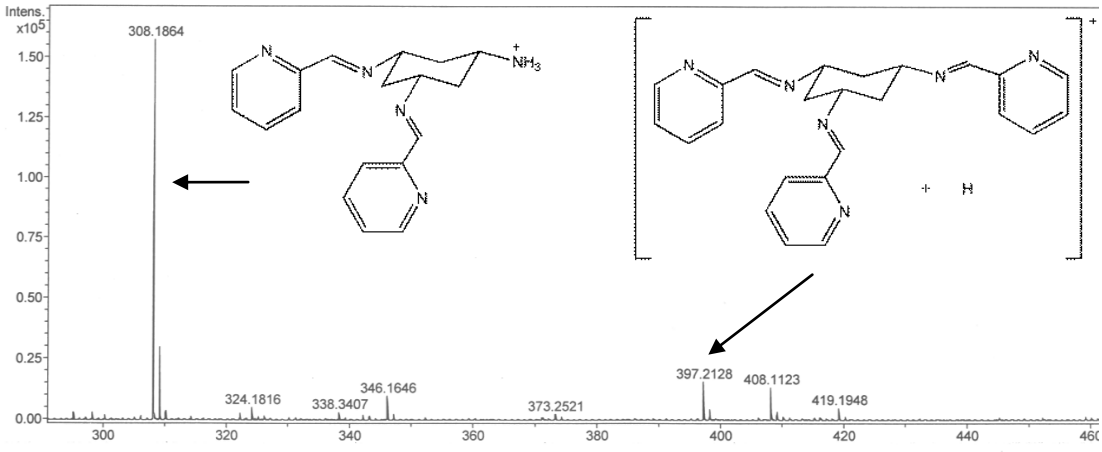

Figure 2.17: Positive mode high resolution ESI-MS of tachimpyr **[3a]**; *m/z* values reported on the x axis.

2.4.2 Tri-amines

The Schiff bases presented in section **2.4.1** were reduced with sodium borohydride to form the corresponding tri-amines (**Figure 2.18**).

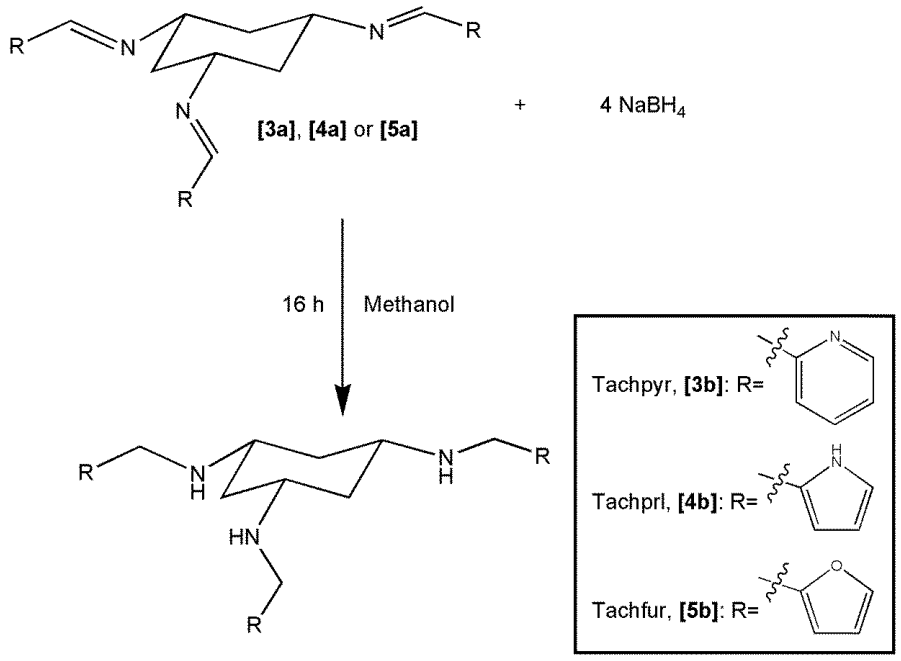

Figure 2.18: General synthetic scheme for the reduction of Schiff bases to tri-amines.

The reducing agent was slowly added to a solution of tri-imine in methanol and the mixture stirred for 16 h. Extraction with chloroform or dichloromethane gave the final tri-amine compounds in high yields (96, 94 and 97% for **[3b]**, **[4b]** and **[5b]**, respectively) and high purity, as confirmed by elemental analysis. ^{1}H NMR spectroscopy shows disappearance of the imine signal with the corresponding appearance of the methylene signal at 3.5-4 ppm, a clear indication of the success of the reduction. Similarly, ^{13}C and DEPT 135 NMR experiments show the signal of the amine carbon at 44-52 ppm. **Figure 2.19** shows the ^{1}H NMR of compound **[3b]** overlaid with the spectrum of the analogous Schiff base **[3a]**. After reduction, several changes in the ^{1}H NMR are present: the majority of the signals are shifted, the imine singlet at 8.48 ppm can no longer be observed, while a new signal at 3.80 ppm with a relative integration of six protons, which can be assigned to the CH_2 of the amine, dominates the spectrum.

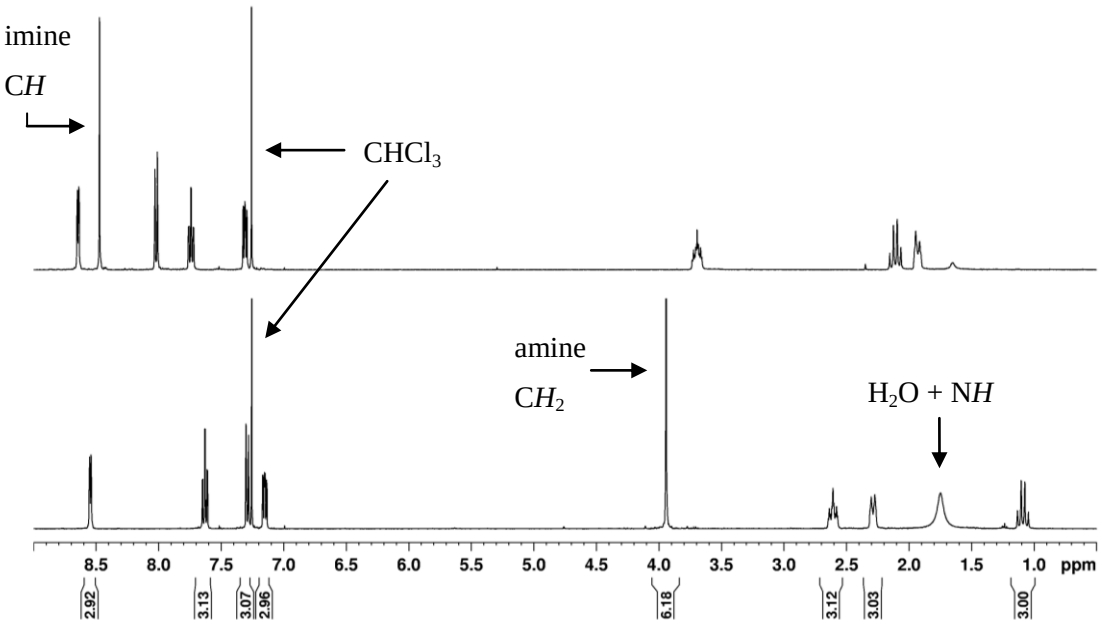

Figure 2.19: ^{1}H NMR spectra of tachimpyr **[3a]** (top) and tachpyr **[3b]** (bottom). Relative integration is shown for **[3b]**; spectra recorded in $CDCl_3$.

Full characterisation of the compounds was performed by NMR and MS, as explained for compound **[3a]** in section **2.4.1.1**. The amines were usually isolated as pure compounds, with no further purification needed. Tachpyr and tachfur were light yellow or bright orange oils, respectively, whilst tachprl was isolated as a cream coloured solid.

The ^{1}H NMR spectrum of compound **[4b]** shows the characteristic signal of the pyrrolyl proton at 8.99 ppm and COSY NMR (**Figure 2.20**) highlights the coupling between the pyrrolyl proton and all the other protons on the aromatic ring. This coupling is the cause of the fine structure of the aromatic protons, which appear as multiplets.

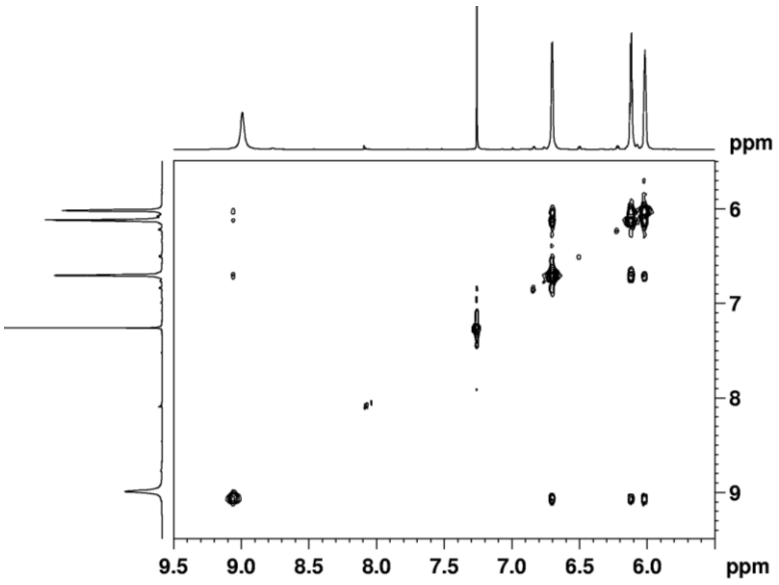

Figure 2.20: COSY NMR of tachprl **[4b]**, detail of the aromatic region; recorded in $CDCl_3$.

Compound **[4b]** was crystallised as fine needle-like crystals suitable for X-ray diffraction by slow evaporation of chloroform. The asymmetric unit, shown in **Figure 2.21**, contains two molecules of **[4b]** and three molecules of chloroform. The diagram of the crystal structures, as the other presented in this thesis, were done using Ortep3 software.[164]

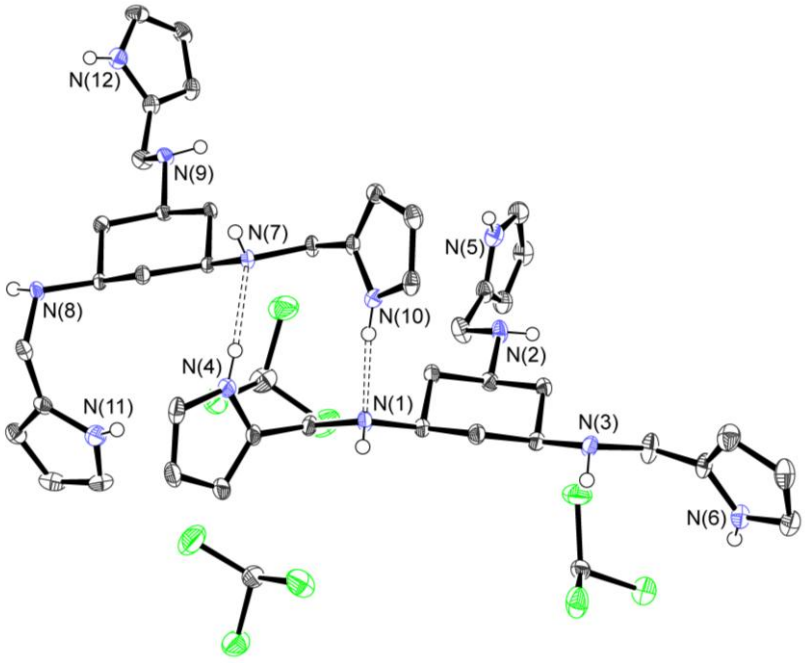

Figure 2.21: ORTEP diagram (thermal ellipsoids at 50% probability level) of tachprl **[4b]**. Hydrogen atoms omitted for clarity, except for hydrogens bound to heteroatoms.

An intermolecular hydrogen bond (defined as the non-covalent interaction between H and an atom carrying a full or partial negative charge)[165] network is present in the lattice of the crystal structure between amines and pyrrolyl moieties, with the pyrroles acting as hydrogen bond donors and the amines as hydrogen bond acceptors. All H-bonding hydrogen atoms were located by difference electron density maps. Hydrogen bond distances and angles are presented in **Table 2.1**.

D	H	A	d(D-H) / Å	d(H···A) / Å	d(D···A) / Å	D-H···A / °
N(4)	H(4)	N(7)	0.82(3)	2.14(3)	2.944(3)	166(3)
N(6)	H(6)	N(8)[1]	0.87(3)	2.09(3)	2.947(3)	169(3)
N(10)	H(10A)	N(1)	0.84(3)	2.09(3)	2.918(3)	174(3)

Table 2.1: Hydrogen bond lengths and angles in the crystal structure of tachprl **[4b]**. [1]Symmetry generated N(8), symmetry operator: -1+X,1+Y,+Z.

Table 2.1 contains also the hydrogen bond between N(6) and the symmetry generated N(8) contained in the next asymmetric unit, which is not shown in the ORTEP plot in **Figure 2.21**.

2.5 Synthesis and characterisation of salicylaldehyde derivatives

The synthesis of salicylaldehyde derivatives was based on the PhD thesis by E. Lewis.[166-167] The rationale for making this series of derivatives was to investigate the biological role of the heteroatom present on the compounds showed in section **2.4**. The hypotheses behind these structural modifications are described in further details in **Chapter 4**. Compounds **[3b]**, **[4b]** and **[5b]** have a heteroatom as part of the rings which compose the arms of the derivatives. The compounds described in this section were made using various salicylaldehyde derivatives, therefore the heteroatom was no longer part of the ring, but now substituent at the 2-position of the phenyl ring. An alternative would have been to use 2-aminobenzaldehyde, which has previously been used for the condensation with different amines,[168] instead of salicylaldehyde, in order to keep the nitrogen atoms as in tachpyr **[3b]**. However, salicylaldehyde derivatives

had proven to offer a facile synthesis with tach,[167] and so were well suited candidates for a preliminary investigation. Furthermore, as explained in detail in **Chapter 4**, the role of the oxygen atom was subjected to investigation in relation to the biological activity.

2.5.1 Schiff bases

The general scheme for the synthesis of these derivatives is shown in **Figure 2.22**.

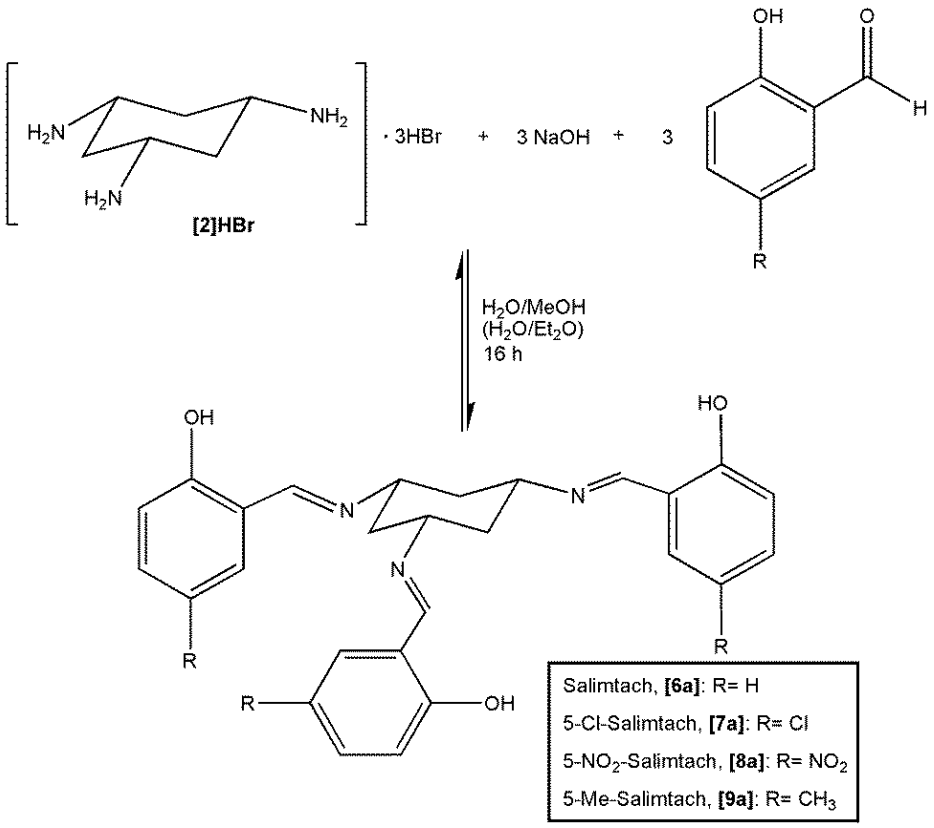

Figure 2.22: Synthetic scheme for salicyl tri-imine tach ligands.

The salicyl tri-imine tach (salimtach) ligands were readily synthesised from the condensation between tach·3HBr and the appropriate salicylaldehyde derivative either in a water/methanol mixture or as a bi-layer reaction in water/diethyl ether, allowing the ether to evaporate over a 16 h period. Usually a clear colour change from colourless to bright yellow was observed upon addition of the aldehyde. The tri-imine product precipitated from the water solution to give the desired compound in good to high yield (63-89%) and good purity. As for the heterocyclic Schiff-bases, the imine

group gave a characteristic signal at 8.5-9 ppm in the ^{1}H NMR and 163-165 ppm in the ^{13}C NMR. With the exception of salimtach, the other compounds of the series displayed the distinctive splitting pattern, shown in **Figure 2.23** for compound **[7a]**, due to 1,2,5-substitution on the phenyl ring.

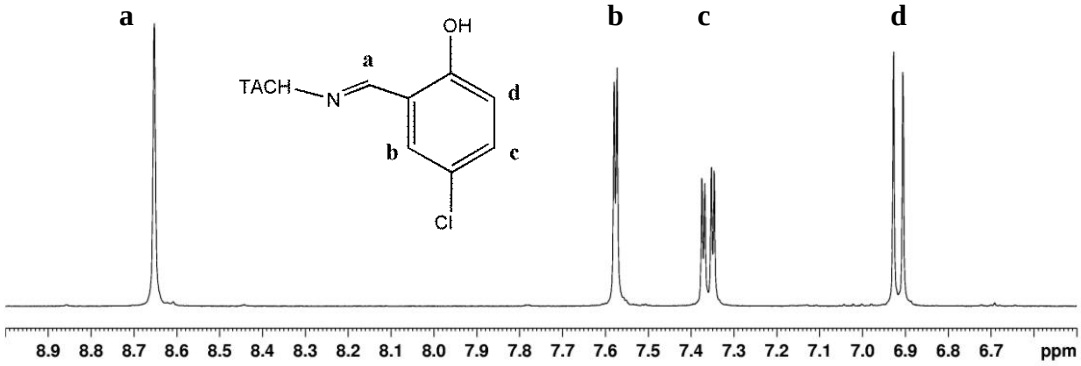

Figure 2.23: Aromatic region of ^{1}H NMR of 5-Cl-salimtach **[7a]**; recorded in d_6-DMSO.

The protons labelled as **b** appear as a doublet with a small ^{4}J coupling constant (2.8 Hz) with protons **c**. The signal from protons **c** is split by the large ^{3}J coupling with protons **d** (8.8 Hz) and the ^{4}J coupling with **b**, resulting in a doublet of doublets. Finally, protons **d** show the coupling with **c** only, appearing as a doublet.

Salimtach **[6a]** and 5-Me-salimtach **[9a]** were crystallised, respectively, from slow diffusion of ethanol layer into a chloroform solution of **[6a]** or slow diffusion of water layer into a DMSO solution of **[9a]**, producing single crystals suitable for X-ray diffraction. For compound **[6a]**, the bright yellow needle-like crystals were sent to the National Crystallography Service for data collection due to their very weak diffraction. The two structures are very similar, both showing an intramolecular hydrogen bond between the –OH on the aromatic rings and the imine nitrogen atoms. As an example, an ORTEP diagram of compound **[6a]** is presented in **Figure 2.24**, which shows such intramolecular hydrogen bonds. The H-bonding hydrogen atoms were located by difference electron density maps and lengths and angles of these hydrogen bonds are reported in **Table 2.2**.

D	H	A	d(D-H) / Å	d(H···A) / Å	d(D···A) / Å	D-H···A / °
O(1)	H(1A)	N(1)	1.01(4)	1.67(4)	2.580(3)	147(3)
O(2)	H(2)	N(2)	0.96(3)	1.72(3)	2.585(2)	149(3)
O(3)	H(3A)	N(3)	1.02(4)	1.69(4)	2.591(3)	145(3)

Table 2.2: Hydrogen bond lengths and angles of salimtach **[6a]**.

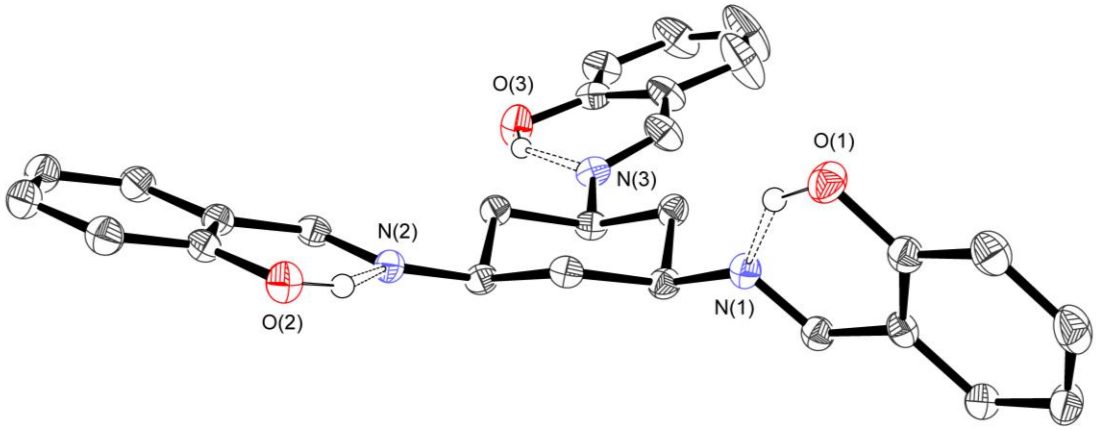

Figure 2.24: ORTEP diagram (thermal ellipsoids at 50% probability level) of salimtach **[6a]**. Hydrogen atoms omitted for clarity, except for oxygen-bound hydrogens.

It can be noticed that the hydrogen bonds observed in the crystal structures of the salimtach derivatives are much shorter than those found in the crystal structure of compound **[4b]**. This difference is likely to be due to the difference in the nature of the H-bond (intra- or intermolecular). Similarly, the angles of the bonds are restrained by the structure, resulting in a smaller value than that found in tachprl.

The intramolecular hydrogen bond can be observed in other crystal structures of Schiff bases derived from salicylaldehyde.[169-171]

2.5.2 Tri-amines

The Schiff bases **[6a]-[9a]** were reduced with sodium borohydride in methanol, either under reflux for 4 h or at ambient temperature for 16 h, to form the corresponding tri-amine tach ligands in good yields (63-92%), as shown in **Figure 2.25**.

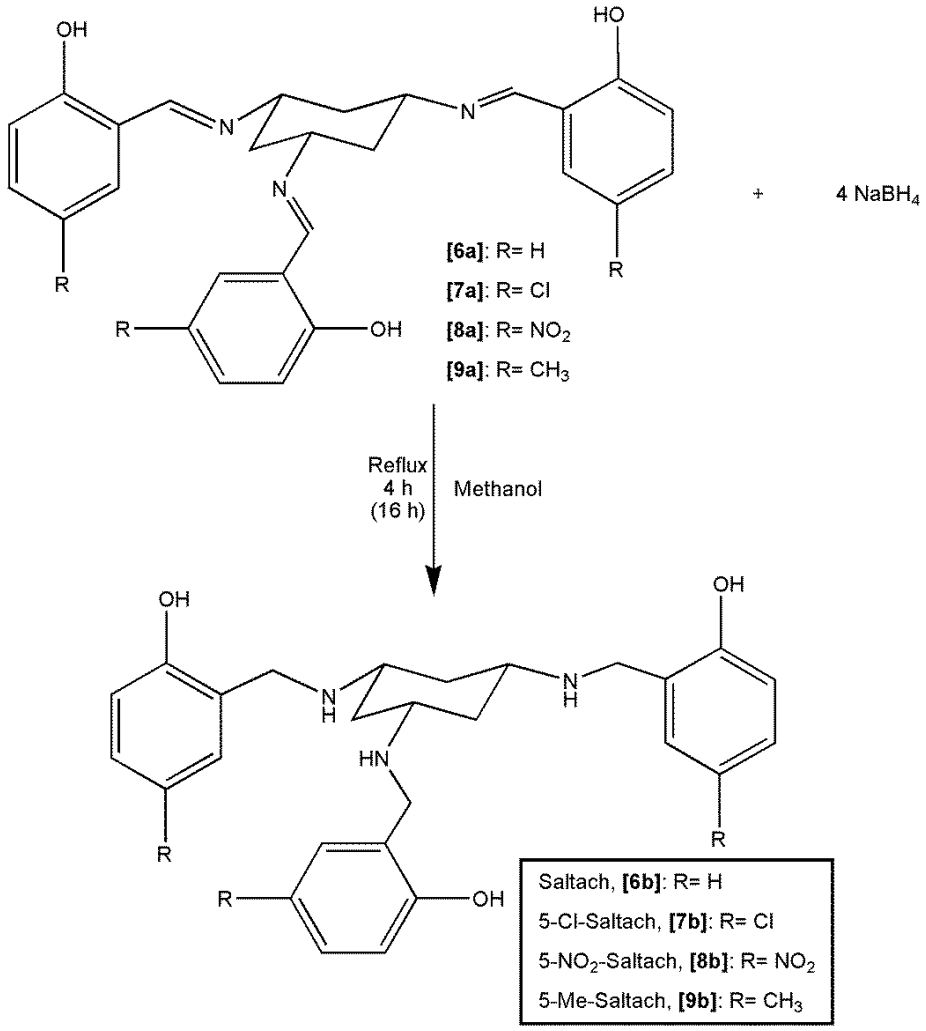

Figure 2.25: General synthetic scheme for saltach derivatives.

As for the heterocyclic tri-amines, the formation of the product was easily monitored by ^{1}H NMR, which showed the disappearance of the signal for the imine protons and the emergence of the C*H*$_2$ protons at 3.8-4.0 ppm as a sharp singlet.

Single crystals suitable for X-ray diffraction were obtained for compounds **[6b]**, **[7b]** and **[9b]** from slow diffusion of water into a concentrated DMSO solution of the salicylaldehyde derivative in an NMR tube. The crystals obtained were yellow or colourless fine needles.

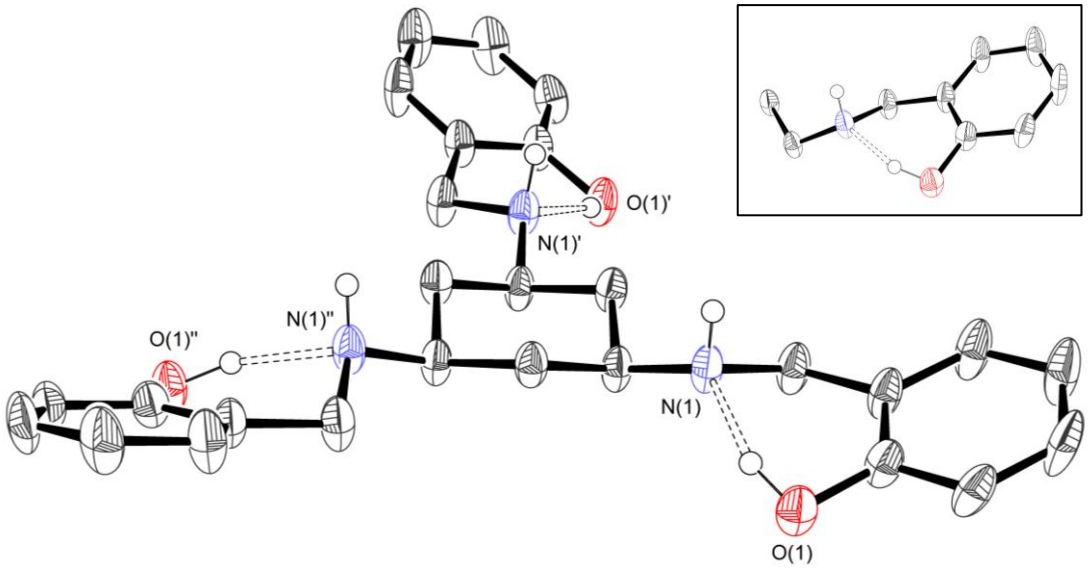

Figure 2.26: ORTEP diagram (thermal ellipsoids at 50% probability level) of saltach **[6b]**; in the box, the asymmetric unit of the crystal lattice. Hydrogen atoms omitted for clarity, except for hydrogen atoms bound to heteroatoms.

In the crystal lattice of **[6b]**, **[7b]** and **[9b]** the asymmetric unit is given by only one third of the whole molecule due to the three-fold axis present in the structure (space group for all three compounds is $P3_1c$). An ORTEP diagram of the crystal structure of **[6b]** and the asymmetric unit (in the box) are shown in **Figure 2.26**. The intramolecular hydrogen bond observed in the crystal structures of the imine derivatives **[6a]** and **[9a]** is still present in the reduced compounds, as shown for compound **[6b]**. Hydrogen bond distances and angles for saltach **[6b]** are presented in **Table 2.3**, the positions of the hydrogen atom was found by electron density difference maps.

D	H	A	d(D-H) / Å	d(H···A) / Å	d(D···A) / Å	D-H···A / °
O(1)	H(1)	N(1)	0.95(5)	1.73(5)	2.594(3)	155(4)

Table 2.3: Hydrogen bond lengths and angles of saltach **[6b]**.

All the compounds described so far in this section (**[6b]**-**[9b]**) showed very poor water solubility (cf. section **4.3.2**), probably due to the intramolecular hydrogen bond observed in the solid state and highlighted in **Figure 2.26**. In order to increase the water solubility, which is an important requirement for biological applications, 5-Cl-

saltach **[7b]** was added to a solution of approximately 3 equivalents of HCl in water to form the hydrochloride salt **[7b]HCl**. A clear downfield shift of all signals in the ^{1}H NMR spectrum was evident after protonation, and two broad signals integrating for 3 and 6 protons at very low field were observed. These were assigned to the phenol and ammonium protons respectively (**Figure 2.27**).

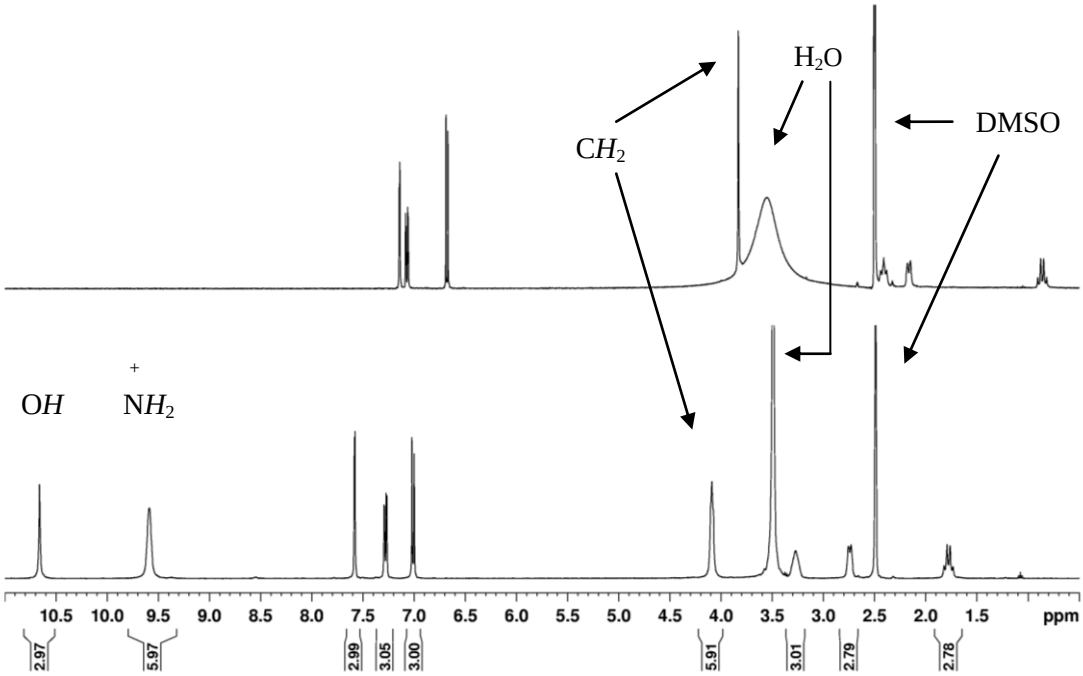

Figure 2.27: ^{1}H NMR spectra of compounds **[7b]** (top) and **[7b]HCl** (bottom); recorded in d_6-DMSO.

The effect of protonation of the amines is noticeable in the chemical shifts of the surrounding protons. The positive charge on the nitrogen atoms causes a greater electron withdrawing effect, with consequent downfield shifts of the tach and methylene protons. On the other hand, the phenol proton can no longer form a hydrogen bond with the nitrogen lone pair of electrons, hence decreasing the electron donating effect of the oxygen to the aromatic ring and causing a downfield shift of the aromatic protons compared to the neutral compound. Although the hydrochloride salt **[7b]HCl** showed excellent water solubility, it was very poorly soluble in buffer or cell culture medium (cf. section **4.3.2**). For this reason, no other attempts were made to synthesise salts of the amine ligands and the class of derivatives was not developed further.

2.6 Synthesis and characterisation of benzaldehyde derivatives

A further series of derivatives based on the benzaldehyde moiety was developed to investigate the biological role of the heteroatom on the tach arms of the compounds presented in section **2.4** and to understand if the electronic properties of the aromatic rings had an effect on the cytotoxicity of the ligands. The results of the biological tests for the compounds described in this chapter, together with some preliminary structure-activity relationships (SARs), are presented and analysed in **Chapter 4**.

2.6.1 Schiff bases

The unsubstituted benzaldehyde derivative tachimben **[10a]** was made by a modified version of the reported synthesis[172-173] and the general scheme is shown in **Figure 2.28**.

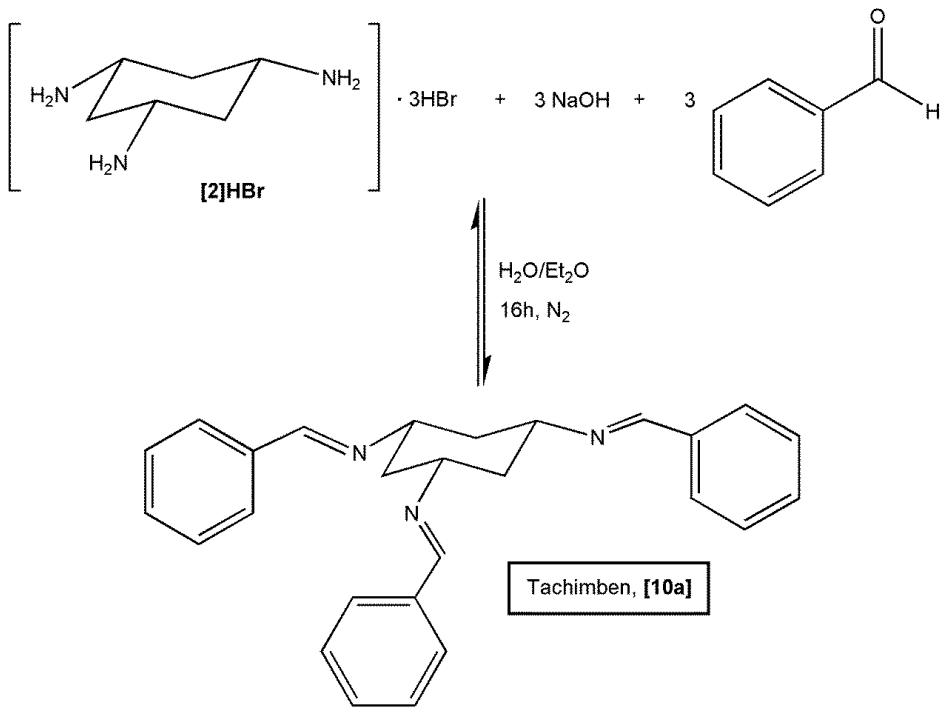

Figure 2.28: Synthetic scheme for tachimben **[10a]**.

Tach·3HBr was dissolved in water with 3 equivalents of sodium hydroxide and benzaldehyde was added as a solution in diethyl ether. The bi-layer reaction was vigorously stirred at room temperature for 16 h under a N_2 atmosphere. The layers

were then separated and extraction of the aqueous layer with diethyl ether afforded the desired Schiff base in a 71% yield. Traces of the aldehyde starting material were seen by ^{1}H NMR, and so the crude reaction mixture was purified by re-crystallisation at 4 °C from diethyl ether/hexane to give white fine needles. Unfortunately the crystals, although single, were too small for X-ray diffraction and gave very weak diffraction, so a crystal structure of this compound could not be obtained.

The synthetic route used for tachimben **[10a]** proved to be unsuitable when a substituent was present on the aromatic ring. A new general procedure was developed, with adaptations made for the different 4-substituted aldehydes according to the substituent. The final isolated yields were usually good and ranged between 65% and 93%. 4-NMe_2-, 4-OMe- and 4-CF_3-tachimben derivatives, **[11a]**, **[12a]** and **[15a]** respectively, were synthesised by leaving the reaction mixture under reflux for 16 h in methanol or ethanol. The synthesis of compound **[15a]** was carried out under nitrogen to minimise oxidation of the aldehyde to the corresponding carboxylic acid. The 4-Br- and 4-F-tachimben derivatives were synthesised in methanol, but reflux was not necessary to obtain good yields and the reactions were therefore performed at room temperature. The general synthetic scheme is reported in **Figure 2.29**.

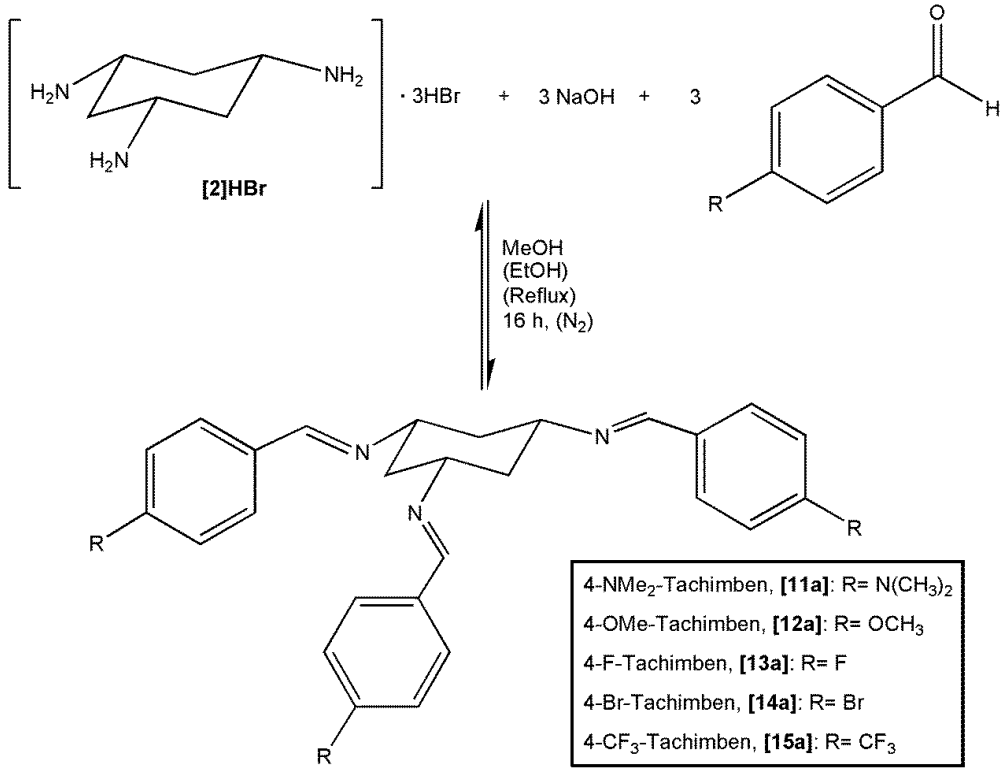

Figure 2.29: General synthetic scheme of 4-substituted tachimben derivatives.

The products were isolated adding diethyl ether or chloroform to the mixture after evaporation of the reaction solvent. This addition caused the precipitation of unreacted tach and NaBr salt, which could be removed by filtration. Evaporation of the solvent yielded the Schiff base derivative. The only exception to this general procedure was 4-Br-tachimben **[14a]**, because this derivate precipitated from the methanol solution and was therefore isolated as pure compound by vacuum filtration. When aldehyde was still present in the crude of the reaction, the Schiff base derivatives were washed with the appropriate solvent or re-crystallised. Due to stability problems, the Schiff bases were often used for the reduction step without further purification from the aldehyde starting material, as discussed in more detail in section **2.6.2**. Similarly to the other Schiff bases described in previous sections, the benzaldehyde derivatives showed the typical ^{1}H NMR splitting pattern of the tach moiety and the imine signal between 8.2 and 8.5 ppm, in agreement with what has been reported for related molecules.[174] The yields of the Schiff base condensation for the benzaldehyde derivatives were usually very good, ranging between 65 and 93%. When the imine was not purified from the

aldehyde, the yield was calculated with respect to the equivalents of aldehyde visible in the ^{1}H NMR spectrum relative to the Schiff base.

The electronic properties of the aromatic rings in compounds **[10a]-[15a]** are affected by the different substituents in the 4-position. Although not with a strong correlation, these trends can be seen by NMR spectroscopy, as shown in **Figure 2.30**.

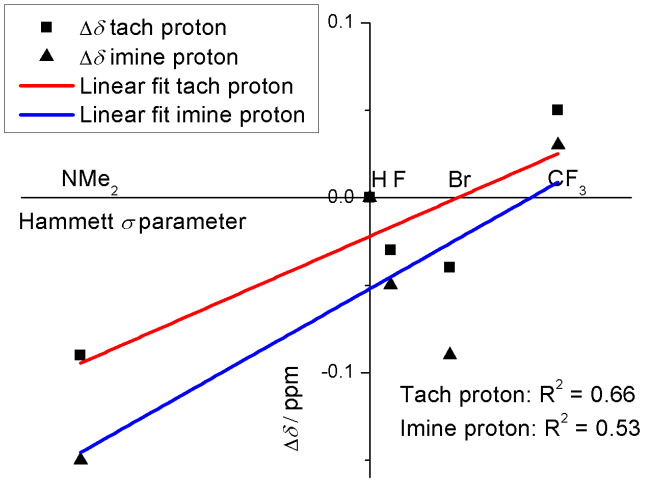

Figure 2.30: Plot of difference chemical shift ($\Delta\delta = \delta_{subst} - \delta_{H}$) against Hammett σ parameter for compounds **[10a]-[15a]**. Points represent single measurements.

Plotting the difference of chemical shift between the substituted compound and compound **[10a]** ($\Delta\delta$) against the σ Hammett parameter, a trend can be seen for both the tach C*H* and the imine protons, although with a non-perfect fit. The imine signal shows a downfield shift of 0.18 ppm going from the electron-donating NMe_2 to the electron-withdrawing CF_3 compound. The partial trend can still be observed in the tach C*H* proton, quite far away from the aromatic ring, with a $\Delta\delta$ of 0.14 ppm. The ^{13}C NMR of the imine signal, instead, does not seem to be affected by the substituent on the ring, with no real trend present. The values of chemical shift for the tach CH proton (C*H*-N), the imine proton (N=C*H*) and the imine carbon (N=*C*H) for compounds **[10a]-[15a]** are reported in **Table 2.4**. The unsubstituted compound is a slight outlier in the series when the derivatives are listed in order of increasing Hammett parameter,[175] but the reasons for this are not really clear. 4-OMe-tachben **[12a]** was not included in the analysis of the trend because the spectra could not be run in chloroform due to solubility issues.

Compound	*σ*-para	C*H*-N	N=C*H*	N=*C*H
[11a], NMe_2	-0.83	3.50	8.24	159.2
[10a], H	0.00	3.59	8.39	159.6
[13a], F	0.06	3.56	8.34	158.1
[14a], Br	0.23	3.55	8.30	158.4
[15a], CF3	0.54	3.64	8.42	158.3

Table 2.4: ^{1}H and ^{13}C chemical shift on the Schiff base series, compounds in increasing order of Hammett σ parameter. All spectra run in $CDCl_3$.

Single crystals suitable for X-ray diffraction were obtained for compounds **[11a]** and **[15a]**, which are shown in **Figure 2.31**.

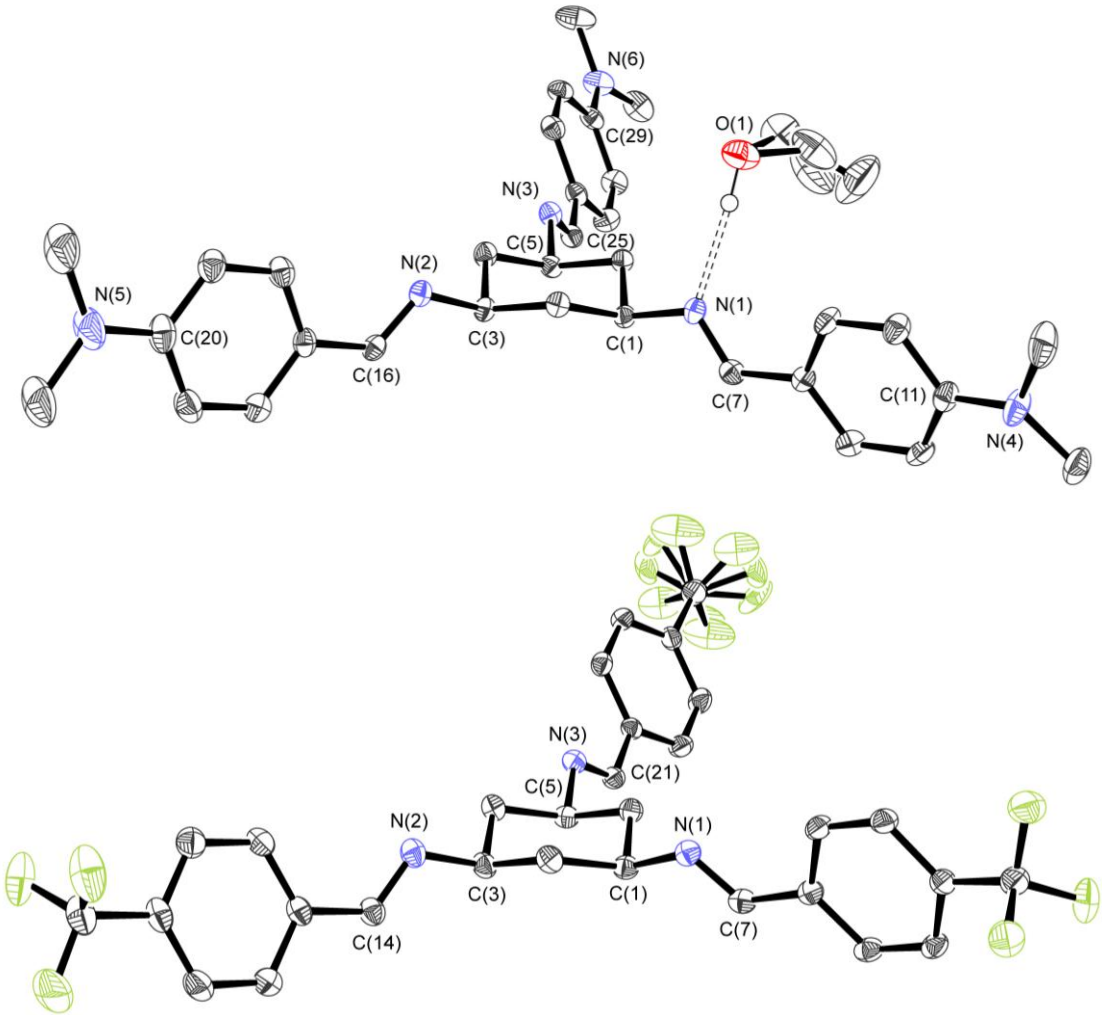

Figure 2.31: ORTEP diagram (thermal ellipsoids at 50% probability level) of compounds **[11a]** (top) and **[15a]** (bottom). Hydrogen atoms omitted for clarity, except EtOH hydrogen.

The crystal structure of 4-NMe_2-tachimben **[11a]** shows one of the imine nitrogen atoms, N(1), engaged in a hydrogen bond with an ethanol molecule, disordered over two positions. 4-CF_3-tachimben **[15a]** presents some disorder of one of the CF_3 groups, which was modelled over 3 positions. Selected bond lengths and angles are reported in **Table 2.5**. Ebrahimpour *et al.* reported the crystal structures of three tach-benzaldehyde molecules: 2,6-$(OMe)_2$-, 2-CF_3- and 2-OMe- derivatives.[174] The imine bond lengths reported for these compounds range between 1.267(2) and 1.272(2) Å,[174] in agreement with those observed in compounds **[11a]** and **[15a]**.

[11a]·EtOH		**[15a]**	
C(7)-N(1)	1.276(2)	C(7)-N(1)	1.266(2)
C(16)-N(2)	1.265(2)	C(14)-N(2)	1.268(2)
C(25)-N(3)	1.264(2)	C(21)-N(3)	1.265(2)
C(1)-N(1)	1.462(2)		
C(3)-N(2)	1.465(2)		
C(5)-N(3)	1.464(2)		
C(11)-N(4)	1.376(3)		
C(20)-N(5)	1.370(3)		
C(29)-N(6)	1.366(2)		
C(7)-N(1)-C(1)	116.94(16)	C(7)-N(1)-C(1)	118.35(15)
C(16)-N(2)-C(3)	117.10(17)	C(14)-N(2)-C(3)	116.44(16)
C(25)-N(3)-C(5)	115.68(17)	C(21)-N(3)-C(5)	115.69(15)

Table 2.5: Selected bond lengths (Å) and angles (°) for compounds **[11a]** and **[15a]**.

The hydrogen bond of N(1) with the molecule of ethanol in the crystal lattice of compound **[11a]** causes an increase in the bond length of the N(1)-C(7) bond, which is slightly longer than the other imine bonds. Furthermore, the bond lengths between

N(4), N(5) and N(6) and the carbons they are bound to on the aromatic rings, C(11), C(20) and C(29) respectively, are approximately 0.1 Å shorter than a pure single bond (e.g. tach-nitrogen bond C(1)-N(1)) and 0.1 Å longer than a pure double bond (e.g. the imine bond C(7)-N(1)). This demonstrates the effect of the resonance of the electron donating group NMe_2 with the aromatic ring, with the C-N bonds displaying partial double bond character.

2.6.2 Tri-amines

The Schiff bases **[10a]-[15a]** were then reduced with sodium borohydride to give the corresponding tri-amines, as shown in **Figure 2.32**.

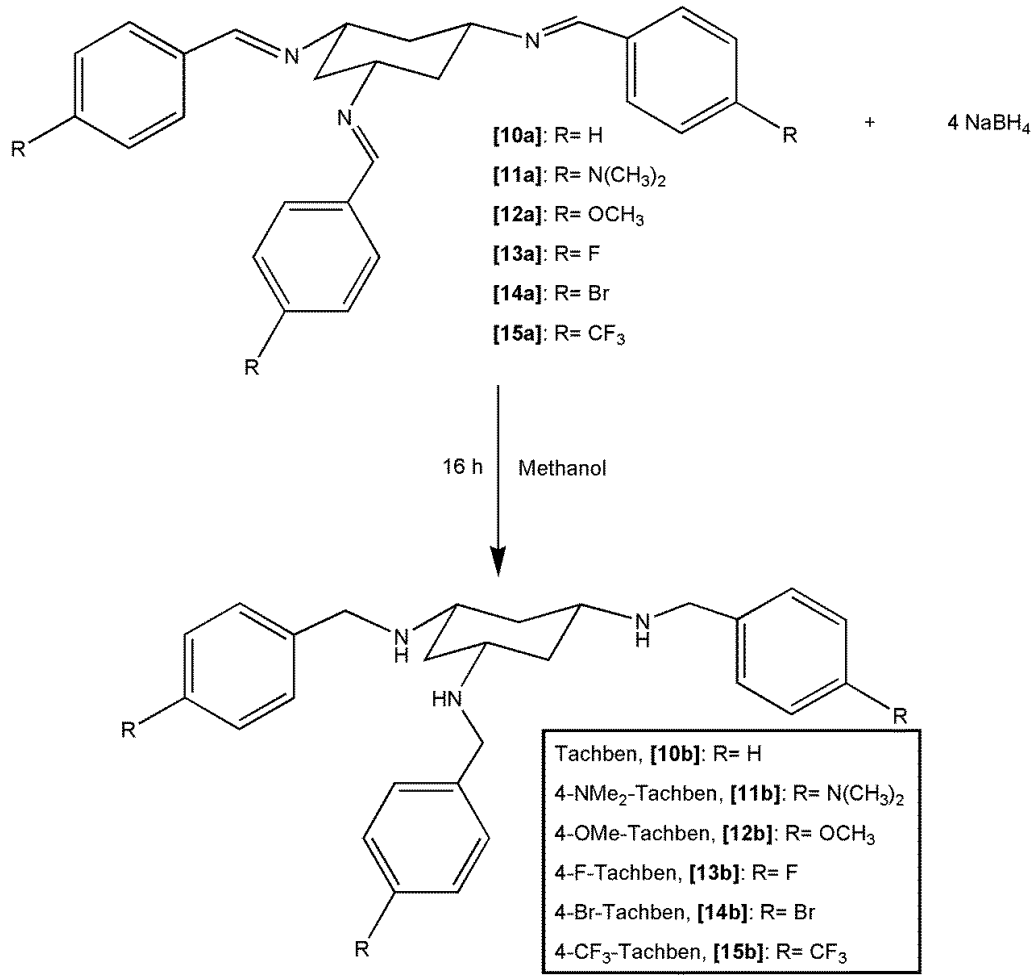

Figure 2.32: General synthetic scheme of tachben derivatives.

In some cases, the crude reaction mixture from the Schiff base reaction was used for the reduction step without purification and the benzyl alcohol derived from the reduction of the aldehyde starting material was separated from the desired tri-amine product. After the standard work-up of the reduction step, which involves extraction of the product and evaporation of the solvent, the residue was dissolved in 0.1 M HCl solution and washed with diethyl ether to remove the benzyl alcohol. Change of pH to basic (pH = 12-14) with NaOH and extraction with dichloromethane allowed for isolation of the final tri-amine in good yields (63-98%). This purification method was usually preferred to the purification of the Schiff base due to better stability of the tri-amine compared to the tri-imine. Furthermore, for the compounds presented, the purification of the Schiff bases was often challenging, with the low stability of the imines to different pHs and water restricting the range of possible purification methods. Moreover, not all the different tri-imines could be easily crystallised. The process led to lower yields and sometimes the resulting tri-amine still needed an acid/base wash after the reduction to be isolated as pure compound. For all these reasons, when the purification of the Schiff base could not be achieved in a straightforward way, they were considered as a "reaction intermediate" and used directly for the reduction, while the tri-amines underwent an extra wash to eliminate all the impurities. Elemental analysis confirmed the purity of the final compounds.

The tri-amines were fully characterised by MS and NMR and purity confirmed by elemental analysis. Compounds **[13b]** and **[15b]**, as their precursors **[13a]** and **[15a]**, were characterised also by ^{19}F NMR spectroscopy. The presence of fluorine (^{19}F I=½, 100% abundance) gave a characteristic splitting pattern in both ^{1}H and ^{13}C NMR spectra. As an example, the ^{13}C spectrum of 4-F-tachben is shown in **Figure 2.33**.

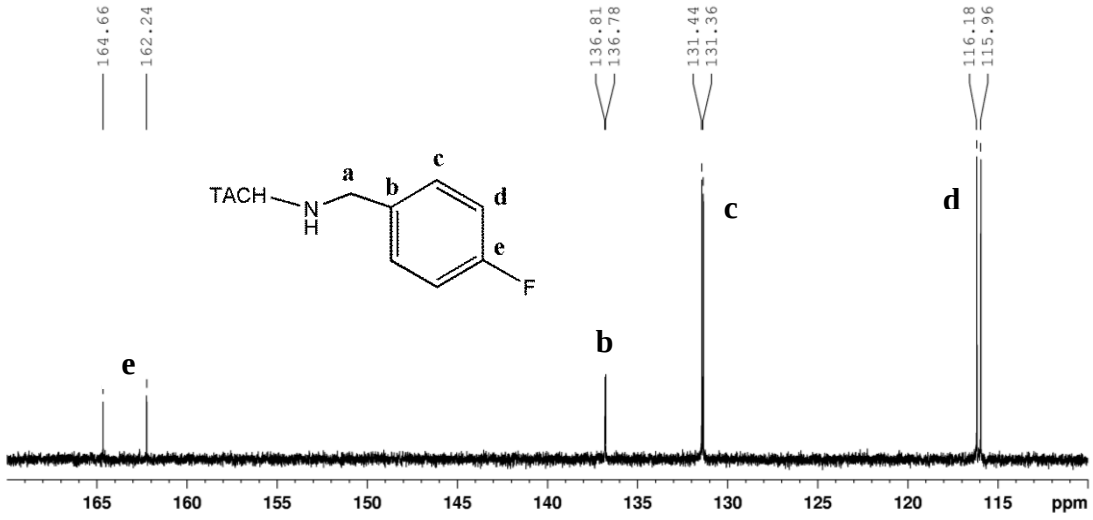

Figure 2.33: Detail of the aromatic region of the ^{13}C NMR spectrum of 4-F-tachben [14b], recorded in d_4-MeOH.

All signals in the aromatic region appear as doublets due to the coupling with fluorine. The quaternary carbon bound to the fluorine is, as expected, the most deshielded due to the *–I* effect of the halogen atom. Assignment of the signals was completed using the $J_{C\text{-}F}$ coupling constants, which decrease from 243.6 Hz for the ^1J with carbon **e** to 3.1 Hz for the ^4J with carbon **b** in relation to the number of bonds dividing carbon and fluorine. All C-F coupling constants for compounds **[13a-b]** and **[15a-b]** were compared to literature values and found in good agreement with the reported ranges.[176]

Similar to the ^{13}C spectrum, the effect of coupling between the aromatic protons and the fluorine is displayed in the ^{1}H NMR spectrum of compound **[13b]**, as shown in **Figure 2.34**.

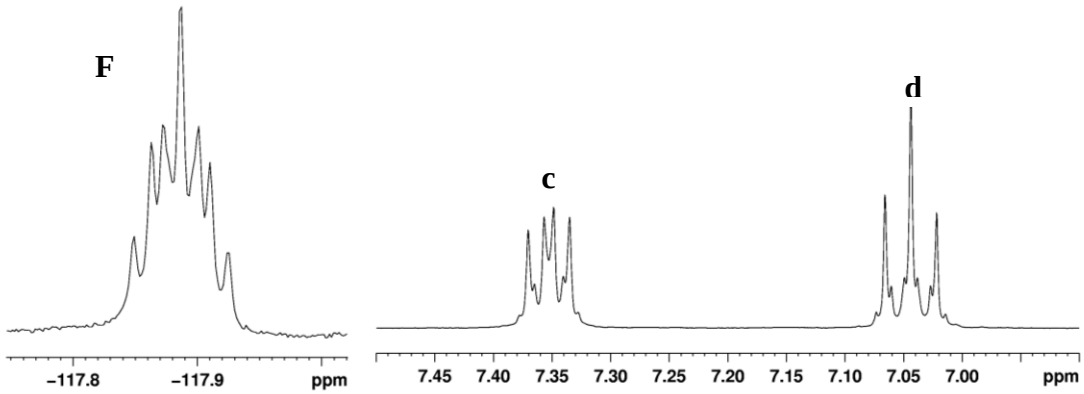

Figure 2.34: ^{19}F (left) and ^{1}H (right) NMR spectra of compound **[13b]**, recorded in d_4-MeOH.

The ^{1}H NMR of compound **[13b]** shows the characteristic fine splitting of a AA'BB' system,[177] due to the magnetic inequivalence of the two **c** protons and the two **d** protons (which should be labelled as **c**/**c'** and **d**/**d'**). The small inside lines visible in the spectrum are the result of this inequivalence and are due to the coupling between all four kind of protons. If approximated to a simple AB system, the spitting pattern observed in both ^{19}F and ^{1}H spectra can be explained as follows. The protons labelled as **d**, in ortho position to the fluorine, appear as a triplet, due to the *J* coupling to both proton **c** and fluorine which are similar in value (8.4 Hz). Protons **c**, instead, are a doublet of doublets due to a larger $^{3}J_{H\text{-}H}$ coupling of 8.4 Hz with **d** (in the range of 7-10 Hz, typical $^{3}J_{ortho}$ coupling[162]), and a smaller $^{4}J_{H\text{-}F}$ coupling of 5.2 Hz with fluorine. The same coupling constant values, which are in agreement with literature values,[177] are observed in the ^{19}F spectrum to give a triplet of triplets. The multiplicity of the fluorine signal is not a classic triplet of triplets, although its shape can be rationalised as explained in the diagram below.

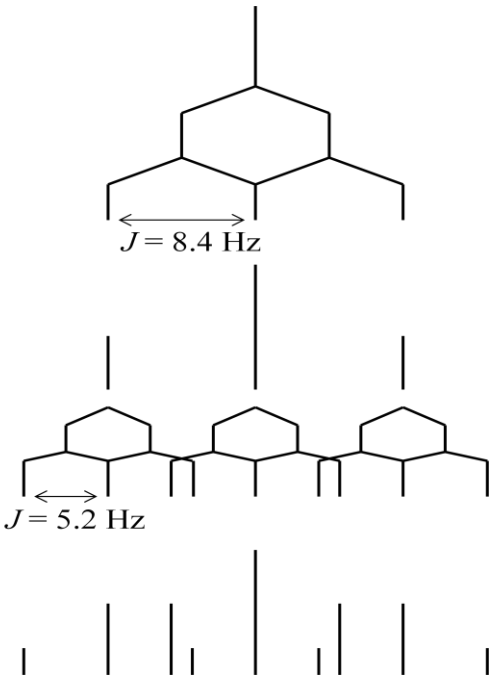

In 4-F-tachben, the fluorine signal is split by the two protons in the ortho position first, protons **d**, with a coupling constant of 8.4 Hz, giving the first set of triplets. Each signal is then split by the two protons in the *meta* position to the fluorine, protons **c**, *J* = 5.2 Hz, to form the triplet of triplets. However, due to the value of the coupling constants, the signals in the centre of the multiplet are very close to each other, so that the signal in ^{19}F NMR spectrum gains the shape shown in **Figure 2.34**.

As for the Schiff bases, a chemical shift trend is visible in ^{1}H NMR spectra in relation to the electronic properties of the substituent in the 4-position of the aromatic ring, whilst the ^{13}C signals are not affected. A 0.21 ppm downfield shift is evident moving from the electron donating NMe_2 to the electron withdrawing CF_3 derivative. The effect on the tach proton C*H*-NH is now negligible (0.05 ppm), although the shift follows the same trend. **Figure 2.35** and **Table 2.6** highlight these trends for the signals close to the nitrogen atoms.

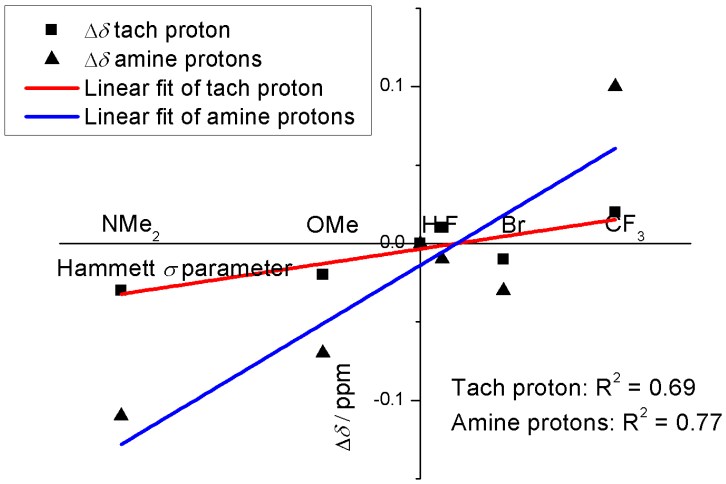

Figure 2.35: Plot of difference chemical shift ($\Delta\delta = \delta_{subst} - \delta_H$) against Hammett σ parameter for compounds **[10b]-[15b]**.

Compound	σ-para	C*H*-NH	NH-CH_2	NH-CH_2
[11b], NMe_2	-0.83	2.44	3.67	50.8
[12b], OMe	-0.27	2.45	3.71	50.7
[10b], H	0.00	2.47	3.78	51.4
[13b], F	0.06	2.48	3.77	50.6
[14b], Br	0.23	2.46	3.75	50.7
[15b], CF_3	0.54	2.49	3.88	50.9

Table 2.6: ^{1}H and ^{13}C chemical shift on the tri-amine series, compounds in increasing order of Hammett σ parameter. All spectra run in d_4-MeOH.

2.7 Mono-armed ligands

All the ligands presented so far in the chapter have the same substituent on the three tach amines. The synthesis of mono-substituted tach compounds was investigated with the idea of understanding the importance of the arms for the biological activity. Furthermore, having a reliable synthetic method to make "mono-armed" derivatives

would open to the possibility of adding different substituents on the three tach amines, with widening of the possible pharmacological applications.

Two mono-armed compounds were investigated: the mono-benzyl and the mono-cyclohexylmethyl derivatives, shown in **Figure 2.36**. These two compounds were chosen for different reasons: compound **[16]**, tachmonoben, allows a direct comparison with the corresponding three-armed derivative tachben **[10b]** in terms of biological activity. On the other hand, compound **[17]**, tachmonocyc, can give insights on the biological role of the aromatic ring, to evaluate if aromaticity is an essential requirement for activity. The results of the biological tests are presented in **Chapter 4**. The two mono-armed ligands were synthesised in two different ways: tachmonoben from modification of reported literature procedures,[166, 178] tachmonocyc through a Boc-protection route.

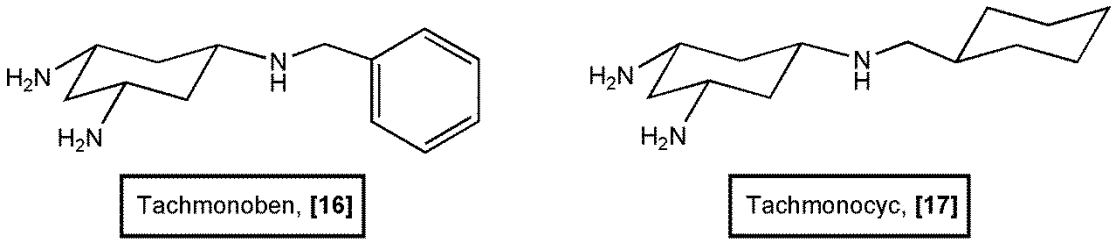

Figure 2.36: Tachmonoben **[16]** (left) and tachmonocyc **[17]** (right).

2.7.1 Tachmonoben

Tachmonoben **[16]** was synthesised following the reported literature procedures. Greener *et al.* reported the selective hydrolysis of tach derivatives upon complexation with copper[172] and Archibald *et al.* used nickel nitrate to synthesise mono-substituted tach derivatives.[166, 178]

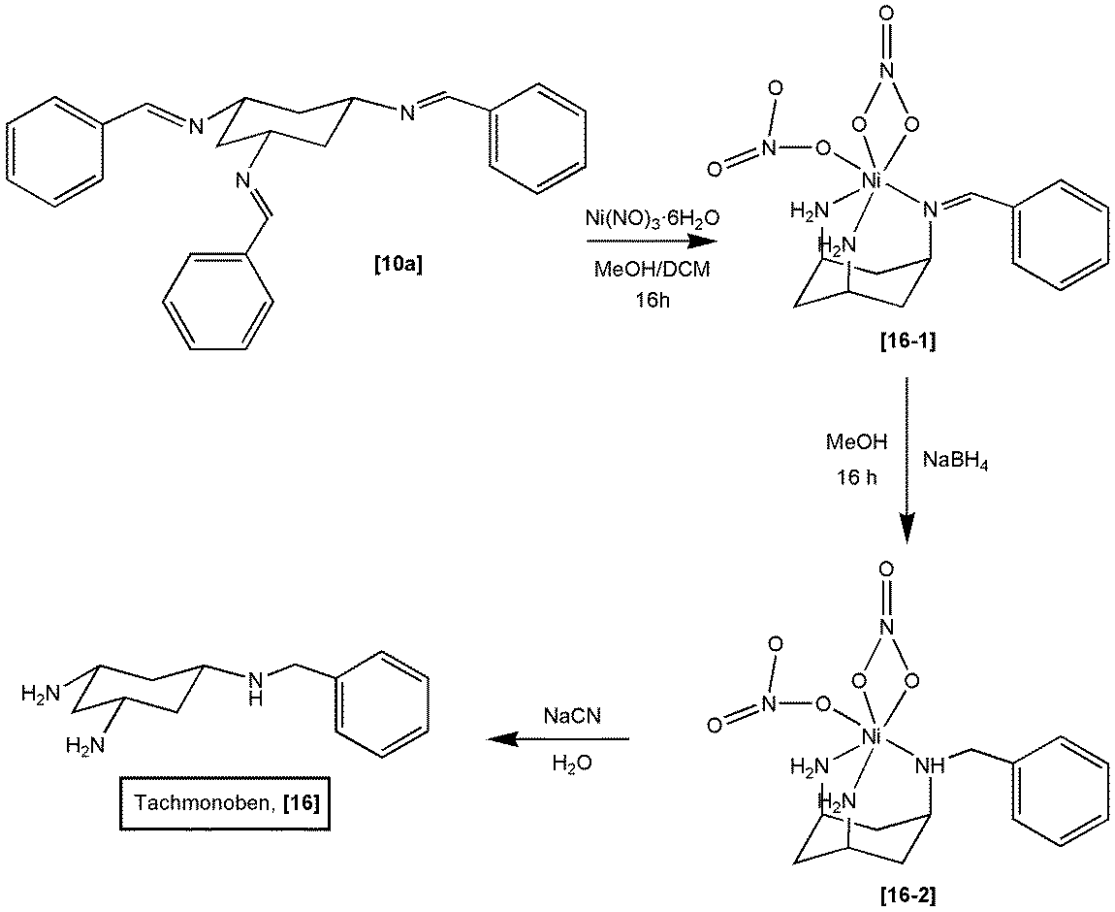

Figure 2.37: Synthetic scheme of tachmonoben **[16]**.

The reaction scheme for the synthesis of tachmonoben **[16]** is shown in **Figure 2.37**. The three-armed tachimben **[10a]** was synthesised as described in section **2.6.1** and added to one equivalent of nickel nitrate hexahydrate in a 2:1 methanol/dichloromethane mixture. Complexation with nickel selectively hydrolyses two of the three arms,[178] resulting in the Ni(II)-mono-substituted-tach complex. Diethyl ether was added to the reaction mixture to help precipitation and compound **[16-1]** was isolated by filtration as a bright turquoise powder in 68% yield. The complex was then suspended in MeOH and sodium borohydride added to reduce the imine bond and form compound **[16-2]**, which was used for the demetallation step without being isolated. Sodium cyanide was added to the reaction mixture to remove the nickel and the free ligand was isolated as a colourless oil. Although the metal hydrolysis gave very good yields, the reduction/demetallation step was very low yielding (7%) and the final product could not be isolated as pure compound. Several purification methods were attempted, but with little success.

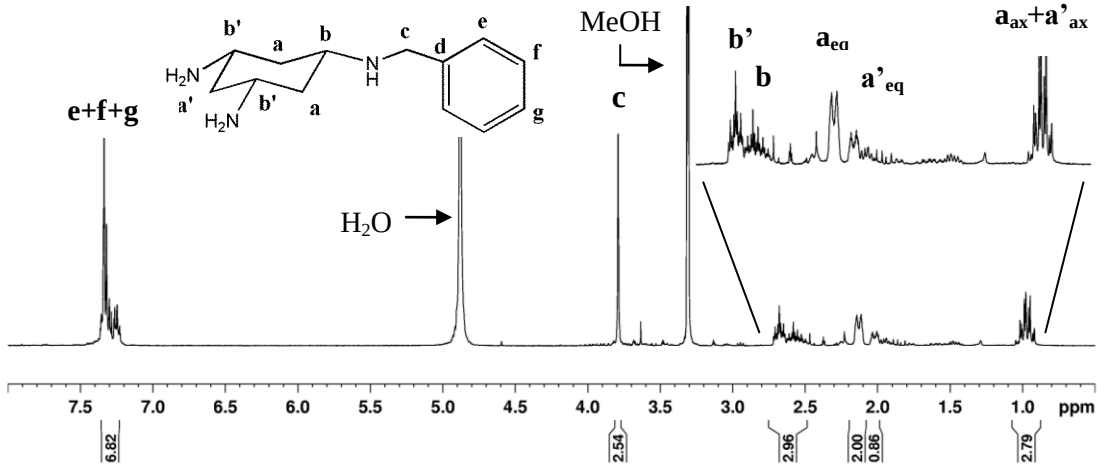

Figure 2.38: ^{1}H NMR spectrum of tachmonoben **[16]** with relative integration of the signals, recorded in d_4-MeOH.

The ^{1}H NMR of the impure tachmonoben is shown in **Figure 2.38**. It is immediately possible to notice the difference in the characteristic tach signals in comparison to the ligands described so far. Mono-substitution of the tach moiety causes the lost of the C_3 symmetry shown by the fully substituted compounds. Tachmonoben, as tachmonocyc described in the next section, presents instead a mirror plane containing the arm. For this reason, two sets of signals for each of the tach protons are evident in the NMR, one for the protons contained in the mirror plane and one for the others. Similarly, ^{13}C NMR shows five signals in the aliphatic region of the spectrum: one for the benzyl carbon and four belonging to the tach moiety. Although promising for the possibility of forming mono-substituted benzaldehyde derivatives, this synthetic method proved to be unreliable and low yielding for the unsubstituted benzaldehyde. Furthermore, the final product could not be obtained as a pure compound, as also evident by ^{1}H NMR spectrum in **Figure 2.38**. The integration of the tach protons is very close to what expected, but the aromatic and the CH_2 signals, which should integrate for five and two protons, respectively, show instead a higher value of relative integration, suggesting the presence of impurities. Further minor unidentified impurities are clear in the aliphatic region of the spectrum.

2.7.2 Tachmonocyc

Due to the difficulties experienced in the synthesis of **[16]** and the high toxicity of the reagents used (i.e. nickel and cyanide), a different strategy was developed for the synthesis of tachmonocyc **[17]**, as shown in **Figure 2.39** and **Figure 2.40**.

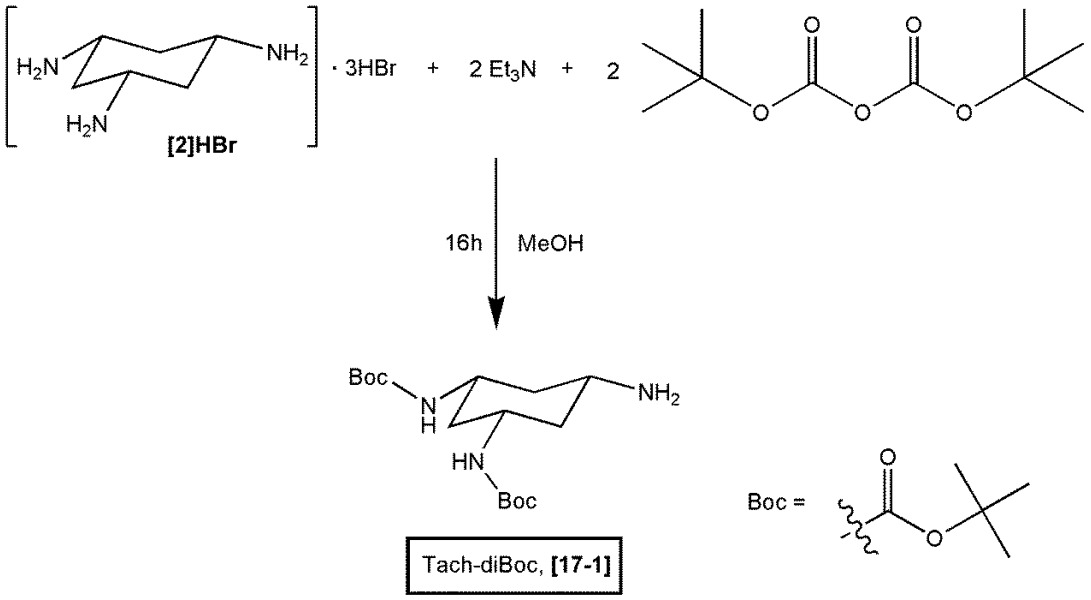

Figure 2.39: Synthetic scheme for Boc-protection of tach·3HBr.

The first step of the synthesis of compound **[17]** was the protection of two out of three tach nitrogens with di-*tert*-butyl dicarbonate (Boc anhydride, Boc_2O), as presented in **Figure 2.39**. Boc is widely used in organic synthesis as a protecting group for amines due to its low cost, the relatively good stability and the facility of the deprotection step in acidic conditions.[179] Tach·3HBr was dissolved in methanol and two equivalents of triethylamine were added to the solution. A dilute solution of Boc anhydride in methanol was slowly added dropwise over a 16 h period to the dilute solution of tach. The addition was very slow to minimise as much as possible the possibility of forming the tri-protected tach. The solvent was then evaporated and the residue was dissolved with basic water (pH = 10) and ethyl acetate. Using this method, the protected product was extracted into the organic layer, while unreacted tach and triethylamine were left in the aqueous layer. The procedure afforded the di-protected product tach-diBoc **[17-1]** as a bright white solid in good yield (75%). The splitting pattern of the tach region and the relative integration of the signals in the ^1H NMR showed complete selectivity

for the di-Boc product, although a small peak of protonated tri-Boc derivative was usually present in the positive mode high resolution ESI-MS at *m/z* 430.2900. However, the presence of tri-protected tach is not to be considered an issue for the synthesis because the tri-Boc tach would not subsequently react with the aldehyde and, in the deprotection step, the Boc group would be hydrolised releasing free tach, which could be easily separated from the product with a simple extraction in the appropriate conditions. On the other hand, there is no evidence of mono-Boc tach, which instead would represent a problem, in either NMR or ESI-MS. Having a synthetic method to protect only one or two tach amines is a great advantage for the synthesis of tach derivatives with different functionalities on the amines.

Tach-diBoc **[17-1]** was used for the condensation with cyclohexanecarboxaldehyde as shown in **Figure 2.40**. The synthetic procedure used reductive amination of the tach amine and was based on modifications of the synthesis of related compounds reported in the literature.[180] One equivalent of aldehyde was added to compound **[17-1]** and the mixture was stirred at room temperature for 24 h, after which sodium borohydride was added in portion to reduce the imine bond formed. The presence of the Schiff base was monitored by ESI-MS on small aliquots of the reaction mixture. Compound **[17-2]** could be isolated as a white solid, but the yields of the reaction were usually low and the NMR showed presence of cyclohexylmethanol, derived from the reduction of unreacted aldehyde. The lability of Boc to acid conditions made the purification of compound **[17-2]** very difficult, hence it was used for the hydrolysis without further purification.

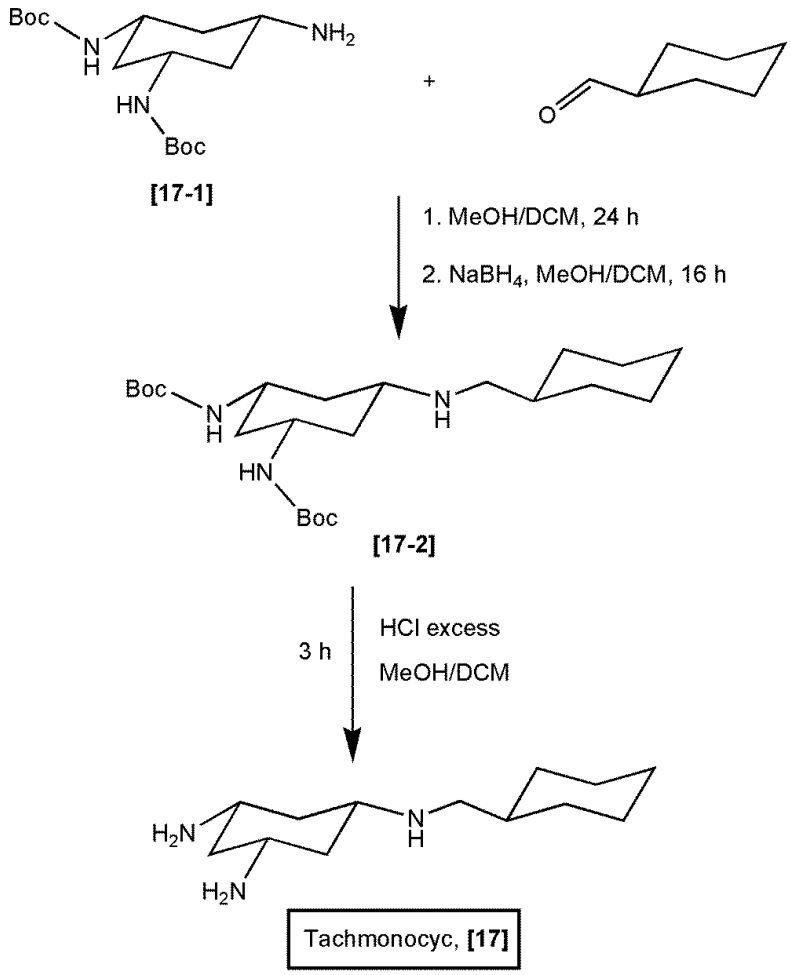

Figure 2.40: Synthetic scheme of tachmonocyc **[17]**.

Trifluoroacetic acid (TFA) is usually the preferred choice for Boc hydrolysis,[181] but when used on compound **[17-2]** problems were encountered. Although the amines were successfully deprotected, compound **[17]** could not be isolated in high purity and a signal in the ^{19}F NMR was observed, showing the presence of TFA tightly bound to the compound, although the compound had been extracted with organic solvent from a very basic water solution. For these reasons, the hydrolysis was performed using HCl, which overcame these problems. The final yield for **[17]** were usually very low (8%), making the purification and characterisation of tachmonocyc very difficult. ESI-MS showed evidence for the protonated molecule at *m/z* 266.2273, in agreement with the expected elemental composition, and no peaks for the di-armed compound where present. Furthermore, ^{1}H NMR showed the characteristic mono-substitution pattern seen in compound **[16]** with the correct integration of the protons. The presence of the cyclohexylmethyl substituent makes the aliphatic region of the spectrum very difficult

to assign, as shown in **Figure 2.41**, although the main tach signals and the doublet due to the amine protons (**c**) are clearly present.

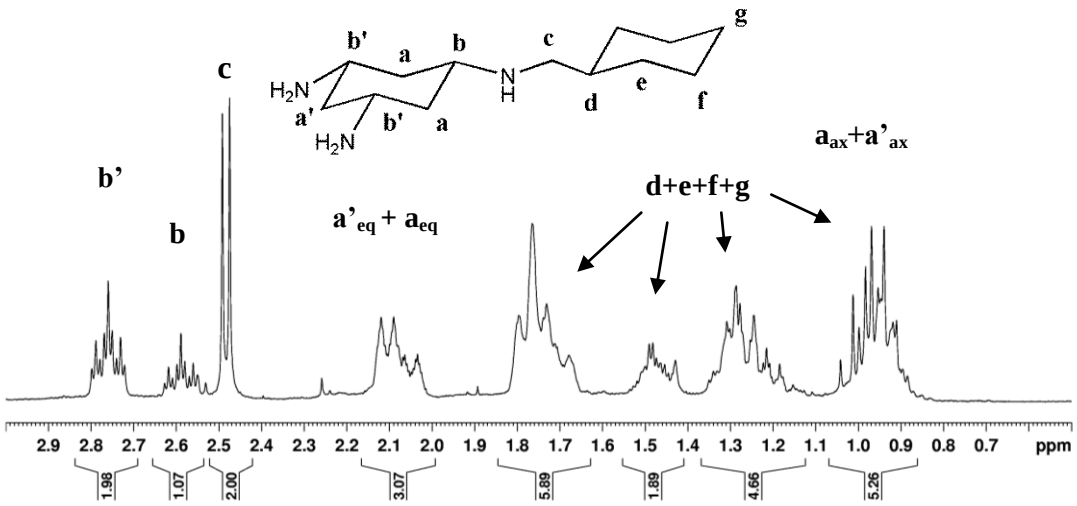

Figure 2.41: ^{1}H NMR spectrum of tachmonocyc **[17]**, with relative integration of the signals, recorded in d_4-MeOH.

Reduction with sodium borohydride and Boc deprotection are generally very high yielding reactions, therefore the low yields obtained for compound **[17]** are likely to be due to very poor rate of Schiff base formation in the reductive amination step. This would not be surprising, considering that the Schiff base formation for compound **[17]** is not driven by increased conjugation of the system. The Boc protection route was used to attempt the synthesis of compound **[16]** as an alternative to the method described in section **2.7.1**. In this case, the diBoc-monoarmed derivative could easily be made in 78% yield, confirming that the condensation efficiency plays a crucial role in the synthesis. Unfortunately, the deprotection conditions used to remove the Boc groups caused also the hydrolysis of the benzyl arm. These preliminary studies had shown that, with optimisation of the reaction conditions, a promising synthetic route for the synthesis of mono-armed tach derivatives can be obtained.

2.8 Chapter conclusions

Cis,cis-1,3,5-triaminocyclohexane (tach) offers a good scaffold for the facile synthesis of Schiff bases. The amine nitrogens of **[2]HBr** were used for the condensation with different classes of aldehydes. To overcome solubility and stability problems, the Schiff base derivatives were reduced with sodium borohydride to obtain the corresponding tri-amine compounds. All the ligands made were fully characterised by NMR spectroscopy, mass spectrometry and, when good quality crystals were obtained, X-ray diffraction. Elemental analysis was performed on all the tri-amines to ensure purity for the biological tests and on most of the Schiff bases.

Synthetic methods for the preparation of mono-substituted derivatives were explored and two mono-armed compounds were made. Although the procedures need optimisation to improve purity and yields, they formed the basis for further investigation and expansion of tach-related library of compounds.

The ligands reported were designed to investigate structure-activity relationships, which are presented in **Chapter 4**.

Chapter 3

Synthesis, characterisation and biological evaluation of tachpyr-containing metal complexes

3. Synthesis, characterisation and biological evaluation of tachpyr-containing metal complexes

3.1 Introduction

Cis-diaminodichloroplatinum, cisplatin, and its derivatives (**Figure 3.1**) are among the few inorganic drugs that have been approved in cancer therapy to date. Since the fortuitous discovery of the cytotoxic properties of cisplatin[182] and its introduction on the market in the late 70s, several other inorganic, organometallic and coordination compounds have been synthesised and tested as potential anticancer agents or diagnostic tools, but a small number of them have entered clinical trials and only few have been introduced in therapy.[183-184]

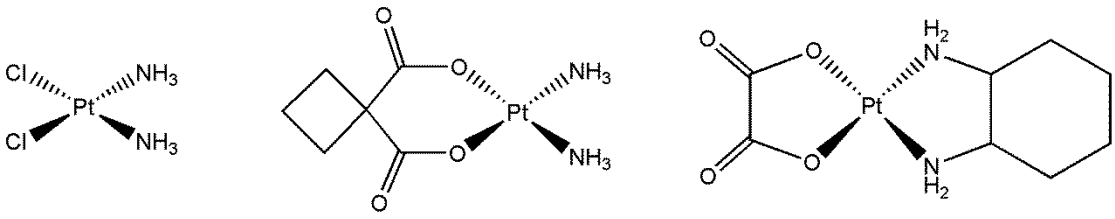

Figure 3.1: Structure of cisplatin (left), carboplatin (centre) and oxaliplatin (right).

Cisplatin (**Figure 3.1**, on the left) has proved to be active on several different tumours, in particular against testicular cancer, for which it increases greatly the chances of survival,[185] as this particular kind of cancer appears to have an intrinsic sensitivity to this compound[186] due to lack of DNA-repair mechanisms of DNA-platinum-adducts compared to other cell lines.[187] Unfortunately, cisplatin presents several side effects, including nephro- and neuro-toxicity. Also, resistance to cisplatin can occur during the treatment or it can be inherent, limiting the efficacy of the therapy.[28] The mechanism of resistance might involve several pathways: reduced uptake of the drug inside the cells or increased efflux;[28, 188] inhibition of cisplatin by glutathione or other sulfur-containing proteins;[189-190] increased ability to repair the DNA damage due to cisplatin binding[188] or to ignore apoptosis signals.[191] In order to improve the activity profile and overcome resistance, several cisplatin derivatives have been made, but only two of them, carboplatin and oxaliplatin (**Figure 3.1**), have been introduced in therapy and reached world-wide usage.

The mechanism of action of these compounds has still not been completely clarified, but it is understood that they undergo an aquation process which leads to the active species, able to bind DNA. For cisplatin, the chloride atoms are replaced with water molecules, mostly in cells, where the chloride concentration is quite low. In the blood stream the high concentration of chloride ions reduces the extent of aquation process.[186] Once the compound is in its active form, it can irreversibly bind the DNA with both intra-[192-193] and inter-[194] strand links (**Figure 3.2**), preferably through coordination bonds between guanine residues.[186, 195] The main product responsible for action (and side effects) of cisplatin is the intra-strand compound, whilst the inter-strand contributes a small percentage to the total amount of Pt-DNA adduct.[196] The distortion of the DNA after coordination with cisplatin prevents replication and transcription of the genetic material, leading to apoptosis, i.e. programmed cell death. For this reason, cisplatin is regarded as a genotoxic agent, even if its mode of action is still a matter of debate and other mechanisms, such as interaction with proteins, may be possible.

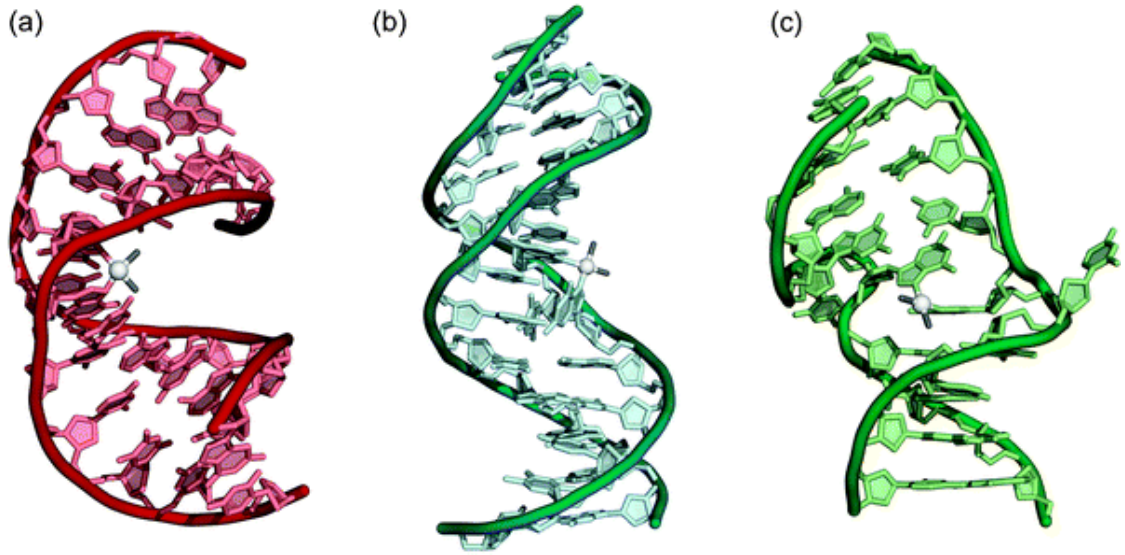

Figure 3.2: X-ray crystal structures of cisplatin-DNA adducts. Examples of intrastrand (**a** and **b**, PDB codes 1AIO and 1DA4, respectively) and interstrand (**c**, PDB code 1A2E) complexes. Image adapted from Todd and Lippard.[195]

The activity of cisplatin seems to be related to the kinetics of the aquation process.[183] In order to decrease the side-effects of cisplatin, a compound with slower exchange rate, carboplatin, was designed. It is less reactive than cisplatin, therefore it can be

administered at higher doses than the parent compound. Carboplatin can form the same DNA adducts as cisplatin with the only difference in the kinetics of binding[197] and it is usually used for the same kind of tumours.[183]

A further development was obtained with the introduction into therapy of another cisplatin derivative, oxaliplatin. This compound was found to be active on cisplatin-resistant and other types of tumours, such as for example metastases and colorectal cancer, probably due to the slightly different DNA-binding mode.[183, 195, 198]

3.1.1 Non-platinum metal-based anticancer agents

Following the considerable success of platinum-based anticancer drugs, several other complexes with different metals have been synthesised and tested in the last 30 years, with some promising results.[184] Resistance and side effects are the two main problems related with cisplatin therapy; furthermore, some patients can develop cisplatin-induced cancer several years after the end of the treatment due to the DNA adducts formed with cisplatin, because the cross link is irreversible and, over the years, can cause mutations of the genetic material due to mistakes in the DNA replication process and post-replication mechanisms.[199] For all these reasons, developing new compounds able to overcome the problems related with cisplatin therapy is a big challenge in anticancer research.

Metal complexes offer several advantages in drug design due to some unusual characteristics of metals; for example different redox states for the same metal, possible *in situ* activation (e.g. photo-activation), a relatively rigid structure and the possibility to bind, more or less strongly, to biomolecules. Furthermore, all these features can in theory be finely tuned, a key feature in drug design. A classification based on the role played by the metal, rather than the biological target, of inorganic, organometallic or coordination compounds which have shown interesting activity against tumour cells has been attempted by Gianferrara, Bratsos and Alessio.[200] It is interesting to note from this study that the same compound can present more than one

mode of action. The uncertainty about the mechanism of action can make its assignment to a class a challenging task.

One way to exploit some of the properties of metal complexes is to combine them with bioactive organic molecules. In this way, the metal complex might have either a merely structural role, protecting the ligand from early activation (or de-activation), or it might improve some bio-physical characteristic of the organic moiety (e.g. solubility) and actively play a role in cell toxicity. An interesting example is given by ferrocifen, (**Figure 3.3**) in which the organometallic complex ferrocene has been added to the anticancer agent hydroxytamoxifen (**Figure 3.3**). Tamoxifen and hydroxytamoxifen are potent anticancer agents for breast cancers which express the estrogen receptor (ER+), but it is inactive when this receptor is not present. Combination with ferrocene makes the resulting compound active on both ER+ and ER− breast cancers, showing that the ferrocene moiety added a further mechanism of action to the organic molecule.[200]

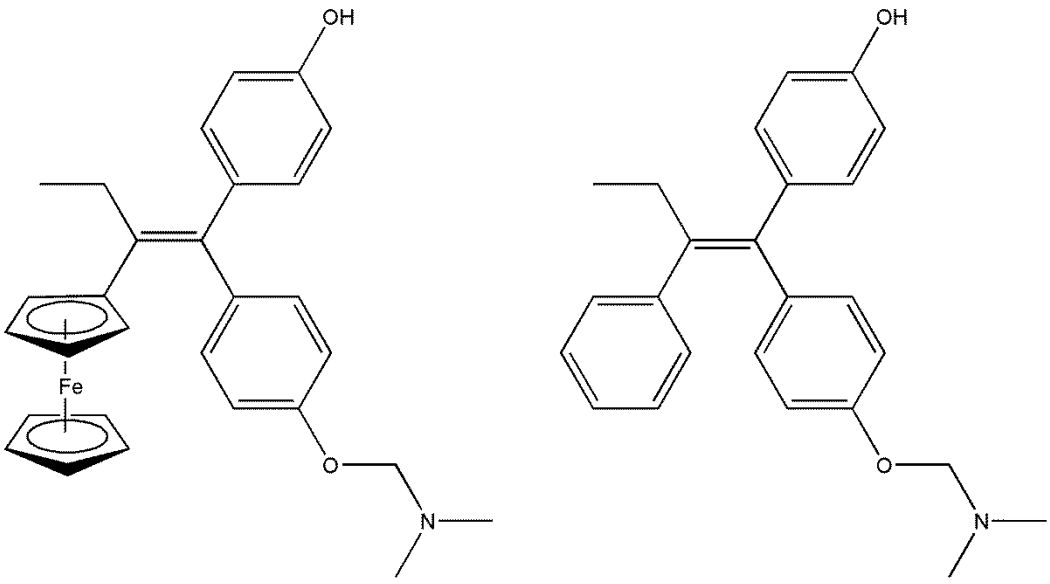

Figure 3.3: Ferrocifen (left) and hydroxytamoxifen (right).

To evaluate the role played by the ferrocene moiety, the iron atom was substituted with ruthenium by Pigeon *et al.*[201] and the resulting compound showed to be active only against ER+ tumours, with no activity on ER− cells. This result seems to suggest a possible redox mechanism involved in the action of ferrocifen, supported by

electrochemical studies of the ruthenocene derivatives, which demonstrated that the ruthenium-moiety decomposes after electron transfer.[201]

In other cases, the metal centre might be used only for a structural role, to maintain a particular conformation of the ligand. For example, the ruthenium complex outlined in **Figure 3.4** was made to mimic the structure of the anticancer agent staurosporine,[202] a protein kinase inhibitor, showing good inhibitory activity against this enzyme.[203]

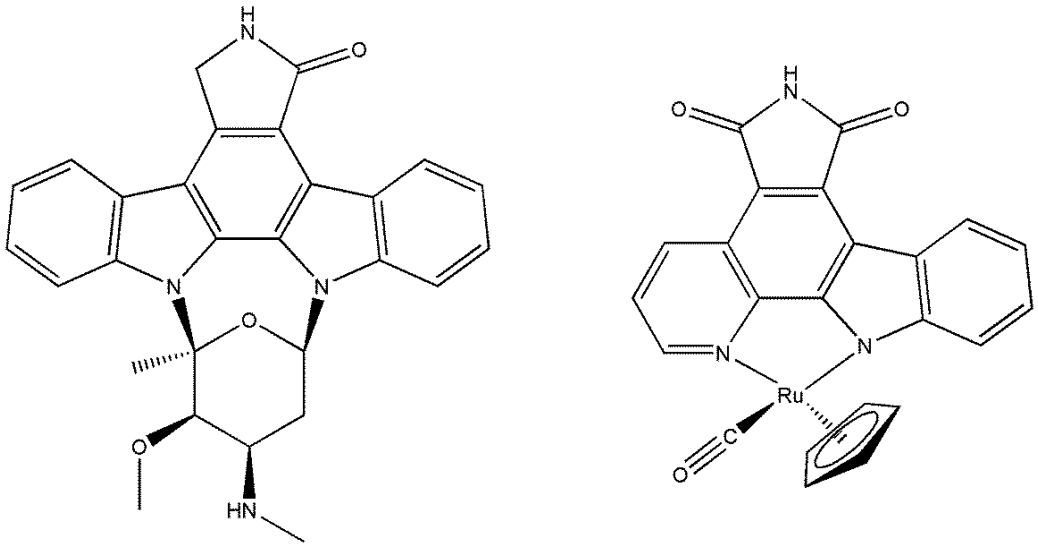

Figure 3.4: Structure of staurosporine (left) and the ruthenium complex made to mimic it (right).

In 1993 the first non-platinum-based complex to enter clinical trials for the treatment of cancer was titanocene dichloride (**Figure 3.5**).

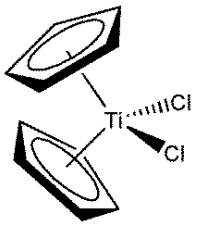

Figure 3.5: Titanocene dichloride.

The mechanism of action for titanocene dichloride has not been completely clarified, but titanocene has been found in cellular compartments rich in nucleic acids and it seems to inhibit nucleic acid synthesis.[204] It has been reported by Guo *et al.* that

titanocene binds to DNA, but in a different way than cisplatin. Instead of coordinating nitrogen atoms of nucleotides, titanocene seems to interact with the phosphate groups present in the backbone,[205] which is in contrast with an early study of its binding mode which showed the possibility of formation of complexes with nitrogen atoms on DNA bases.[206] It has been proven that titanocene can bind serum transferrin, the protein responsible for delivering iron to cells,[207] and that serum albumin might play an important role in transport and delivery of this compound.[208] Despite the fact that titanocene was found to be active on cisplatin resistant cell lines *in vitro* and was shown to have mild toxicity (except for hepatotoxicity, which was the dose-limiting side-effect), the response *in vivo* was poor and the clinical trials on the molecule were stopped in 1998.[209] Since the introduction in clinical trials of titanocene dichloride, several derivatives have been synthesised in order to improve the activity, the solubility profile and the coordination properties. Mono- and di-alkylamino,[210-211] alkenyl[212] and peptide-substituted[213] derivatives have been synthesised so far, but none of them has passed through clinical trials, in spite of showing even better results *in vitro* than titanocene dichloride.[210-211, 214]

Among the transition metals, cobalt has proved to be a good candidate for anticancer agents, also thanks to its cytotoxicity. Some pyrrolo[3,2-*f*]quinoline cytotoxins,[215] nitrogen mustards[216] and a cobalt complex of marimastat (a potent inhibitor of an enzyme called matrix metalloproteinase (MMP) involved in connective-tissue breakdown, overexpressed in tumour)[217] have been made. Examples of these compounds are shown in **Figure 3.6**.

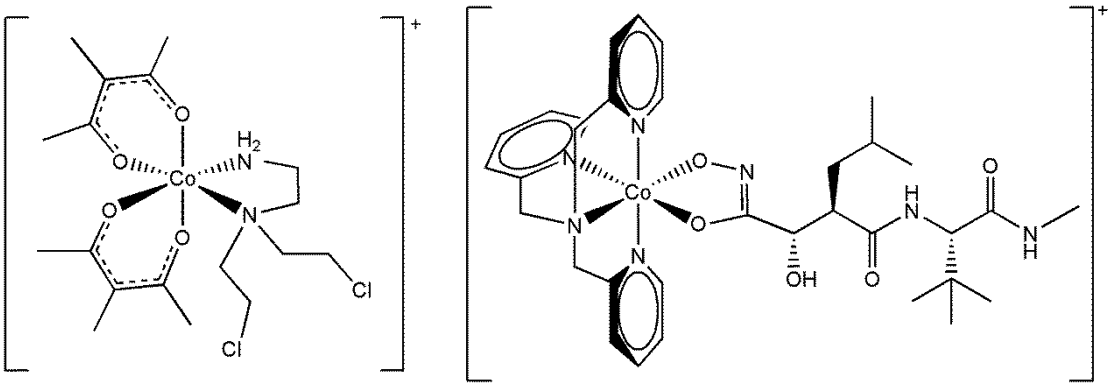

Figure 3.6: Structure of a cobalt (III) complex of a nitrogen mustard[216] (left) and marimastat[217] (right).

In these complexes, the metal usually has a protective role for the ligand, preventing it from early activation and reducing side-effects. The complex acts as a prodrug, in which the oxidation state of the metal avoids dissociation of the ligand. In this context Co(III) complexes have potential as the complexes are relatively inert but, when in cancerous cells, the metal can be reduced to a Co(II) species by the reducing environment often found in tumours.[23] The complex so formed is more labile than the starting one and can dissociate, releasing both the cytotoxic ligand and the metal. The latter might have its own role in the apoptotic process (cobalt is known to be cytotoxic), possibly increasing the effect of the ligand.

Among the metal complexes made and tested for anticancer activity, ruthenium complexes have been proved to possess interesting characteristics and often very good anticancer properties.[218-220] Two ruthenium-based compounds, called NAMI-A and KP1019[221] and shown in **Figure 3.7**, are currently in Phase II clinical trials.[218]

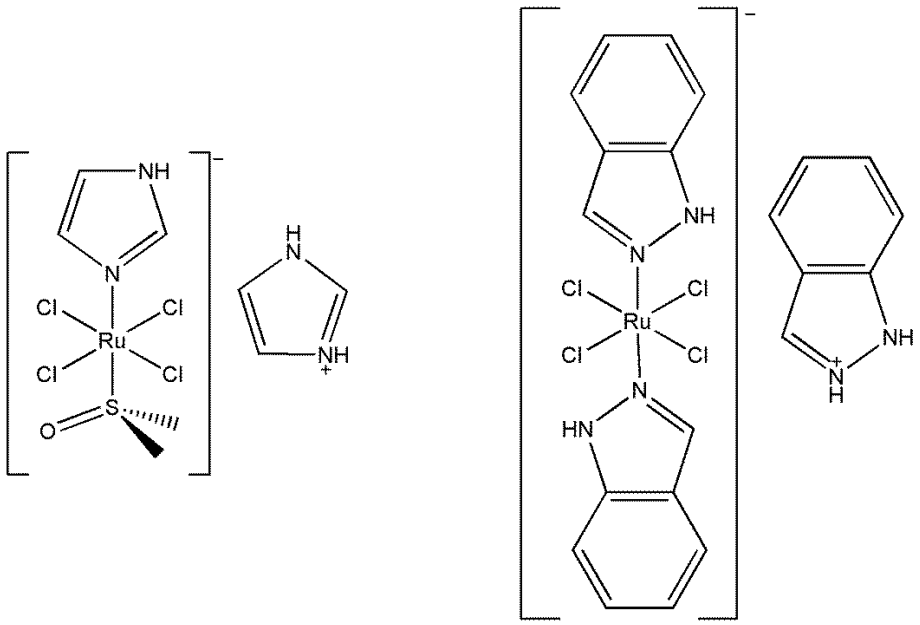

Figure 3.7: Ruthenium-based anticancer complexes in clinical trials: NAMI-A (left) and KP1019 (right).

The mechanism of action of these compounds has not been clarified yet, but, similar to cisplatin, they are believed to be activated by chloride dissociation, with a possible activation by a reduction step. NAMI-A has shown antimetastatic properties,[222-223] and KP1019 is able to promote apoptosis in several cell lines.[224]

Besides these two compounds, several other Ru-based complexes have been made; among them, RAPTA compounds synthesised by Dyson's group[225-226] and Sadler's ethylenediamino complexes,[227] shown in **Figure 3.8**, have proven to possess interesting activity against tumours.

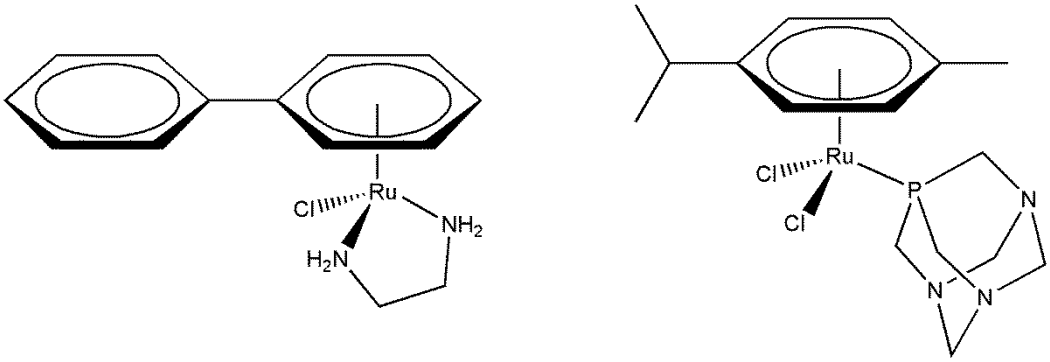

Figure 3.8: Example of Sadler's Ru-ethylenediamino complex[228] (left) and Dyson's RAPTA-C complex[229] (right).

Ethylenediamino compounds cause DNA damage similarly to cisplatin,[228] showing potent cytotoxicity against tumour cells. RAPTA compounds, instead, seem to target other cellular components than DNA, probably proteins, with very low toxicity against healthy cells.[229-230]

Due to the very promising results showed by ruthenium complexes and the cytotoxicity of cobalt which could potentially be exploited against cancer cells, these two metals were used for the complexation with tachpyr **[3b]**. This chapter describes the synthesis and characterisation of such complexes and their *in vitro* evaluation against cancer cells.

3.2 Synthesis and characterisation of cobalt complexes

Tachimpyr **[3a]** and tachpyr **[3b]** were used to synthesise the corresponding cobalt(II) complexes **[18]Cl_2** and **[19]Cl_2**, as shown in **Figure 3.9**. Both reactions were performed in deoxygenated solvent under N_2 atmosphere for 16 h. Addition of one equivalent of cobalt dichloride hexahydrate to the colourless ligand solution caused an immediate change of colour to the mixture, which turned orange for both **[3a]** and **[3b]**.

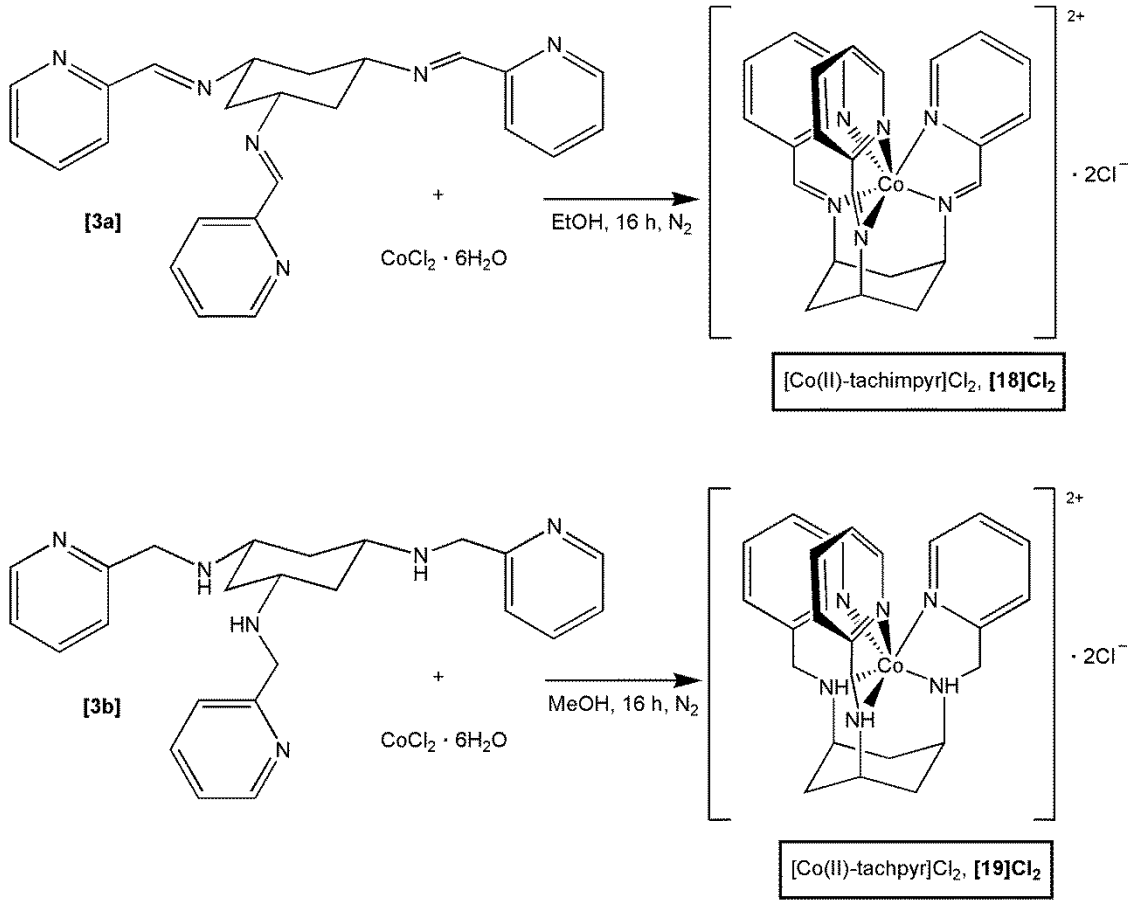

Figure 3.9: Synthetic scheme for the formation of [Co(II)-tachimpyr]Cl_2, **[18]Cl_2** (top), and [Co(II)-tachpyr]Cl_2, **[19]Cl_2** (bottom).

Addition of diethyl ether to the solutions caused the precipitation of a yellow/brown solid, which was isolated by filtration (crude yield of 53 and 30% for **[18]Cl_2** and **[19]Cl_2**, respectively) and stored under N_2 atmosphere.

As expected for a d^7 Co^{2+} system, the ^{1}H NMR was very broad and featureless. ESI-MS showed the presence of both the singly and doubly charged ions, with the charge deriving from the metal centre, for compound **[18]** at *m/z* 455.1395 and 227.5689, respectively, in agreement with the molecular composition, $C_{24}H_{24}CoN_6^{n+}$. The ESI-MS of the Co(II)-tachpyr complex **[19]**, on the other hand, did not show any peak for the complex. The spectrum was dominated by the doubly charged peak at *m/z* 228.5754, which could be assigned to the compound with formula $C_{24}H_{26}CoN_6^{2+}$ (error = 1.6 mDa). A small peak at *m/z* 459.1696, corresponding to the molecular formula $C_{24}H_{28}CoN_6^{+}$ (error = 0.6 mDa), was also observed. These two peaks

correspond to the partially oxidised complexes, whose structures are shown in **Figure 3.10**.

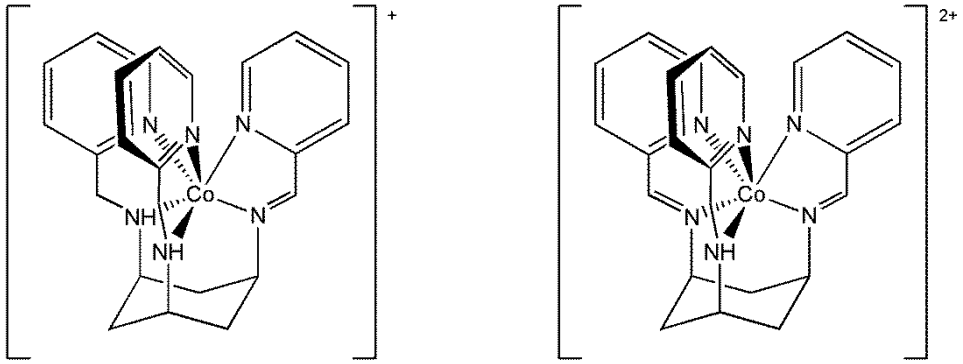

Figure 3.10: Proposed structures for the molecular ion peaks observed in the ESI-MS spectrum of compound **[19]**.

The presence of these peaks could be explained by the oxidation of compound **[19]** inside the MS instrument and Park *et al.* observed a similar behaviour for the equivalent Fe(II) complex of tachpyr, which could easily form the mono-, di- or tri-imine when exposed to air.[135] Unfortunately, elemental analysis did not match the calculated values for the expected elemental composition, hence the purity of neither compound **[18]Cl_2** nor **[19]Cl_2** could be proven, although crystals for both compounds were obtained.

3.2.1 Structural investigation of cobalt complexes

Crystals of **[18]Cl_2** suitable for X-ray diffraction could be grown from EtOH/Et_2O layer as orange blocks and the crystal structure obtained is shown in **Figure 3.11**.

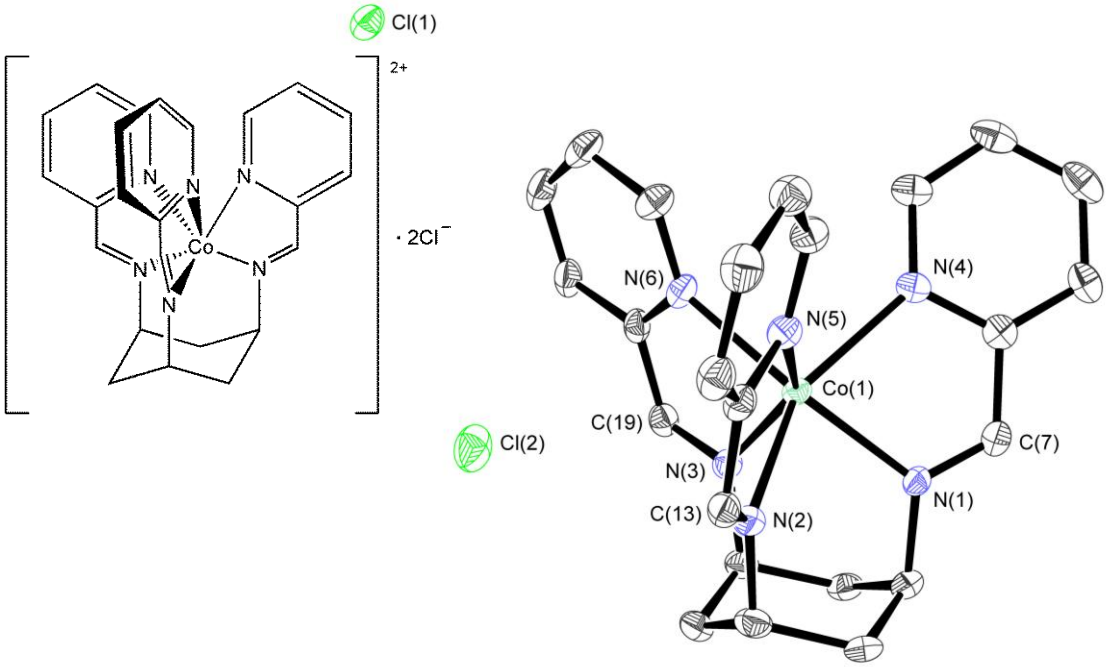

Figure 3.11: Structure (left) and ORTEP diagram (thermal ellipsoids at 50% probability level) of [Co(II)-tachimpyr]Cl_2 **[18]Cl_2**. Hydrogen atoms and EtOH solvent molecules omitted for clarity.

The metal presents a distorted trigonal prismatic geometry, as already reported by Wentworth *et al.*,[231] due to the presence of the ligand, which forces the metal ion to assume this particular geometry rather than an octahedral structure. The coordination geometry around the cobalt, showing the six coordinating nitrogen atoms, is shown in **Figure 3.12**. Looking at the structure from the pseudo three-fold rotation axis, it is possible to determine that the complex is in the Δ configuration and the twist of the pyridine arms, which contributes to the distortion of the geometry compared to an idealised trigonal prism, becomes very visible.

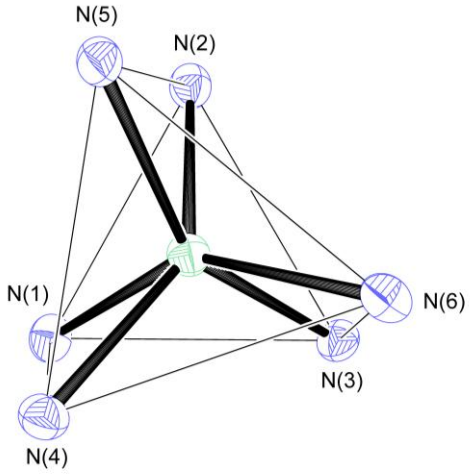

Figure 3.12: Detail of the distorted trigonal prismatic geometry of **[18]Cl_2**.

A way to estimate the geometry and the extent of the distortion around the metal centre is to calculate the twist angle α of the pyridine nitrogen atoms compared to the imines, as shown in **Figure 3.13**.[232]

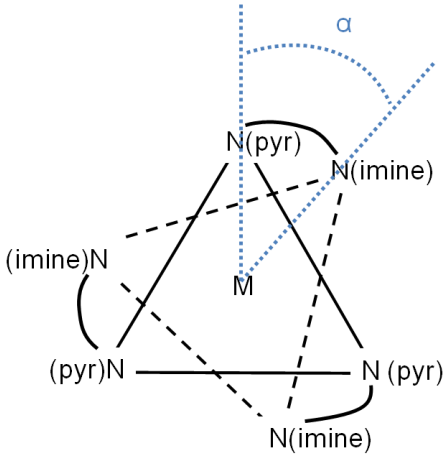

Figure 3.13: Scheme of the arrangement around the metal centre and the twist angle of the complex.

In a perfect trigonal prismatic geometry, α = 0°, while the angle is 60° for a perfect octahedral. For **[18]Cl_2** the three twist angles were 20.40°, 19.90° and 19.73°, giving an average of 20.01°. The complex, therefore, tends to trigonal prismatic geometry, but it is very distorted. The equivalent Zn(II) complex with tachimpyr reported by Gillum *et al.* had an almost perfect trigonal prismatic geometry, with an average twist angle of 4.6°,[233] whilst the Ni(II)-tachimpyr reported by Fleischer *et al.* showed an

arrangement around the metal centre halfway between trigonal prismatic and octahedral, with an average α = 32°.[234] Fleischer *et al.* rationalised these findings by considering the different factors which can affect the geometry of the complex, most notably the rigidity of the ligand and the ligand-field stabilisation energies of the different metals.[234] The rigidity of the ligand due to the presence of the imine bonds forces the complex in a trigonal prismatic conformation, which is the most suited to minimise the strain on the conformation. On the other hand, ligand-field stabilisation energies are greater for octahedral geometry than trigonal prismatic, and the greater the electronic stabilisation, the more the complex would tend towards an octahedral geometry. The balance between conformation strain and ligand-field energy gives the shape of the final complex, which, in the case of **[18]Cl$_2$**, was a distorted trigonal prism.

Crystals suitable for X-ray diffraction were also obtained for the Co(II)-tachpyr complex **[19]** from MeOH/Et$_2$O layer. The crystal structure of the complex is shown in **Figure 3.14**. The hydrogen atoms of the amines were found by electron density difference maps.

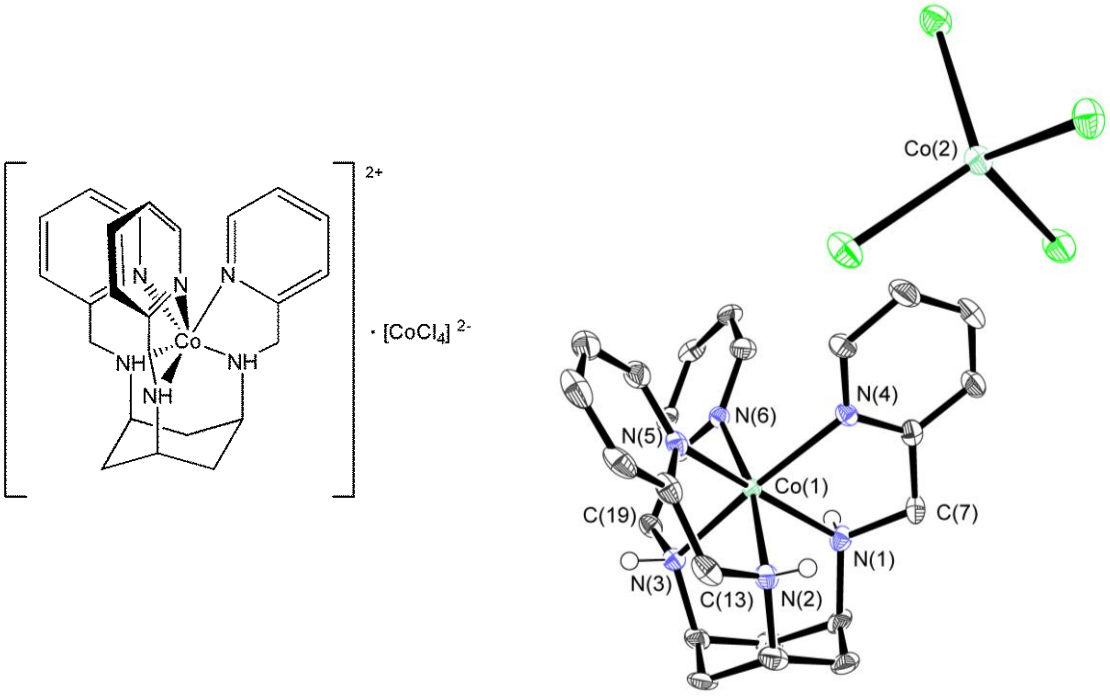

Figure 3.14: Structure (left) and ORTEP diagram (thermal ellipsoids at 50% probability level) of [Co(II)-tachpyr]CoCl$_4$ **[19]CoCl$_4$**. Hydrogen atoms omitted for clarity, except for amine hydrogen atoms.

As shown in **Figure 3.14**, the complex crystallised with an unexpected counter ion. The two positive charges due to the cobalt were balanced by a tetrachlorocobaltate anion, instead of the expected dichloride seen in the crystal structure of compound **[18]**. Differently from compound **[18]**, the Co(II)-tachpyr complex adopts the Λ configuration in the solid state.

The Co(II)-tachpyr complex shows a distorted octahedral geometry for the metal centre, with an average twist angle of 44.95°. The higher flexibility of the ligand due to the reduction of the imine double bonds decreases the strain on the structure. As a result, the complex tends towards a more octahedral geometry, which is the favoured by electronic factors. **Table 3.1** and **Table 3.2** show selected bond lengths and angles for the two cobalt complexes **[18]** and **[19]**.

Bond	**Bond length / Å**	
	[18]Cl_2·2.5EtOH	**[19]$CoCl_4$**
Co(1) - N(1)	2.099(2)	2.143(3)
Co(1) - N(2)	2.138(2)	2.126(3)
Co(1) - N(3)	2.111(2)	2.129(3)
Co(1) - N(4)	2.187(2)	2.146(3)
Co(1) - N(5)	2.197(2)	2.118(3)
Co(1) - N(6)	2.196(2)	2.133(3)
C(7) - N(1)	1.267(4)	1.471(5)
C(13) - N(2)	1.269(4)	1.464(5)
C(19) - N(3)	1.271(4)	1.475(5)

Table 3.1: Selected bond lengths (Å) in Co(II)-tachimpyr **[18]** and Co(II)-tachpyr **[19]** complexes.

Bond	**Bond angle / °**	
	[18]Cl_2·2.5EtOH	**[19]$CoCl_4$**
N(1) – Co(1) – N(2)	83.09(9)	89.80(12)
N(1) – Co(1) – N(3)	85.64(9)	89.31(12)
N(3) – Co(1) – N(2)	83.08(9)	89.98(12)
N(4) – Co(1) – N(5)	90.89(9)	93.98(12)
N(4) – Co(1) – N(6)	93.47(9)	91.76(11)
N(6) – Co(1) – N(5)	89.99(9)	98.52(11)
N(1) – Co(1) – N(4)	76.58(9)	78.95(12)
N(2) – Co(1) – N(5)	75.12(9)	79.48(12)
N(3) – Co(1) – N(6)	76.10(9)	79.73(12)

Table 3.2: Selected bond angles (°) in Co(II)-tachimpyr **[18]** and Co(II)-tachpyr **[19]** complexes.

A literature search for the Co(II)-tachpyr complex shows that this compound was previously synthesised by Park *et al.*,[137] although its crystal structure has not been previously reported. Several other tachpyr complexes with different metals have been analysed by X-ray crystallography in the past, which include Ga(III) and In(III),[232] Zn(II), Cd(II) and Hg(II),[235] Cu(II),[236] Ni(II) and Mn(II).[137] The complexes have different geometries around the metal centre, highlighted by the twist angles shown in **Table 3.3**.

Metal complex	Ionic radius[237-238] / Å	Twist angle / °
Mn(II)-tachpyr[137]	0.97	2.5(1)
Co(II)-tachpyr	0.88	44.9
Ni(II)-tachpyr[137]	0.83	45.5(2)
Cu(II)-tachpyr[236]	0.87	-
Zn(II)-tachpyr[235]	0.88	43.7(2)
Cd(II)-tachpyr[235]	1.09	20.8(4) / 11.4(9)
Hg(II)-tachpyr[235]	1.16	5(1)
Ga(III)-tachpyr[232]	0.76	22.40
In(III)-tachpyr[232]	0.94	18.23

Table 3.3: Table of the twist angles in different complexes of tachpyr. The value for the Cu(II) complex was not reported in the literature, as well as some standard deviation values.

As shown, the metal complexes of the first row transition metal prefer to adopt a distorted octahedral geometry over trigonal prismatic, with the Mn(II) complex being the only exception. Increasing the size of the metal from Zn(II) to Cd(II) to Hg(II), the complex moves from a distorted octahedral to more and more a trigonal prismatic geometry, in order to accommodate the bigger cation.[235] A similar behaviour was shown by Hilfiker *et al.* for the Ga(III)- and In(III)-tachpyr complexes.[232]

3.3 Synthesis and characterisation of ruthenium complex

As briefly described in section **3.1.1**, ruthenium has been extensively employed for the development of new anti-cancer compounds, with very promising results. The complexation of tachpyr **[3b]** with ruthenium to form the Ru(II)-complex was therefore explored, as shown in **Figure 3.15**.

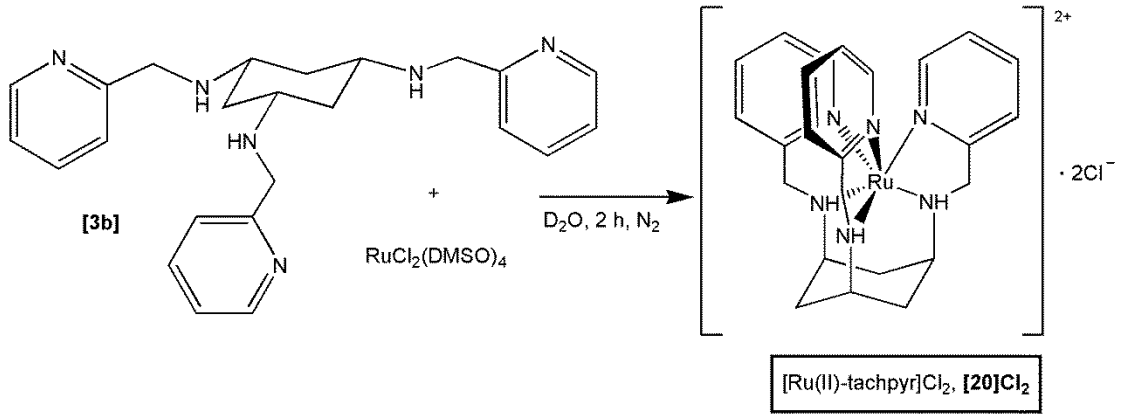

Figure 3.15: Synthetic scheme for the formation of [Ru(II)-tachpyr]Cl_2, **[20]Cl_2**.

The reaction was attempted in several different solvents and with several different methodologies because the complexation was quite difficult to achieve.

When performed in methanol, the ^{1}H NMR spectrum of the reaction showed the presence of different compounds, including **[3b]** starting material and several unknown by-products, with little Ru-complex in the reaction mixture. To try to drive the reaction towards the final complex, potassium hexafluorophosphate was added to tachpyr **[3b]** and $RuCl_2(DMSO)_4$ in ethanol to cause the precipitation of the desired ruthenium complex from the reaction mixture. A red precipitate was indeed formed during the reaction, but both ESI-MS and ^{1}H MNR showed no evidence for the Ru(II)-tachpyr complex. In particular, the ^{1}H NMR did not exhibit the aromatic signals due to the pyridyl rings, suggesting that hydrolysis of the arms might have occurred during the reaction.

Water was found to give better results when used as the solvent for the complexation reaction. The reaction was first done on a 5 mg scale in a sealed NMR tube using degassed deuterated solvent, in order to monitor the formation of the product by ^{1}H NMR spectroscopy. Addition of the Ru(II) precursor to the colourless solution of tachpyr did not cause any change of colour at room temperature, but the reaction mixture turned to a dark orange colour upon heating. Leaving the reaction at reflux for a further 2 h led to a dark red/brown solution.

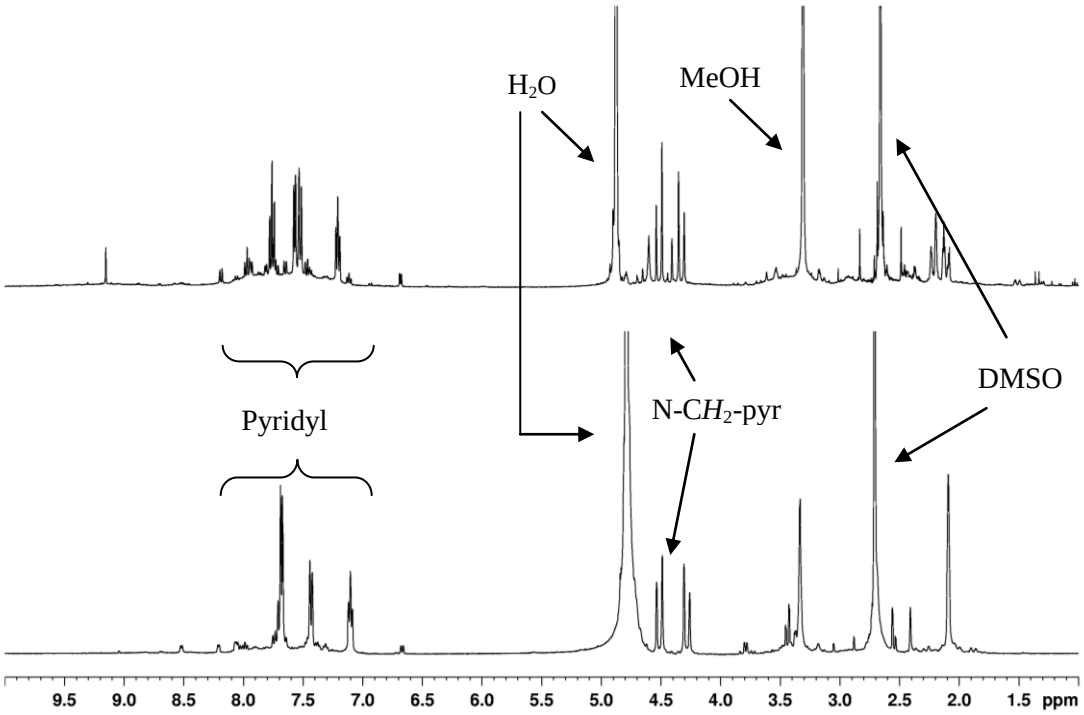

Figure 3.16: ^{1}H NMR spectra of the reaction mixture of Ru(II)-tachpyr **[20]** after reaction in d_4-MeOH (top) and D_2O (bottom).

Figure 3.16 shows the improvement in the reaction obtained by changing the solvent used for the reaction from deuterated methanol to D_2O. Although still containing some unknown by-products, the reaction in D_2O appeared to give more selective conversion. The presence of the Ru(II)-tachpyr complex could be easily determined by ^{1}H NMR due to the appearance of two characteristic doublets at 4.47 and 4.24 ppm, belonging to the methylene protons bound to the amines, as also observed for other tachpyr complexes.[139-140, 232] The C*H*$_2$ protons of the ligand are diastereotopic and give rise to the two doublets (^{2}J = 18.9 Hz), which is an indication of the rigidity of the complex on a NMR timescale. Although clear evidence for the presence of the complex was given by NMR spectroscopy, the charged complex or any other related peak could not be observed by ESI-MS, whilst the signals present in the mass spectrum were not identified.

After assessing the procedure for the synthesis of complex **[20]** in a NMR tube, the reaction was scaled up, but unfortunately all attempts were unsuccessful. Several reaction conditions were tested, but no product could be isolated unless the reaction

was performed in a Young's tap sealed NMR tube. Using a sealed vessel for the synthesis of the compound causes an increase in the pressure upon heating, with consequent increase in the boiling point of the solvent used for the reaction. For this reason, the synthesis of Ru(II)-tachpyr was attempted both in 1-butanol (b.p. = 117 °C) and in a sealed ampoule to reproduce the conditions used in the NMR tube, but in neither case the complex could be isolated. Increasing the reaction time also caused problems due to the hydrolysis of the pyridyl arms of the ligand. For all these reasons, Ru(II)-tachpyr could never be isolated pure and yields of reaction could not be determined.

Several crystallisations methods were tried in the effort of isolating the complex, which led to single crystals suitable for X-ray diffraction. The crystals appeared from MeOH/Et_2O layer as pink blocks and, surprisingly, solution and refinement of the structure showed that the crystal obtained did not belong to the expected Ru(II) complex, but to the Ru-dimer showed in **Figure 3.17**.

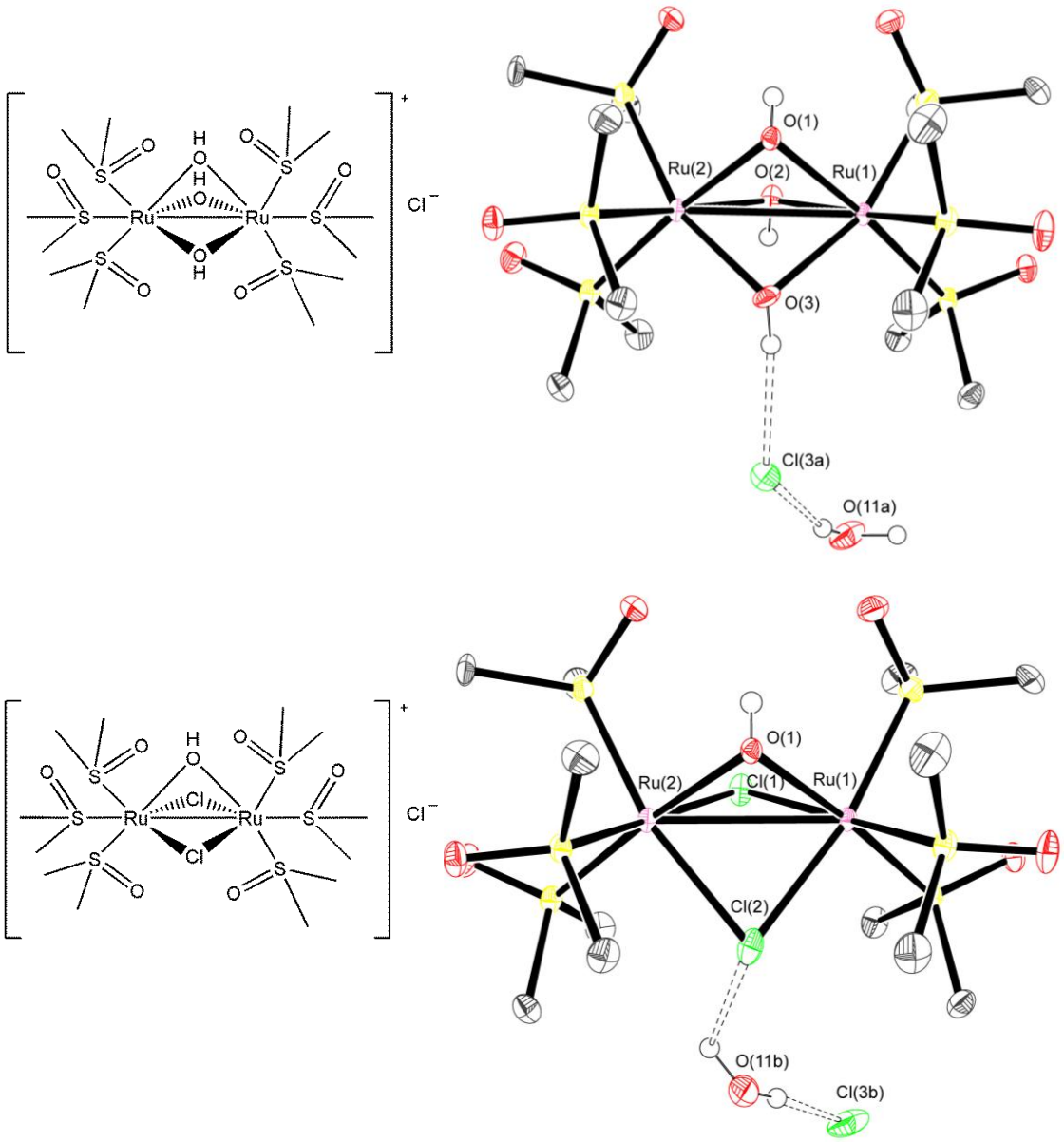

Figure 3.17: Structures (left) and ORTEP diagrams (thermal ellipsoids at 50% probability level) of Ru-dimers. Methanol solvent molecule and hydrogen atoms omitted for clarity, except for hydroxo and water hydrogen atoms.

The crystal contained two different species, both of them containing two ruthenium atoms bound to three DMSO molecules and connected by three bridging atoms. The difference between the two complexes was found in the bridging groups between the two ruthenium centres, which gave rise to the diRu(II)-trihydroxo dimer $[Ru_2(OH)_3(DMSO)_6]Cl$ and the diRu(II)-dichlorido-hydroxo dimer $[Ru_2Cl_2(OH)(DMSO)_6]Cl$. The relative occupancies for the two complexes were 0.77

and 0.23 for the $Ru_2(OH)_3$ and the $Ru_2Cl_2(OH)$ dimer, respectively. The bridging groups had an influence in the arrangement of the chloride counter ion and the water molecule present in the crystal lattice. In the trihydroxo dimer (**Figure 3.17**, top), one of the hydroxyl groups forms a hydrogen bond with the chloride counter ion, which is in turn engaged in a hydrogen bond interaction with a water molecule. In the dichlorido dimer (**Figure 3.17**, bottom), instead, one of the chlorido ligands shows a hydrogen bond with a water molecule, which is also bound to the chloride counter ion through a hydrogen bond interaction. The hydrogen bond distances between the atoms were ranging between 3.19 and 3.24 Å, in agreement with what reported in literature for O-H···Cl hydrogen bond interactions.[239-240]

Bond	**Bond length / Å**
Ru(1) – Ru(2)	2.9588(4)
Ru(1) – O(1)	2.080(3)
Ru(1) – O(2)	2.099(16)
Ru(1) – O(3)	2.100(9)
Ru(2) – O(1)	2.072(3)
Ru(2) – O(2)	2.108(17)
Ru(2) – O(3)	2.072(9)
Ru(1) – Cl(1)	2.35(2)
Ru(1) – Cl(2)	2.394(10)
Ru(2) – Cl(1)	2.34(2)
Ru(2) – Cl(2)	2.407(11)

Table 3.4: Selected bond lengths (Å) in the crystal structure of the Ru-dimers.

The Ru–Ru distance was found in good agreement with the similar Ru(II)-dinuclear complex $[Ru_2(OH)_3(\eta^6\text{-}C_6H_6)_2]Cl\cdot 3H_2O$ reported in the literature (Ru(1)-Ru(2) distance = 2.9812(7) Å)[241] and is indicative of a metal-metal bond. Similarly, the Ru-O bond distances are in very close agreement with the reported values.[241] For the Ru(II)-dichlorido complex, a literature search did not show any related structures, therefore a comparison of bond angles could not be performed.

The presence of the Ru dimer in the reaction mixture might be one of the reasons for the difficulty in obtaining the Ru(II)-tachpyr complex, because the formation of the dimer would decrease the amount of ruthenium available for the complexation with tachpyr **[3b]**.

After several attempts, the Ru(II)-tachpyr complex **[20]Cl_2** was crystallised from MeOH/Et_2O diffusion as dark red blocks. The structure of the complex is shown in **Figure 3.18**. The hydrogen atoms bound to the amine groups were found by difference electron density maps.

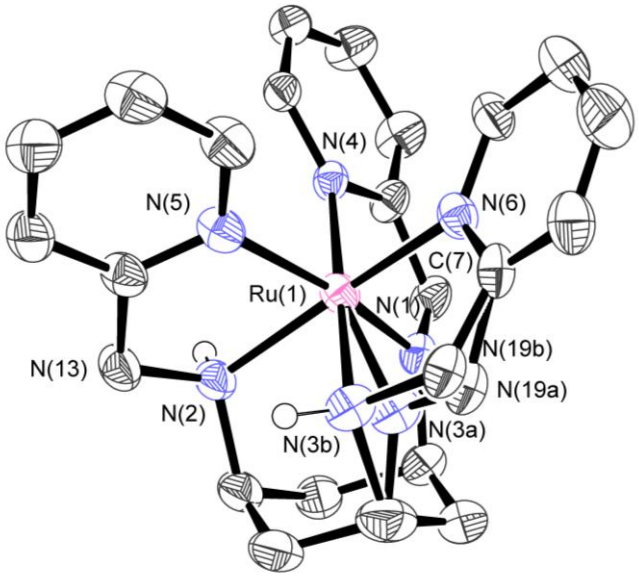

Figure 3.18: ORTEP diagram (thermal ellipsoids at 50% probability level) of [Ru(II)-tachpyr]Cl_2 **[20]Cl_2**. Chloride counter ions and hydrogen atoms omitted for clarity, except for hydrogen atoms bound to amines.

As clear from **Figure 3.18**, the structure presented disorder around one of the arms due to partial oxidation of ligand. In particular, one of the N - C bonds was always an imine bond (N(1) - C(7)), one bond was always a single bond (N(2) - C(13)), whilst the last N - C bond was present in the imine form in the 70.5% of the crystal and as an amine bond in the remaining 29.5% of the cases. Due to the mixed oxidation state of the ligand, any evaluation of the geometry around the metal centre would be affected by uncertainty, therefore the twist angles were not calculated. Partial oxidation of the

tri-amine bonds to Schiff base might be one of the causes of the difficulty of isolating the complex in good yields and high purity.

3.4 *In vitro* evaluation

A preliminary evaluation of the activity against cancer cells of compounds **[18]Cl_2**, **[20]Cl_2** and the Ru-dimer was carried out against A549 human lung adenocarcinoma cells. As further discussed in section **4.2**, the metal complexes presented in this chapter were made to, on one hand, exploit the cytotoxic activity of metals such as cobalt and ruthenium and, on the other hand, tune the cytotoxic action of tachpyr against cancer cells (cf. section **4.2**). The tests were performed being aware that the purity of the compounds had not been proven by elemental analysis, therefore the results should be looked at only as indicative of a trend rather than to produce a value of activity. Co(II)-tachpyr **[19]** was not used for the tests due to the possible presence of the tetrachlorocobaltate counter ion, which is not suitable for cell cultures due to possible intrinsic toxicity. All compounds showed complete water and culture medium solubility up to mM concentrations, which is an essential requirement for cell tests.

All tests were carried out following the procedure described in detail in **Chapter 4**. Briefly, A549 human adenocarcinoma cancer cells were plated at the seeding concentration of 1000 cells/well in a 96 well plate. The cells were incubated at 37°C, 90% RH for 16 h, after which time a solution of the metal complex in medium was added to the wells. The cells were then incubated with the complex for 3 days and the cell viability was visualized using 3-(4,5-dimethylthiazol-2-yl)-2,5-diphenyltetrazolium bromide (MTT).

Surprisingly, no loss of viability was observed for any of the compounds up to 250 µM (data not shown), implying, in the case of the Ru(II)-tachpyr complex, that not only did the metal not show toxicity, but it also stopped the action of the free ligand, which is reported to be cytotoxic (section **1.3**).[133]

The ruthenium dimer was also inactive, although other Ru(II) and Ru(III) complex with sulfur-based ligands have been reported to have extremely high toxicity against cancer cells.[242-244]

Due to their poor cytotoxic activity, the metal complexes were not developed further, whilst a detailed investigation of the activity of tachpyr and related molecules was carried out, as outlined in **Chapter 4**.

3.5 Chapter conclusions

The ligands tachimpyr **[3a]** and tachpyr **[3b]** were used for the complexation with Co(II) and Ru(II).

Both cobalt complexes Co(II)-tachimpyr **[18]** and Co(II)-tachpyr **[19]** could be characterised by ESI-MS and their X-ray crystal structure obtained, although their purity could not be confirmed by elemental analysis. The crystal structures showed that the geometry of the complex is related to the ligand used for the complexation and changes from distorted trigonal prismatic in **[18]** to distorted octahedral in complex **[19]** due to the greater flexibility of the tachpyr ligand present in complex **[19]**.

The complexation with Ru(II) proved to be challenging, and, although the Ru(II)-tachpyr complex **[20]** could be characterised by NMR spectroscopy, no purity data was obtained. X-ray diffraction showed the unexpected presence of dinuclear Ru(II) species, which appeared to be relatively rare in the literature. The crystal structure of the Ru(II)-tachpyr complex was also obtained and showed partial oxidation of the ligand to the relative Schiff base.

Preliminary evaluation of the cytotoxic effect of these compounds against cancer cells showed complete lack of activity, which suggested that a detailed investigation of the biological activity of tachpyr and its mechanism of action was needed. Given the poor cytotoxicity, these compounds were not pursued further.

Chapter 4

Biological evaluation of tach-based compounds

4. Biological evaluation of tach-based compounds

4.1 Introduction

The biological evaluation of the activity of drug candidates is a crucial step in the assessment of potential hits for new compounds. Similarly, study of the possible mechanism of action of new or commercially available molecules can lead to structural modifications to improve binding to the cellular target(s) and, hence, improve the activity or decrease the side effects.

The investigation of the mechanism of action of tachpyr **[3b]** is discussed in this chapter, with particular focus on the hypotheses developed during this evaluation. Furthermore, the *in vitro* assessment of the cytotoxic activity of the tach-based amines described in **Chapter 2** is presented and analysed. The purity of all the compounds analysed in this chapter was confirmed by elemental analysis (± 0.4% deviation from the calculated values) prior to their use on cancer cells.

4.1.1 *In vitro* evaluation of activity via MTT assay

In order to evaluate the cytotoxic activity of the compounds described in **Chapter 2**, several *in vitro* tests have been carried out against A549 human adenocarcinoma and A2780 human ovarian cancer cell lines following the general procedure described by Torti *et al*.[133] The tests were conducted *via* the 3-(4,5-dimethylthiazol-2-yl)-2,5-diphenyltetrazolium bromide (MTT) assay.

MTT is a widely used assay to evaluate cell viability.[245-246] It exploits the change in solubility and absorbance of the tetrazolium salt (MTT) after reduction to formazan, as shown in **Figure 4.1**.

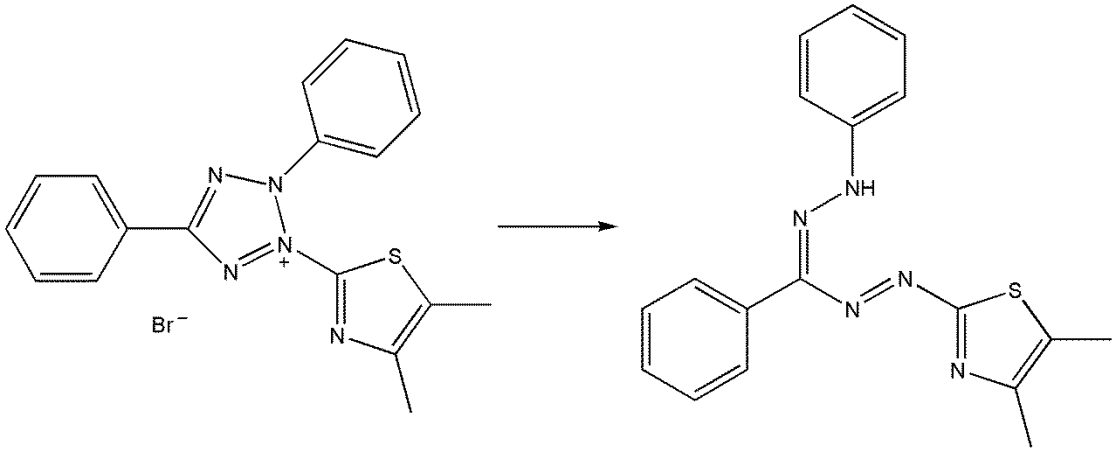

Figure 4.1: Schematic of the reduction of MTT bromide to formazan.

This reduction happens in mitochondria in viable cells only, transforming the yellow water soluble MTT compound to the insoluble formazan product, which precipitates in the aqueous medium.[247] The blue-purple formazan crystals can be dissolved using an organic solvent and the UV/Vis absorbance at 540 nm of the obtained solution measured. The intensity of the purple colour is related to the amount of formazan formed, therefore to the number of viable cells present in the well. The percentage of viable cells can therefore be determined from the value of the absorbance in comparison to the negative and positive controls and plotted against concentration of compound added as a logarithmic dose-response curve.

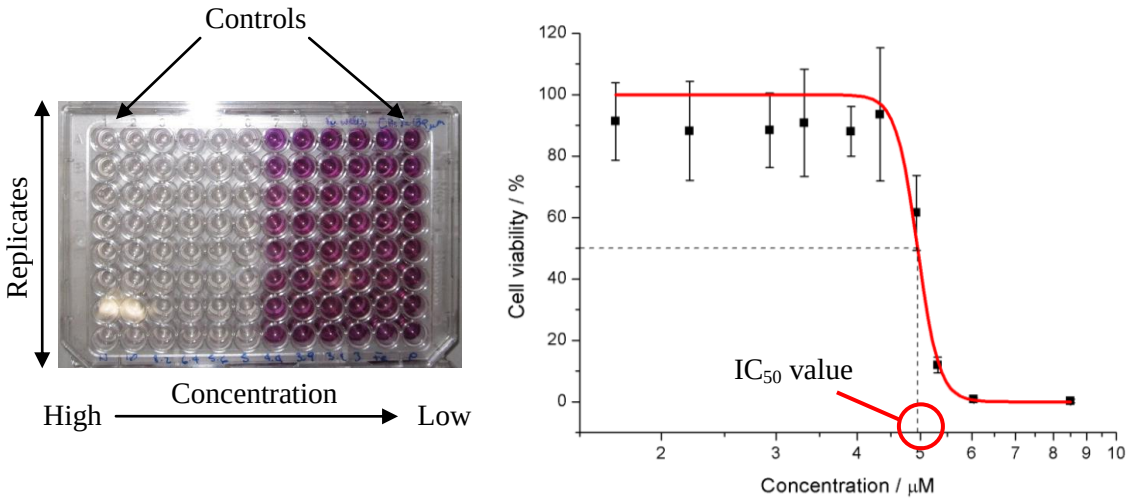

Figure 4.2: Picture of a 96-well plate at the end of the MTT assay (left) and viability against concentration plot (right).

Figure 4.2 shows a picture of a 96-well plate after addition of MTT and dissolution of formazan in DMSO (on the left) and the obtained cell viability against concentration plot (on the right). One plate enables the testing of each concentration in octuplicate, from which the standard deviation for each measurements is calculated. A sigmoidal line can be fitted to the data and the IC_{50} value estimated as the concentration which gives 50% loss of cell viability. Two controls are always added to the plates: the positive control, which consisted in medium only to reference as 0% viability; and the negative control, which contained cells, but no compound, to have a reference for 100% viability. As a control for activity (positive control), cisplatin, well known for its anti-tumour activity, was used against the cells. As a control of reproducibility of the tests on different batches of cells, tachpyr was tested at least once on every batch, to ensure that the resulting cytotoxicity was consistent across the experiments.

Due to the inherit characteristics of non-cancerous cells, the first stages of development of new anti-cancer compounds are generally carried out on immortalised (cancerous or non-cancerous) cells, which are robust, have a fast growth and can be kept in culture for long periods of time. For this reason, and in common with this accepted approach, the compounds described in this thesis were also tested against cancer cells. Compounds **[3b]** and **[11b]** were also tested against a non-cancerous immortalised cell line.

Every compound presented in this chapter was tested in at least triplicate and the different IC_{50} values obtained with their standard deviations were combined according to the formula reported by Lyons[248] and shown in **Equation 4.1**. An average value expressed as $(a \pm \sigma)$, where a is the average IC_{50} value and σ is the average standard deviation on the measure, was obtained. The IC_{50} values and the corresponding standard deviations derived from the fitted sigmoid of the plates are expressed as a_i and σ_i.

$$a = \frac{\Sigma\left(\frac{a_i}{\sigma_i^2}\right)}{\Sigma\left(\frac{1}{\sigma_i^2}\right)} \; ; \qquad \sigma = \pm\sqrt{\frac{1}{\Sigma\left(\frac{1}{\sigma_i^2}\right)}}$$

Equation 4.1: Average IC_{50} and standard deviation values calculated from plate replicates.

4.1.1.1 General procedure for MTT assays

A detailed method description for the MTT assay can be found in **Chapter 6**. As a general overview, the general procedure for all *in vitro* tests discussed in the chapter consisted of adding the cells to a 96-well plate in appropriate seeding density and incubating them for 18 h before addition of a solution of compound in medium. When the tested compound was not freely soluble in culture medium, DMSO was added to dissolve the molecule and the solution was then diluted with medium; all the tachben derivatives (compounds **[10b]-[15b]**) required DMSO to be dissolved in medium. 4-Br-tachben **[14b]** was insoluble in medium even when DMSO was present, therefore it was not tested. The concentration of DMSO added to the wells containing the cells was never higher than 1% and in these cases DMSO was also added to the controls. DMSO did not cause detectable loss of cell viability at these concentrations. The solution of tested compound was filtered to be sterilised, added at different concentrations to the wells and left with the cells for 72 h. Cell viability was then evaluated by MTT assay and the cytotoxicity of the compound against the particular cell line was expressed as IC_{50} value, standardised to the positive and negative controls.

4.1.2 DNA and correlated techniques

Deoxyribonucleic acid (DNA) is the molecule in which the inherited genetic information of every cell of every living organism is encoded. DNA, whose double helical structure was firstly deduced by Watson and Crick in 1953, is made by four nucleobases, shown in **Figure 4.3**, and 2-deoxyribose monosaccharide units alternated with phosphate groups, which form the negative backbone of the DNA strand.[77]

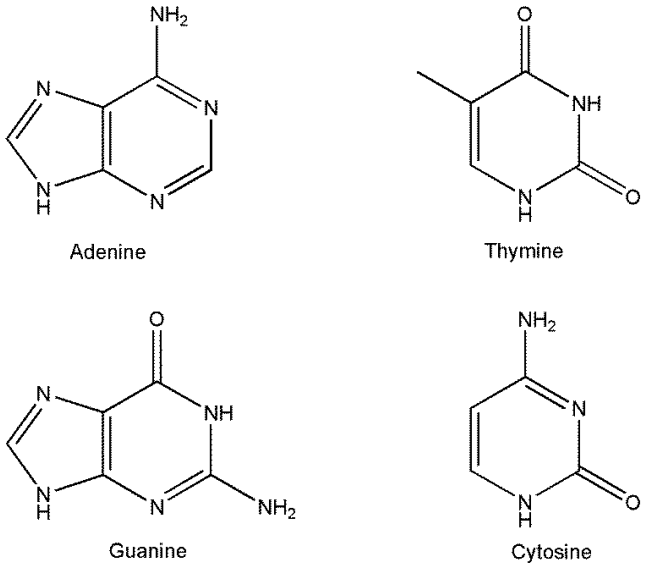

Figure 4.3: Nucleobases found in DNA.

The nucleobases are divided in purines, adenine (A) and guanine (G), and pyrimidines, thymine (T) and cytosine (C). The bases can interact with each other through hydrogen bond interactions and, in particular, the A-T pair is bound by two hydrogen bonds, while the G-C pair has three. This interaction is a fundamental characteristic of the double helix found in the DNA.[77] The sequence of DNA is usually reported following the 5' → 3' direction, according to the numbering of the monosaccharide unit, as shown in **Figure 4.4**.

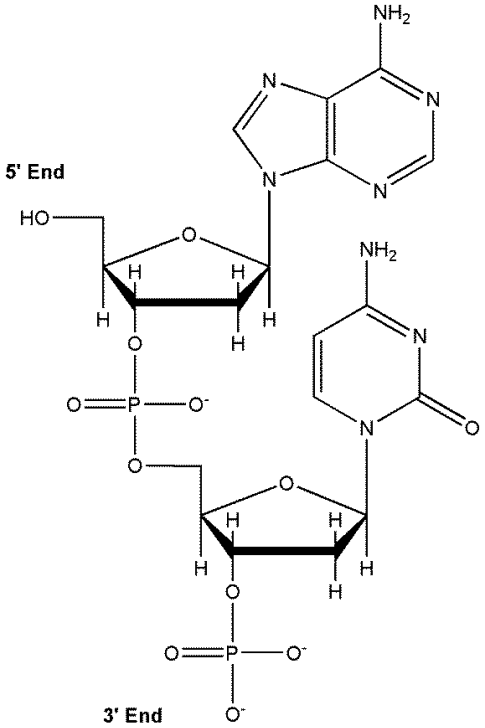

Figure 4.4: Example of a DNA dinucleotide.

The DNA double helix can assume different conformations, called polymorphs, as shown in **Figure 4.5**.

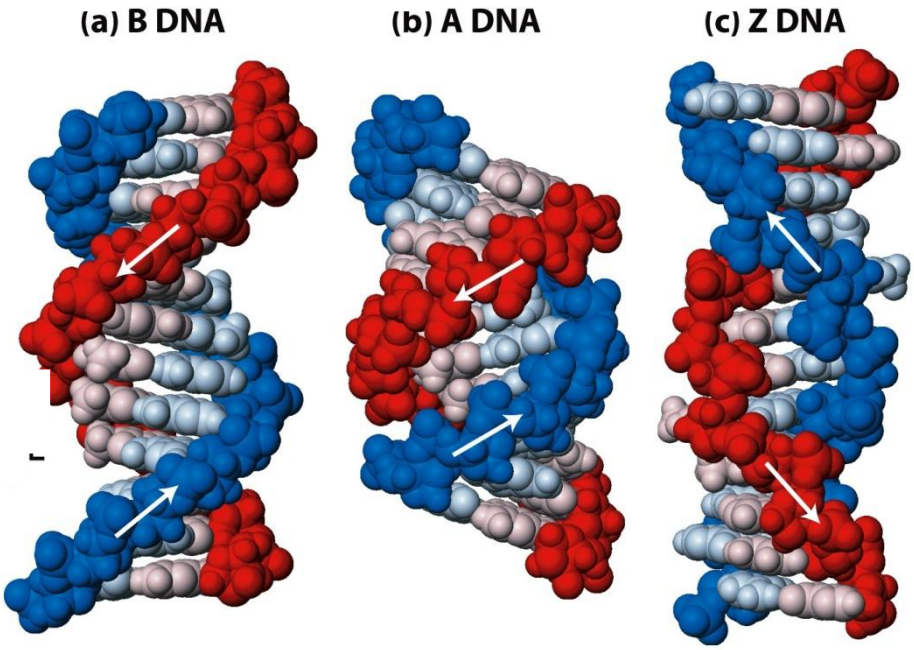

Figure 4.5: B-, A- and Z- form of DNA double helix. The arrows represent the 5' → 3' direction. Image adapted from Lodish *et al*.[249]

The B-DNA is the classic, right-handed Watson and Crick's double helix, characterised by 3.4 Å rise per base pair and 10.1 base pairs per turn of the helix. When the hydration state of the DNA is reduced, the A-form of the DNA can be observed. This structure still shows a right-handed turn, but now the rise-per-base is of only 2.3 Å and every turn of the helix contains 11 base pairs. The Z-DNA form has been reported in the literature for short oligonucleotides and often in conditions of high salt concentration. The Z-DNA conformation presents a left-handed turn, with 12 base pairs per turn of the helix and a rise per base pair of 3.8 Å.[77] The biological function of the different forms of DNA is not completely clear, especially for the Z-DNA. This form is so different from the B-DNA that it is usually not recognised by DNA-binding proteins, although it has been reported that a RNA editing enzyme was able to specifically bind Z-DNA,[250] opening up the possibility that this polymorph of the DNA might have some biological functions. Several other alternative structures of DNA have been characterised and their biological functions explored,[251-253] but they are not going to be the main focus of this discussion.

The interest in DNA and its interaction with different molecules has increased in the last years in the continuous effort to find compounds able to regulate gene expression.[254] Among the various techniques employed for the study, circular and linear dichroism offer a facile procedure to study nucleic acids and their interaction with other molecules.[255] Both techniques are based on the interaction between DNA and polarised light. Circular dichroism (CD) exploits the difference absorption of left- and right-handed circularly-polarised light by chiral molecules.[256] For this reason, circular dichroism is highly suited for DNA. The double helix of the DNA is a source of very high asymmetry and gives therefore very intense CD spectra.[256] The CD spectra of DNA are usually recorded in the UV/Vis range and this technique is very sensitive to conformational changes in the DNA structure, and for this reason it is often used to study modifications of the secondary structure of DNA.[257-259] As an example, the left-handed Z-DNA was observed for the first time during CD experiments.[260] Linear dichroism (LD), on the other hand, exploits the difference in absorption of parallel and perpendicular polarised light by oriented molecules. Electronic transitions in isolated molecules usually happen in a particular direction,

but when the molecules are in solution, their random arrangement in the solvent causes the absorption to be the same regardless of the direction of the light. If the molecules are mostly oriented in a particular direction, however, the absorption will change according to the direction of the incident light beam.[256, 261] For this reason, LD is very suited for molecules that can be easily oriented, like fibres or long polymers, which can be oriented using a flow apparatus, or polymeric electrolytes, which can be oriented with an electric field.[256] If the binding of molecules to the DNA affects its orientation, a change in the absorption of the light is obtained and, hence, also a change in the LD spectrum is visible. For these reasons, linear dichroism is often used, together with circular dichroism, to study the interaction between DNA and other molecules.[262-263] An extensive review on this technique and its use in the study of nucleic acids has been published by Nordén *et al.*.[264]

4.2 *In vitro* evaluation of tachpyr and Fe assays

The cytotoxicity of tachpyr **[3b]** was evaluated via MTT assay against A549 human adenocarcinoma and A2780 human ovarian cancer cell lines in order to compare the activity against these two cell lines with the results reported in the literature (IC_{50} = 4.6 ± 2.0 μM).[133]

The effect of tachpyr on cells was very noticeable when cells were observed with a microscope. Addition of **[3b]** to the cell culture caused a complete change in the appearance of the cells, as shown in **Figure 4.6**. The cells became small, dark masses and their number decreased clearly upon addition of tachpyr. The loss of viability was usually clear after 20-24 h from addition.

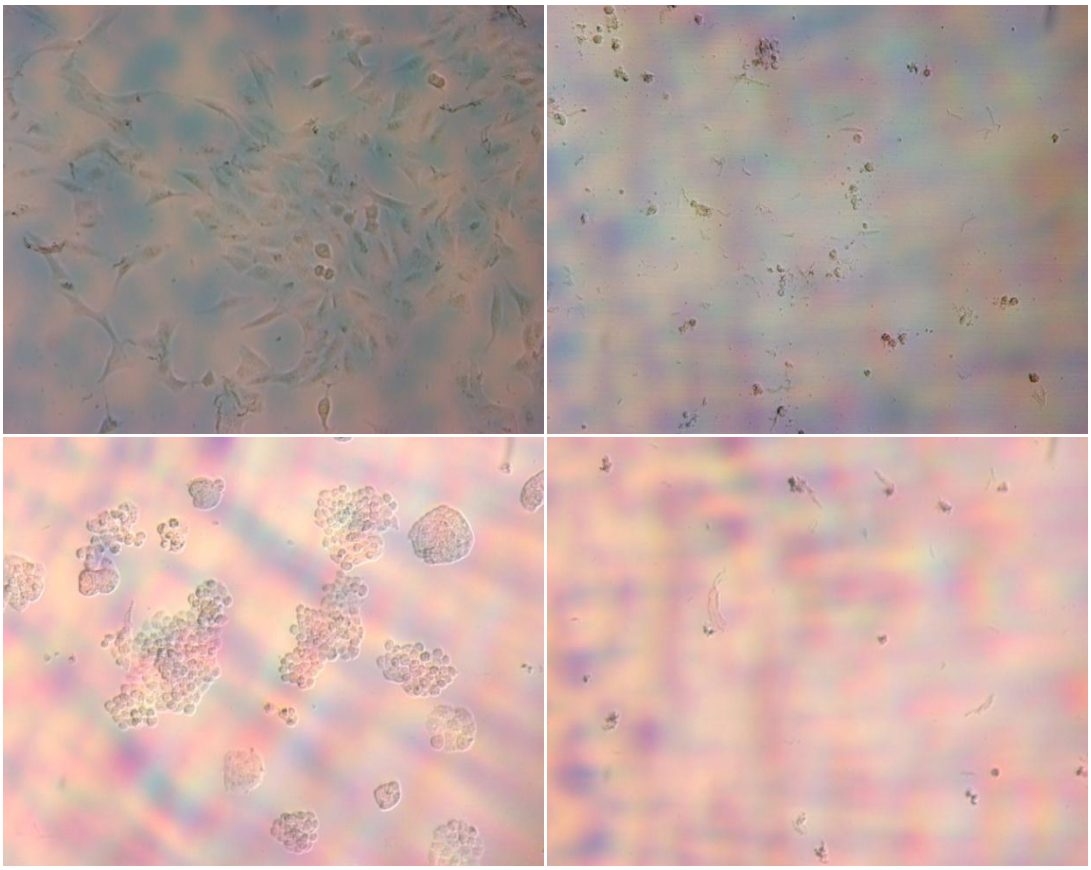

Figure 4.6: Pictures of cells before and after addition of tachpyr **[3b]** and 72 h incubation. Top, A549 lung cells before (left) and after (right) addition. Bottom, A2780 ovarian cells before (left) and after (right) addition.

The MTT tests were performed according to the protocol described in section **4.1.1.1** and **Chapter 6** and repeated in triplicate on both cell lines, resulting in an average IC_{50} value of 4.99 ± 0.02 μM against A549 and 4.01 ± 0.03 μM against A2780 cells, in line with the reported value of 4.6 ± 2.0 μM, obtained against MBT2 mouse bladder tumour cells.[133] **Figure 4.7** shows an example of IC_{50} plots of tachpyr against the two cell lines.

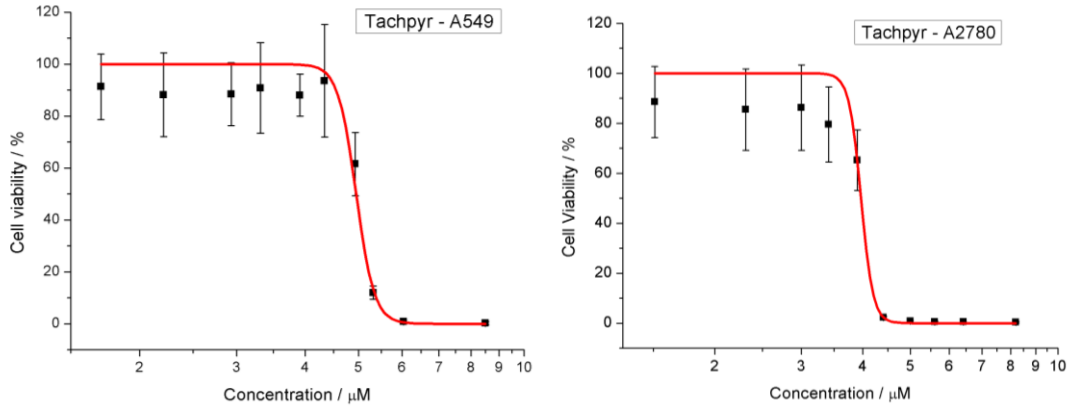

Figure 4.7: IC_{50} graphs of tachpyr **[3b]** against A549 (left) and A2780 (right) cells.

The *in vitro* tests of tachpyr against cancer cells highlighted a distinctive property of this compound. The profile of the fitted sigmoidal line was shown to be sharp, going from 100% to 0% cell viability within a small concentration range (2-3 μM). The steepness of the sigmoid can be expressed by the value of the *power* (*p*), which can be obtained from the equation of the fitted sigmoid, shown in **Equation 4.2**. The higher the value of *p*, the sharper the sigmoid is.

$$y = \frac{100}{1 + \left(\frac{x}{\mathrm{IC}_{50}}\right)^{p}}$$

Equation 4.2: Equation of the fitted sigmoidal line.

A profile like the one shown in **Figure 4.2** is not ideal for a candidate compound to therapy, because the therapeutical concentration is restricted to a very small range. This implies that the toxic dose can be too close to the active dose needed, which would make the compound dangerous to use. Similar cases are very rare in therapy, with probably the only main exception represented by digoxin, which can illustrate how the measure of *p* is used. Digoxin is a compound used to treat various heart conditions, the therapeutic range of which is 0.8-1.9 ng/mL.[265] A small therapeutic range is accepted for therapy only if the advantages derived from the use of that molecule overcome the risks of toxicity, as in the case of digoxin.

To compare the activity of tachpyr (and the other tach-based compounds) to commercial anti-cancer drugs, *cis*-diaminodichloroplatinum, cisplatin, was used as a

reference for activity against these cell lines. Cisplatin was tested in the same experimental conditions employed for the tach-derivatives and an example of viability plot is shown in **Figure 4.8**.

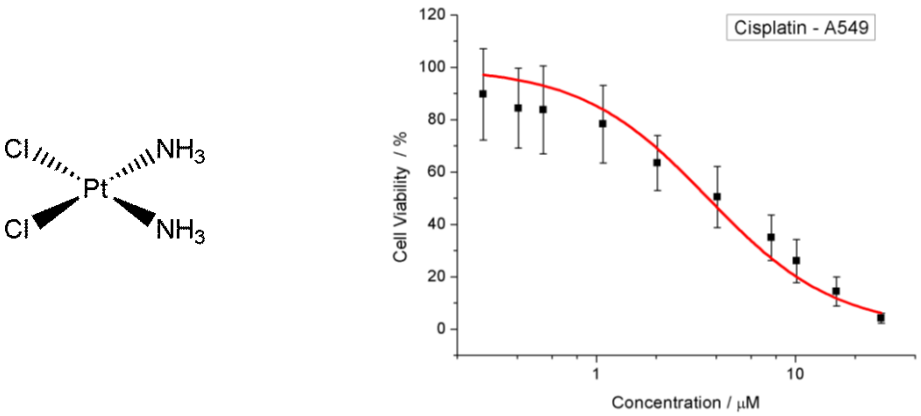

Figure 4.8: Structure of cisplatin (left) and its IC_{50} plot against A549 cells (right).

The viability plot of cisplatin shows clearly the difference in the shape of the sigmoid compared to tachpyr. IC_{50} values and *p* values for tachpyr and cisplatin against the two cells lines are reported in **Table 4.1**.

Compound	**A549**		**A2780**	
	IC_{50} /μM	***p***	**IC_{50} /μM**	***p***
Tachpyr **[3b]**	4.99 ± 0.02	29.9 ± 1.9	4.01 ± 0.03	39.4 ± 2.4
Cisplatin	2.85 ± 0.24	1.3 ± 0.1	0.40 ± 0.01	1.0 ± 0.1

Table 4.1: Table of IC_{50} and power values for tachpyr **[3b]** and cisplatin.

It should be noted that possible activation processes of cisplatin (cf. section **3.1**) might play a role in the resulting cytotoxicity profile. Nevertheless, cisplatin shows a better activity profile against the cancer cells than tachpyr, with a shallow profile of the dose-response curve. It has to be noticed that the value of *p* is not necessarily related to the range of adverse side effects shown by a compound, but it is merely an indication of the possible safety range related to a molecule. Furthermore, *in vivo* absorption processes and interaction with plasma proteins can greatly alter the pharmacokinetics of a molecule. For this reason, the value of *p* is usually not reported in the literature, so no comparisons can be done with other anti-cancer compounds.

Improving the activity profile of tachpyr was one of the challenges of the project and for this reason the metal complexes presented in **Chapter 3** were made and tested. The hypothesis was that addition of a metal to the free ligand would, on one hand, add a dissociation step to the cytotoxic mechanism, possibly slowing down and tuning the activity of the free ligand and, on the other hand, addition of a toxic metal could improve the overall activity against cancer cells. As reported in section **3.4**, metal complexes of tachpyr surprisingly did not show significant cytotoxicity, therefore more detailed investigation of the mechanism of action was performed. As described in **Chapter 1**, the reported mechanism of action[133-136] for tachpyr involves iron chelation and apoptosis resulting from iron deprivation, therefore the starting point for a further investigation was a study of how the activity profile of tachpyr changed upon addition of different concentrations of iron.

A series of experiments was therefore designed to further investigate the possible interaction between tachpyr and iron in solution. Iron(II) sulfate heptahydrate was added to the plate where cells were incubated and the IC_{50} of tachpyr evaluated by MTT assay. The main purpose of the experiments was to evaluate how the shape of the sigmoidal curve and the IC_{50} value changed depending on the concentration of iron added to the wells. Each plate had two negative controls: cells with added iron solution, but no compound; and cells with no iron and no compound, to monitor any possible effect of iron itself on cell growth. The medium enriched with iron was used to suspend the cells or added to the plate at different times of the assay; the concentration of iron added to the cells was either 47 μM, 94 μM, 188 μM or 377 μM. The Fe-enriched medium was sterile-filtered prior of use on the cells and the final concentration of Fe in the culture medium was confirmed by atomic absorption spectroscopy (AAS).

Furthermore, to evaluate if the moment of addition of iron had an influence on the result, the metal ion was added at different stages of the assay:

- with the cell suspension on day 1 of the assay;
- with tachpyr on day 2, either pre-incubating the solutions of iron and tachpyr together before adding the mixture to the cells or adding the Fe solution first,

followed by tachpyr;

- 8 h after addition of tachpyr to the cells.

The experiment reported by Zhao *et al.*[134] was also repeated: cells were plated in medium enriched with 200 μM Fe for 24 h, then the medium was removed, the cells were washed with phosphate buffer saline (PBS) and tachpyr was added in Fe-free medium. Detailed methods can be found in **Chapter 6** and all IC_{50} values are reported in the **Appendix**. Examples of IC_{50} plots and a table of illustrative experiments are shown in **Figure 4.9**, **Table 4.2** and **Table 4.3**.

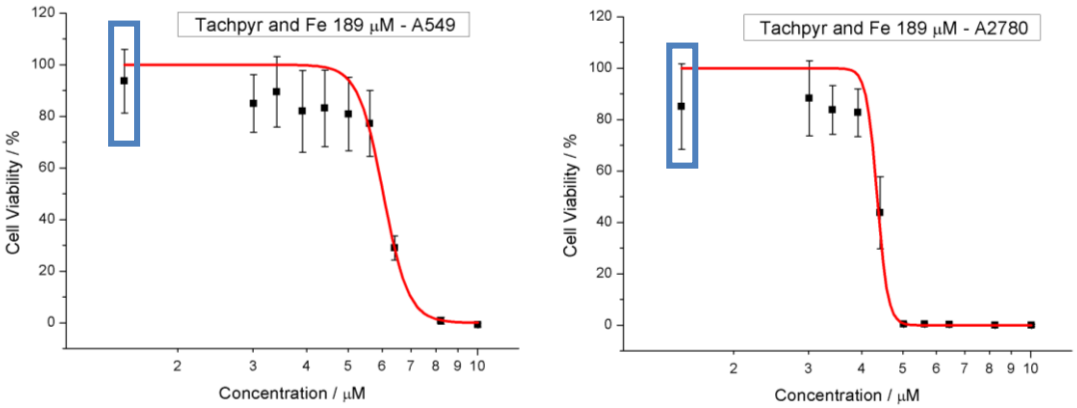

Figure 4.9: Cell viability plots of tachpyr **[3b]** in the presence of 189 μM of iron against A549 (left) and A2780 (right) cells. The graphs are referred to addition of Fe on day 2 of the assay followed by tachpyr. In the box, the value of viability of the negative control with Fe.

Iron concentration / μM	IC_{50} / μM - A549	IC_{50} / μM - A2780
0	4.99 ± 0.02	4.01 ± 0.02
47	5.59 ± 0.15	4.40 ± 0.02
94	5.28 ± 0.14	4.18 ± 0.12
189	6.46 ± 0.15	4.50 ± 0.02
377	7.27 ± 0.34	5.26 ± 0.14

Table 4.2: Selected IC_{50} values of tachpyr **[3b]** against A549 and A2780 cells in the presence of increasing concentrations of iron. The values are referred to addition of Fe with tachpyr on day 2 of the experiment.

Moment of Fe addition	IC_{50} / µM - A549	IC_{50} / µM - A2780
day 1	5.02 ± 0.09	2.98 ± 0.07
day 2, Fe first-then **[3b]**	6.03 ± 0.15	4.35 ± 0.08
day 2, Fe incubated with **[3b]**	6.46 ± 0.15	4.50 ± 0.02
day 2, 8 h after **[3b]**	5.27 ± 0.16	2.03 ± 0.17

Table 4.3: Selected IC_{50} values of tachpyr **[3b]** against A549 and A2780 cells in the presence of iron 189 µM added at different times of the assay.

In all cases, the activity profile and IC_{50} values of tachpyr were not or very little affected by the concentration of iron in the plate and the time of addition of the metal. The presence of iron did not generally affect the cell viability in the controls; a partial loss of viability could be observed only when the iron enriched medium was used to plate the cells on day 1 of the assay. **Figure 4.9** shows that the shape of the fitted sigmoidal line is not affected by the presence of iron if compared to the experiment with no iron in the culture medium (cf. **Figure 4.7**). In the same way, the IC_{50} values of tachpyr against the two cell lines show only a very small change upon increasing concentrations of iron or time of addition of the metal, **Table 4.2** and **Table 4.3**. The change in IC_{50} can be plotted against the concentration of Fe added to the cells to give the graph shown in **Figure 4.10**.

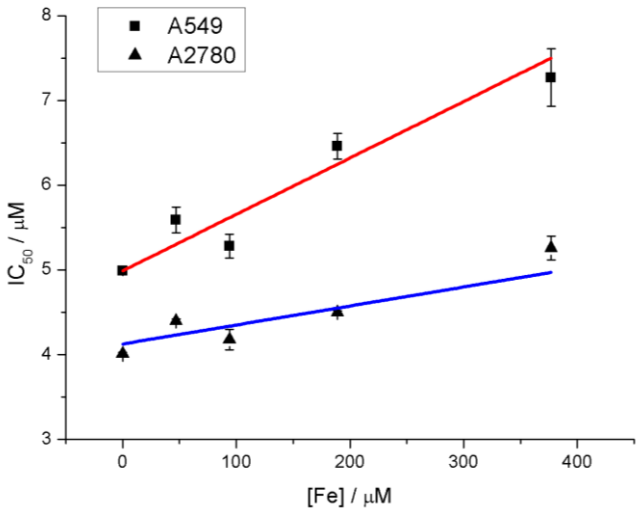

Figure 4.10: IC_{50} values of tachpyr **[3b]** against Fe concentration. The data refers to the addition of Fe with tachpyr on day 2 of the experiment.

As shown above, the change in IC_{50} value follows the increase in iron concentration and a line can be fitted for the two sets of data, with R^2 values of 0.59 and 0.90 for A549 and A2780 data, respectively. However, the IC_{50} values increased by a maximum of 3 μM, which is almost negligible if considered that the Fe concentration ramped from 0 to 400 μM and that the lowest concentration of iron is about five times higher than the highest concentration of tachpyr.

The results obtained from the other experiments, in which iron was added at different moments of the assay, are very similar to what is reported above. Also the repetition of the experiment reported by Zhao *et al.*[134] gave completely different results from those published in the original paper, with no loss of activity detected for compound **[3b]** when Fe was added. These results show that pre-treatment with iron, as well as presence of iron in the extracellular medium, is not able to inhibit the cytotoxic activity of tachpyr **[3b]**. The results are even more surprising if it is considered that complexation between iron and **[3b]** is essentially instantaneous: addition of Fe(II) to a solution of tachpyr shows an immediate change of colour from colourless to a dark red, sign of successful formation of the metal complex, as also reported by Park *et al.*[135] Also complexation with Fe(III) causes an immediate change of colour of the colourless tachpyr solution to a dark emerald green. Therefore, a change in the IC_{50} value was expected at least when iron and tachpyr were pre-incubated together before addition to the cells if iron was involved in the mechanism of action. This result is clearly in contrast with that reported in the literature,[133-136] but the data in our hands seem to suggest that the extracellular concentration of iron does not play any particular role on the activity of tachpyr and that chelation is unlikely to be the only mechanism of action. The reasons for the difference in the experimental results compared to those reported by Zhao *et al.* against SUM149 breast cancer cells[134] are not clear, but the experiments reported in this chapter were repeated several times and no change in the activity of tachpyr was ever observed.

If the concentration of iron is the limiting factor in the growth of cells, then on increasing the concentration of iron in solution a change in either the IC_{50} value or the slope of the sigmoid would have been expected in the case of complexation between

tachpyr and the metal ion. However, very little difference can be observed. The intracellular concentration of iron is well controlled by cells,[266] therefore addition of iron to the cell culture medium does not affect the amount of iron present in the cells. However, the extra-iron added to the medium should prevent cell death due to iron deprivation, either binding tachpyr before entering the cells or re-supplying the cells with the iron sequestered by the ligand. The cytotoxic activity of tachpyr should hence be completely suppressed in these conditions, especially considering that iron is in great excess. As compound **[3b]** keeps its activity, chelation can be considered not important for cytotoxicity.

These experiments therefore placed doubts on the reported mechanism of action of compound **[3b]**. Further investigation was needed to evaluate different possible cellular targets as a better understanding of the mechanism of action is a main requirement to improve the activity and the selectivity towards cancer cells.

4.3 Evaluation of the mechanism of action of tachpyr

In the light of the previous results, showing that tachpyr does not inhibit tumour cells growth by iron sequestration, it was decided to investigate other modes of action. The possible targets for tachpyr inside the cells can vary from enzymes to DNA to various kind of proteins, without considering possible disruption of cell pathways.

In the first instance, analysis of the structure of tachpyr gave some clues as to the feasible targets. Some important features of this compound need to be highlighted: first of all, the planar, yet still quite flexible, structure of compound **[3b]**. The tach moiety and the free rotation of the pyridine arms around the amine bond gives a few degrees of flexibility for possible binding to biomolecules. In addition, the presence of the planar aromatic rings as N-substituents on the tach moiety is optimal for possible π-stacking interactions with other aromatic rings of amino acids in proteins or intercalation to DNA nucleotides. Another important structural characteristic of tachpyr is the presence of the nitrogen atoms of the tach moiety, which, due to their

basic nature (pK_a of secondary ammonium ion = 10 - 11),[267] will be protonated in biological conditions. The cation so formed can interact with negatively charged molecules inside the cells, making negatively charged phosphate within the backbone of DNA and other ribonucleic acids a possible target.

Whilst the pyridine nitrogen atoms are unlikely to be protonated at pH 7 (pK_a of pyridium = 5.2),[267] the tach amines give tachpyr three possible sites of protonation, making the molecule structurally quite similar to the natural polyamines, shown in **Figure 4.11**.

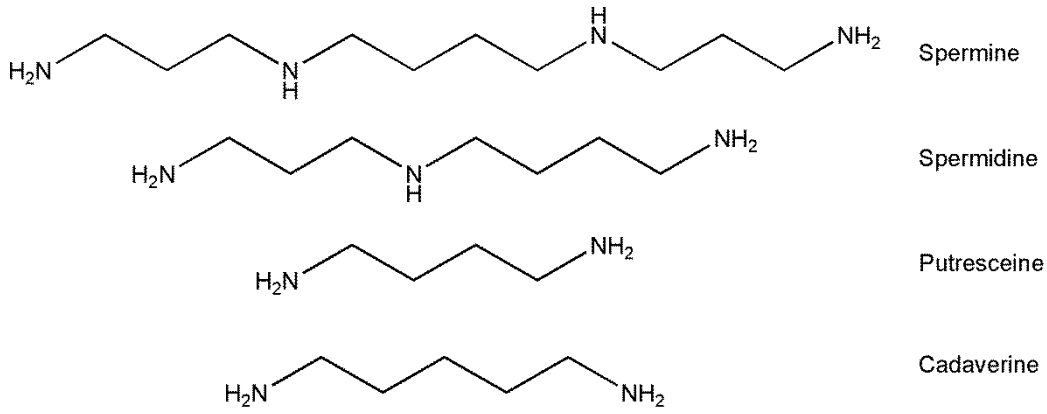

Figure 4.11: Natural polyamines.

It is well established that natural polyamines play a very important role in the cell cycle and they are able to interact and stabilise DNA,[268] with the binding getting stronger with the number of amine groups.[269] The metabolism of the natural polyamines is highly controlled and is regulated by several feedback mechanisms, and if, for any reason, the natural polyamine concentration in cells is too low, apoptosis occurs within a few cell cycles.[268, 270-271] Natural polyamines seem to play also a role in cancer growth[272-273] and for this reason their metabolic pathway has been considered as a possible target for cancer treatment.[274] Some spermine derivatives are already reported in the literature as potential anti-cancer agents interfering with the metabolism of the natural polyamine.[275-276] The molecules shown in **Figure 4.12**, for example, are cytotoxic against cancer cell in the range of 1-10 μM.[274]

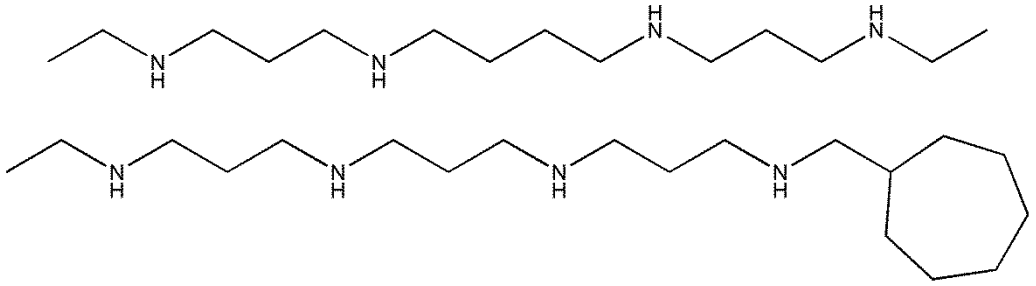

Figure 4.12: Examples of cytotoxic spermine derivatives.[274]

The mechanism of action of spermine-like derivatives seems to involve depletion of the natural polyamine pool. These synthetic derivatives up-regulate all biochemical pathways involving spermine, inhibiting its synthesis and uptake and accelerating its catabolism. They can be recognised as spermine by the cell, but they cannot achieve the same biological functions that spermine has, leading to apoptosis.[268]

One of the hypothesis considered evaluating the potential sites of interaction of tachpyr was therefore the possibility that **[3b]** could interfere with the polyamine metabolism acting as a spermine mimic, inhibiting the polyamine cycle and/or interacting with the phosphate groups of the DNA, leading to cell apoptosis.

For these reasons, the hypothesis that DNA could be the target of the action was investigated and DNA was used for the preliminary study of the mechanism of action of compound **[3b]**.

4.3.1 Interaction with DNA

The first step in the investigation of the mechanism of action of tachpyr was to establish if it could bind to DNA. Various techniques were employed, with particular focus on circular and linear dichroism.

Circular dichroism (CD) was used to evaluate the effect of tachpyr on the structure of DNA. A titration was performed adding increasing amounts of the test compound to a buffered solution of calf thymus (ct)-DNA at a constant concentration of 300 μM bp (bp = base pair). As a control, tach **[2]**, inactive against A549 and A2780 cells (IC_{50} >

250 μM, see section **4.3.2**), was also tested, in order to compare the results from the cytotoxic compound **[3b]** with the non-cytotoxic compound **[2]**. The CD spectra of the titrations are shown in **Figure 4.13**.

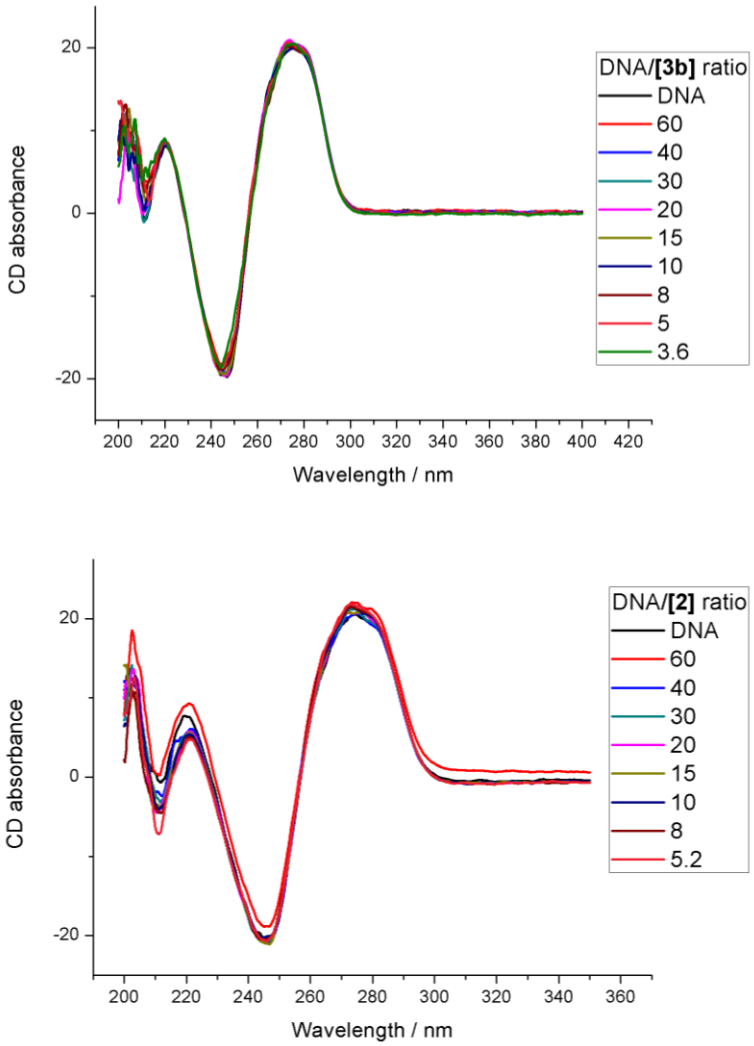

Figure 4.13: Plots of CD titrations of ct-DNA with tachpyr **[3b]** (top) and tach **[2]** (bottom).

As evident from **Figure 4.13**, the CD spectra did not show changes for either compound across the range of concentration tested. This result indicates that tachpyr and tach do not interfere with the secondary structure of DNA, unwinding or disrupting the double helix.

Different results were obtained by linear dichroism (LD), again using ct-DNA at a constant concentration of 300 μM bp and titrating with either tachpyr or tach. This

time, a change in the spectra was recorded for both compounds (**Figure 4.14**), in particular for tachpyr.

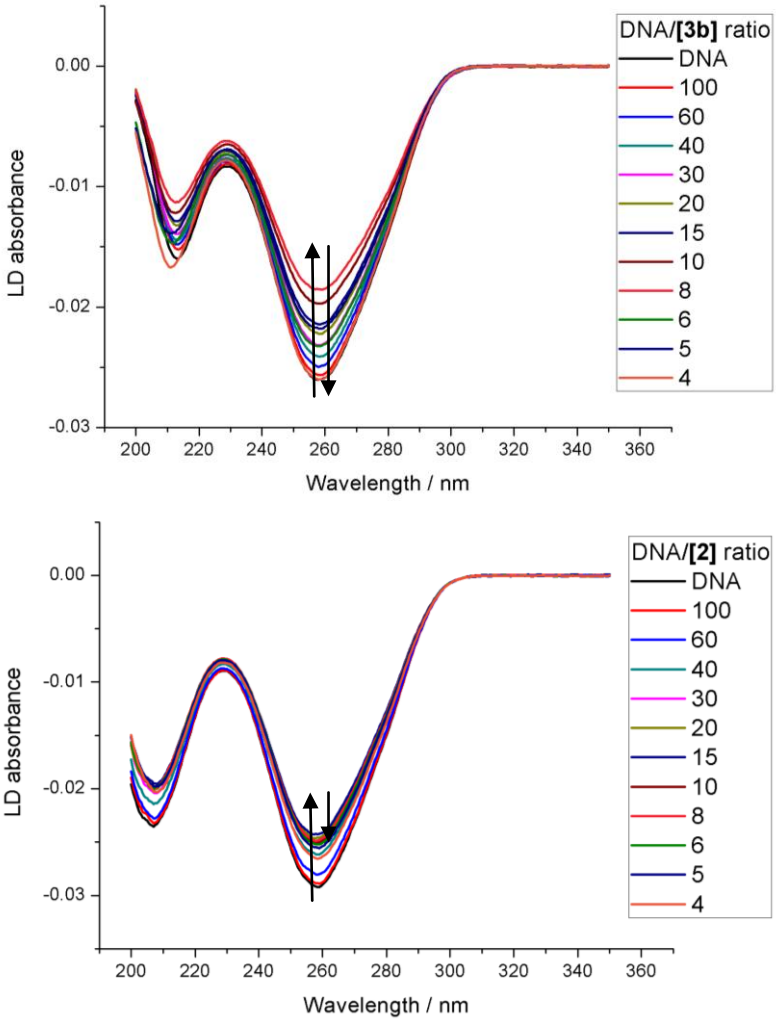

Figure 4.14: Plots of LD titrations of ct-DNA with tachpyr **[3b]** (top) and tach **[2]** (bottom). The arrows exemplify the direction and relative intensity of the LD change (e.g. arrow up shows a positive change in the LD absorbance).

The change in the LD spectra is due to a loss of orientation, consistent with the DNA losing linearity on interaction with the compound. Although both compounds showed the ability to interact with DNA, the cytotoxic tachpyr gave a greater shift in the recorded LD signals. In particular, it is possible to observe two different interactions, as outlined by plotting the LD absorbance against concentration or LD absorbance against the ratio DNA/compound (**Figure 4.15**).

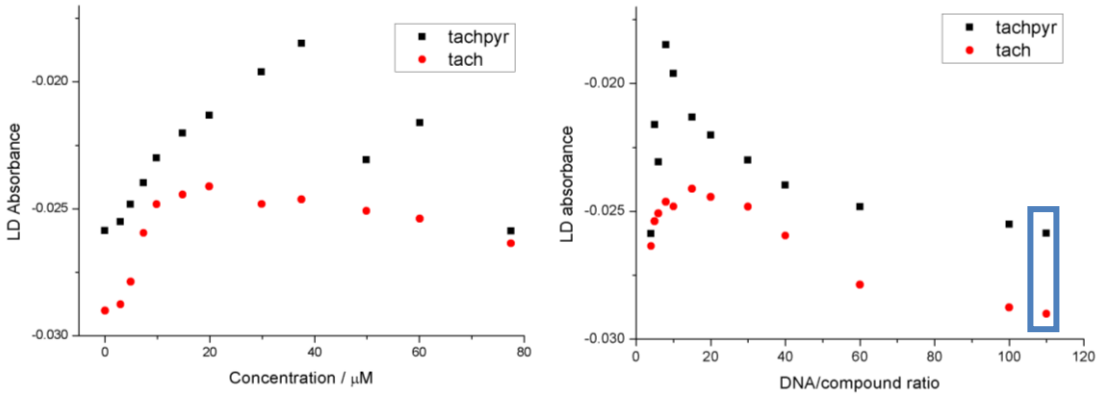

Figure 4.15: Plots of LD absorbance against concentration (left) or DNA/compound ratio (right) for tachpyr **[3b]** and tach **[2]**. In the box, the absorbance of DNA alone.

The plots show clearly that the effect of tachpyr is greater than the change caused by tach. The graphs shown in **Figure 4.15** are complementary and, observing the plot of the absorbance against DNA/compound ratio, it is possible to notice that both compounds gave the maximum change when they were in a 8:1 ratio with DNA. After that point, tach shows just a small change, while tachpyr presumably starts a second kind of interaction which reverses the effect on the LD spectrum. What is evident from the LD experiments is that these molecules are able to interact with DNA and disrupt the linearity of the double helix, but not its helicity. Spermine was shown to cause a change in the LD spectrum of DNA, although the effect did not reverse upon further addition of spermine.[277] The spermine derivative shown in **Figure 4.16**, instead, gave LD spectra similar to those observed for tachpyr, with a change in the direction of the LD signal at high concentration of spermine derivative,[277] similar to what happened during the titration with compound **[3b]**.

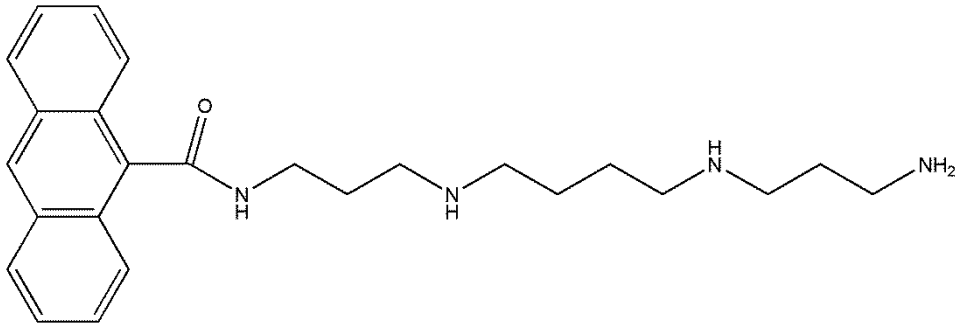

Figure 4.16: Structure of the spermine derivative anthracene-9-carbonyl-*N*'-spermine.

LD experiments gave evidence that tachpyr might potentially work as a spermine-mimic, binding to the DNA and causing apoptosis. The structure of **[3b]** has a main difference if compared to spermine, which is due to the presence of the aromatic rings. From a structural point of view, tachpyr presents several similarities with the anthracene derivative shown in **Figure 4.16**, which was found to be a groove binder rather than an intercalator,[277] despite the presence of the flat aromatic anthracene moiety. However, for tachpyr, the possibility that a spermine-like kind of binding directs the compound to the DNA, where intercalation of the pyridine rings to the base pairs might happen, could not be excluded. In order to gain some information about this hypothesis, an ethidium bromide displacement titration was performed.

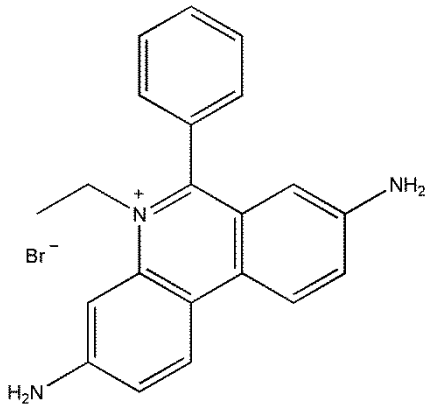

Figure 4.17: Ethidium bromide.

Ethidium bromide displacement is often used to evaluate possible intercalating agents,[70, 278-279] exploiting the change of fluorescence when ethidium bromide (**Figure 4.17**) is displaced from its binding with DNA. The fluorescence of ethidium bromide in solution is quenched by the interaction with the solvent, but this compound shows strong fluorescence in the presence of DNA due to the intercalation of the molecule between base pairs. In the presence of other intercalating agents able to displace the molecule from its binding sites with DNA, fluorescence is quenched and a decrease in the maximum of emission can be measured.[71, 280-281] Ethidium bromide was added to ct-DNA and the fluorescence measured before starting the titration. Tachpyr **[3b]** or tach **[2]** were added up to a 1:1 ratio with ethidium bromide, whilst the concentrations of ethidium bromide and DNA were kept constant during the titration at 15 μM and 12 μM, respectively. The experiments did not show any change in the fluorescent

emission of ethidium bromide for either compound. This result is not surprising for compound **[2]**, which does not possess aromatic rings, while it suggests that tachpyr is not an intercalating agent, that its binding constant is lower than that of ethidium bromide, or that the binding of tachpyr does not affect the binding of ethidium bromide. The first option would support a spermine-like binding to the DNA and also the results of the CD experiments, because intercalation causes major changes in the CD spectra, while backbone and groove binding is typically not visualised by CD.[282]

Agarose gel electrophoresis was carried out on compounds **[3b]** and **[2]** mixed with pBR-322 circular plasmid DNA, to evaluate a possible change in the coiling of the DNA double helix. Tachpyr or tach were incubated with pBR-322 plasmid DNA for 3 h at 37 °C at different DNA/compound ratios. The solutions were then analysed using gel electrophoresis and the results visualised with ethidium bromide, as shown in **Figure 4.18**.

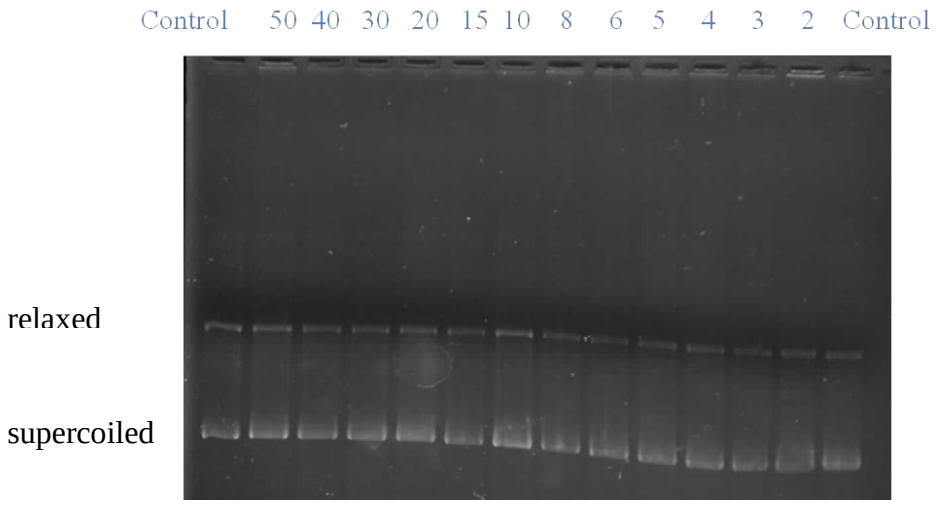

Figure 4.18: Agarose gel of tachpyr **[3b]** and plasmid DNA. Controls contained DNA only. The numbers refer to the DNA/tachpyr ratio.

Development of the agarose gel did not show change in the supercoiled/relaxed ratio of the DNA compared to the controls for either compound, which is indicative that **[3b]** and **[2]** did not affect the coiling of the circular plasmid in the experimental conditions used. The results support the hypothesis of a mechanism of action which does not involve intercalation, because increase in the supercoiling of plasmid DNA is not shown.

4.3.2 Structural modifications

Another method to gain information about the mechanism of action of a compound is to modify its structure and evaluate structure-activity relationships (SARs), and so to highlight which are the principal pharmacophores of the molecule. For this reason, the structure of tachpyr **[3b]** was modified and the compounds presented in **Chapter 2** were made and tested using MTT assay.

Firstly, the pyridyl rings of compound **[3b]** were substituted with different heterocycles to evaluate the role of the heteroatom (section **2.4**); for the same reason, the salicylaldehyde derivatives were prepared (section **2.5**). The nitrogen atom of the pyridine ring of **[3b]** was then completely eliminated in the tachben series (section **2.6**). Finally, mono-N-substituted compounds were made (section **2.7**) and a preliminary evaluation of their activity was performed and compared to the three-armed derivatives. A scheme of the structural modifications made on the tach moiety is shown in **Figure 4.19**.

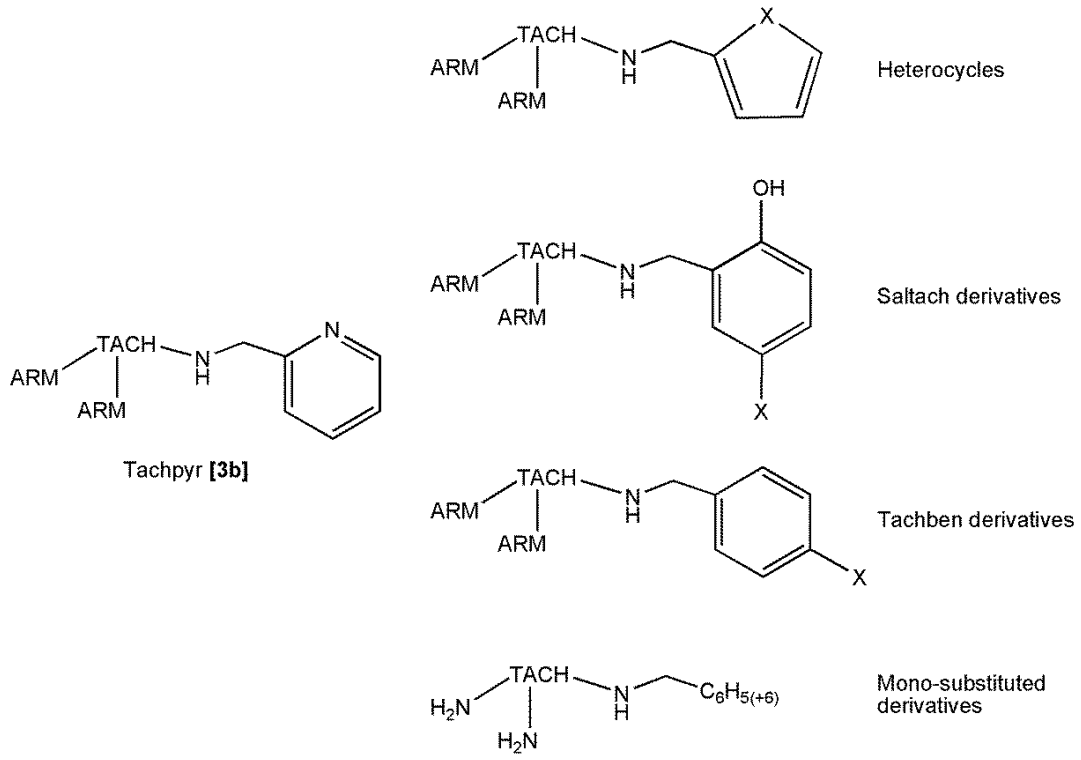

Figure 4.19: Scheme of the structural modifications of the tachpyr ligand.

The activity of tach **[2]** was also evaluated, both to have information about the cytotoxicity of the non-substituted molecule and as a control of starting material. Similarly, pyridine-2-carboxaldehyde and furfural were evaluated for activity as negative controls, to ensure that the toxicity shown by the N-substituted derivatives was not due to the parental aldehyde after hydrolysis in the cells.

Unfortunately, the saltach derivatives **[6b]**–**[9b]** (section **2.5**) were completely insoluble in culture medium, even in the presence of 1% DMSO, therefore they could not be tested for activity. The lack of solubility of these compounds could be due to the intramolecular hydrogen bond between the tach amines and the OH group of the aromatic ring, highlighted in the crystal structures of these derivatives (section **2.5.2**). In an attempt to increase the water solubility of these compounds and so to evaluate their cytotoxic effect, the HCl salt of compound **[7b]**, 5-Cl-saltach, was made, as described in section **2.5.2**. Compound **[7b]HCl** showed complete water solubility up to mM concentration, but it was very poorly soluble in the buffered medium used for the biological tests. The concentration of **[7b]HCl** in phosphate buffer saline (PBS) solution was evaluated by UV/Vis absorption. **[7b]HCl** was dissolved in water at different concentrations and the UV/Vis spectra recorded and used to determine the value of the molar extinction coefficients (ε = 21077 $dm^3 \cdot mol^{-1} \cdot cm^{-1}$ for maximum at 228 nm, ε = 8168 $dm^3 \cdot mol^{-1} \cdot cm^{-1}$ for maximum at 286 nm). PBS was then added to 5-Cl-saltach·3HCl and the mixture was left for 16 h, after which time it was filtered to eliminate the undissolved **[7b]HCl**. The UV/Vis spectrum of the obtained solution was measured, from which it was possible to calculate the concentration of tach-derivative in PBS. To do so the molar extinction coefficients calculated from water were used as a first approximation, although we were aware that the change of pH could have an impact on them. The concentration of **[7b]HCl** in PBS was found to be 11 µM, therefore very low, especially considering that, due to the MTT protocol, the concentration of compound in solution is halved upon addition to the cells, hence the highest concentration added to the cells could not exceed 5.5 µM. However, compound **[7b]HCl** was tested against A549 cells, but it was found to be completely inactive at such concentration. For this reason, the saltach derivatives were not further developed.

Except for the saltach derivatives, all the amines presented in **Chapter 2** were tested in triplicate against A549 and A2780 cells and the results are reported in **Table 4.4**. The mono-armed derivatives were tested only on one plate against A549 cells due to very low yields obtained from the reaction (section **2.7**).

Compound	**IC_{50} / µM - A549**	**IC_{50} / µM - A2780**
Cisplatin	2.85 ± 0.24	0.40 ± 0.01
Tach **[2]**	> 250	> 250
Tachpyr **[3b]**	4.99 ± 0.02	4.01 ± 0.03
Tachprl **[4b]**	188.2 ± 21.4	147.7 ± 7.1
Tachfur **[5b]**	34.6 ± 2.6	85.2 ± 1.0
Tachben **[10b]**	6.65 ± 0.21	3.03 ± 0.10
4-NMe_2-tachben **[11b]**	1.03 ± 0.03	1.24 ± 0.02
4-OMe-tachben **[12b]**	2.07 ± 0.08	1.72 ± 0.03
4-F-tachben **[13b]**	3.49 ± 0.06	2.62 ± 0.04
4-CF_3-tachben **[15b]**	2.42 ± 0.09	6.06 ± 0.07
Tachmonoben **[16]**	73.1 ± 6.4	-
Tachmonocyc **[17]**	86.9 ± 11.8	-
Pyridine-2-carboxaldehyde	108.9 ± 13.1	69.0 ± 3.2
Furfural	> 250	> 250

Table 4.4: IC_{50} values for all the compounds tested against A459 and A2780 cells. Values are reported as average of three triplicate tests with their standard deviation. Refer to fold-in page.

Comparisons between the two cell lines cannot be drawn because different cell lines might have different interactions with the same compound (e.g. absorption, membrane proteins, etc.) which would cause a difference in the final IC_{50} value. General trends in the IC_{50} values for all compounds, however, can give some insights on possible structure-activity relationships in the series. Tach **[2]** is completely inactive against cancer cells, but the lack of activity might be due to the inability of compound **[2]** to cross the cell membrane due to its very polar nature. As a control experiment, the water soluble aldehydes pyridine-2-carboxaldehyde and furfural were tested to assess

if they were responsible for the cytotoxic activity after possible hydrolysis of the tach-compound inside the cells, but these were all shown to be inactive. This indicates that the cytotoxicity is probably not due to the singular components of the compounds, but the overall molecule (tach and arms) is the active pharmacophore. Pyridine-2-carboxaldehyde showed mild toxicity, but the IC_{50} value is a lot higher than that of tachpyr to consider the aldehyde as the only responsible for activity.

4.3.2.1 Heterocyclic derivatives

The heterocyclic compounds, tachprl and tachfur, showed very low activity against the cells, with tachprl **[4b]** being almost completely inactive. The change from the basic nitrogen atoms of the pyridine rings in tachpyr (pK_a of pyridinium ion = 5.2)[267] to the acidic pyrrole nitrogen atoms of tachprl (pK_a pyrrolium ion = -3.8)[267] causes a complete loss of activity, which might be due to a different interaction of these two groups with the target molecule. The effect of the arm on the cytotoxicity of compounds **[3b]** and **[4b]** could be rationalised considering that the nature of the two different aromatic rings can have an influence also on the tach nitrogen atoms, as illustrated in **Figure 4.20**. This difference might completely change the interaction with the target by changing the pK_a of the tach amines, which might be crucial if the amine nitrogens are responsible for the cytotoxic activity of the molecule.

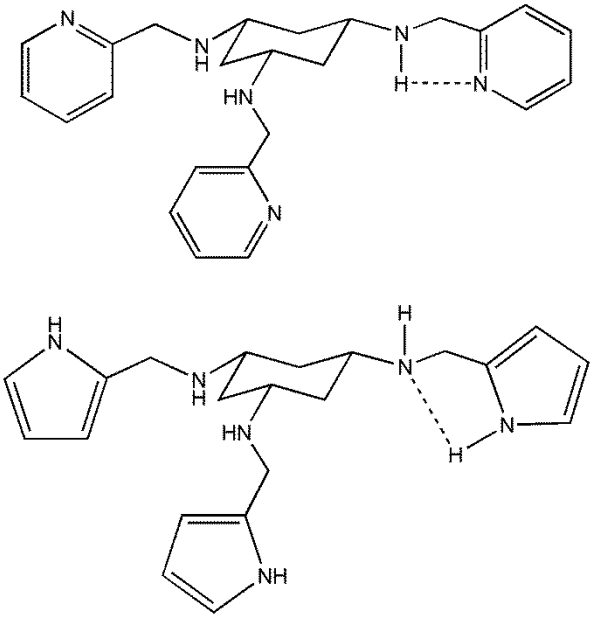

Figure 4.20: Diagram of possible intramolecular hydrogen bond interaction in tachpyr **[3b]** and tachprl **[4b]**.

In compound **[3b]**, the basic nature of the pyridine nitrogen atoms might form an intramolecular hydrogen bond with the tach amines, in which the amine acts as the hydrogen bond donor and the pyridine as the hydrogen bond acceptor. This hydrogen bond would make the lone pair of electrons on the tach amines more available for an interaction with the target molecule or a proton to form the protonated species. On the other hand, in compound **[4b]** the nitrogen atoms of the tach moiety would be the hydrogen bond acceptor while the pyrrole atoms could act as the hydrogen bond donor in case of intramolecular hydrogen bond. In this situation, the lone pair of electrons of the amines would be mostly unavailable to interact with the target/protonation. It should be highlighted that such an intramolecular hydrogen bond was not observed in the crystal structure of compound **[4b]** (section **2.4.2**), but the solid state might not be representative of the equilibria present in solution.

To test the hypothesis that an intramolecular hydrogen bond might be the cause of the lack of activity in tachprl, tachfur **[5b]** was synthesised. If the hypothesis was correct, the presence of a hydrogen bond acceptor on the aromatic rings would allow the compound to re-gain the cytotoxic activity lost with tachprl **[4b]**. As shown in **Table 4.4**, tachfur showed mild activity against the two cell lines, although the IC_{50} values

were not as low as those shown by tachpyr. The experiment seemed to support the hypothesis that the protonated tach amines might be involved in the interaction with the target, however further experiments, such as expanding the library of compounds containing H-bond donor or acceptor groups on the arms, are needed. It should also be noted that, together with the change of heteroatom, the size of the rings was modified, which is another parameter that can affect the activity.

In order to maintain the size of the aromatic ring and add the oxygen atom as in tachfur, the salicylaldehyde series was developed, but for the reasons mentioned above it could not be tested. Furthermore, the crystal structures of these derivatives (**section 2.5.2**) showed that the oxygen atom acts as the hydrogen bond donor in the interaction, therefore these compounds would not be able to test the hypothesis evaluated with tachfur.

4.3.2.2 Tachben derivatives

The change in the IC_{50} values of compounds **[3b]**, **[4b]** and **[5b]** suggests that the heteroatom present on the arm of the derivative influences the activity against cancer cells. The results suggested the next obvious step for the investigation: evaluate if the presence of a heteroatom is crucial for the activity. Tachben **[10b]** was tested and it showed IC_{50} values comparable to tachpyr on both cell lines, as shown in **Table 4.4**. Similarly, all the 4-substituted tachben derivatives showed very high cytotoxicity against both cell lines, in some cases even higher than tachpyr and cisplatin. The result gives important insights about the mechanism of action of tachpyr, showing that the nitrogen atoms of the aromatic rings are clearly not required for activity. The data also support the hypothesis of a mechanism of action not based on iron chelation: the tridentate tachben molecule (or its 4-substituted derivative) is a much weaker ligand for iron than the hexadentate tachpyr, but their cytotoxic activity against the two cell lines is very similar, from which one can infer that the stability of the Fe complex is not relevant for the cytotoxic activity.

The different tachben derivatives (compounds **[11b]-[15b]**) were synthesised also to evaluate if the presence of a substituent in the 4-position of the ring and the electronic

properties of the phenyl ring make a difference in the activity of the compounds. As shown in **Table 4.4**, the change in IC_{50} value is very small within the whole tachben series with no linear correlation between IC_{50} values and chemical properties of the compounds, which shows that the cytotoxic effect of these derivatives is not closely associated with the presence of a 4-substituent or the nature of the substituent. Another piece of information that can be gained from the test of the tachben series concerns the sterics around the site of interaction to accommodate the ligand. The data show that substituents as big as dimethylamino or methoxide can be accommodated when they are in the 4-position, with not distinct preference for a particular substituent over the others. The sterics of the substituents are therefore not important for the interaction with the target. All tachben derivatives showed the same steep sigmoidal fitting as was seen for tachpyr (section **4.2**), suggesting that they are likely to share the same kind of general mechanism of action.

4.3.2.3 Mono-N-substituted derivatives

The importance of the aromatic rings was then evaluated by making the mono-substituted derivatives **[16]** and **[17]**. MTT assays of the unsubstituted tach molecule had shown that the compound does not possess cytotoxic activity up to 250 μM, while, as said, the three-armed compounds can give very good IC_{50} values, which would suggest that the arms help cytotoxicity, either by making tach more lipophilic, hence increasing its ability of crossing membranes, or by actively interacting with the target. Tachmonoben **[16]** was synthesised and tested to verify if mono-substitution gave increased cytotoxicity to compound **[2]** and to have a direct comparison with the equivalent tri-amine tachben **[10b]**. For similar reasons, tachmonocyc **[17]** was tested to assess if aromaticity of the ring played a crucial role. It has to be highlighted that purity of compounds **[16]** and **[17]** could not be confirmed by elemental analysis (see also section **2.7**), therefore their evaluation against cancer cells might have been affected by possible impurities and should hence been seen as a preliminary result. The data in **Table 4.4** shows that both mono-armed derivatives have mild cytotoxicity against A549 cells with comparable IC_{50} values. The presence of at least one arm seems to be necessary to have some cytotoxic action, but having an aromatic rather

than an aliphatic substituent might not be crucial. Although the exact role played by the "arms" is yet to be clarified, their presence seems to improve the activity.

4.3.2.4 SARs conclusions

The analysis of the cytotoxicity of the tach derivatives highlights some key characteristics which these molecules should posses to show cytotoxicity. Firstly, the presence of the arms on the tach moiety is an essential requirement to have at least mild toxicity, although no major differences were shown between aromatic and aliphatic substituents. The presence of the nitrogen atom on the pyridine ring is not crucial to have high toxicity, but the presence of hydrogen bond donors on the arm decreases notably the cytotoxic action of the compound. Finally, substituents on the 4-position of the aromatic rings do not affect the activity and the electronic nature of the substituent was found to be irrelevant for the cytotoxicity. Summarising all these findings together, two main properties seem to be important for the activity: the pK_a of the tach nitrogen atoms and the lipophilicity of the tach derivative. The lipophilicity of a compound is often measured by its water/n-octanol partition coefficient, log*P*,[283] which gives an indication about the ability to cross the biological membrane. The IC_{50} values of the tach derivatives can be plotted against pK_a and log*P* to give the graph shown in **Figure 4.21**.

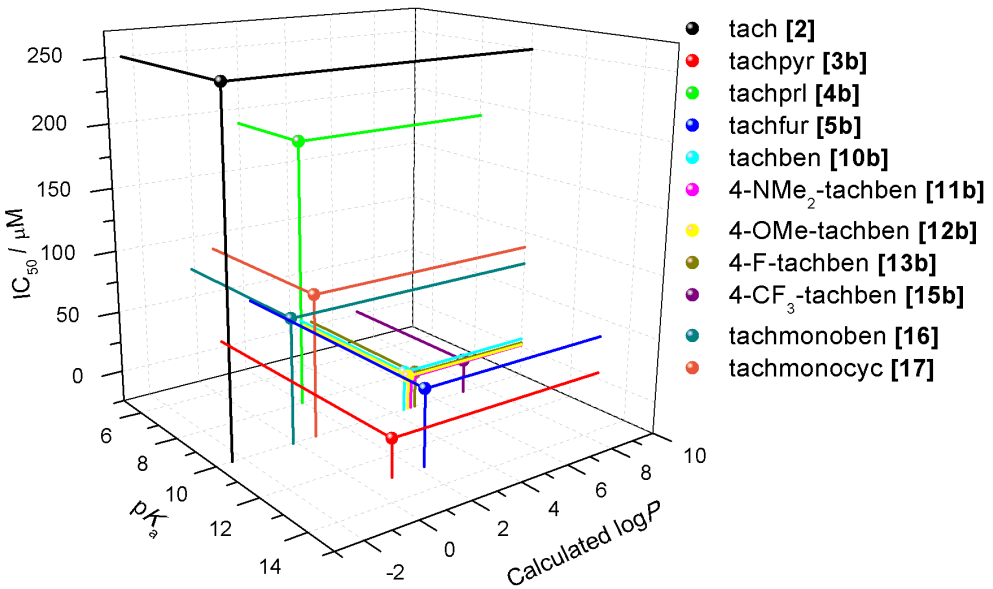

Figure 4.21: Diagram of IC_{50} values against pK_a against log*P* of the tach derivatives. The IC_{50} values were taken from the MTT assays against A549 cells.

The log*P* values for the different compounds were calculated using the Molinspiration Property Calculation Service software. The pK_a values were estimated starting from literature values[267] and should be viewed only as an indication rather than an experimental measure. The pK_a values were set to be equal to the literature value for secondary amines (compounds **[2]** and **[10b]-[17]**, pK_a = 10), higher than the literature value for compounds containing a hydrogen bond acceptor on the arms (compounds **[3b]** and **[5b]**, pK_a = 13), or lower than the literature value for compounds containing a hydrogen bond donor on the arms (compound **[4b]**, pK_a = 8). The graph in **Figure 4.21** shows a possible correlation between the basicity of the amines, the lipophilicity of the compound and the observed IC_{50} value. Most of the active (i.e. low IC_{50} value) compounds appear in the log*P* range between 4 and 7. Log*P* values lower than 4 give rise to poorly active or inactive compounds, unless the loss in lipophilicity is counter weighted by a greater basicity (i.e. higher pK_a), as in the case of tachpyr **[3b]**. It is interesting to notice how compounds with very similar log*P* values, such as **[4b]** and **[5b]** or **[3b]** and **[17]**, show very different cytotoxicity according to the basicity of the amines, which seems to support the hypothesis of a major involvement of the tach moiety in the interaction with the target for all the compounds presented. Although in need of further experiments to validate the hypothesis (e.g. measuring the pK_a and log*P* of the tach compounds and evaluate if a correlation with the toxic activity is present), the pK_a and log*P* properties of the compound should be considered important in the design of cytotoxic tach derivatives.

4.3.3 Crystal structure

The experiments described so far in this chapter showed that tachpyr **[3b]** is able to interact with DNA and this interaction might be responsible for the cytotoxic effect of this compound. In the hope of gaining a deeper understanding of the modality of the binding, which could not be determined from the experiments conducted so far, several attempts of co-crystallising **[3b]** with a short DNA oligonucleotide were made.

One of the crucial points for the experiment was the choice of the oligonucleotide. This choice was made following the hypothesis that tachpyr could bind to the DNA in

a spermine-like fashion, to the phosphate backbone due to the positive charge(s) on the protonated amine nitrogen atoms. If the hypothesis was correct, the binding to DNA would be mainly non-specific, so independent of the base pair sequence. A non-specific binding would be problematic for structural determination, especially if the DNA sequence was made by several base pairs, because the compound might be disordered on several positions across the oligonucleotide. The number of base pairs should be kept to a minimum to avoid this problem, but the shorter the sequence, the lower the melting temperature (temperature at which half of the DNA appears as single strand) of the DNA. A very low melting temperature would make the crystallisation difficult to achieve, because it would require low crystallisation temperatures to maintain the DNA as a double helix. For this reason, the oligomer was designed to have only G-C pairs, which increase the stability of the double helix due to the three hydrogen bonds between the bases. The oligonucleotide chosen for the experiment was the self-complementary $(GC)_3$ hexamer, which has a melting temperature of 17 °C. The length of the oligomer was set to six base pairs, so that the fragment of DNA obtained would be long enough to allow binding of tachpyr, but not too long in order to minimise disorder due to the binding of tachpyr over several different positions.

Several crystallisation screens and conditions were tested, including the conditions reported by Brzezinski *et al.*[284] for their ultra-high resolution structure of a very similar DNA oligomer. The crystallisations were set up for both native DNA and a solution of DNA and tachpyr. Both commercial and proprietary screens were used, including Hampton and PACT screens, although modifications of successful literature conditions for similar DNA sequences[284-285] produced the highest number of hits. The crystals were typically grown by hanging drop/vapour diffusion method against a reservoir of 2-methyl-2,4-pentan-diol (MPD) at 10 °C, isolated from the crystallisation drop with a rayon loop and frozen in liquid nitrogen without use of cryoprotectants. Several crystals, of different sizes and shapes, were obtained from the plates, but exclusively when DNA and tachpyr were both present in the starting solution. All attempts to crystallise native DNA were unsuccessful. Some of the crystals obtained are shown in **Figure 4.22**.

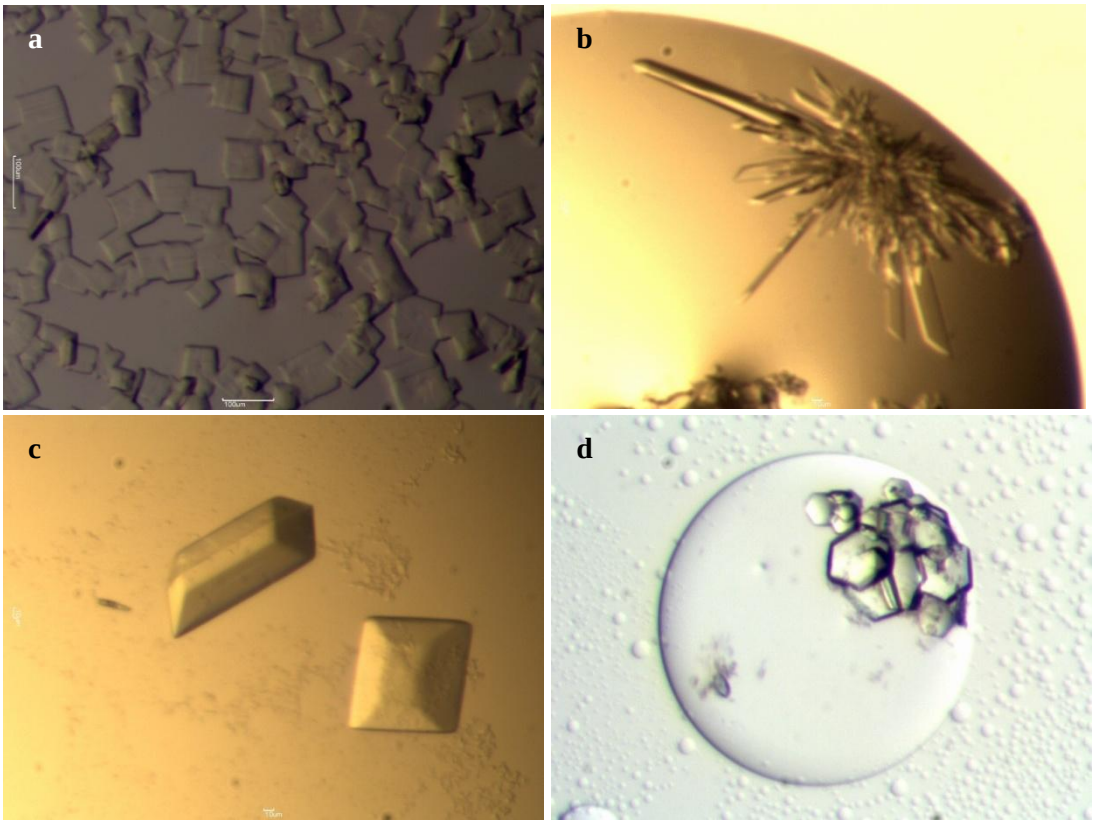

Figure 4.22: Examples of crystals obtained from DNA and tachpyr **[3b]** in different experimental conditions: **a**. 30 mM sodium cacodylate pH = 7.0, 10 mM spermine, 7.5 mM tachpyr, 0.7 mM DNA, 5% MPD; **b**. 50 mM HEPES pH = 7.0, 100 mM $CaCl_2$, 2.5 mM spermine, 3.7 mM tachpyr, 0.7 mM DNA, 11% PEG 8K; **c**. 15 mM sodium cacodylate pH = 7.0, 2.5 mM spermine, 5 mM tachpyr, 0.7 mM DNA, 5% MPD; **d**. 20 mM sodium cacodylate pH = 6.0, 40 mM NaCl, 10 mM $BaCl_2$, 6 mM spermine, 7.5 mM tachpyr, 0.37 mM DNA, 22.5% MPD. Concentration of DNA reported for the double strand.

Cycles of optimisation of the crystallisation conditions were performed to improve the quality and the size of the crystals. Despite the number of crystals obtained, the quality was usually not very good, with very weak diffraction and resolution lower than 5 Å.

After several attempts, better quality crystals were obtained from sitting drop/vapour diffusion method from a Natrix HT™ screen after 9 months at 10 °C (experimental details can be found in **Chapter 6**) and diffraction data collected at 1.5 Å resolution at the Diamond Light Source synchrotron. The crystal was a cluster, shown in **Figure 4.22** (**d**), and it contained several hexagonal shaped crystals, but it provided good enough quality data for structural determination. A detail of the diffraction pattern is

shown in **Figure 4.23**, in which it is possible to see reflections almost at the edge of 1.47 Å resolution.

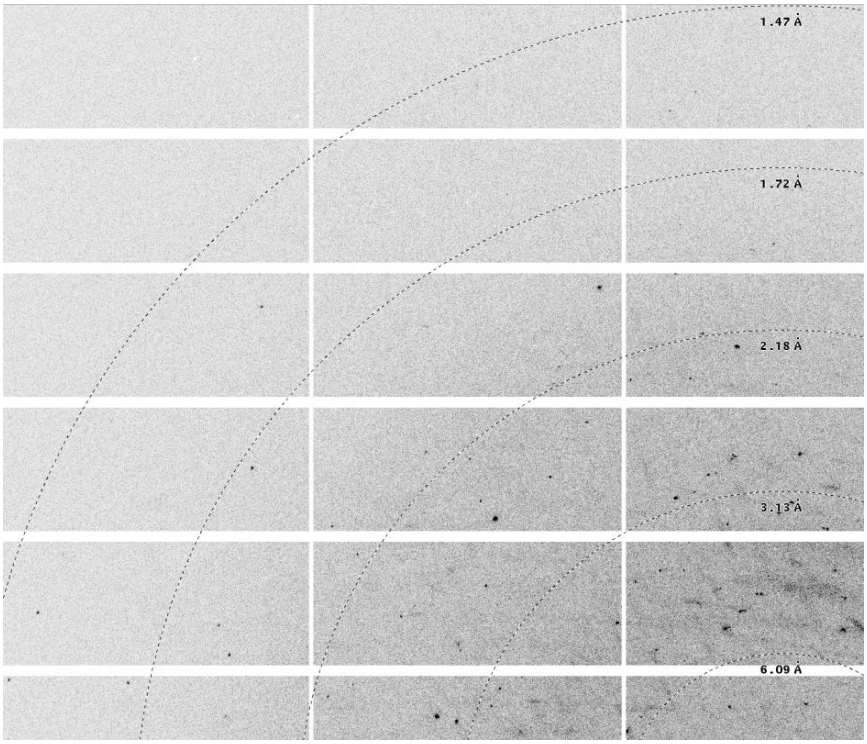

Figure 4.23: Diffraction pattern of DNA-tachpyr crystals, detail of reflections at high resolution. Data collected at Diamond Light Source synchrotron.

The data presented a very strong anomalous signal, which is due to the interaction of the X-ray wave with heavy metals present in the structure.[286] The crystallisation conditions included barium chloride, therefore the presence of a heavy atom in the crystal lattice could not be excluded. The structure was solved and refinement carried out using MOLREP,[287] CCP4[288] and Coot.[289]

An image of the crystal structure is shown in **Figure 4.24**. The image shows clearly the DNA hexamers forming a left-handed double helix, characteristic of Z-DNA, a barium atom, disordered over two positions (shown as the grey cylinder in the picture), and residual electron density which could be assigned to a disordered tachpyr molecule.

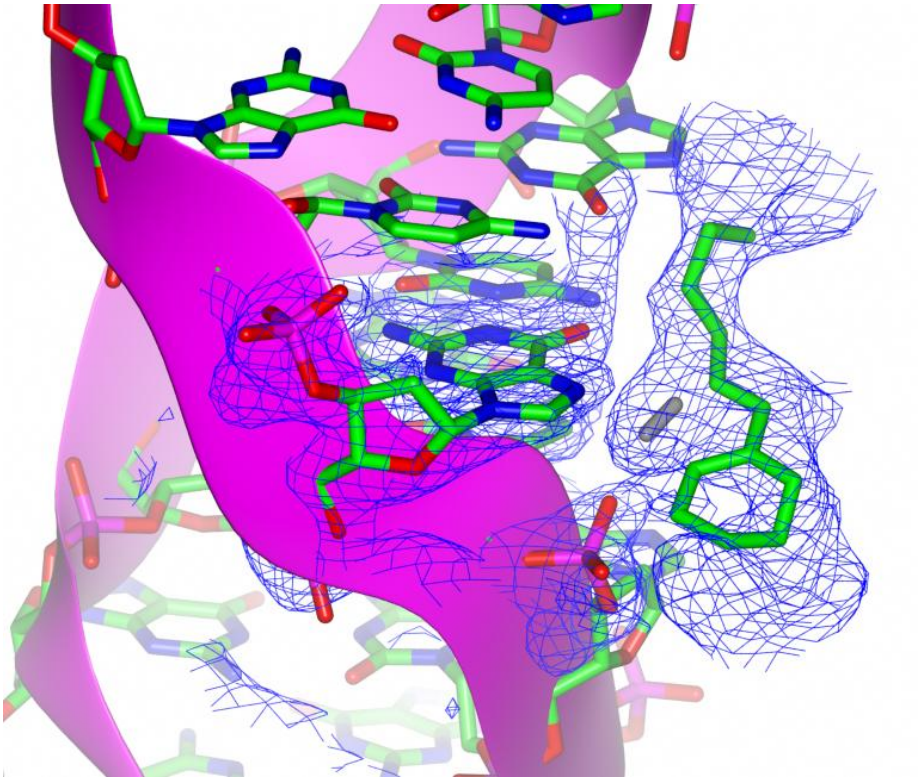

Figure 4.24: Crystal structure of DNA and tachpyr **[3b]**, electron density shown at 0.3 σ. Image produced with CCP4mg software.[290]

The determination of the structure represented a crystallographic challenge for several reasons, which are briefly discussed herein. The structure showed very high symmetry, with the asymmetric unit formed by only two consecutive nucleobases (i.e. GC). The structure was modelled as both a left- and right-handed double helix, and the data showed a better fitting for the left-handed structure, which gave the crystal a $P6_522$ space group assignment. This solution was quite surprising, because the literature reports very few examples of a 5'-purine start DNA sequence which gives Z-DNA. For small oligonucleotides (up to 12 base pairs) the direction of the rotation of the double helix seems to be associated to the sequence[291-293] and to the nucleobase (purine or pyrimidine) found in the 5'-position.[294] Z-DNA is typically found in sequences with a 5'-pyrimidine start,[284-285, 295-296] while 5'-purine oligos produce A-DNA. The only exception to date is given by the decamer $(GC)_5$ reported by Ban *et al.* (PBD code 279D)[297], which showed a left-handed helix although possessing a purine start. Several other similarities between the structure reported by Ban *et al.*[297] and our structure were found: both have the same asymmetric unit and belong to the hexagonal

$P6_522$ space group. In both our study and Ban's, DNA forms pseudo-continuous chains, with no clear distinction between one oligonucleotide and the next. **Figure 4.25** shows the arrangement of the DNA double helices in the unit cell and the detail of one double helix observed in the structure.

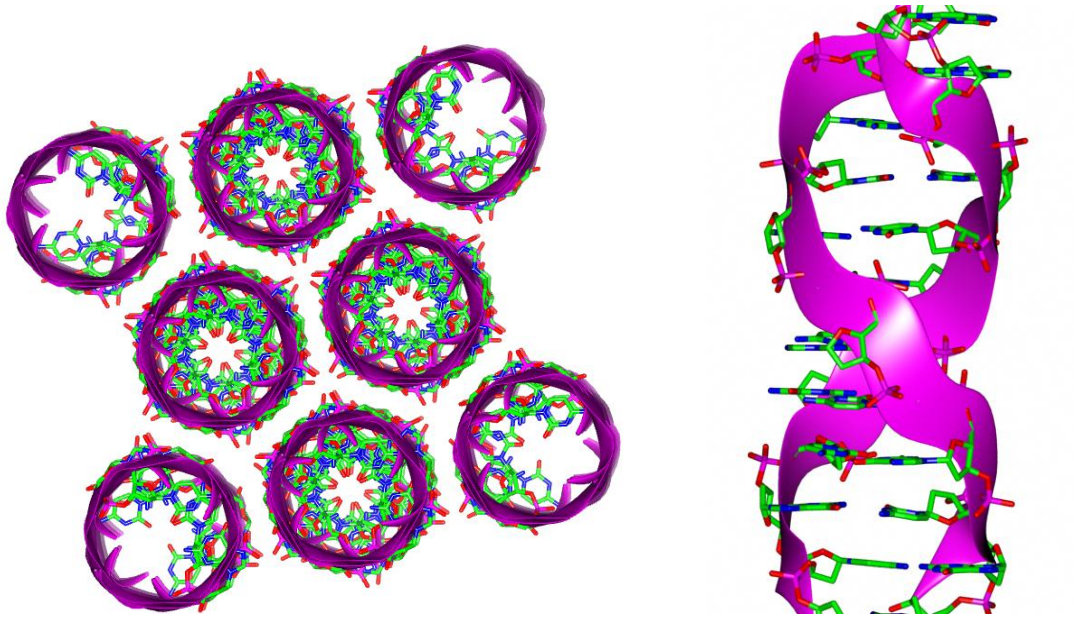

Figure 4.25: Image of arrangement of the DNA double helices in the crystal packing (left) and example of continuous chain formed in the crystal lattice (right). Barium atom and **[3b]** omitted for clarity, image produced with CCP4mg software.[290]

If the phosphate groups are represented as "p", the DNA sequence used for the crystallisation can be expressed as 5'-GpCpGpCpGpC-3'. To have a continuous chain, an extra phosphate, which would act as the linker, is needed. What can be observed in the structure is that all the phosphate groups present in the double helix have 5/6 of occupancy and they are all equal, resulting therefore statistically disorder across the structure and giving the arrangement observed. The same behaviour was observed and reported by Ban *et al.*[297] for their Z-DNA crystals.

The presence of these "quasi-polymers", as described by Ban *et al.*[297], is probably the cause of streaks observed in the diffraction pattern, which are shown in **Figure 4.26**.

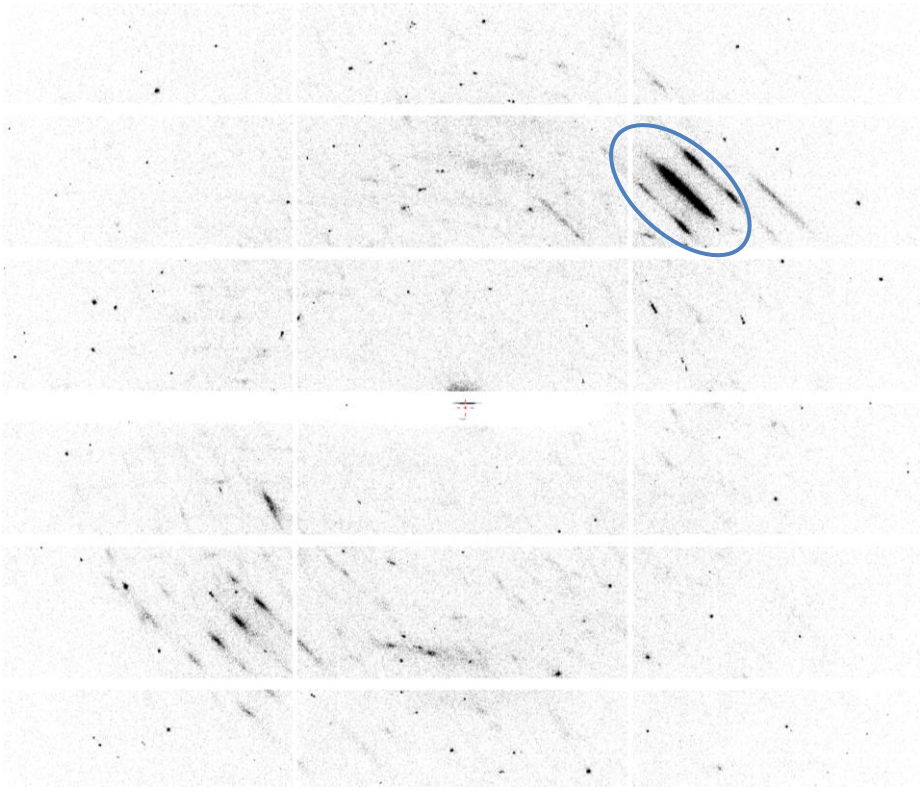

Figure 4.26: Example of diffraction pattern of DNA crystals. In the circles, streaks observed in the diffraction.

These reflections could not be included in the integration of the reflections, with consequent partial loss of information.

As shown in **Figure 4.27**, the structural model of the nucleotides forming the DNA oligomer fits very well the electron density observed in the crystal. Next to the double helix, a clear ring of residual electron density is present. Tachpyr **[3b]**, or at least part of it, gives a very good match with this residual electron density. The crystallisation conditions contained also spermine, which was checked for fitting in the residual electron density observed, but it did not give a good solution. This electron density was therefore modelled as a disordered tachpyr molecule.

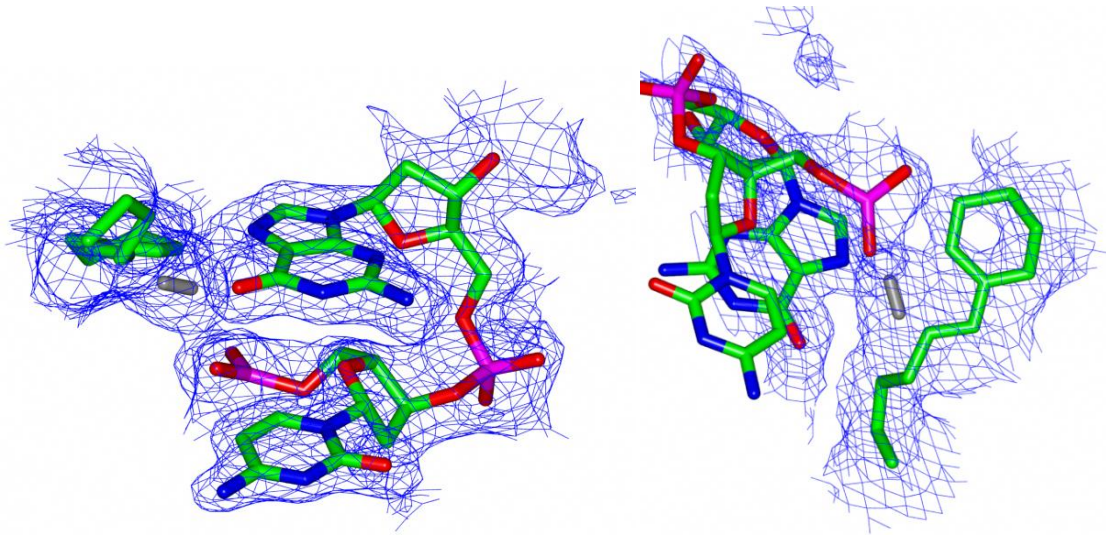

Figure 4.27: Images of model and electron density in the asymmetric unit: the nucleotides forming the DNA oligo (left) and the residual electron density due to the ligand (right). Electron density shown at 0.3 σ, image produced with CCP4mg software.[290]

The whole of the molecule of **[3b]** was not visible for probably two main reasons: the molecule is disordered across the lattice and the asymmetric unit is too small to accommodate the whole molecule of tachpyr. The ligand, in fact, cannot fit into the required symmetry, so what is modelled can be considered as an average of different arrangements around the DNA fragment and all the atoms have indeed only partial occupancies. From the electron density it is not possible to distinguish clearly if the ring observed in the structure belongs to the tach moiety or it is one of the pyridine rings, therefore no final conclusions can be drawn about the possible binding mode. However, what can be deduced is that the tachpyr molecule interacts with the "outside" of the DNA, probably in a hydrogen bond interaction with the phosphate backbone, as shown in **Figure 4.28**.

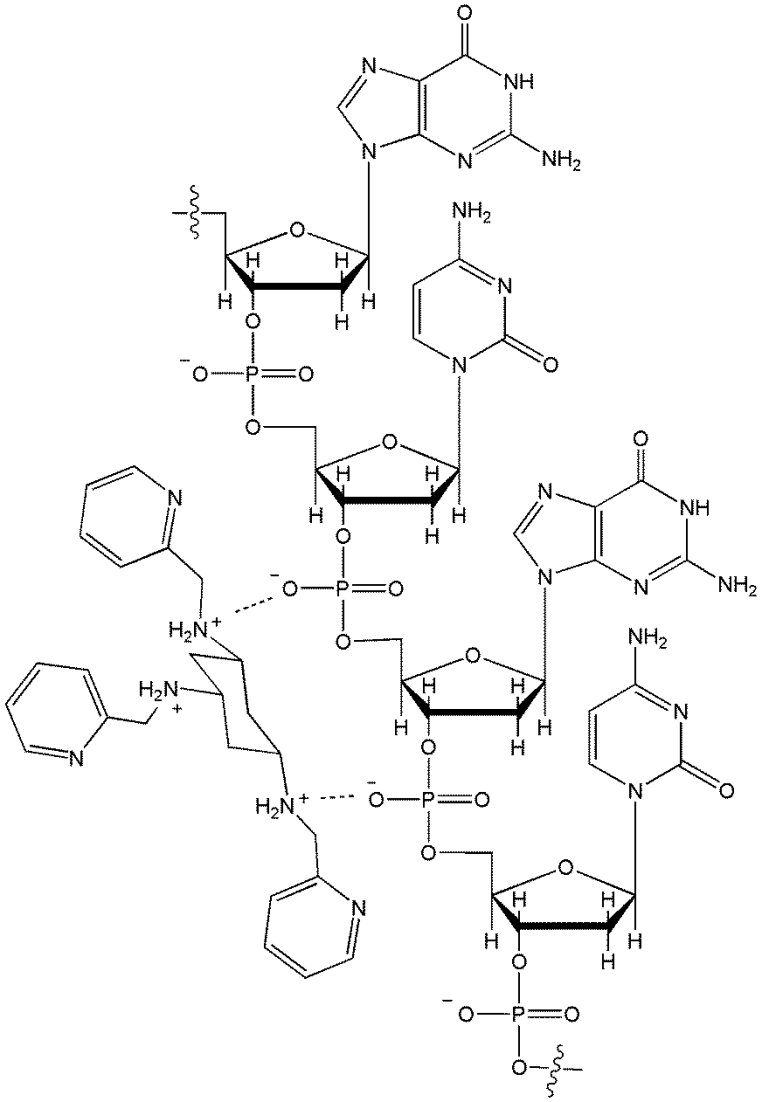

Figure 4.28: Scheme of possible interaction between tachpyr **[3b]** and the phosphate backbone of DNA.

The final structure and refinement parameters for the crystal are shown in **Table 4.5**.

Parameter	
Unit cell dimensions (Å)	$a = b = 17.869$
	$c = 42.398$
Space group	$P6_522$
Resolution range (Å)	15.68 – 1.52
Final R value (%)	33.1
R free value (%)	36.8
RMS deviation from ideal geometry:	
Bond lengths (Å)	0.009
Bond angles (°)	2.213

Table 4.5: Crystal and refinement parameters of the DNA hexamer d(GCGCGC) and tachpyr **[3b]**.

The very high final R value after refinement can be explained by the presence of all the problems discussed in this section: intrinsic disorder, partial integration of the data and possibly some bad reflection due to the clustering of the crystal. Nonetheless, crystallography showed clearly a very rare structure of a 5'-purine oligonucleotide in the Z-DNA form and, most importantly for our study, the presence of tachpyr in the proximity of the DNA double helix. Although the structure does not allow to establish with absolute certainty the mode of binding to the DNA, it supports the data obtained from the other experiments: tachpyr is able to interact with DNA in the solid state as well as in solution (as shown by LD experiments), is found in close proximity of the phosphate backbone of the DNA and does not show intercalation. Structure activity relationships obtained by the study of the different tach derivatives were also consistent with these findings: the tach moiety plays a central role in the interaction, with the pK_a of the amines being crucial for activity, as it would be expected in case of binding to the negatively charged phosphates of DNA. The hypothesis that **[3b]** might show a spermine-like binding to the DNA is therefore a valid alternative to the reported metal chalation mechanism.[133-136]

4.4 Evaluation of activity on non-cancerous cells

The cytotoxic activity against cancer cells of the compounds presented in the previous sections shows that these molecules can potentially be active against tumours, but a control against non-cancerous cells is needed. Selectivity is an essential requirement to decrease side effects and have an effective therapeutic drug. For this reason, cisplatin, tachpyr **[3b]** and 4-NMe_2-tachben **[11b]** were tested against 293T human embryonic kidney immortalised cells as a preliminary evaluation of selectivity. Immortalised cells were plated in a 96-well plate following the standard MTT procedure, the IC_{50} evaluated and the results after triplicate test are reported in **Table 4.6**.

Compound	**IC_{50} value / μM**
Cisplatin	2.20 ±0.14
Tachpyr **[3b]**	3.82 ± 0.11
4-NMe_2-tachben **[11b]**	0.57 ± 0.02

Table 4.6: IC_{50} values against 293T cells.

As shown, none of the compound tested presented significant difference in activity between the non-cancerous and the cancer cell lines. 4-NMe2-tachben was actually more active on 293T cells than A2780 (cf. **Table 4.4**). Although this result is not very promising, a few considerations should be made. Cisplatin, which is the benchmark reference, did not show selectivity toward cancer cells either. Furthermore, this particular cell line was made immortal by silencing genes involved in the replication cycle[298] to allow the line to survive for long periods in culture. For this reason, the immortalised cells present some of the characteristics of cancer cells. The lack of selectivity might be a consequence of the immortalisation process and/or the interaction of the compounds with elements of the immortalised cells. To have a more accurate description of possible selectivity of action, the compounds should be tested on non-cancerous, non-immortalised cells in order to discriminate if the molecules are anti-tumour compounds or poisons.

4.5 Chapter conclusions

The iron chelation mechanism of action of tachpyr **[3b]**, previously considered as the cause of the cytotoxic activity of this compound, was investigated. This study led to the conclusion that metal chelation is not involved in the cytotoxic activity of this compound and a new possible target for the action was found in DNA.

Tachpyr showed the ability to interact with DNA, highlighted in LD experiments, without acting as an intercalator. The structural investigation of tachpyr and its derivatives showed the pharmacologically-important features of these compounds, helped develop new hypotheses about the potential mechanism of action, such as the interaction with the phosphate backbone of DNA via a spermine-like binding, and offered new molecules with very high cytotoxic activity.

Co-crystallisation of DNA and tachpyr **[3b]** was attempted and produced crystals of good enough quality for structural determination. The obtained crystal structure is one of the first examples of a 5'-purine oligo in the Z-DNA form and it clearly shows residual electron density that can be associated to tachpyr. The experimental data represents clear evidence that Fe chelation is unlikely to be the mechanism of action of tachpyr and that DNA (or possibly other ribonucleic acids in the cells) might be a target for the action. The data obtained can also explain some of the results reported by Planalp and co-workers during their investigation. The loss of activity due to substitution on the 6-position of the pyridine ring described by Childers *et al.*[140] might be explained by steric hindrance and inhibition of the interaction with the DNA. Similarly, the tris(ethylendiamine) derivatives reported by Ye *et al.*[139] showed poor toxicity, which could be due to a low log*P* value derived by the presence of six amine groups on the molecule.

Tachpyr **[3b]** and the most active of its derivatives, 4-NMe_2-tachben **[11b]**, were tested against non-cancerous immortalised cells, and they did not show any selectivity for cancer over non-cancerous cells. Similarly, cisplatin showed the same lack of selectivity, therefore a deeper evaluation of selectivity against different cell lines, including non-cancerous non-immortalised cells, is needed.

Chapter 5

Conclusions and future work

5. Conclusions and future work

5.1 Conclusions

The aims of this project involved the synthesis and *in vitro* evaluation of tach derivatives, and the study of the mechanism of action of these molecules, with particular focus on tachpyr.

Several tach-based Schiff bases were synthesised and reduced to the corresponding tri-amines. The choice of the N-substituent on the tach amines was led by the need to incorporate the structural modifications into the tachpyr molecule required to explore structure activity relationships. The heterocyclic compounds **[4a-b]** and **[5a-b]** were synthesised to study the effect of different heteroatoms on the aromatic rings, whilst compounds **[6a-b]-[9a-b]** were made to explore the effect of the oxygen atom of the salicyl moiety, although the *in vitro* evaluation of these molecules could not be performed. The roles of the pyridyl nitrogen atom of tachpyr and the 4-substituents on the aromatic ring were evaluated in the tachben series (compounds **[10a-b]-[15a-b]**). Finally, new synthetic methods for the development of mono-N-substituted derivatives were explored, which led to promising procedure to expand the tach-based library of compounds.

The complexation of tachpyr with Co(II) and Ru(II) was studied and new crystal structures obtained for the two complexes. The geometry of the cobalt complex was shown to be dependent on the oxidation of the ligand, changing from distorted trigonal prismatic to distorted octahedral for the complex with **[3a]** or **[3b]**, respectively. The complexation with Ru(II) proved to be challenging and yielded an unexpected Ru(II)-dimer. Preliminary *in vitro* tests against cancer cells were performed for the complexes and the Ru(II)-dimer, however they all showed very poor cytotoxicity.

The mechanism of action of tachpyr **[3b]** was investigated and this study led to the conclusion that iron chelation, which was reported to be the cause of the cytotoxic action of tachpyr,[133-136] is unlikely to be the main cause of the cytotoxic activity of this molecule. Tachpyr showed the ability to interact with the DNA in a non-intercalating

fashion. The study of tach and its derivatives, compounds **[2]-[17]**, highlighted the structural features (basic nitrogen atoms on the tach moiety, presence of at least one arm to improve lipophilicity) of the molecule necessary for activity and gave new molecules with high toxicity against cancer cells.

A crystal structure was obtained which showed tachpyr **[3b]** in close proximity to the DNA phosphate backbone. This is consistent with the hypothesis of a mechanism of action different from iron chelation. Furthermore, the structure represents one of the first examples of a 5'-purine start oligonucleotide crystallising in the Z-DNA form. All data obtained represent clear evidence that the action of tachpyr in cells does not involve metal chelation and the crystal structure indicates that DNA or other nucleic acid might be the target of the cytotoxicity. The set of evidence collected by Planalp and co-workers during their studies explores the ability of tachpyr and its derivatives to be effective hexadentate iron chelators,[133, 135-136, 140] but the metal binding abilities of the ligands might not be related to its mechanism of action. The evidence collected and presented in **Chapter 4** suggested clearly a non-chelating mechanism, which should be considered and further investigated.

Evaluation of the mechanism of action of a molecule is a long process that can require decades. Cisplatin, for example, was studied since the discovery of its cytotoxic properties during the 1960s and the full mechanism of action is still not completely understood. In recent years new research highlighted a new activation mechanism and possible binding target of cisplatin in sulfur-containing membrane molecules.[299] Similarly, the evaluation of the mechanism of action of tachpyr, started about 15 years ago, is far from complete. This thesis described the hypothesis-driven evaluation of the mechanism of action of tachpyr and other tach-based molecules. The results obtained open up the possibility of having a cellular target not previously considered for these molecules, with further investigation of the binding to DNA and other ribonucleic acids needed. New active cytotoxic compounds have been described and synthetic methods for mono-substituted tach derivatives developed. The promising and exciting results obtained are worth further investigation to expand the understanding and knowledge of the action of tachpyr on cancer cells.

5.2 Future work

The possible developments in the study of tach-based ligands and their action against cancer cells are numerous.

Several alternatives to continue the evaluation of structure activity relationships are available. The tachben series of derivatives might be expanded with more 4-substituents and the position of the substituent on the aromatic ring could also be varied, to explore the steric effects around the site of interaction and, hence, the effect on the activity. Furthermore, if ketones are used for the Schiff base condensation with tach, chiral derivatives would be produced after reduction of the imine bond. This modification would obviously raise the problem of obtaining pure stereoisomers, but important structure activity relationships might be gained by this evaluation. Similarly, the mono-substituted derivatives might be developed, with almost endless variations possible. The addition of fluorescent probes to visualise sites of accumulation in cells should also be evaluated.

Considering the promising results reported by Gamble *et al.*[131-132] for the cytotoxicity of Ru(II)-tach complexes, but the lack of activity shown by Ru(II)-tachpyr, the mono-armed tach derivatives might be used for complexation with ruthenium or other metals. This might lead to improved cytotoxicity and further understanding of the mechanism of action for both the free ligand the metal complex.

The molecules described in this thesis were tested against two cancer cell lines only, therefore more *in vitro* tests should be carried out against several other cell lines, including cisplatin-resistant cells. The ultimate goal in cancer treatment is to obtain compounds highly cytotoxic against cancer cells, but inactive against normal cells, therefore the activity of the most promising compounds should be evaluated against non-cancerous, non-immortalised cell lines to assess the selectivity profile of the derivatives. More co-crystallisations with DNA, both with tachpyr and other derivatives (e.g the highly cytotoxic tachben derivatives), might be attempted, together with the evaluation of possible interaction with other nucleic acids, such as mRNA and tRNA.

The hypothesis of the correlation between log*P*, pK_a and cytotoxicity exposed in **Chapter 4** might be explored through evaluation of experimental log*P* and pK_a values. The synthesis of more derivatives and their evaluation against cancer cells might give insights on the validity of this hypothesis, which, if confirmed, might give a powerful tool for the design of new active compounds.

Finally, computational methods such as density functional theory (DFT) and molecular dynamics may be used for the evaluation of the interaction with biomolecules.

Chapter 6

Experimental

6. Experimental

6.1 Notes

For clarity, the ESI-MS ions and fragments were assigned according to the following nomenclature:

- The protonated molecule is indicated as $[M+H]^+$ or $[M+2H]^{2+}$ in case of double protonation.
- The fragment ions are indicated as $[M+H-Arm]^+$ to represent structures as the ones shown below for the tri-imines and tri-amines, respectively:

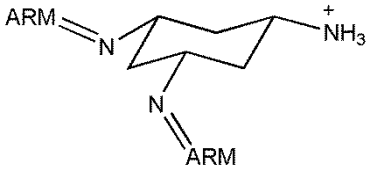

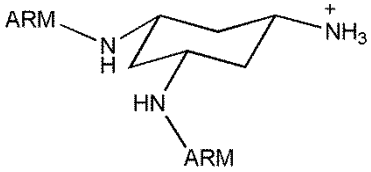

6.2 Synthesis and characterisation of ligands - Materials and methods

Materials and solvents were used as supplied by Sigma Aldrich, Alfa Aesar and Fluka without further purification. *Cis,cis*-1,3,5-cyclohexanetricarboxylic acid was purchased from TCI UK and used for the synthesis of *cis,cis*-1,3,5-triaminocyclohexane according to literature procedures.[128, 161] Compounds **[3a-b]**,[161] **[5a-b]**,[163] **[6a-b]** to **[9a-b]**,[166] **[10a-b]**[172-173] and **[16]**[166, 178] were made following reported literature procedures or by their modification. ^{1}H, ^{19}F and ^{13}C NMR spectra were recorded either on a JEOL EXC-400 or a JEOL ECS-400 spectrometer (^{1}H 400 MHz, ^{13}C 100.6 MHz, ^{19}F 376.2 MHz) at 295 K. Chemical shifts (δ) are quoted in parts per million referenced to residual proton signal of the solvent; *J* values are quoted in Hz and are referred to ^{1}H-^{1}H couplings, unless otherwise stated. All ^{13}C NMR spectra were recorded with ^{1}H decoupling. Mass spectra were recorded on a Bruker micrOTOF electrospray mass spectrometer (ESI-MS). Elemental analyses were performed using an Exeter Analytical Inc. CE-440 analyser. Melting points were

measured on a Stuart Scientific SMP3 apparatus. Diffraction data for X-ray crystallography was collected using an Oxford Diffraction SuperNova system with EOS CCD camera at 110 K. Crystal structures were solved with Olex2[300] using Superflip[301] structure solution program and refined with ShelXL.[302]

6.3 Synthesis of ligands

6.3.1 Synthesis of tach

***Cis,cis*-1,3,5-cyclohexanetris(benzylcarbamate), [1]**

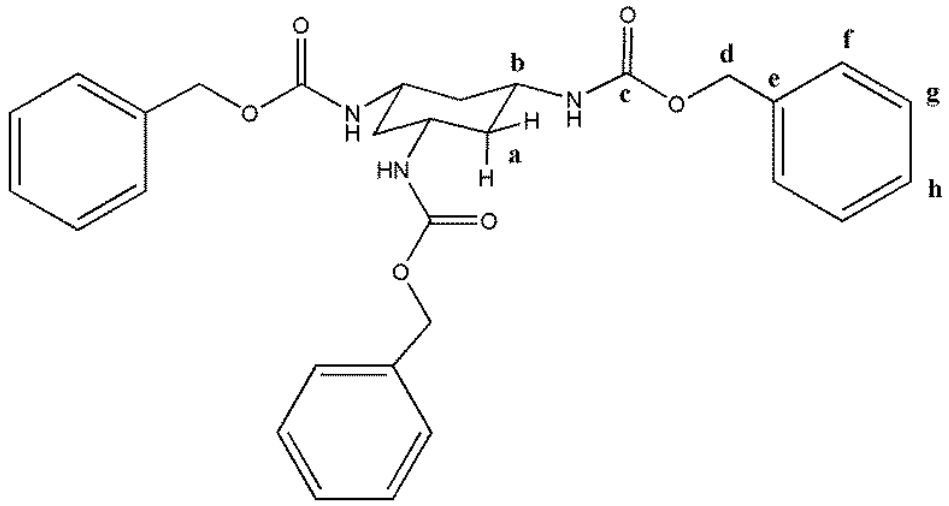

Triethylamine (7.02 g, 9.7 mL, 69.38 mmol, 3 eq.) and diphenylphosphorylazide (DPPA) (19.09 g, 14.9 mL, 69.38 mmol, 3 eq.) were added to a suspension of *cis,cis*-1,3,5-cyclohexane tricarboxylic acid (5.0 g, 23.13 mmol, 1 eq.) in 125 mL of benzene. The mixture was heated at reflux until it became a clear solution. Benzyl alcohol (7.50 g, 7.2 mL, 69.38 mmol, 3 eq.) was added and the reaction mixture was maintained at reflux for 16 h. The resulting cream suspension was filtered and the white solid washed with cold diethyl ether. The compound was used without further purification.
Yield: 8.2 g, 15.4 mmol, 67%

^{1}H NMR: (d_6-DMSO) δ 7.34 (15H, m, **f**+**g**+**h**), 5.00 (6H, s, **d**), 3.40 (3H, m, **b**), 1.88 (3H, bd, $\mathbf{a_{eq}}$), 1.05 (3H, ap.q, $\mathbf{a_{ax}}$).

Cis,cis-1,3,5-triaminocyclohexane trihydrobromide, tach·3HBr, [2]HBr

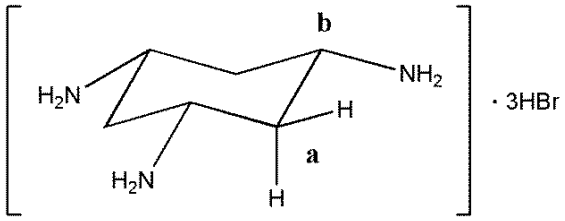

A solution of HBr 33% wt in acetic acid (60 mL) was added to tach(benzylcarbamate) (5.5 g, 10.3 mmol, 1 eq.) and the mixture was left stirring at room temperature for 16 h. Ethanol (100 mL) was then added and the mixture was left stirring at room temperature for a further 24 h. The white precipitate formed was isolated by filtration and washed with chilled ethanol, then dried under vacuum. The compound was used without further purification.

Yield: 3.3 g, 8.76 mmol, 91%

^{1}H NMR: (d_6-DMSO) δ 3.50 (3H, tt, $^3J_{ax\text{-}ax}$ = 12.2, $^3J_{ax\text{-}eq}$ = 4.0, **b**), 2.44 (3H, bd, ^2J = 12.2, $\mathbf{a_{eq}}$), 1.62 (3H, ap.q, $^3J = {}^2J$ = 12.2, $\mathbf{a_{ax}}$).

Cis,cis-1,3,5-triaminocyclohexane, tach, [1]

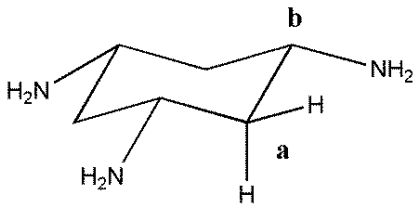

Cis,cis-1,3,5-triaminocyclohexane trihydrobromide, tach·3HBr, (1.0 g, 2.69 mmol) was dissolved in the minimum amount of water and passed through a Dowex 1X4-50 (300 g) ion exchange column, which had previously been washed with, in order, water, 1 M HCl, 1 M NaOH and finally with water again till neutral pH. The fractions with basic pH were collected and solvent evaporated. The residue was sublimed at 10^{-2} mbar at 70 °C using a liquid nitrogen cold finger, giving a bright white solid which was stored under inert gas.

Yield: 0.081 g, 0.63 mmol, 23%.

^{1}H NMR: (D_2O) δ 2.75 (3H, tt, $^3J_{ax\text{-}ax}$ = 11.6, $^3J_{ax\text{-}eq}$ = 3.2, **b**), 1.94 (3H, ap.d, ^2J = 11.6, $\mathbf{a_{eq}}$), 0.89 (3H, ap.q, $^3J = {}^2J$ = 11.6, $\mathbf{a_{ax}}$).

6.3.2 Synthesis of heterocyclic ligands

***Cis,cis*-1,3,5-tris(pyridine-2-carboxaldimino)cyclohexane, tachimpyr, [3a]**

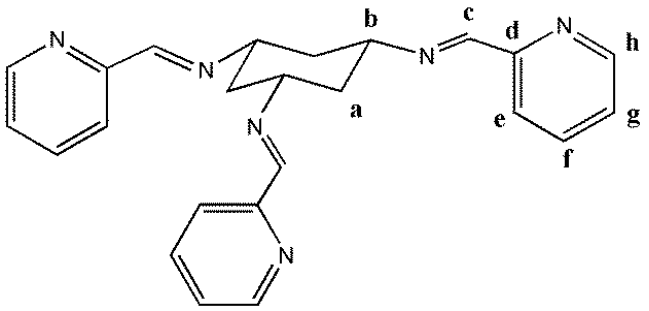

Tach·3HBr (250 mg, 0.67 mmol, 1 eq.) was dissolved in 1 mL of water and NaOH (80 mg, 2.01 mmol, 3 eq.) added. The mixture was stirred until the solid was completely dissolved and 50 mL of toluene were then added. The reaction was heated at reflux and water was removed by azeotropic distillation using a Dean-Stark apparatus. When no water remained in the reaction flask, pyridine-2-carboxaldehyde (215 mg, 190 μL, 2.01 mmol, 3 eq.) was added and the mixture was maintained at reflux with the Dean-Stark under nitrogen for 16 h. After cooling to room temperature, the mixture was filtered and toluene was evaporated under vacuum, leaving a yellow solid, which was washed with pentane and diethyl ether. The resulting white solid was dried under vacuum for 16 h and used without further purification.

Yield: 180 mg, 0.45 mmol, 68%. Melting point: 138-140°C.

^{1}H NMR: ($CDCl_3$) δ 8.64 (3H, dd, ^{3}J = 4.8, ^{4}J = 1.2, **h**), 8.48 (3H, s, **c**) 8.02 (3H, d, ^{3}J = 7.6, **e**), 7.74 (3H, td, ^{3}J = 7.6, ^{4}J = 1.2, **f**), 7.31 (3H, ddd, $^{3}J_{g\text{-}f}$ = 7.6, $^{3}J_{g\text{-}h}$ = 4.8, ^{4}J = 1.2, **g**), 3.70 (3H, tt, $^{3}J_{ax\text{-}ax}$ = 12.0, $^{3}J_{ax\text{-}eq}$ = 3.5, **b**), 2.11 (3H, ap.q, $^{3}J = {}^{2}J$ = 12.0, $\mathbf{a_{ax}}$), 1.93 (3H, ap.d, ^{2}J = 12.0, $\mathbf{a_{eq}}$).

^{13}C{^{1}H} NMR: ($CDCl_3$) δ 160.8 (**c**), 154.8 (**d**), 149.5 (**h**), 136.7 (**f**), 124.9 (**g**), 121.7 (**e**), 66.3 (**b**), 40.7 (**a**).

ESI-MS: positive ion *m/z* 397.2128 ($[M+H]^+$, calc. for $C_{24}H_{25}N_6^+$: 397.2135, error 0.7 mDa); *m/z* 308.1864 ($[M+H-Arm]^+$, calc. for $C_{18}H_{22}N_5^+$: 308.1870, error 0.6 mDa).

Elemental Analysis: for $C_{24}H_{24}N_6$: Calc. C 72.70; H 6.10; N 21.20; Rest 0.00%. Found C 72.44; H 6.09; N 20.96; Rest 0.50%.

***N,N',N''*-tris(2-pyridylmethyl)-*cis,cis*-1,3,5-triaminocyclohexane, tachpyr, [3b]**

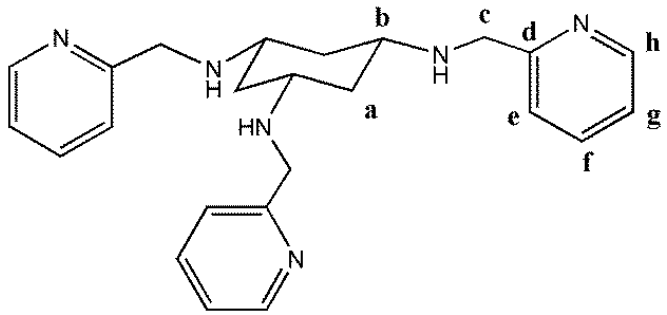

Cis,cis-1,3,5-tris(pyridine-2-carboxaldimino)cyclohexane, tachimpyr, (120 mg, 0.30 mmol, 1 eq.) was dissolved in 10 mL of methanol and sodium borohydride (40 mg, 1.06 mmol, 3.5 eq.) was slowly added in portions. The mixture was left stirring at room temperature for 16 h. Methanol was evaporated and the residue dissolved in 10 mL of $CHCl_3$. A 1:1 mixture of $NaHCO_3$ sat. solution and NaCl sat. solution (10 mL in total) was added to the organic solvent and the mixture was left stirring vigorously for 1 h. The layers were separated and the aqueous one was extracted with $CHCl_3$ (3×6 mL). The organic layers combined were washed with brine (2×6 mL), dried over Na_2SO_4 and filtered. The solvent was removed by rotary evaporation, leaving a pale yellow oil.

Yield: 116 mg, 0.29 mmol, 96%.

^{1}H NMR: (d_6-DMSO) δ 8.46 (3H, ddd, ^3J = 4.8, ^4J = 1.8, ^5J = 0.9, **h**), 7.71 (3H, td, ^3J = 7.6, ^4J = 1.8, **f**) 7.40 (3H, bd, ^3J = 7.6, **e**), 7.20 (3H, ddd, $^3J_{g\text{-}f}$ = 7.6, $^3J_{g\text{-}h}$ = 4.9, ^4J = 0.9, **g**), 3.80 (6H, s, **c**), 2.36 (3H, ap.t, $^3J_{ax\text{-}ax}$ = 11.2, **b**), 2.11 (3H, ap.d, ^2J = 11.2, $\mathbf{a_{eq}}$), 0.84 (3H, ap.q, $^3J = {}^2J$ = 11.2, $\mathbf{a_{ax}}$).

^{13}C{^{1}H} NMR: (d_6-DMSO) δ 159.8 (**d**), 149.3 (**h**), 136.5 (**f**), 122.4 (**e**), 122.0 (**g**), 53.8 (**b**), 52.5 (**c**), 40.1 (**a**).

ESI-MS: positive ion *m/z* 403.2606 ($[M+H]^+$, calc. for $C_{24}H_{31}N_6^+$: 403.2605, error −0.1 mDa); *m/z* 425.2425 ($[M+Na]^+$, calc. for $C_{24}H_{30}N_6Na^+$: 425.2424, error −0.1 mDa); *m/z* 202.1302 ($[M+2H]^{2+}$, calc. for $C_{24}H_{32}N_6^{2+}$: 202.1338, error 3.6 mDa).

Elemental Analysis: for $C_{24}H_{30}N_6 \cdot 1.7H_2O$: Calc. C 66.85; H 7.76; N 19.49; Rest 5.90%. Found C 66.60; H 7.45; N 19.44; Rest 6.50%.

***Cis,cis*-1,3,5-tris(pyrrole-2-carboxaldimino)cyclohexane, tachimprl, [4a]**

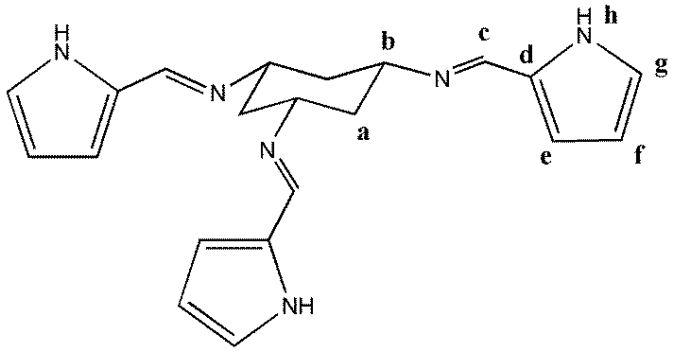

Tach·3HBr (500 mg, 1.34 mmol, 1 eq.) was dissolved in 3 mL of water and NaOH (160 mg, 4.03 mmol, 3 eq.) added. The mixture was stirred until the solid was completely dissolved and 80 mL of toluene were then added. The mixture was heated at reflux and water was removed by azeotropic distillation using a Dean-Stark apparatus. When no water remained in the reaction flask, pyrrole-2-carboxaldehyde (383 mg, 4.03 mmol, 3 eq.) was added and the mixture was maintained at reflux with a Dean-Stark apparatus under nitrogen for 16 h. After cooling to room temperature, the mixture was filtered and toluene was evaporated under vacuum, leaving a cream solid, which was washed with pentane and dried. The resulting white solid was then washed again with cold pentane and cold diethyl ether, dried under vacuum and used without further purification.

Yield: 218 mg, 0.60 mmol, 45%.

^{1}H NMR: ($CDCl_3$) δ 8.09 (3H, s, **c**), 6.82 (3H, bs, **g**) 6.46 (3H, dd, ^{3}J = 3.6, ^{4}J = 1.2, **e**), 6.19 (3H, m, **f**), 3.40 (3H, bs, **b**), 1.83 (6H, m, $\mathbf{a_{ax+eq}}$)

^{13}C{^{1}H} NMR: ($CDCl_3$) δ 150.5 (**c**), 129.8 (**d**), 122.2 (**g**), 114.9 (**e**), 109.6 (**f**), 65.5 (**b**), 41.5 (**a**).

ESI-MS: positive ion *m/z* 361.2123 ($[M+H]^+$, calc. for $C_{21}H_{25}N_6^+$: 361.2135, error 1.2 mDa); *m/z* 181.1106 ($[M+2H]^{2+}$, calc. for $C_{21}H_{26}N_6^{2+}$: 181.1104, error −0.2 mDa).

***N,N',N''*-tris(2-pyrrolylmethyl)-*cis,cis*-1,3,5-triaminocyclohexane, tachprl, [4b]**

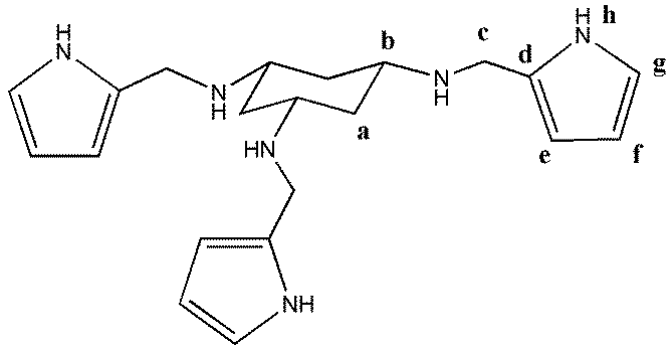

Cis,cis-1,3,5-tris(pyrrole-2-carboxaldimino)cyclohexane, tachimprl, (150 mg, 0.42 mmol, 1 eq.) was suspended in 20 mL of methanol and sodium borohydride (65 mg, 1.66 mmol, 4 eq.) was slowly added in portions. The mixture was stirred for 16 h at room temperature. Methanol was concentrated to about 2 mL and 15 mL of water were added. The pale yellow mixture was extracted with $CHCl_3$ (3×15 mL), the organic layers combined were dried over Na_2SO_4, filtered and the solvent removed by rotary evaporation, leaving a white solid. Needle-like crystals suitable for X-ray diffraction were grown from slow evaporation of $CHCl_3$.

Yield: 145 mg, 0.39 mmol, 94%

^{1}H NMR: ($CDCl_3$) δ 8.99 (3H, bt, **h**), 6.70 (3H, m, **g**) 6.12 (3H, m, **f**), 6.02 (3H, bt, **e**), 3.79 (6H, s, **c**), 2.52 (3H, ap.t, $^3J_{ax\text{-}ax}$ = 11.6, **b**), 2.13 (3H, ap.d, ^2J = 11.6, $\mathbf{a_{eq}}$), 0.86 (3H, ap.q, $^3J_{ax\text{-}ax} = {}^2J$ = 11.6, $\mathbf{a_{ax}}$).

^{13}C{^{1}H} NMR: ($CDCl_3$) δ 130.2 (**d**), 117.6 (**g**), 108.1 (**f**), 106.4 (**e**), 53.3 (**b**), 43.9 (**c**), 39.8 (**a**).

ESI-MS: positive ion *m/z* 367.2594 ($[M+H]^+$, calc. for $C_{21}H_{31}N_6^+$: 367.2605, error 1.1 mDa); *m/z* 288.2182 ($[M+H-Arm]^+$, calc. for $C_{16}H_{26}N_5^+$: 288.2183, error 0.1 mDa); 209.1756 ($[M+H-2Arm]^+$, calc. for $C_{11}H_{21}N_4^+$: 209.1761, error 0.5 mDa); *m/z* 130.1359 ($[M+H-3Arm]^+$, calc. for $C_6H_{16}N_3^+$: 130.1339, error −2.0 mDa).

Elemental Analysis: for $C_{21}H_{30}N_6 \cdot 0.25Et_2O \cdot 1.3H_2O$: Calc. C 64.55; H 8.67; N 20.53; Rest 6.25%. Found C 64.42; H 8.45; N 20.37; Rest 6.75%.

***Cis,cis*-1,3,5-tris(furan-2-carboxaldimino)cyclohexane, tachimfur, [5a]**

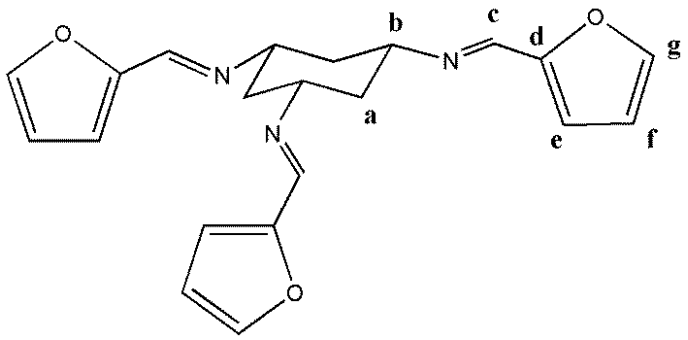

Tach·3HBr (250 mg, 0.67 mmol, 1 eq.) was dissolved in 1 mL of water and NaOH (80 mg, 2.01 mmol, 3 eq.) added. The mixture was stirred until the solid was completely dissolved and 20 mL of benzene were then added. The mixture was heated at reflux and water was removed by azeotropic distillation using a Dean-Stark apparatus. When no water remained in the reaction flask, furfural (194 mg, 167 μL, 2.01 mmol, 3 eq.) was added and the mixture was maintained at reflux with the Dean-Stark for 16 h. After cooling to room temperature, the mixture was filtered and benzene was evaporated under vacuum, leaving a yellow oil.

Yield: 152 mg, 0.42 mmol, 62%

^{1}H NMR: ($CDCl_3$) δ 8.16 (3H, s, **c**), 7.51 (3H, dd, ^{3}J = 1.6, ^{4}J = 0.4, **g**), 6.74 (3H, dd, ^{3}J = 3.2, ^{4}J = 0.4, **e**), 6.47 (3H, dd, ^{3}J = 3.2, ^{4}J = 1.6, **f**), 3.50 (3H, ap.tt, $^{3}J_{ax\text{-}ax}$ = 12, $^{3}J_{ax\text{-}eq}$ = 4, **b**), 2.05 (3H, ap.q, $^{3}J_{ax\text{-}ax}$ = ^{2}J = 12.0, $\mathbf{a_{ax}}$), 0.86 (3H, ap.q, ^{2}J = 12.0, $\mathbf{a_{eq}}$).

^{13}C{^{1}H} NMR: ($CDCl_3$) δ 151.6 (**d**), 148.3 (**c**), 145.0 (**g**), 114.6 (**e**), 111.7 (**f**), 66.7 (**b**), 40.9 (**a**).

ESI-MS: positive ion *m/z* 364.1641 ($[M+H]^+$, calc. for $C_{21}H_{22}N_3O_3^+$: 364.1656, error 1.5 mDa); *m/z* 386.1454 ($[M+Na]^+$, calc. for $C_{24}H_{30}N_6NaO_3^+$: 386.1475, error 2.1 mDa); *m/z* 286.1547 ($[M+H-Arm]^+$, calc. for $C_{16}H_{20}N_3O_2^+$: 286.1550, error 0.3 mDa); 208.1447 ($[M+H-2Arm]^+$, calc. for $C_{11}H_{18}N_3O^+$: 208.1444, error −0.3 mDa); *m/z* 182.5862 ($[M+2H]^{2+}$, calc. for $C_{21}H_{23}N_3O_3^{2+}$: 182.5864, error 0.2 mDa).

_N,N',N''_-tris(2-furanylmethyl)-_cis,cis_-1,3,5-triaminocyclohexane, tachfur, [5b]

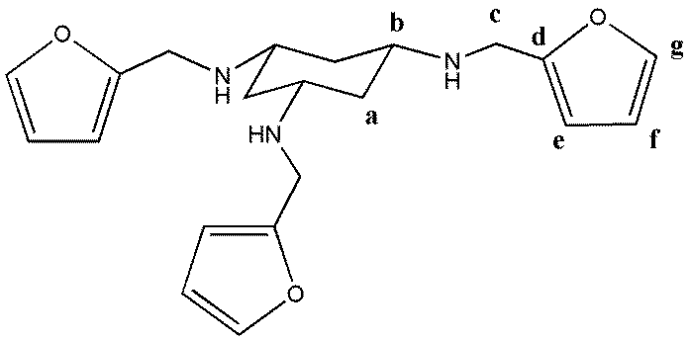

Cis,cis-1,3,5-tris(furan-2-carboxaldimino)cyclohexane, tachimfur, (152 mg, 0.42 mmol, 1 eq) was dissolved in methanol (15 mL) and sodium borohydride (63 mg, 1.67 mmol, 4 eq.) was slowly added in portions. The mixture was left stirring at room temperature for 16 h. Methanol was evaporated and the residue dissolved in 10 mL of $CHCl_3$. A 1:1 mixture of $NaHCO_3$ sat. solution and NaCl sat. solution (10 mL in total) was added to the organic solvent and the mixture was left stirring vigorously for 1 h. The layers were separated and the aqueous layer was extracted with $CHCl_3$ (3×7 mL). The organic layers combined were dried over $MgSO_4$, filtered and the solvent removed by rotary evaporation, leaving a yellow oil.

Yield: 150 mg, 0.26 mmol, 97%

^{1}H NMR: ($CDCl_3$) δ 7.35 (3H, dd, ^3J = 2.0, ^4J = 0.4, **g**), 6.30 (3H, dd, ^3J = 3.2, ^3J = 2.0, **f**), 6.15 (3H, dd, ^3J = 3.2, ^4J = 0.4, **e**), 3.81 (6H, s, **c**), 2.54 (3H, tt, $^3J_{ax\text{-}ax}$ = 11.2, $^3J_{ax\text{-}eq}$ = 3.6, **b**), 2.15 (3H, ap.d, ^2J = 11.2, $\mathbf{a_{ax}}$), 0.86 (3H, ap.q, $^3J_{ax\text{-}ax}$ = ^2J = 11.2, $\mathbf{a_{eq}}$).

^{13}C{^{1}H} NMR: ($CDCl_3$) δ 154.0 (**d**), 141.9 (**g**), 110.3 (**f**), 106.9 (**e**), 52.9 (**b**), 43.6 (**c**), 40.1 (**a**).

ESI-MS: positive ion *m/z* 370.2110 ($[M+H]^+$, calc. for $C_{21}H_{28}N_3O_3^+$: 370.2125, error 1.6 mDa); *m/z* 290.1856 ($[M+H-Arm]^+$, calc. for $C_{16}H_{24}N_3O_2^+$: 290.1863, error 0.7 mDa).

Elemental Analysis: for $C_{21}H_{27}N_3O_3 \cdot 0.5H_2O$: Calc. C 66.64; H 7.46; N 11.10; Rest 14.80%. Found C 66.87; H 7.27; N 11.08; Rest 14.78%.

6.3.3 Synthesis of salicylaldehyde derivatives

***Cis,cis*-1,3,5-tris(salicylidenamino)cyclohexane, salimtach, [6a]**

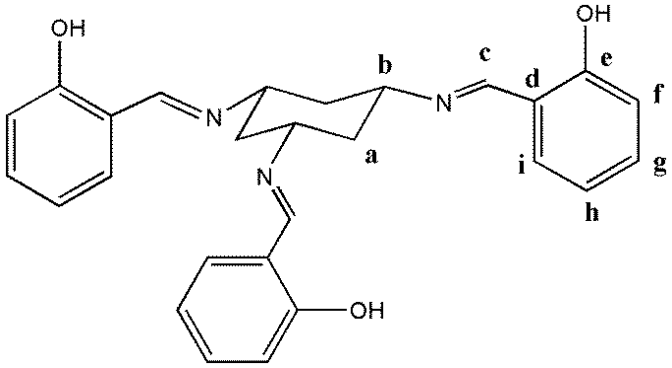

Tach·3HBr (250 mg, 0.67 mmol, 1 eq.) was dissolved in 7 mL of water and NaOH (80 mg, 2.01 mmol, 3 eq.) was added to the solution, which was left stirring at room temperature for 10 min. A solution of salicylaldehyde (245 mg, 213 μL, 2.01 mmol, 3 eq.) in 1 mL of diethyl ether was then added to the colourless water solution, which immediately turned to a bright yellow suspension. The mixture was left stirring at room temperature for 16 h, allowing ether to evaporate. The yellow solid was isolated by filtration and washed with chilled ethanol. The compound was used without further purification. Crystals suitable for X-ray diffraction were grown from $CHCl_3$/EtOH layer as bright yellow fine needles.

Yield: 260 mg, 0.59 mmol, 88%. Melting point: 206-207°C.

^{1}H NMR: ($CDCl_3$) δ 8.44 (3H, s, **c**), 7.32 (3H, m, ^3J = 8.0, ^4J = 1.6, **g**), 7.24 (3H, dd, ^3J = 7.5, ^4J = 1.6, **i**), 6.97 (3H, d, ^3J = 8.0, **f**), 6.88 (3H, td, ^3J = 7.5, ^4J = 0.9, **h**), 3.57 (3H, tt, $^3J_{ax\text{-}ax}$ = 11.6, $^3J_{ax\text{-}eq}$ = 4.0, **b**), 2.10 (3H, ap.d, ^2J = 11.6, $\mathbf{a_{eq}}$), 1.98 (3H, ap.q, ^3J = ^2J = 11.6, $\mathbf{a_{ax}}$).

^{13}C{^{1}H} NMR: ($CDCl_3$) δ 163.8 (**c**), 161.1 (**e**), 132.6 (**g**), 131.5 (**i**), 118.8 (**f**), 118.8 (**d**), 117.2 (**h**), 64.6 (**b**), 40.9 (**a**).

ESI-MS: positive ion *m/z* 442.2126 ($[M+H]^+$, calc. for $C_{27}H_{28}N_3O_3^+$: 442.2125, error −0.1 mDa); *m/z* 221.6081 ($[M+2H]^{2+}$, calc. for $C_{27}H_{29}N_3O_3^{2+}$: 221.6099, error 1.8 mDa).

Elemental Analysis: for $C_{27}H_{27}N_3O_3 \cdot 0.2H_2O$: Calc. C 72.85; H 6.20; N 9.44; Rest 11.51%. Found C 72.97; H 6.11; N 9.24; Rest 11.68%.

***Cis,cis*-1,3,5-tris(salicylamino)cyclohexane, saltach, [6b]**

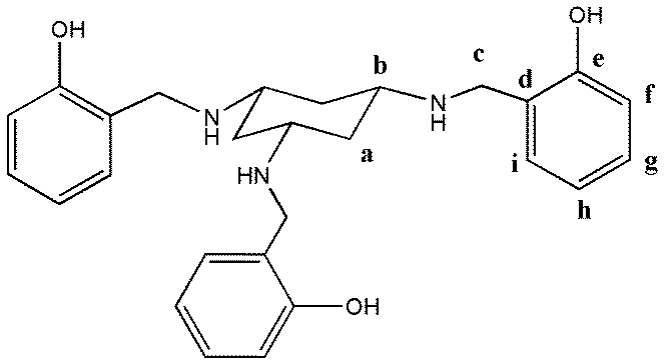

Cis,cis-1,3,5-tris(salicylidenamino)cyclohexane, salimtach, (150 mg, 0.34 mmol, 1 eq.) was suspended in 28 mL of methanol and sodium borohydride (102 mg, 2.7 mmol, 8 eq.) was slowly added in portions at 0°C. The mixture was stirred for 1 h at room temperature and, subsequently, heated at reflux for 16 h. Methanol was concentrated to about 7 mL and 30 mL of water were added. The pale yellow mixture was extracted with DCM (3×15 mL), the organic layers combined were dried over Na_2SO_4, filtered and the solvent removed by rotary evaporation, leaving a light yellow solid. Crystals suitable for X-ray diffraction were grown from DMSO/H_2O layer as colourless fine needles.

Yield: 140 mg, 0.31 mmol, 92%. Melting point: 198-199°C.

^{1}H NMR: (d_6-DMSO) δ 7.05 (6H, m, **g+i**), 6.69 (6H, m, **f+h**), 3.85 (6H, s, **c**), 2.40 (3H, ap.t, $^3J_{ax\text{-}ax}$ = 11.4, **b**), 2.18 (3H, ap.d, ^2J = 11.4, $\mathbf{a_{eq}}$), 0.87 (3H, ap.q, ^3J = ^2J = 11.4, $\mathbf{a_{ax}}$).

^{13}C{^{1}H} NMR: (d_6-DMSO) δ 157.7 (**e**), 128.2 (**g/i**), 127.7 (**g/i**), 124.1 (**d**), 118.3 (**f**), 115.4 (**h**), 52.3 (**b**), 47.8 (**c**), 38.3 (**a**).

ESI-MS: positive ion *m/z* 448.2607 ($[M+H]^+$, calc. for $C_{27}H_{34}N_3O_3^+$: 448.2595, error −1.2 mDa); *m/z* 224.6308 ($[M+2H]^{2+}$, calc. for $C_{27}H_{35}N_3O_3^{2+}$: 224.6333, error 2.5 mDa).

Elemental Analysis: for $C_{27}H_{33}N_3O_3 \cdot 0.6H_2O$: Calc. C 70.75; H 7.52; N 9.17; Rest 12.56%. Found C 70.63; H 7.32; N 9.09; Rest 12.96%.

***Cis,cis*-1,3,5-tris(5-chlorosalicylidenamino)cyclohexane, 5-Cl-salimtach, [7a]**

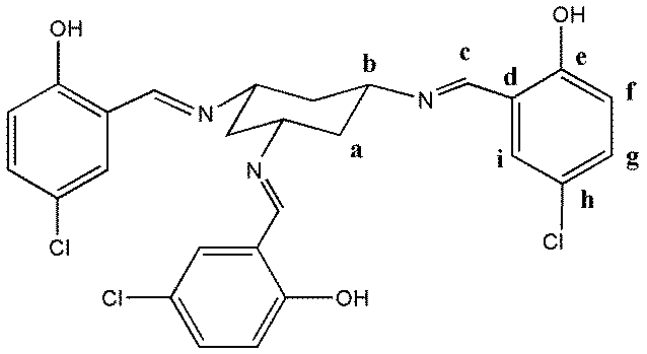

Tach·3HBr (250 mg, 0.67 mmol, 1 eq.) was dissolved in 7 mL of water and NaOH (80 mg, 2.01 mmol, 3 eq.) was added to the solution, which was left stirring at room temperature for 10 min. A solution of 5-chlorosalicylaldehyde (314 mg, 2.01 mmol, 3 eq.) in 2 mL of methanol was then added dropwise to the colourless water solution, which immediately turned to a bright yellow suspension. The mixture was left stirring at room temperature for 16 h. The yellow solid was isolated by filtration and washed with chilled ethanol.

Yield: 299 mg, 0.55 mmol, 82%.

^{1}H NMR: (d_6-DMSO) δ 8.65 (3H, s, **c**), 7.57 (3H, d, ^{4}J = 2.8, **i**), 7.36 (3H, dd, ^{3}J = 8.8, ^{4}J = 2.8, **g**), 6.91 (3H, d, ^{3}J = 8.8, **f**), 3.73 (3H, ap.t, $^{3}J_{ax\text{-}ax}$ = 11.3, **b**), 2.04 (3H, ap.d, ^{2}J = 11.3, $\mathbf{a_{eq}}$), 1.79 (3H, ap.q, $^{3}J = {}^{2}J$ = 11.3, $\mathbf{a_{ax}}$).

^{13}C{^{1}H} NMR: (d_6-DMSO) δ 163.4 (**c**), 159.2 (**e**), 131.8 (**g**), 130.4 (**i**), 121.7 (**h**), 119.6 (**d**), 118.4 (**f**), 62.4 (**b**), 39.6 (**a**).

ESI-MS: positive ion *m/z* 544.0955 ($[M+H]^+$, calc. for $C_{27}H_{25}Cl_3N_3O_3^+$: 544.0961, error 0.6 mDa); *m/z* 406.1079 ($[M+H-Arm]^+$, calc. for $C_{20}H_{22}Cl_2N_3O_2^+$: 406.1084, error 0.5 mDa); *m/z* 272.5497 ($[M+2H]^{2+}$, calc. for $C_{27}H_{26}Cl_3N_3O_3^{2+}$: 272.5514, error 1.7 mDa).

***Cis,cis*-1,3,5-tris(5-chlorosalicylamino)cyclohexane, 5-Cl-saltach, [7b]**

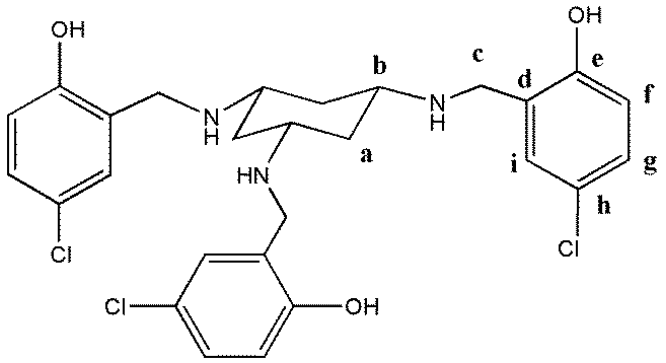

Cis,cis-1,3,5-tris(5-chlorosalicylidenamino)cyclohexane, 5-Cl-salimtach, (150 mg, 0.27 mmol, 1 eq.) was dissolved in 20 mL of methanol and sodium borohydride (82 mg, 2.16 mmol, 8 eq.) were slowly added in portions. Immediately the bright yellow solution became a cream suspension. The mixture was left stirring for 2 h at room temperature and, subsequently, heated at reflux for 4 h. Methanol was concentrated to about 4 mL and 20 mL of water were added. The precipitate was isolated by filtration and washed with small amounts of chilled ethanol. Crystals suitable for X-ray diffraction were grown from DMSO/H_2O layer as pale yellow fine needles.

Yield: 119 mg, 0.22 mmol, 78%. Melting point: 202-203°C.

^{1}H NMR: (d_6-DMSO) δ 7.14 (3H, d, ^4J = 2.8, **i**), 7.07 (3H, dd, ^3J = 8.4, ^4J = 2.8, **g**), 6.68 (3H, d, ^3J = 8.4, **f**), 3.83 (6H, s, **c**), 2.41 (3H, ap.t, $^3J_{ax\text{-}ax}$ = 11.6, **b**), 2.16 (3H, ap.d, ^2J = 11.6, $\mathbf{a_{eq}}$), 0.86 (3H, ap.q, ^3J = ^2J = 11.6, $\mathbf{a_{ax}}$).

^{13}C{^{1}H} NMR: (d_6-DMSO) δ 156.4 (**e**), 127.7 (**i**), 127.1 (**g**), 126.6 (**d**), 121.7 (**h**), 116.8 (**f**), 52.3 (**b**), 46.9 (**c**), 38.3 (**a**).

ESI-MS: positive ion *m/z* 550.1432 ($[M+H]^+$, calc. for $C_{27}H_{31}Cl_3N_3O_3^+$: 550.1426, error −0.6 mDa).

Elemental Analysis: for $C_{27}H_{30}Cl_3N_3O_3 \cdot 0.2H_2O$: Calc. C 58.48; H 5.53; N 7.58; Rest 28.41%. Found C 58.34; H 5.40; N 7.52; Rest 28.74%.

Cis,cis-1,3,5-tris(5-chlorosalicylamino)cyclohexane trihydrochloride, 5-Cl-salimtach·3HCl, [7b]HCl

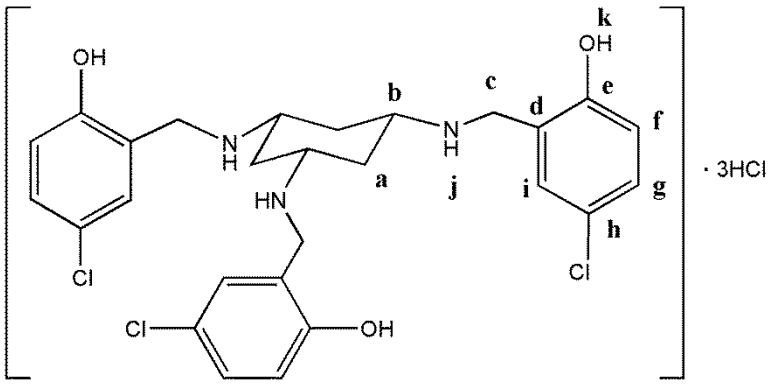

Cis,cis-1,3,5-tris(5-chlorosalicylamino)cyclohexane, 5-Cl-saltach, (80 mg, 0.14 mmol, 1 eq.) was dissolved in a 86 mM solution of HCl in water (0.43 mmol, 3 eq.).

The mixture was left stirring for 10 min, allowing the solid to completely dissolve in the acid solution. Water was evaporated under vacuum, leaving a white solid.

Yield: 90 mg, 0.14 mmol, 98%. Melting point: dec. >210°C.

^{1}H NMR: (d_6-DMSO) δ 10.66 (3H, s, **k**), 9.59 (6H, s, **j**), 7.58 (3H, d, ^4J = 2.4, **i**), 7.28 (3H, dd, ^3J = 8.4, ^4J = 2.4, **g**), 7.01 (3H, d, ^3J = 8.4, **f**), 4.09 (6H, s, **c**), 3.27 (3H, bs, **b**), 2.74 (3H, d, ^2J = 11.8, $\mathbf{a_{eq}}$), 1.77 (3H, ap.q, ^3J = ^2J = 11.8, $\mathbf{a_{ax}}$).

ESI-MS: positive ion *m/z* 550.1426 ($[M+H]^+$, calc. for $C_{27}H_{31}Cl_3N_3O_3^+$: 550.1426, error 0.0 mDa).

Elemental Analysis: for $C_{27}H_{33}Cl_6N_3O_3 \cdot 2.5H_2O$: Calc. C 45.98; H 5.43; N 5.96; Rest 42.63%. Found C 45.94; H 5.14; N 6.10; Rest 42.82%.

Cis,cis-1,3,5-tris(5-nitrosalicylidenamino)cyclohexane, 5-NO_2-salimtach, [8a]

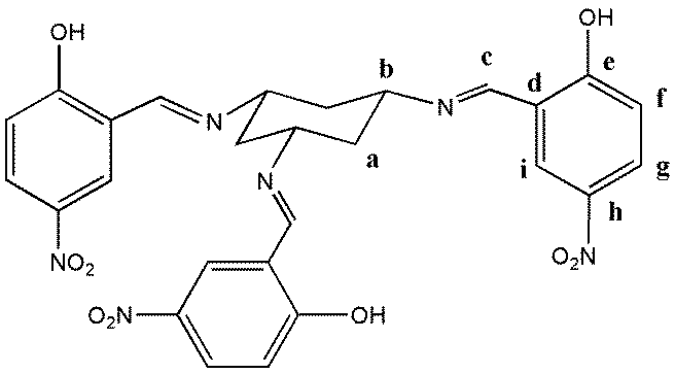

Tach·3HBr (250 mg, 0.67 mmol, 1 eq.) was dissolved in 7 mL of water and NaOH (80 mg, 2.01 mmol, 3 eq.) was added to the solution, which was left stirring at room temperature for 10 min. A methanolic solution of 5-nitrosalicylaldehyde (336 mg, 2.01 mmol, 3 eq.) was added dropwise to the colourless water solution, which immediately turned to a bright yellow suspension. The mixture was left stirring at room temperature for 16 h. The yellow solid was isolated by filtration and washed with chilled ethanol and a small amount of cold ether.

Yield: 306 mg, 0.53 mmol, 79%

^{1}H NMR: (d_6-DMSO) δ 8.90 (3H, s, **c**), 7.52 (3H, d, ^{4}J = 3.2, **i**), 8.13 (3H, dd, ^{3}J = 9.2, ^{4}J = 3.2, **g**), 6.84 (3H, d, ^{3}J = 9.2, **f**), 3.96 (3H, ap.t, $^{3}J_{ax\text{-}ax}$ = 11.5, **b**), 2.31 (3H, ap.d, ^{2}J = 11.5, $\mathbf{a_{eq}}$), 1.94 (3H, ap.q, $^{3}J = {}^{2}J$ = 11.5, $\mathbf{a_{ax}}$).

^{13}C{^{1}H} NMR: (d_6-DMSO) δ 172.5 (**e**), 164.7 (**c**), 136.1 (**h**), 130.3 (**i**), 128.6 (**g**), 120.4 (**f**), 115.4 (**d**), 58.6 (**b**), 37.5 (**a**).

ESI-MS: positive ion *m/z* 577.1667 ($[M+H]^+$, calc. for $C_{27}H_{25}N_6O_9^+$: 577.1683, error 1.6 mDa).

<u>*Cis,cis*-1,3,5-tris(5-nitrosalicylamino)cyclohexane, 5-NO_2-saltach, [8b]</u>

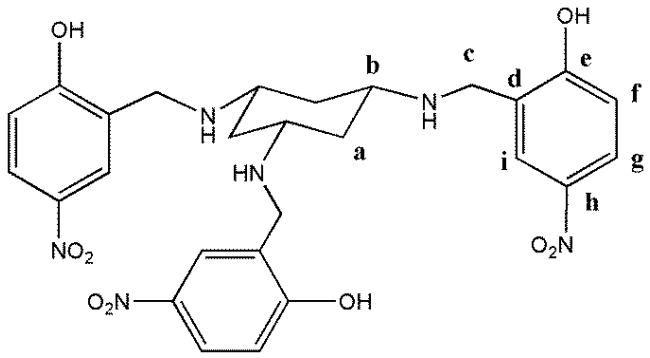

Cis,cis-1,3,5-tris(5-nitrosalicylidenamino)cyclohexane, 5-NO_2-salimtach, (150 mg, 0.26 mmol, 1 eq.) was suspended in 20 mL of methanol and sodium borohydride (79 mg, 2.08 mmol, 8 eq.) was slowly added in portions. The mixture was left stirring for 4 h at room temperature and, subsequently, heated at reflux for 2 h. The resulting yellow/orange solution was cooled to room temperature, methanol was concentrated to about 4 mL and 20 mL of water were added. The pH of the solution was adjusted to 7 with 1 M HCl, resulting in the precipitation of a bright yellow compound, which was isolated by filtration and washed with chilled EtOH.

Yield: 131 mg, 0.22 mmol, 87%.

^{1}H NMR: (d_6-DMSO) δ 8.05 (3H, d, ^4J = 2.8, **i**), 7.93 (3H, dd, ^3J = 9.2, ^4J = 2.8, **g**), 6.56 (3H, d, ^3J = 9.2, **f**), 3.97 (6H, s, **c**), 2.76 (3H, ap.t, $^3J_{ax\text{-}ax}$ = 11.2, **b**), 2.32 (3H, ap.d, ^2J = 11.2, $\mathbf{a_{eq}}$), 1.14 (3H, ap.q, ^3J = ^2J = 11.2, $\mathbf{a_{ax}}$).

^{13}C{^{1}H} NMR: (d_6-DMSO) δ 169.7 (**e**), 135.0 (**h**), 125.4 (**g/i**), 125.3(**g/i**), 122.8 (**d**), 116.7 (**f**), 51.7 (**b**), 45.9 (**c**), 34.8 (**a**).

ESI-MS: positive ion *m/z* 583.2162 ($[M+H]^+$, calc. for $C_{27}H_{31}N_6O_9^+$: 583.2147, error −1.5 mDa).

***Cis,cis*-1,3,5-tris(5-methylsalicylidenamino)cyclohexane, 5-Me-salimtach, [9a]**

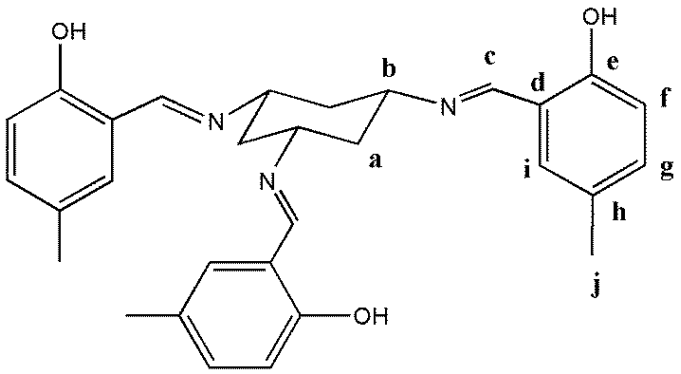

Tach·3HBr (250 mg, 0.67 mmol, 1 eq.) was dissolved in 10 mL of water and NaOH (80 mg, 2.01 mmol, 3 eq.) was added to the solution, which was left stirring at room temperature for 10 min. A solution of 5-methylsalicylaldehyde (273 mg, 2.01 mmol, 3 eq.) in 2.5 mL of diethyl ether was then added dropwise to the colourless water solution, which immediately turned to a bright yellow suspension. The mixture was left stirring at room temperature for 16 h, allowing the ether to evaporate. The yellow solid was isolated by filtration and washed with chilled ethanol. Crystals suitable for X-ray diffraction were grown from DMSO/H_2O layer in a NMR tube as bright yellow plates.

Yield: 205 mg, 0.42 mmol, 63%. Melting point: 176-179°C.

^{1}H NMR: (d_6-DMSO) δ 8.60 (3H, s, **c**), 7.24 (3H, d, ^4J = 2.0, **i**), 7.14 (3H, dd, ^3J = 8.2, ^4J = 2.0, **g**), 6.78 (3H, d, ^3J = 8.4, **f**), 3.66 (3H, ap.t, $^3J_{ax\text{-}ax}$ = 11.6, **b**), 2.24 (9H, s, **j**), 2.01 (3H, ap.d, ^2J = 11.6, $\mathbf{a_{eq}}$), 1.77 (3H, ap.q, ^3J = ^2J = 11.6, $\mathbf{a_{ax}}$).

^{13}C{^{1}H} NMR: (d_6-DMSO) δ 164.3 (**c**), 158.0 (**e**), 132.8 (**g**), 131.4 (**i**), 127.0 (**h**), 118.2 (**d**), 116.1 (**f**), 62.8 (**b**), 40.2 (**a**), 19.8 (**j**).

ESI-MS: positive ion *m/z* 484.2604 ($[M+H]^+$, calc. for $C_{30}H_{34}N_3O_3^+$: 484.2595, error −0.9 mDa); *m/z* 242.6321 ($[M+2H]^{2+}$, calc. for $C_{27}H_{35}N_3O_3^{2+}$: 242.6333, error 1.2 mDa).

<u>*Cis,cis*-1,3,5-tris(5-methylsalicylamino)cyclohexane, 5-Me-saltach, [9b]</u>

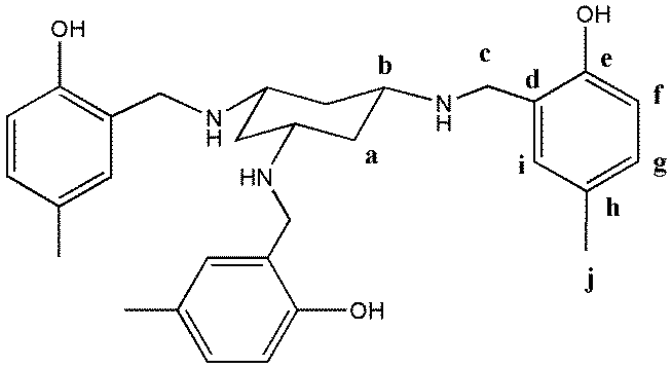

Cis,cis-1,3,5-tris(5-methylsalicylidenamino)cyclohexane, 5-Me-salimtach (100 mg, 0.21 mmol, 1 eq.) was dissolved in 20 mL of methanol and sodium borohydride (79 mg, 2.1 mmol, 10 eq.) were slowly added in portions at 0°C. The mixture was left stirring for 1 h at room temperature and, subsequently, heated at reflux for 4 h. Methanol was concentrated to about 3 mL and 7 mL of water were added. The resulting cloudy mixture was extracted with DCM (3×7 mL), the organic layers combined were dried over Na_2SO_4, filtered and the solvent removed by rotary evaporation, leaving a light yellow solid. Crystals suitable for X-ray diffraction were grown from DMSO/H_2O layer as yellow needles.

Yield: 64 mg, 0.13 mmol, 63%. Melting point: 194-196°C.

^{1}H NMR: ($CDCH_3$) δ 6.97 (3H, dd, ^3J = 8.4, ^4J = 1.6, **g**), 7.77 (3H, dd, ^4J = 1.4, **i**), 6.73 (3H, d, ^3J = 8.4, **f**), 3.97 (6H, s, **c**), 2.58 (3H, ap.t, $^3J_{ax\text{-}ax}$ = 11.6, **b**), 2.37 (3H, ap.d, ^2J = 11.6, $\mathbf{a_{eq}}$), 2.24 (9H, s, **j**), 0.93 (3H, ap.q, $^3J = {}^2J$ = 11.6, $\mathbf{a_{ax}}$).

^{13}C{^{1}H} NMR: ($CDCH_3$) δ 155.7 (**e**), 129.4 (**g**), 128.9 (**i**), 128.3 (**h**), 122.1 (**d**), 116.3 (**f**), 52.6 (**b**), 49.9 (**c**), 34.4 (**a**), 20.5 (**j**).

ESI-MS: positive ion *m/z* 490.3079 ($[M+H]^+$, calc. for $C_{30}H_{40}N_3O_3^+$: 490.3064, error −1.5 mDa); *m/z* 370.2425 ($[M+H-Arm]^+$, calc. for $C_{22}H_{32}N_3O_2^+$: 370.2489, error 6.4 mDa); *m/z* 245.6553 ($[M+2H]^{2+}$, calc. for $C_{30}H_{41}N_3O_3^{2+}$: 245.6568, error 1.5 mDa).
Elemental Analysis: for $C_{30}H_{39}N_3O_3 \cdot 0.1H_2O$: Calc. C 73.32; H 8.04; N 8.55; Rest 10.09%. Found C 73.24; H 8.16; N 8.45; Rest 10.15%.

6.3.4 Synthesis of benzaldehyde derivatives

***Cis,cis*-1,3,5-tris(benzylidenamino)cyclohexane, tachimben, [10a]**

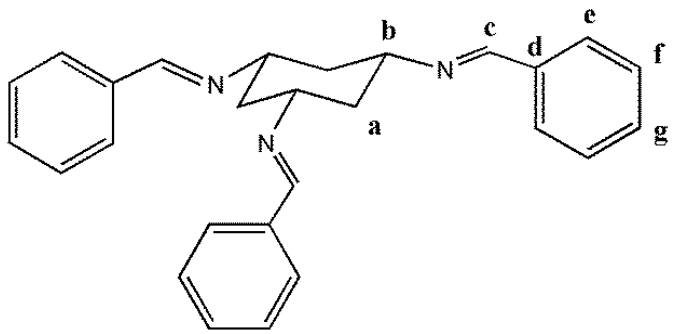

Tach·3HBr (500 mg, 1.34 mmol, 1 eq.) was dissolved in 5 mL of water and NaOH (161 mg, 4.03 mmol, 3 eq.) added. The solution was left stirring for 10 min, then a solution of benzaldehyde (428 mg, 0.409 mL, 4.03 mmol, 3 eq.) in diethyl ether (7 mL) was slowly added and the reaction mixture was left stirring at room temperature for 16 h under a N_2 atmosphere. The two layers were separated and the aqueous one was extracted with ether (3x5 mL). The organic layers combined were dried over $MgSO_4$, filtered and solvent evaporated by rotary evaporation, leaving a white solid, which was generally used without further purification. Colourless crystals of the compound could be obtained from a 1:1 mixture of diethyl ether and hexane at 4°C.
Yield: 400 mg, 0.95 mmol, 71%
^{1}H NMR: ($CDCl_3$) δ 8.39 (3H, s, **c**), 7.75 (6H, dd, ^3J = 6.0, ^4J = 2.3, **e**) 7.41 (9H, m, **f**+**g**), 3.59 (3H, ap.tt, $^3J_{ax\text{-}ax}$ = 11.2, $^3J_{ax\text{-}eq}$ = 4.0, **b**), 2.06 (3H, ap.q, $^3J_{ax\text{-}ax}$ = ^2J = 11.2, $\mathbf{a_{ax}}$), 1.92 (3H, ap.d, ^2J = 11.2, $\mathbf{a_{eq}}$).
^{13}C{^{1}H} NMR: ($CDCl_3$) δ 159.6 (**c**), 136.5 (**d**), 130.7 (**f/g**), 128.7 (**f/g**), 128.3 (**e**), 66.5 (**b**), 41.0 (**a**).

ESI-MS: positive ion *m/z* 394.2261 ($[M+H]^+$, calc. for $C_{27}H_{28}N_3^+$: 394.2278, error 1.7 mDa); *m/z* 306.1958 ($[M+H-Arm]^+$, calc. for $C_{20}H_{24}N_3^+$: 306.1965, error 0.7 mDa); 218.1627 ($[M+H-2Arm]^+$, calc. for $C_{13}H_{20}N_3^+$: 218.1652, error 2.5 mDa).

<u>*Cis,cis*-1,3,5-tris(benzylamino)cyclohexane, tachben, [10b]</u>

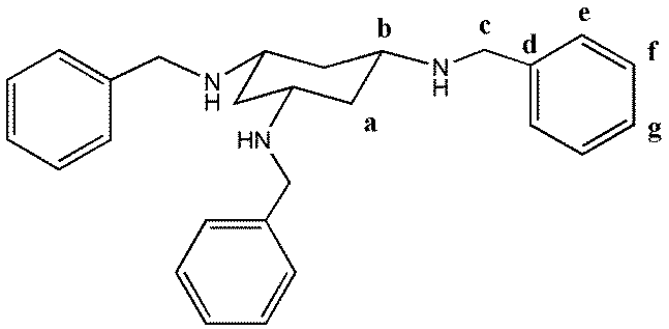

Cis,cis-1,3,5-tris(benzylidenamino)cyclohexane, tachimben, (316 mg, 0.80 mmol, 1 eq.) was dissolved in methanol (4 mL) and sodium borohydride (60 mg, 1.6 mmol, 2 eq.) was slowly added in portions. The solution was heated to reflux for 2 h in the presence of molecular sieves type 4A. After cooling to room temperature, the mixture was filtered and water added until a white suspension persisted (ca. 12 mL). The mixture was then extracted with diethyl ether, dried over $MgSO_4$, filtered and the solvent removed by rotary evaporation, leaving a colourless oil, which was dried on a high vacuum line.

Yield: 202 mg, 0.50 mmol, 63%

^{1}H NMR: (d_6-DMSO) δ 7.28 (12H, m, **e**+**f**), 7.20 (3H, tt, ^3J = 6.8, ^4J = 1.8, **g**), 3.70 (6H, s, **c**), 2.29 (3H, ap.t, $^3J_{ax\text{-}ax}$ = 11.2, **b**), 2.12 (3H, ap.d, ^2J = 11.2, $\mathbf{a_{eq}}$), 0.79 (3H, ap.q, $^3J_{ax\text{-}ax} = {}^2J$ = 11.2, $\mathbf{a_{ax}}$).

^{13}C{^{1}H} NMR: (d_6-DMSO) δ 141.4 (**d**), 128.0 (**f/e**), 127.8 (**f/e**), 126.3 (**g**), 52.8 (**b**), 50.0 (**c**), 39.9 (**a**).

ESI-MS: positive ion *m/z* 400.2736 ($[M+H]^+$, calc. for $C_{27}H_{34}N_3^+$: 400.2747, error 1.1 mDa); *m/z* 310.2274 ($[M+H-Arm]^+$, calc. for $C_{20}H_{28}N_3^+$: 310.2278, error 0.4 mDa); 220.1791 ($[M+H-2Arm]^+$, calc. for $C_{13}H_{22}N_3^+$: 220.1808, error 1.7 mDa).

Elemental Analysis: for $C_{27}H_{33}N_3 \cdot 0.8H_2O$: Calc. C 78.33; H 8.42; N 10.15; Rest 3.10%. Found C 78.35; H 8.37; N 10.12; Rest 3.16%.

***Cis,cis*-1,3,5-tris(4-(dimethylamino)benzylidenamino)cyclohexane, 4-NMe_2-tachimben , [11a]**

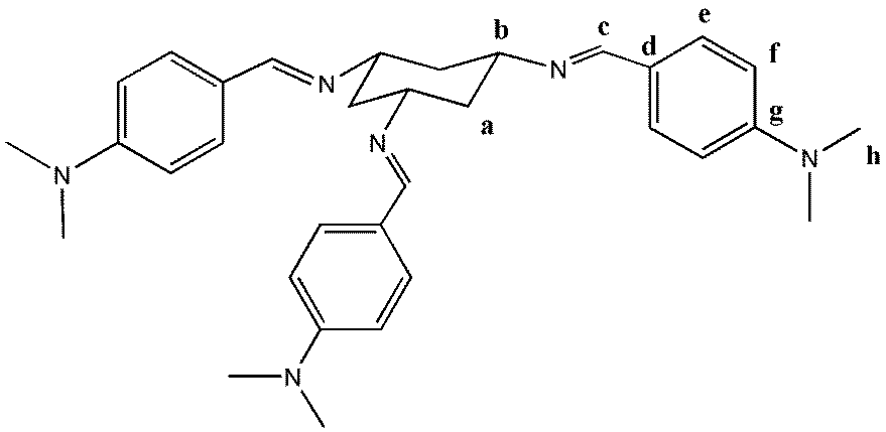

Tach·3HBr (200 mg, 0.54 mmol, 1 eq.) was dissolved in 14 mL of EtOH and NaOH (64 mg, 1.61 mmol, 3 eq.) added. The solution was left stirring for 10 min, then 4-(dimethylamino)benzaldehyde (240 mg, 1.61 mmol, 3 eq.) was slowly added and the reaction mixture was heated at reflux for 16 h. Upon heating, the initially colourless reaction mixture became a bright yellow solution. After cooling down, the solvent was evaporated and 30 mL of $CHCl_3$ added to the residue, causing the precipitation of a white solid (unreacted tach and NaBr) from the yellow solution, which was filtered and solvent evaporated by rotary evaporation, leaving a yellow solid. The solid was re-crystallised from slow evaporation of a EtOH/DCM mix. The yellow crystals were filtered and washed several times with cold EtOH. Needle-like crystals suitable for X-ray diffraction were grown with the same method.

Yield: from reaction: 264 mg, 0.50 mmol, 93%; from crystals: 130 mg, 0.25 mmol, 46%. Melting point: decomposition 218-221° C

^{1}H NMR: ($CDCl_3$) δ 8.24 (3H, s, **c**), 7.61 (6H, d, ^3J = 8.4, **e**), 6.68 (6H, d, ^3J = 8.4, **f**), 3.50 (3H, ap.t, $^3J_{ax\text{-}ax}$ = 11.2, **b**), 2.99 (18H, s, **h**), 1.95 (6H, m, **a**).

^{13}C{^{1}H} NMR: ($CDCl_3$) δ 159.2 (**c**), 152.1 (**g**), 129.7 (**e**), 124.8 (**d**), 111.7 (**f**), 66.5 (**b**), 41.5 (**a**), 40.4 (**h**).

ESI-MS: positive ion *m/z* 523.3533 ($[M+H]^+$, calc. for $C_{33}H_{43}N_6^+$: 523.3544, error 1.0 mDa); *m/z* 262.1800 ($[M+2H]^{2+}$, calc. for $C_{33}H_{44}N_6^{2+}$: 262.1808, error 0.8 mDa).

Elemental Analysis: for $C_{33}H_{42}N_6$·1.1EtOH: Calc. C 73.73; H 8.54; N 14.66; Rest 3.07%. Found C 73.50; H 8.42; N 14.89; Rest 3.19%.

Cis,cis-1,3,5-tris(4-(dimethylamino)benzylamino)cyclohexane, 4-NMe_2-tachben, [11b]

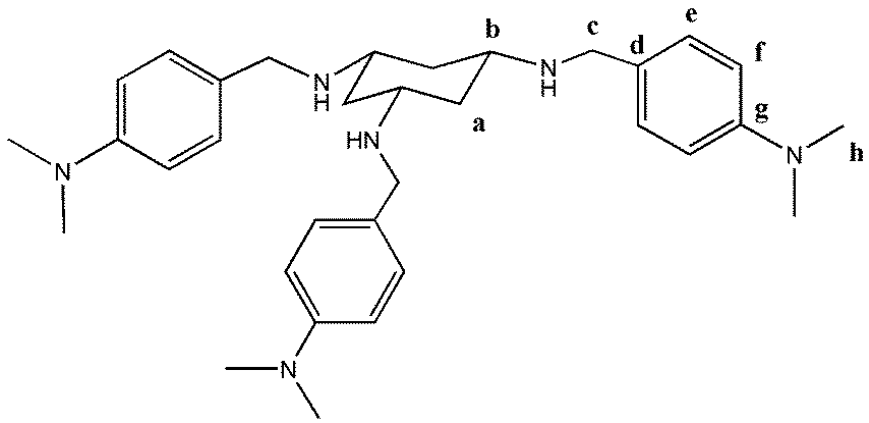

Cis,cis-1,3,5-tris(4-(dimethylamino)benzylidenamino)cyclohexane, 4-NMe_2-tachimben, (130 mg, 0.25 mmol, 1 eq.) was suspended in methanol (15 mL) and sodium borohydride (38 mg, 1.0 mmol, 4 eq.) was slowly added in portions. The pale yellow suspension turned in to a colourless solution. The mixture was stirred at room temperature for 16 h. Methanol was evaporated and the residue was taken with H_2O (7 mL) and DCM (7 mL). The layers were separated and the aqueous layer was extracted with DCM (3×7 mL). The organic layers combined were dried over $MgSO_4$, filtered and the solvent removed by rotary evaporation, leaving a colourless oil.

Yield: 109 mg, 0.21 mmol, 82%

^{1}H NMR: (CD_3OD) δ 7.16 (6H, d, ^3J = 8.8, **e**), 6.74 (6H, d, ^3J = 8.8, **f**), 3.67 (6H, s, **c**), 2.89 (18H, s, **h**), 2.44 (3H, ap.t, $^3J_{ax\text{-}ax}$ = 11.6, **b**), 2.18 (3H, ap.d, ^2J = 11.6, $\mathbf{a_{eq}}$), 0.98 (3H, ap.q, $^3J_{ax\text{-}ax} = {}^2J$ = 11.6, $\mathbf{a_{ax}}$).

^{13}C{^{1}H} NMR: (CD_3OD) δ 151.6 (**g**), 130.5 (**e**), 128.6 (**d**), 114.2 (**f**), 53.5 (**b**), 50.8 (**c**), 41.1 (**h**), 39.1 (**a**).

ESI-MS: positive ion *m/z* 529.3991 ($[M+H]^+$, calc. for $C_{33}H_{49}N_6^+$: 529.4013, error 2.3 mDa); *m/z* 396.3111 ($[M+H-Arm]^+$, calc. for $C_{24}H_{38}N_5^+$: 396.3122, error 1.1 mDa).

Elemental Analysis: for $C_{33}H_{48}N_6 \cdot 0.55H_2O$: Calc. C 74.58; H 9.19; N 15.60; Rest 0.63%. Found C 74.07; H 9.17; N 15.07; Rest 1.69%.

***Cis,cis*-1,3,5-tris(4-methoxybenzylidenamino)cyclohexane, 4-OMe-tachimben, [12a]**

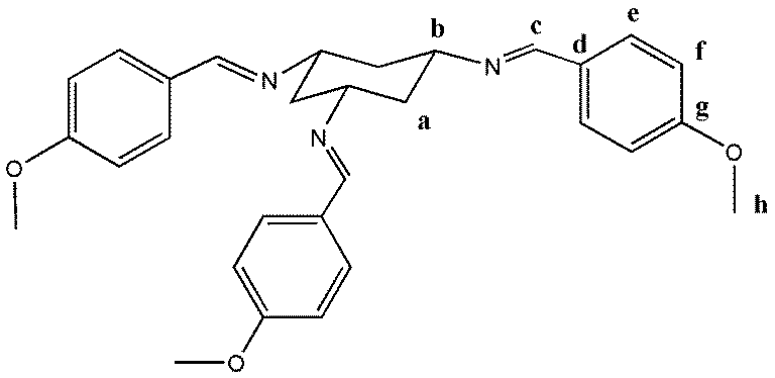

Tach·3HBr (150 mg, 0.40 mmol, 1 eq.) was dissolved in 10 mL of EtOH and NaOH (48 mg, 1.21 mmol, 3 eq.) added. The solution was left stirring for 10 min, then 4-methoxybenzaldehyde (163 mg, 143 μL, 1.21 mmol, 3 eq.) was slowly added and the reaction mixture was heated at reflux for 16 h. After cooling down, the solvent was evaporated and 20 mL of $CHCl_3$ added to the residue, causing the precipitation of a white solid (unreacted tach and NaBr) from the solution, which was filtered and solvent evaporated by rotary evaporation, leaving a yellow solid. The compound was usually used without further purification.

Yield: 140 mg, 0.29 mmol, 72%.

^{1}H NMR: (CD_3OD) δ 8.39 (3H, s, **c**), 7.72 (6H, d, ^3J = 8.8, **e**), 6.98 (6H, d, ^3J = 8.8, **f**), 3.83 (9H, s, **h**), 3.60 (3H, ap.t, $^3J_{ax\text{-}ax}$ = 11.6, **b**), 1.98 (3H, ap.q, $^3J_{ax\text{-}ax}$ = ^{2}J = 11.6, $\mathbf{a_{ax}}$), 1.87 (3H, ap.d, ^2J = 11.6, $\mathbf{a_{eq}}$).

^{13}C{^{1}H} NMR: ($CDCl_3$) δ 163.6 (**g**), 162.8 (**c**), 131.2 (**e**), 129.8 (**d**), 115.1 (**f**), 67.5 (**b**), 55.9 (**h**), 42.0 (**a**).

ESI-MS: positive ion *m/z* 484.2575 ($[M+H]^+$, calc. for $C_{30}H_{34}N_3O_3^+$: 484.2585, error 2.0 mDa); *m/z* 366.2170 ($[M+H-Arm]^+$, calc. for $C_{22}H_{28}N_3O_2^+$: 366.2176, error 0.6 mDa); *m/z* 242.6284 ($[M+2H]^{2+}$, calc. for $C_{30}H_{35}N_3O_3^{2+}$: 242.6333, error 4.9 mDa).

***Cis,cis*-1,3,5-tris(4-methoxybenzylamino)cyclohexane, 4-OMe-tachben, [12b]**

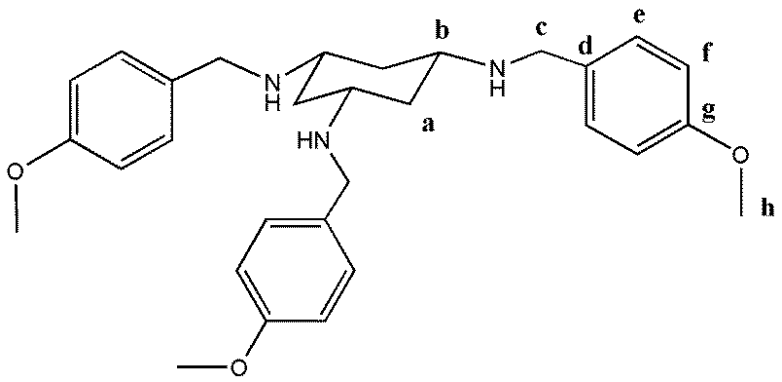

Cis,cis-1,3,5-tris(4-methoxybenzylidenamino)cyclohexane, 4-OMe-tachben, (140 mg, 0.29 mmol, 1 eq.) was dissolved in methanol (15 mL) and sodium borohydride (44 mg, 1.16 mmol, 4 eq.) was slowly added in portions. The pale yellow solution turned immediately colourless. The mixture was stirred at room temperature for 16 h. Methanol was evaporated and the residue was taken with H_2O (10 mL) and $CHCl_3$ (10 mL). The layers were separated and the aqueous layer was extracted with $CHCl_3$ (3×10 mL). The organic layers were combined and the solvent removed by rotary evaporation. The residue was re-dissolved in 12 mL of 0.1 M HCl solution and washed with diethyl ether (2×10 mL). The aqueous solution was basified with NaOH, becoming a white cloudy suspension as soon as the pH became basic. The mixture was extracted with $CHCl_3$ (4×10 mL), dried with $MgSO_4$, filtered and the solvent evaporated, leaving a colourless oil.

Yield: 116 mg, 0.24 mmol, 82%

^{1}H NMR: (CD_3OD) δ 7.24 (6H, d, ^3J = 8.4, **e**), 6.87 (6H, d, ^3J = 8.4, **f**), 3.78 (9H, s, **h**), 3.71 (6H, s, **c**), 2.45 (3H, ap.t, $^3J_{ax\text{-}ax}$ = 11.6, **b**), 2.20 (3H, ap.d, ^2J = 11.6, $\mathbf{a_{eq}}$), 1.00 (3H, ap.q, $^3J_{ax\text{-}ax} = {}^2J$ = 11.6, $\mathbf{a_{ax}}$).

^{13}C{^{1}H} NMR: (CD_3OD) δ 160.4 (**g**), 132.6 (**d**), 130.8 (**e**), 114.8 (**f**), 55.6 (**h**), 53.8 (**b**), 50.7 (**c**), 39.3 (**a**).

ESI-MS: positive ion *m/z* 490.3056 ($[M+H]^+$, calc. for $C_{30}H_{40}N_3O_3^+$: 490.3064, error 0.8 mDa); *m/z* 370.2480 ($[M+H-Arm]^+$, calc. for $C_{22}H_{32}N_3O_2^+$: 370.2489, error 0.9 mDa); *m/z* 350.1888 ($[M+H-2Arm]^+$, calc. for $C_{14}H_{24}N_3O^+$: 250.1914, error 2.6 mDa).

Elemental Analysis: for $C_{30}H_{39}N_3O_3 \cdot 0.3H_2O$: Calc. C 72.78; H 8.06; N 8.49; Rest 10.67%. Found C 72.74; H 7.90; N 8.53; Rest 10.83%.

***Cis,cis*-1,3,5-tris(4-fuorobenzylidenamino)cyclohexane, 4-F-tachimben, [13a]**

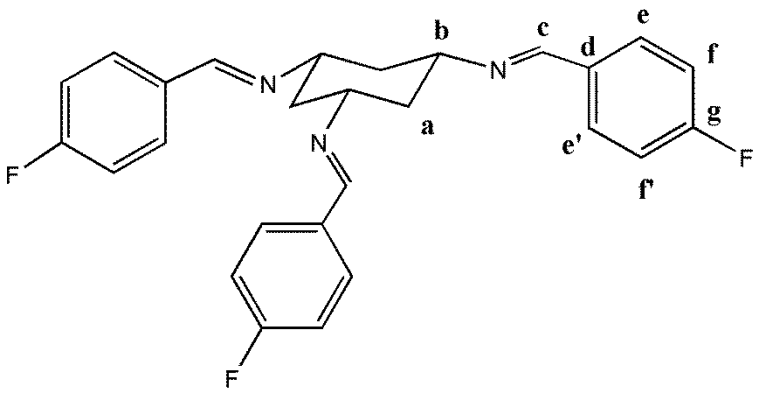

Tach·3HBr (150 mg, 0.40 mmol, 1 eq.) was dissolved in 10 mL of MeOH and NaOH (48 mg, 1.21 mmol, 3 eq.) added. The solution was left stirring for 10 min, then 4-fluorobenzaldehyde (150 mg, 130 μL, 1.21 mmol, 3 eq.) was added and the reaction mixture was stirred at room temperature for 16 h, during which time the initially colourless reaction mixture became a pale yellow solution. The solvent was evaporated and 20 mL of $CHCl_3$ added to the residue, causing the precipitation of a white solid (unreacted tach and NaBr) from the solution, which was filtered and the solvent evaporated by rotary evaporation, leaving a white solid. The compound was usually used without further purification.

Yield: 120 mg, 0.27 mmol, 68%.

^{1}H NMR: ($CDCl_3$) δ 8.34 (3H, s, **c**), 7.73 (6H, dd, $^3J_{H\text{-}H}$ = 8.6, $^4J_{H\text{-}F}$ = 5.5, **e**), 7.09 (6H, ap.t, $^3J_{H\text{-}H}$ = $^3J_{H\text{-}F}$ = 8.6, **f**), 3.56 (3H, tt, $^3J_{ax\text{-}ax}$ = 11.6, $^3J_{ax\text{-}eq}$ = 4.0, **b**), 2.02 (3H, ap.q, $^3J_{ax\text{-}ax}$ = ^2J = 11.6, $\mathbf{a_{ax}}$), 1.88 (3H, dt, ^2J = 11.6, $^3J_{ax\text{-}eq}$ = 4.0, $\mathbf{a_{eq}}$). NOTE: protons **e**/**e'** and **f**/**f'** showed magnetic inequivalence.

^{13}C{^{1}H} NMR: ($CDCl_3$) δ 164.4 (d, ^1J = 250.5, **g**), 158.1 (**c**), 132.8 (d, ^4J = 3.0, **d**), 130.1 (d, ^3J = 8.6, **e**), 115.8 (d, ^2J = 21.8, **f**), 66.3 (**b**), 41.0 (**a**).

^{19}F NMR: ($CDCl_3$) δ -109.6 (tt, $^3J_{H\text{-}F}$ = 8.6, $^4J_{H\text{-}F}$ = 5.5).

ESI-MS: positive ion *m/z* 448.1994 ($[M+H]^+$, calc. for $C_{27}H_{25}F_3N_3^+$: 448.1995, error 0.1 mDa); *m/z* 342.1776 ($[M+H-Arm]^+$, calc. for $C_{20}H_{22}F_2N_3^+$: 342.1776, error 0.0 mDa); *m/z* 236.1501 ($[M+H-2Arm]^+$, calc. for $C_{13}H_{19}FN_3^+$: 236.1558, error 5.7 mDa).

***Cis,cis*-1,3,5-tris(4-fuorobenzylamino)cyclohexane, 4-F-tachben, [13b]**

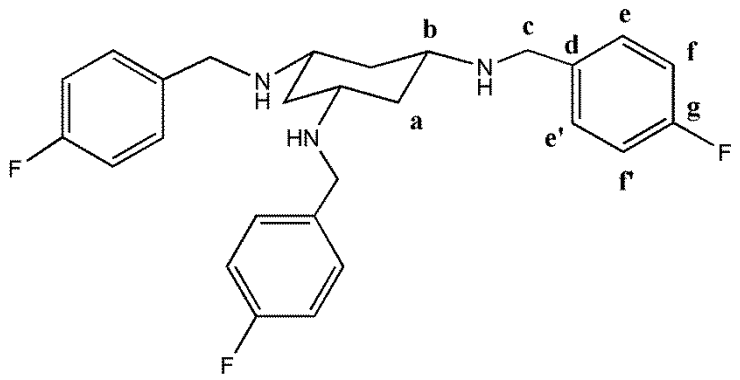

Cis,cis-1,3,5-tris(4-fluorobenzylidenamino)cyclohexane, 4-F-tachimben, (120 mg, 0.27 mmol, 1 eq.) was dissolved in methanol (15 mL) and sodium borohydride (41 mg, 1.08 mmol, 4 eq.) was slowly added in portions. The mixture was stirred at room temperature for 16 h. Methanol was evaporated and the residue was taken with H_2O (10 mL) and DCM (10 mL). The layers were separated and the aqueous layer was extracted with DCM (3×10 mL). The organic layers were combined and the solvent removed by rotary evaporation. The residue was re-dissolved in 10 mL of 0.1 M HCl solution and washed with diethyl ether (2×10 mL). The aqueous solution was basified with NaOH, becoming a white cloudy suspension as soon as the pH became basic. The mixture was extracted with DCM (4×10 mL), dried with $MgSO_4$, filtered and the solvent evaporated, leaving a colourless oil.

Yield: 117 mg, 0.26 mmol, 96%.

^{1}H NMR: (CD_3OD) δ 7.35 (6H, dd, $^3J_{H\text{-}H}$ = 8.4, $^4J_{H\text{-}F}$ = 5.2, **e**), 7.04 (6H, ap.t, $^3J_{H\text{-}H}$ = $^3J_{H\text{-}F}$ = 8.4, **f**), 3.77 (6H, s, **c**), 2.48 (3H, ap.t, $^3J_{ax\text{-}ax}$ = 11.6, **b**), 2.24 (3H, ap.d, ^2J = 11.6, $\mathbf{a_{eq}}$), 1.02 (3H, ap.q, $^3J_{ax\text{-}ax}$ = ^2J = 11.6, $\mathbf{a_{ax}}$). NOTE: protons **e**/**e'** and **f**/**f'** showed magnetic inequivalence.

^{13}C{^{1}H} NMR: (CD_3OD) δ 163.4 (d, ^1J = 243.6, **g**), 136.8 (d, ^4J = 3.1, **d**), 131.4 (d, ^3J = 7.9, **e**), 116.1 (d, ^2J = 21.4, **f**), 54.0 (**b**), 50.6 (**c**), 39.4 (**a**).

^{19}F NMR: (CD_3OD) δ -117.9 (tt, $^3J_{H\text{-}F}$ = 8.4, $^4J_{H\text{-}F}$ = 5.2).

ESI-MS: positive ion *m/z* 454.2475 ($[M+H]^+$, calc. for $C_{27}H_{31}F_3N_3^+$: 454.2465, error −1.0 mDa); *m/z* 346.2104 ($[M+H-Arm]^+$, calc. for $C_{20}H_{26}F_2N_3^+$: 346.2089, error −1.5 mDa).

Elemental Analysis: for $C_{27}H_{30}F_3N_3 \cdot 0.3H_2O$: Calc. C 70.66; H 6.72; N 9.16; Rest 13.43%. Found C 70.54; H 6.67; N 9.35; Rest 13.44%.

***Cis,cis*-1,3,5-tris(4-bromobenzylidenamino)cyclohexane, 4-Br-tachimben, [14a]**

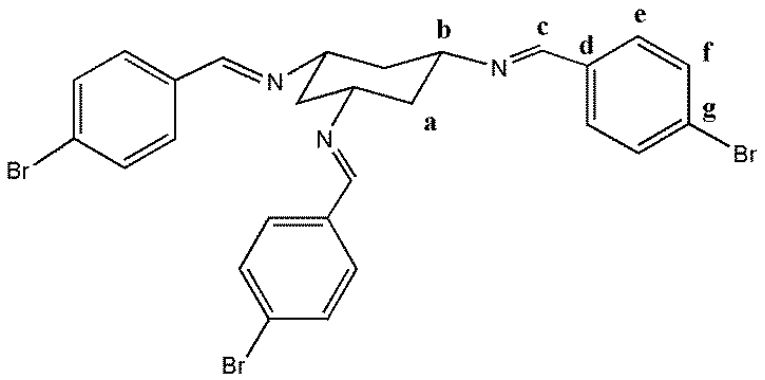

Tach·3HBr (150 mg, 0.40 mmol, 1 eq.) was dissolved in 10 mL of MeOH and NaOH (48 mg, 1.21 mmol, 3 eq.) added. The solution was left stirring for 10 min, then 4-bromobenzaldehyde (224 mg, 1.21 mmol, 3 eq.) was added and the reaction mixture was stirred at room temperature for 16 h, during which time a white precipitate formed. The solid was filtered and washed with cold methanol. The compound was used without further purification.

Yield: 164 mg, 0.26 mmol, 65%. Melting point: 166-167°C.

^{1}H NMR: ($CDCl_3$) δ 8.30 (3H, s, **c**), 7.59 (6H, d, ^{3}J = 8.4, **e**), 7.52 (6H, d, ^{3}J = 8.4, **f**), 3.55 (3H, ap.t, $^{3}J_{ax\text{-}ax}$ = 12.0, **b**), 2.01 (3H, ap.q, $^{3}J_{ax\text{-}ax}$ = ^{2}J = 12.0, $\mathbf{a_{ax}}$), 1.86 (3H, ap.d, ^{2}J = 12.0, $\mathbf{a_{eq}}$).

^{13}C{^{1}H} NMR: ($CDCl_3$) δ 158.4 (**c**), 135.3 (**d**), 131.9 (**f**), 129.7 (**e**), 125.1 (**g**), 66.4 (**b**), 40.9 (**a**).

ESI-MS: positive ion *m/z* 627.9596 ($[M+H]^+$, calc. for $C_{27}H_{25}Br_3N_3^+$: 627.9593, error −0.3 mDa); *m/z* 462.0161 ($[M+H-Arm]^+$, calc. for $C_{20}H_{22}Br_2N_3^+$: 462.0175, error 1.4 mDa); *m/z* 296.0738 ($[M+H-2Arm]^+$, calc. for $C_{13}H_{19}BrN_3^+$: 296.0757, error 1.9 mDa).

Elemental Analysis: for $C_{27}H_{24}Br_3N_3$: Calc. C 51.46; H 3.84; N 6.67; Rest 38.03%. Found C 51.01; H 3.75; N 6.56; Rest 38.50%.

***Cis,cis*-1,3,5-tris(4-bromobenzylamino)cyclohexane, 4-Br-tachben, [14b]**

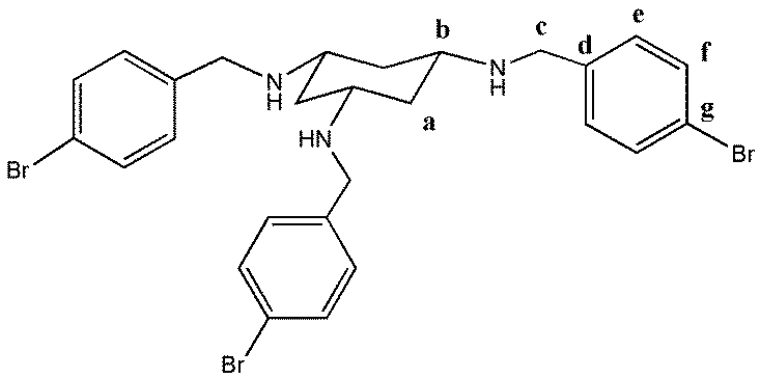

Cis,cis-1,3,5-tris(4-bromobenzylidenamino)cyclohexane, 4-Br-tachimben, (128 mg, 0.20 mmol, 1 eq.) was dissolved in a 2:1 methanol/DCM mixture (12 mL) and sodium borohydride (31 mg, 0.80 mmol, 4 eq.) was slowly added in portions. The mixture was stirred at room temperature for 16 h. Methanol was concentrated to 1 mL and H_2O (10 mL) added. The mixture was extracted with $CHCl_3$ (3×10 mL) and the organic layers combined were dried over $MgSO_4$, filtered and the solvent removed by rotary evaporation, leaving a colourless oil.

Yield: 121 mg, 0.19 mmol, 98%

^{1}H NMR: (CD_3OD) δ 7.47 (6H, d, ^3J = 8.4, **e**), 7.26 (6H, d, ^3J = 8.4, **f**), 3.75 (6H, s, **c**), 2.46 (3H, ap.t, $^3J_{ax\text{-}ax}$ = 11.6, **b**), 2.21 (3H, ap.d, ^2J = 11.6, $\mathbf{a_{eq}}$), 1.00 (3H, ap.q, $^3J_{ax\text{-}ax}$ = ^{2}J = 11.6, $\mathbf{a_{ax}}$).

^{13}C{^{1}H} NMR: (CD_3OD) δ 140.1 (**d**), 132.6 (**f**), 131.5 (**e**), 121.8 (**g**), 54.0 (**b**), 50.7 (**c**), 39.4 (**a**).

ESI-MS: positive ion *m/z* 634.0067 ($[M+H]^+$, calc. for $C_{27}H_{31}Br_3N_3^+$: 634.0063, error −0.4 mDa); *m/z* 466.0480 ($[M+H-Arm]^+$, calc. for $C_{20}H_{26}Br_2N_3^+$: 466.0488, error 0.8 mDa); *m/z* 298.0905 ($[M+H-2Arm]^+$, calc. for $C_{13}H_{21}BrN_3^+$: 298.0913, error 0.8 mDa).

Elemental Analysis: for $C_{27}H_{31}Br_3N_3$: Calc. C 50.97; H 4.75; N 6.60; Rest 37.68%. Found C 50.83; H 4.63; N 6.48; Rest 38.06%.

***Cis,cis*-1,3,5-tris(4-(trifluoromethyl)benzylidenamino)cyclohexane, 4-CF_3-tachimben, [15a]**

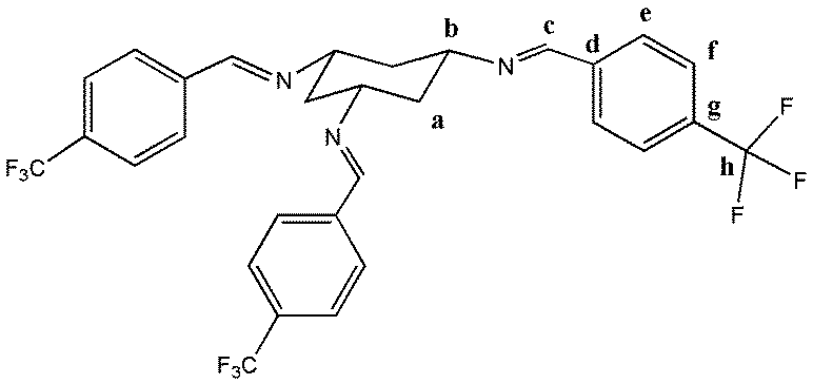

Tach·3HBr (100 mg, 0.27 mmol, 1 eq.) was dissolved in 7 mL of MeOH and NaOH (32 mg, 0.81 mmol, 3 eq.) added. The solution was left stirring for 10 min and nitrogen gas bubbled through, then 4-(trifluoromethyl)benzaldehyde (141 mg, 111 µL, 0.81 mmol, 3 eq.) was added and the reaction mixture was heated at reflux for 16 h under nitrogen. After cooling down, the solvent was evaporated and 20 mL of diethyl ether added to the residue, causing the precipitation of a white solid (unreacted tach and NaBr) from the solution, which was filtered and solvent evaporated by rotary evaporation, leaving a cream solid. The compound was usually used without further purification for the reduction step, but when necessary the solid was washed with pentane and dried. Crystals suitable for X-ray diffraction were grown from $CHCl_3$/pentane layer as colourless plates.

Yield: 132 mg, 0.22 mmol, 82%.

^{1}H NMR: ($CDCl_3$) δ 8.42 (3H, s, **c**), 7.86 (6H, d, ^3J = 8.0, **e**), 7.66 (6H, d, ^3J = 8.0, **f**), 3.64 (3H, ap.t, $^3J_{ax\text{-}ax}$ = 12.0, **b**), 2.08 (3H, ap.q, $^3J_{ax\text{-}ax}$ = ^2J = 12.0, $\mathbf{a_{ax}}$), 1.92 (3H, ap.d, ^2J = 12.0, $\mathbf{a_{eq}}$).

^{13}C NMR: ($CDCl_3$) δ 158.3 (**c**), 139.5 (q, ^5J = 1.5, **d**), 132.4 (q, ^2J = 32.5, **g**), 128.5 (**e**), 125.7 (q, ^3J = 3.6, **f**), 124.0 (q, ^1J = 272.5, **h**), 66.4 (**b**), 40.7 (**a**).

^{19}F NMR: ($CDCl_3$) δ -62.6.

ESI-MS: positive ion *m/z* 598.1925 ($[M+H]^+$, calc. for $C_{30}H_{25}F_9N_3^+$: 598.1899, error −2.6 mDa); *m/z* 442.1723 ($[M+H-Arm]^+$, calc. for $C_{22}H_{22}F_6N_3^+$: 442.1712, error −1.1 mDa); *m/z* 286.1522 ($[M+H-2Arm]^+$, calc. for $C_{14}H_{19}F_3N_3^+$: 286.1526, error 0.4 mDa).

Elemental Analysis: for $C_{30}H_{24}F_9N_3 \cdot 0.55H_2O$: Calc. C 59.32; H 4.16; N 6.62; Rest 29.60%. Found C 59.03; H 3.87; N 6.77; Rest 30.30%.

<u>*Cis,cis*-1,3,5-tris(4-(trifluoromethyl)benzylamino)cyclohexane, 4-CF_3-tachben, [15b]</u>

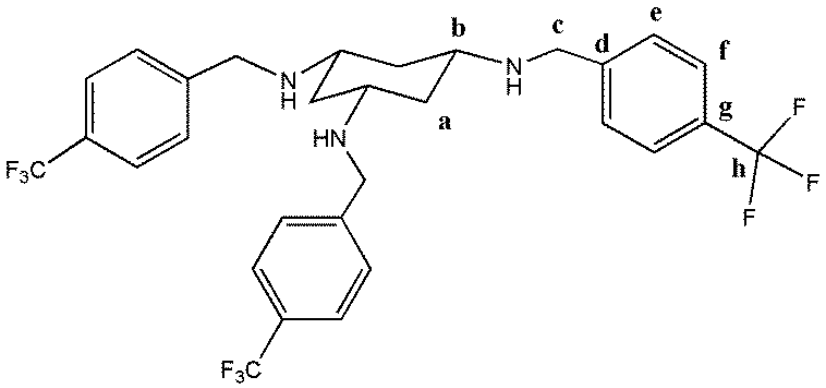

Cis,cis-1,3,5-tris(4-(trifluoromethyl)benzylidenamino)cyclohexane, 4-F-tachimben, (113 mg, 0.19 mmol, 1 eq.) was dissolved in a 2:1 methanol/DCM mixture (12 mL) and sodium borohydride (29 mg, 0.76 mmol, 4 eq.) was slowly added in portions. The mixture was stirred at room temperature for 16 h. The solvent was evaporated and the residue was taken with H_2O (10 mL) and DCM (10 mL). The layers were separated and the aqueous layer was extracted with DCM (3×10 mL). The organic layers were combined and the solvent removed by rotary evaporation. The residue was re-dissolved in 12 mL of 0.1 M HCl solution and washed with diethyl ether (2×10 mL). The aqueous solution was basified with NaOH, becoming a white cloudy suspension as soon as the pH became basic. The mixture was extracted with DCM (4×10 mL), dried with $MgSO_4$, filtered and the solvent evaporated, leaving a colourless oil.

Yield: 98 mg, 0.16 mmol, 85%.

^{1}H NMR: (CD_3OD) δ 7.62 (6H, d, ^{3}J = 8.0, **f**), 7.54 (6H, d, ^{3}J = 8.0, **e**), 3.88 (6H, s, **c**), 2.49 (3H, ap.t, $^{3}J_{ax\text{-}ax}$ = 11.6, **b**), 2.25 (3H, ap.d, ^{2}J = 11.6, $\mathbf{a_{eq}}$), 1.04 (3H, ap.q, $^{3}J_{ax\text{-}ax}$ = ^{2}J = 11.6, $\mathbf{a_{ax}}$).

^{13}C NMR: (CD_3OD) δ 145.6 (**d**), 130.3 (q, ^{2}J = 32.2, **g**), 130.0 (**e**), 126.3 (q, ^{3}J = 3.8, **f**), 125.8 (q, ^{1}J = 271.1, **h**), 54.1 (**b**), 50.9 (**c**), 39.5 (**a**).

^{19}F NMR: (CD_3OD) δ -63.8

ESI-MS: positive ion *m/z* 604.2350 ($[M+H]^+$, calc. for $C_{30}H_{31}F_9N_3^+$: 604.2369, error 1.9 mDa); *m/z* 446.2022 ($[M+H-Arm]^+$, calc. for $C_{22}H_{26}F_6N_3^+$: 446.2025, error 0.3 mDa); *m/z* 302.6204 ($[M+2H]^{2+}$, calc. for $C_{30}H_{32}F_9N_3^{2+}$: 302.6221, error 1.7 mDa).
Elemental Analysis: for $C_{30}H_{30}F_9N_3 \cdot 0.5H_2O$: Calc. C 58.82; H 5.10; N 6.86; Rest 29.22%. Found C 59.06; H 4.90; N 6.61; Rest 29.43%.

6.3.5 Synthesis of mono-armed ligands

Ni(II)[1-benzylideneamino-3,5-diaminocyclohexane] dinitrate, [16-1]

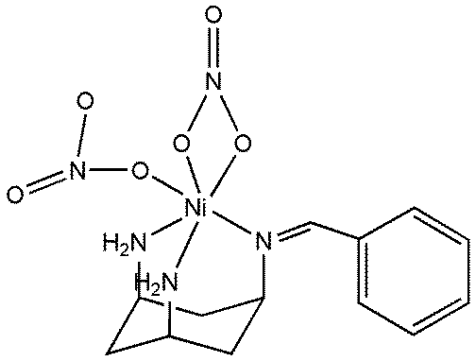

Cis,cis-1,3,5-tris(benzylidenamino)cyclohexane, tachimben, (394 mg, 1.0 mmol, 1 eq.) was dissolved in 5 mL of DCM and a solution of nickel nitrate hexahydrate (291 mg, 1.0 mmol, 1 eq.) in 2 mL of MeOH was slowly added. Further MeOH (8 mL) was added and the green solution was stirred at room temperature for 16 h. Over this period of time, the solution became a turquoise suspension. EtOH (12 mL) was added to the reaction mixture to favour precipitation of the solid and the mixture was cooled in an ice bath for approximately 30 min. The solid was isolated by filtration and washed with diethyl ether. The product was used without further purification. (**caution:** due to its high toxicity, nickel nitrate should be handled with particular care and all nickel contaminated waste disposed of as special waste)
Yield: 273 mg, 0.68 mmol, 68%.
ESI-MS: positive ion *m/z* 320.0897 ($[M]^+$, calc. for $C_{14}H_{20}N_3NiO_2^+$: 320.0904, error 0.6 mDa). N.B.: due to the MS conditions, the formate adduct was detected instead of the dinitrate.

Ni(II)[1-benzylamino-3,5-diaminocyclohexane] dinitrate, [16-2]

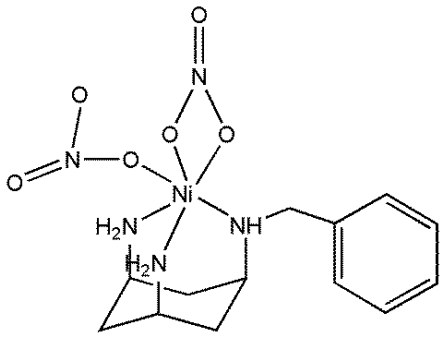

The Ni(II)-complex **[16-1]** (273 mg, 0.68 mmol, 1 eq.) was suspended in 28 mL of MeOH and the mixture was cooled in a ice bath. Sodium borohydride (129 mg, 3.41 mmol, 5 eq.) was slowly added in portion to the reaction mixture, which progressively turned grey/black . The reaction mixture was left to go back to room temperature and stirred for 16 h. The solvent was concentrated to approximately 1 mL and everything was used for the next reaction step.

***Cis,cis*-1-benzylamino-3,5-diaminocyclohexane, tachmonoben, [16]**

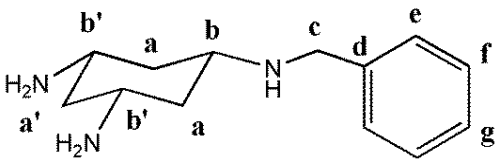

The reaction mixture of **[16-2]** was re-suspended 28 mL of water and sodium cyanide (167 mg, 3.41 mmol, 5 eq., assuming 100% yield in the previous step) was slowly added in portions. The grey suspension turned to a pale yellow colour and the reaction mixture was stirred at room temperature for 10 min and then heated at reflux for 2.5 h, during which time the suspension became a pale yellow solution. Water was evaporated, leaving a yellow oil which was re-dissolved in water (20 mL) and extracted with DCM (3×20 mL). The organic layers combined were dried over $MgSO_4$, filtered and the solvent was evaporated, leaving a light yellow oil. (**caution:** all glassware and water from extraction should be bleached to remove traces of cyanide)

Yield: 10 mg, 0.04 mmol, 7%.

^{1}H NMR: (CD_3OD) δ 7.32 (5H, m, **e**+**f**+**g**), 3.79 (2H, s, **c**), 2.68 (2H, tt, $^{3}J_{ax\text{-}ax}$ = 11.6, $^{3}J_{ax\text{-}eq}$ = 4.0, **b'**), 2.58 (1H, m, **b**), 2.13 (2H, d, ^{2}J = 11.6, $\mathbf{a_{eq}}$), 2.02 (1H, m, $\mathbf{a'_{eq}}$), 0.97 (3H,m, $\mathbf{a_{ax}}$+ $\mathbf{a'_{ax}}$).

^{13}C{^{1}H} NMR: (CD_3OD) δ 140.5 (**d**), 129.6 , 129.5 and 128.2 (**e**+**f**+**g**), 53.8 (**b**), 51.4 (**c**), 48.5 (**b'**), 43.8 (**a'**), 41.1 (**a**).

***Cis,cis*-1,3-di-*tert*-bythylcarbamate-5-aminocyclohexane, tach-diBoc, [17-1]**

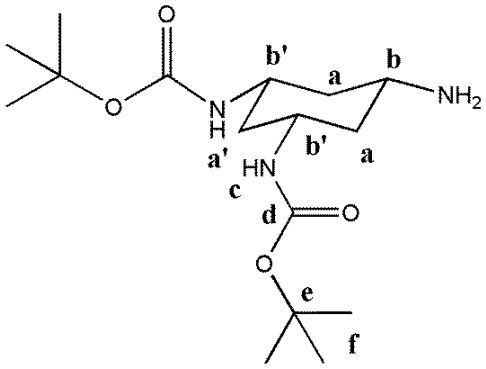

Tach·3HBr (200 mg, 0.54 mmol, 1 eq.) was dissolved in 40 mL and triethylamine (109 mg, 150 µL, 1.08 mmol, 2 eq.) was added to the solution. Boc_2O (236 mg, 248 µL, 1.08 mmol, 2 eq.) was mixed with 40 mL of MeOH and the solution was slowly added dropwise (one drop every 10-12 sec) to the tach solution. The reaction was stirred at room temperature for 16 h. The solvent was evaporated leaving a white solid, which was dissolved with a NaOH solution at pH 10 in water (12 mL) and ethyl acetate (12 mL). The layers were separated and the aqueous layer was extracted with ethyl acetate (3×12 mL). An emulsion was usually formed during the extraction, which was left with the organic layer during the extraction. The organic layers combined were dried over $MgSO_4$, filtered and the solvent was evaporated, leaving a white solid.

Yield: 133 mg, 0.40 mmol, 75%.

^{1}H NMR: (d_6-DMSO) δ 6.84 (2H, m, **c**), 3.23 (3H, s, **b**+**b'**), 1.79 (3H, bt, $\mathbf{a_{eq}}$+ $\mathbf{a'_{eq}}$), 1.37 (18H, s, **f**), 0.98 (2H, ap.q, $\mathbf{a_{ax}}$), 0.87 (1H, ap.q, ^{2}J = 11.6, $\mathbf{a'_{ax}}$).

^{13}C{^{1}H} NMR: (d_6-DMSO) δ 154.8 (**d**), 77.5 (**e**), 47.3 (**b'**), 46.3 (**b**), 28.3 (**f**), 41.1 (**a**/**a'**), 38.3 (**a**/**a'**).

ESI-MS: positive ion *m/z* 330.2373 ($[M+H]^+$, calc. for $C_{16}H_{32}N_3O_4^+$: 330.2387, error 1.4 mDa).

<u>*Cis,cis*-1,3-di-*tert*-bythylcarbamate-5-cyclohexylmethylaminocyclohexane, [17-2]</u>

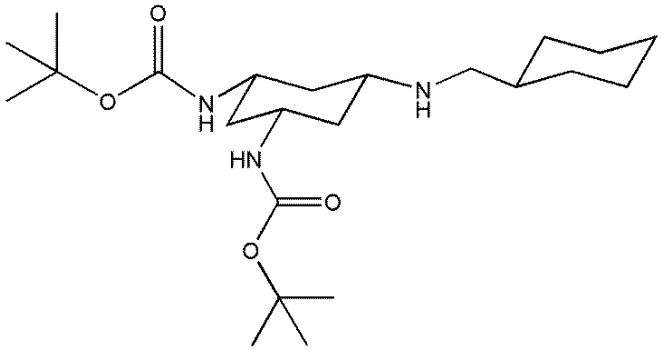

Tach-diBoc **[17-1]** (248 mg, 0.75 mmol, 1 eq.) was dissolved in a 1:2 MeOH/DCM mix (24 mL in total) and cyclohexanecarboxaldehyde (84 mg, 91 μL, 0.75 mmol, 1 eq.) was added to the solution. The mixture was stirred at room temperature for 24 h. Sodium borohydride (142 mg, 3.75 mmol, 5 eq.) was slowly added in portion and the reaction was stirred at room temperature for a further 16 h. The solvent was evaporated and the residue was taken with water (15 mL) and extracted with DCM (4×15 mL). The organic layers combined were dried over $MgSO_4$, filtered and the solvent evaporated, leaving a white solid that was used without further purification although containing cyclohexylmethanol.

Yield: 215 mg of crude product.

^{1}H NMR: (CD_3OD) δ 2.45 (2H, d, NHCH_2-cyclohex.), all other signals covered by impurities.

ESI-MS: positive ion *m/z* 330.2373 ($[M+H]^+$, calc. for $C_{16}H_{32}N_3O_4^+$: 330.2387, error 1.4 mDa).

***Cis,cis*-1-cyclohexylmethylamino-3,5-diaminocyclohexane, Tachmonocyc, [17]**

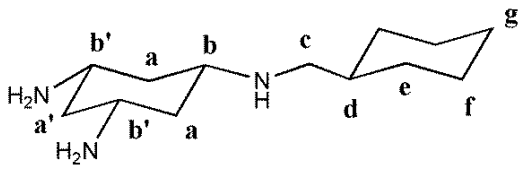

Compound **[17-2]** (215 mg crude) was suspended in 20 mL of MeOH and 4 mL of conc. HCl were added. To dissolve the compound, 8 mL of DCM were added to the mixture, which was left stirring at room temperature for 3 h. The solvent was concentrated down to about 5 mL and 20 mL of water were added. The mixture was extracted with ethyl acetate (2×20 mL) to remove the residual cyclohexylmethanol and the organic layers were discarded. The pH of the solution was basified with NaOH (pH 14) and extracted with DCM (4×20 mL). The organic layers combined were dried over $MgSO_4$, filtered and the solvent evaporated, leaving a white solid.

Yield: 9 mg, 0.04 mmol.

^{1}H NMR: (CD_3OD) δ 2.76 (2H, tt, $^3J_{ax\text{-}ax}$ = 11.6, $^3J_{ax\text{-}eq}$ = 3.6, **b'**), 2.59 (1H, tt, $^3J_{ax\text{-}ax}$ = 11.6, $^3J_{ax\text{-}eq}$ = 3.6, **b**), 2.48 (2H, d, ^{3}J = 6.8, **c**), 2.10 (d, ^2J = 11.6, $\mathbf{a_{eq}}$) and 2.04 (d, ^2J = 11.6, $\mathbf{a'_{eq}}$) (3H between the two signals, partially overlapping), 1.77 – 0.94 (4 sets of multiplets, 17H in total, **d**, **e**, **f**, **g**, $\mathbf{a_{ax}}$ and $\mathbf{a'_{ax}}$).

^{13}C{^{1}H} NMR: (CD_3OD) δ 55.2 (**b**), 54.3 (**c**), 48.5 (**b'**), 44.4 (**a'**), 41.2 (**a**), 38.7 (**d**), 32.5 (**e**), 27.6 (**g**/**f**), 27.1 (**g**/**f**).

ESI-MS: positive ion *m/z* 226.2273 ($[M+H]^+$, calc. for $C_{13}H_{28}N_3^+$: 226.2278, error 0.5 mDa).

6.4 Synthesis of metal complexes

All the complexes were synthesised using general Schlenk line techniques using de-oxygenated solvents. The products were stored under inert atmosphere.

Cobalt(II)-*cis,cis*-1,3,5-tris(pyridine-2-carboxaldimino)cyclohexane dichloride, [Co(II)-tachimpyr]Cl_2, [18]Cl_2

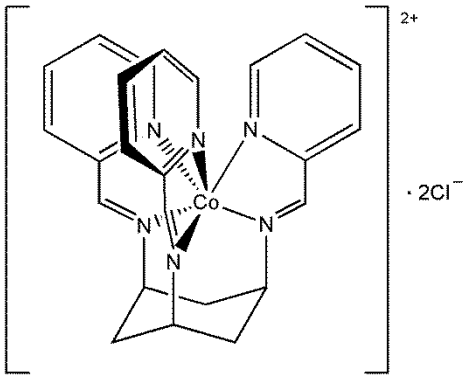

Cis,cis-1,3,5-tris(pyridine-2-carboxaldimino)cyclohexane, tachimpyr, (100 mg, 0.25 mmol, 1 eq.) was dissolved in 5 mL of deoxygenated EtOH and a solution of $CoCl_2 \cdot 6H_2O$ (60 mg, 0.25 mmol, 1 eq.) in 2 mL of EtOH was added. The solution turned immediately dark red and a precipitate was formed. The reaction was left under N_2 atmosphere for 16 h, then the precipitate was filtered and Et_2O was added to the remaining solution. Crystals suitable for x-ray diffraction were formed as orange blocks. To isolate the crystals, the solvent was removed via cannula filtration and the crystals were dried and stored under N_2 atmosphere.

Yield: crude of reaction: 69 mg, 0.13 mmol, 52%.

ESI-MS: positive ion *m/z* 227.5689 ($[M]^{2+}$, calc. for $C_{24}H_{24}CoN_6^{2+}$: 227.5691, error 2.5 mDa); *m/z* 455.1395 ($[M]^+$, calc. for $C_{24}H_{24}CoN_6^+$: 455.1389, error −1.2 mDa).

Cobalt(II)-*N,N',N''*-tris(2-pyridylmethyl)-*cis,cis*-1,3,5-triaminocyclohexane dichloride, [Co(II)-tachimpyr]Cl_2, [19]Cl_2

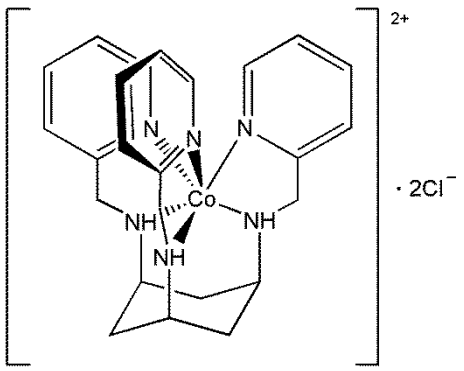

N,N',N''-tris(2-pyridylmethyl)-*cis,cis*-1,3,5-triaminocyclohexane, tachpyr, (72 mg, 0.18 mmol, 1 eq.) was dissolved in 5 mL of MeOH and a solution of $CoCl_2 \cdot 6H_2O$ (43 mg, 0.18 mmol, 1 eq.) in 2 mL of MeOH was added. The colourless solution of ligand solution turned immediately to a yellow/orange colour. The reaction was left under N_2 atmosphere for 16 h, followed by addition of a layer of Et_2O to the solution. Crystals suitable for x-ray diffraction were formed as green needles. To isolate the crystals, the solvent was removed via cannula filtration and the crystals were dried and stored under N_2 atmosphere.

Yield: crude of reaction: 28 mg, 0.05 mmol, 30%.

ESI-MS: positive ion *m/z* 228.5754 ($[M]^{2+}$, calc. for $C_{24}H_{26}CoN_6^{2+}$: 228.5770, error 1.6 mDa); *m/z* 459.1696 ($[M]^+$, calc. for $C_{24}H_{28}CoN_6^+$: 459.1702, error 0.6 mDa).

Ruthenium(II)-*N,N',N''*-tris(2-pyridylmethyl)-*cis,cis*-1,3,5-triaminocyclohexane dichloride, [Ru(II)-tachpyr]Cl_2, [20]Cl_2

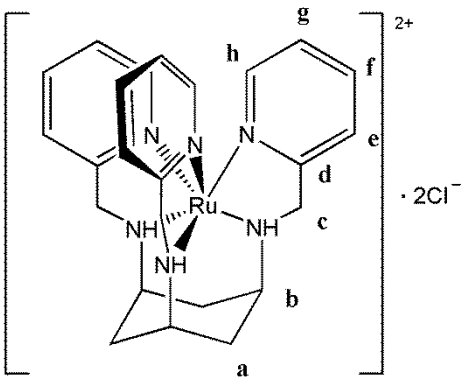

N,N',N''-tris(2-pyridylmethyl)-*cis,cis*-1,3,5-triaminocyclohexane, tachpyr, (5.1 mg, 0.01 mmol, 1 eq.) was dissolved in 1 mL of D_2O in a Young's tap NMR tube under argon and $RuCl_2(DMSO)_4$ (6.1 mg, 0.01 mmol, 1 eq.) was added. The colourless solution of ligand solution turned yellow on addition of the Ru complex, but no further change of colour was noticed. The reaction was heated in the sealed NMR tube at 110 °C under N_2 atmosphere for 2 h. Crystals suitable for X-ray diffraction were formed as dark red blocks after addition of a layer of Et_2O.

^{1}H NMR: (D_2O) δ 7.65 (6H, m, **f**+**h**), 7.39 (3H, d, ^3J = 8.2, **e**), 7.06 (3H, m, **g**), 4.47 (3H, d, ^2J = 18.9, **c**), 4.24 (3H, d, ^2J = 18.9, **c**), 3.30 (3H, partially overlapping with other signals, m, **b**), 2.05 (6H, m, **a**).

$^{13}C\{^{1}H\}$ NMR: (D_2O) δ 165.0 (**d**), 150.9 (**f**), 135.9 (**h**), 124.5 (**g**), 121.2 (**e**), 56.5 (**c**), 52.0 (**b**), 30.3 (**a**).

6.5 Cell culture and MTT assay – Materials and methods

Human lung adenocarcinoma A549 cells were donated by the Department of Biology, University of York. Human ovarian carcinoma A2780 cells were purchased from the European Collection of Cell Cultures (ECACC), Salisbury, UK. Human embryonic kidney 293T cells were kindly donated by Dr Tim Ganderton and Dr Marek Brzozowski, York Structural Biology Laboratory, Department of Chemistry, University of York. All materials were purchased from Sigma, except culture media and FBS (Invitrogen/Gibco), Millex®-MP sterilizing filters (Merck Millipore), 96-well sterile plates and sterile culture flasks (Fisher Scientific). All procedures were carried out in an Envair class II Laminar flow microbiological safety hood BIO 2+ under sterile conditions. Cells were counted using a Beckman Coulter Vi-Cell® Analyser and results of MTT assay visualised with a Hidex Plate Chameleon™V plate reader. Cells were centrifuged with a SciQuip Sigma 1-6 centrifuge. Plates were centrifuged with a Beckman Coulter Allegra™25R Centrifuge using a S5700 rotor. Plates were mixed with an Eppendorf Thermomixer® compact. A549 cells were grown in Dulbecco Modified Eagle Medium (DMEM) in the presence of 10% FBS; A2780 cells were maintained in RPMI 1640 medium enriched with 10% FBS and 1% L-Glutamine; 293T cells were kept in DMEM - GlutaMAX™ medium in the presence of 10% FBS. All cell lines were maintained in 25 cm^2 cell culture flasks at 37°C in a 90% RH, 5% CO_2 Thermo Scientific Forma Steri-Cult incubator. Cells were cultured with 0.25% EDTA-trypsin when 70-80% confluent.

MTT assays were carried out in a 96-well plate following the method reported by Torti *et al.*[133] All non-sterile solutions were filtered using a Millex®-MP 0.22 μm filter in order to sterilise them. Positive and negative controls were added in each plate. For the assay, cells were cultured and centrifuged for 5 min at 1000 rpm, medium was removed and substituted with 10 mL of the appropriate fresh medium. Cells were

suspended and counted using a Vi-Cell® instrument. Cells were then plated at the seeding density of 1000 cells/well for A549 and 293T cells and 3500 cells/well for A2780 cells, adding 100 μL of dilute cell suspension to each well. The plate was then left in the incubator for 16-20 h to allow cells to adhere before adding the drug. The compound to test was dissolved in medium, filtered to sterilise and diluted to have a 2x solution of the desired concentration, then 100 μL of compound solution were added to each well and cells were left incubating for 3 days. When the compounds were not freely soluble in medium, DMSO was used to dissolve the compound and the solution was then diluted with medium. The final concentration of DMSO was never higher than 1%, which was also added to the control. Viability was tested with MTT assay; 50 μL of a sterile solution of 3-(4,5-dimethyltriazol-2-yl)-2,5-diphenyltetrazolium bromide (10.6 mg in 5.5 mL) were added to each well and the plate was left incubating for 2 h. The plate was then centrifuged at 500 rpm for 10 min, 220 μL of medium were taken and substituted with 150 μL of DMSO in each well. Cell viability was evaluated spectrophotometrically reading the absorbance at 540 nm using a Plate Reader. Growth inhibition was calculated as a percentage in relation to the positive and negative controls. Final IC_{50} values were calculated as the average of at least three plates from at least two independent experiments.

6.5.1 MTT assay in the presence of Fe

The general procedure for MTT assay was followed, but a sterile solution of $FeSO_4 \cdot 7H_2O$ in medium was added to the cell culture at different stages of the assay. Due to the dilution occurring in the well, the concentration of the stock Fe-solutions were either two or four times higher than the desired final concentration. The final concentration of iron with cells was 47, 94, 189 or 377 μM. When iron was added on day 1 of the assay, cells were suspended in Fe-enriched medium. Alternatively, when Fe was added on day 2 of the assay, 50 μL of a 4x solution of Fe in medium were either loaded on to the wells, followed by 50 μL of a 4x solution of tachpyr, or mixed with a 4x solution of tachpyr, incubated at 25° C for 15 min and 100 μL of the resulting solution added to the wells. When Fe was added 8 h after the addition of

tachpyr, 50 µL of 4x solution of tachpyr were placed into the wells, the plate was left incubating for 8 h and 50 µL of 4x Fe solution were added to the wells.
In the repetition of the experiment reported by Zhao *et al*,[134] the iron solution in the medium was sterilised and 100 µL of the stock solution were added to the cells to have a final concentration of iron with the cell of 200 µM. The plate was incubated for 24 h, after which time the medium was completely removed, cells were washed with 50 µL of PBS and 100 µL of medium added to the cells. Tachpyr was dissolved in medium and added following the standard protocol. The plate was then placed back in the incubator, proceeding with the test as usual.

6.6 Evaluation of the mechanism of action of tachpyr – Materials and methods

6.6.1 Circular dichroism

Circular dichroism spectra were recorded using a Jasco J-810 spectropolarimeter operated with the following parameters: sensitivity: 100 mdeg, start WL: 350 or 400 nm, end WL: 200 nm; data pitch: 0.5 nm; scanning mode: continuous; scanning speed: 200 nm·min^{-1}; response: 0.1 sec; band width: 1.0; accumulation: 12. All materials were purchased from Sigma Aldrich. A solution containing 300 µM ct-DNA, 20 mM NaCl and 1 mM sodium cacodylate pH 6.8 (1 mL) was added to the spectrometer cell and the CD spectrum recorded. The titration was performed adding different aliquots of a 500 µM stock solution of tachpyr in Milli-Q® water and an equal amount of a 600 µM stock solution of ct-DNA to keep the concentration of DNA in the cuvette constant.

6.6.2 Linear dichroism

Linear dichroism spectra were recorded using a Jasco J-810 spectropolarimeter modified for LD spectroscopic measurements. The instrument was operated with the following parameters: sensitivity: 0.1 dOD, start WL: 350 nm, end WL: 200 nm; data pitch: 0.5 nm; scanning mode: continuous; scanning speed: 500 nm·min^{-1}; response:

0.25 sec; band width: 2.0; accumulation: 8. A solution containing 300 µM ct-DNA, 20 mM NaCl and 0.89 mM sodium cacodylate pH 6.8 (600 µL) was added to the spectrometer cell and the LD spectrum recorded. The titration was performed adding different aliquots of a 500 µM stock solution of tachpyr in Milli-Q® water and an equal amount of a 600 µM stock solution of ct-DNA to keep the concentration of DNA in the cuvette constant.

6.6.3 Ethidium bromide displacement

Ethidium bromide displacement was measured by recording the quenching of fluorescence using a Perking-Elmer LS 50b instrument with the following parameters: excitation WL: 480 nm; emission range: 500-700 nm; resolution: 0.4 nm; excitation split: 5; emission split: 1.5. After measuring the spectrum for ethidium bromide only (600 µL of a 15 µM solution), the solution in the cuvette was substituted with 600 µL of a solution of 12 µM ct-DNA with 15 µM ethidium bromide, 50 mM NaCl and 1 mM sodium cacodylate and the fluorescence recorded. The titration was performed adding aliquots of a 50 µM stock solution of compound in Milli-Q® water and an equal amount of a 60 µM ethidium bromide, 24 µM DNA stock solution with 100 mM NaCl and 2 mM sodium cacodylate to keep the concentration of DNA in the cuvette constant.

6.6.4 Agarose gel electrophoresis

Different aliquots of a 60 µM solution of compound in Milli-Q® water were added to a solution of pBR322 circular plasmid DNA in order to have a final concentration of DNA of 1.54 mM bp. The mixture was incubates for up to 3 h at 37 °C, after which time 4 µL of loading buffer (30% glycerol, 0.05% bromophenol blue, 250 mM EDTA, 40% sucrose, 10% sodium dodecyl sulfate (SDS)) were added to each eppendorf. The solutions were centrifuged for a few seconds to ensure complete mixing and 16 µL of solution were added to 1% agarose gel in TRIS acetate / EDTA buffer pH 8.3 (40 mM TRIS, 1 mM EDTA). The gel was run using a HE99X Maxi (Amersham Biosciences, UK) submarine gel kit at 120 V, 200 A for 3 h. Ethidium bromide (400 µL of a 50 µM

solution) was added and left for 30 min with the gel, which was then washed with water and the results visualised using a UVIdoc Platinum System at the wavelength of 312 nm.

6.7 Crystal structure of DNA – Materials and methods

DNA was obtained by Sigma Aldrich custom oligo service, Natrix screen was purchased by Hampton Research, all other materials were purchased from Sigma Aldrich. DNA (1792.2 g/mol, extinction coefficient = 57.6 OD/µmol, 455.4 µg) was dissolved in Milli-Q® water to have a concentration of 3 mM (single stranded). DNA was annealed using a PCR thermal cycler at 65 °C for 12 min and cooled down to 4 °C over a 1.5 h period. The crystal plate was set up using a TTP Labtech Mosquito instrument. Crystals suitable for X-ray structure determination were obtained with the sitting drop/vapour diffusion method over 9 months from well F8 of the Natrix HT screen, which contained 40 mM sodium cacodylate pH = 6.0, 80 mM NaCl, 20 mM $BaCl_2$, 12 mM spermine and 45% MPD as precipitating solution. A 0.8 µL drop of solution containing 15 mM tachpyr and 1.5 mM DNA (concentration of single strand) was mixed with an equal volume of precipitating solution and the plate was stored at 10 °C to allow for the growth of the crystals. The crystal appeared as a cluster of hexagonal crystals, which were mounted on a rayon loop and frozen in liquid N_2 without use of cryoprotectant. Diffraction data was collected at 1.5 Å resolution at the Diamond Light Source synchrotron. Data was integrated using XDS[303] as implemented in xia2[304], AIMLESS[305] program was used to merge the data, MOLREP[287] for solution and refinement, as well as REFMAC as part of the CCP4 suite[288] and Coot.[289]

Appendix I. X-ray crystallography data

Name	Tachprl **[4b]·3CHCl$_3$**
Identification code	phw1114
Empirical formula	$C_{45}H_{63}Cl_9N_{12}$
Formula weight	1091.12
Temperature / K	109.9
Crystal system	triclinic
Space group	*P*-1
a / Å, b / Å, c / Å	14.3898(12), 14.5637(14), 15.0840(10)
α / °, β / °, γ / °	88.276(7), 63.722(8), 71.729
Volume / Å^3	2669.5(4)
Z	2
ρ_{calc} / mg mm^{-3}	1.357
μ / mm^{-1}	0.516
F(000)	1140.000
Crystal size / mm^3	0.2245 × 0.06 × 0.0362
2θ range for data collection / °	5.76 to 58.06°
Index ranges	-19 ≤ h ≤ 19, -18 ≤ k ≤ 19, -19 ≤ l ≤ 20
Reflections collected	17691
Independent reflections	11923 [R_{int} = 0.0254]
Data / restraints / parameters	11923/0/647
Goodness-of-fit on F^2	1.019
Final *R* indexes [$I > 2\sigma(I)$]	R_1 = 0.0565, wR_2 = 0.1016
Final *R* indexes [all data]	R_1 = 0.0895, wR_2 = 0.1161
Largest diff. peak/hole / e Å^{-3}	0.642/ -0.481

Name	Salimtach **[6a]**
Identification code	phw1101
Empirical formula	$C_{27}H_{27}N_3O_3$
Formula weight	441.52
Temperature / K	120.0
Crystal system	monoclinic
Space group	$P2_1/c$
a / Å, b / Å, c / Å	5.9979(2), 24.6161(8), 15.3079(6)
α / °, β / °, γ / °	90.00, 91.843(2), 90.00
Volume / Å^3	2258.96(14)
Z	4
ρ_{calc} / mg mm^{-3}	1.298
μ / mm^{-1}	0.086
F(000)	936
Crystal size / mm^3	0.32 × 0.05 × 0.04
2θ range for data collection / °	6.28 to 55.14°
Index ranges	$-7 \leq h \leq 7$, $-29 \leq k \leq 31$, $-19 \leq l \leq 19$
Reflections collected	18092
Independent reflections	5165 [R_{int} = 0.0524]
Data / restraints / parameters	5165/0/311
Goodness-of-fit on F^2	1.114
Final *R* indexes [$I > 2\sigma(I)$]	R_1 = 0.0679, wR_2 = 0.1184
Final *R* indexes [all data]	R_1 = 0.1034, wR_2 = 0.1352
Largest diff. peak/hole / e Å^{-3}	0.265/ -0.239

Name	5-Me-salimtach **[9a]**
Identification code	phw1113
Empirical formula	$C_{30}H_{33}N_3O_3$
Formula weight	483.59
Temperature / K	110.0
Crystal system	orthorhombic
Space group	*P*na2_1
a / Å, b / Å, c / Å	18.3543(12), 16.464(11), 8.6727(9)
α / °, β / °, γ / °	90.00, 90.00, 90.00
Volume / Å^3	2620.8(19)
Z	4
ρ_{calc} / mg mm^{-3}	1.226
μ / mm^{-1}	0.080
F(000)	1032
Crystal size / mm^3	0.1749 × 0.1688 × 0.0631
2θ range for data collection / °	5.76 to 57.98°
Index ranges	-14 ≤ h ≤ 24, -13 ≤ k ≤ 22, -11 ≤ l ≤ 11
Reflections collected	10192
Independent reflections	5801 [R_{int} = 0.0197]
Data / restraints / parameters	5801/1/337
Goodness-of-fit on F^2	1.061
Final *R* indexes [$I > 2\sigma(I)$]	R_1 = 0.0422, wR_2 = 0.0983
Final *R* indexes [all data]	R_1 = 0.0511, wR_2 = 0.1034
Largest diff. peak/hole / e Å^{-3}	0.171/ -0.183

Name	Saltach **[6b]**
Identification code	phw1117
Empirical formula	$C_{27}H_{33}N_3O_3$
Formula weight	447.56
Temperature / K	110.0
Crystal system	trigonal
Space group	*P*31c
a / Å, b / Å, c / Å	13.4860(5), 13.4860(5), 7.7069(6)
α / °, β / °, γ / °	90.00, 90.00, 120.00
Volume / Å^3	1213.87(12)
Z	2
ρ_{calc} / mg mm^{-3}	1.225
μ / mm^{-1}	0.080
F(000)	480
Crystal size / mm^3	0.2907 × 0.068 × 0.0524
2θ range for data collection / °	6.08 to 60.78°
Index ranges	$-6 \leq h \leq 17$, $-19 \leq k \leq 15$, $-10 \leq l \leq 9$
Reflections collected	2916
Independent reflections	1846 [R_{int} = 0.0235]
Data / restraints / parameters	1846/1/108
Goodness-of-fit on F^2	1.194
Final *R* indexes [$I > 2\sigma(I)$]	R_1 = 0.0510, wR_2 = 0.1450
Final *R* indexes [all data]	R_1 = 0.0697, wR_2 = 0.1578
Largest diff. peak/hole / e Å^{-3}	0.217/ -0.284

Name	5-Cl-saltach **[7b]**
Identification code	phw1115
Empirical formula	$C_{27}H_{30}Cl_3N_3O_3$
Formula weight	550.89
Temperature / K	110.0
Crystal system	trigonal
Space group	P31c
a / Å, b / Å, c / Å	13.8281(3), 13.8281(3), 8.2311(2)
α / °, β / °, γ / °	90.00, 90.00, 120.00
Volume / Å^3	1363.07(6)
Z	2
ρ_{calc} / mg mm^{-3}	1.342
μ / mm^{-1}	0.370
F(000)	576
Crystal size / mm^3	0.3051 × 0.1453 × 0.116
2θ range for data collection / °	5.9 to 64.54
Index ranges	$-19 \leq h \leq 20$, $-20 \leq k \leq 20$, $-12 \leq l \leq 12$
Reflections collected	8234
Independent reflections	2940 [R_{int} = 0.0270]
Data / restraints / parameters	2940/1/117
Goodness-of-fit on F^2	1.111
Final *R* indexes [$I > 2\sigma(I)$]	R_1 = 0.0404, wR_2 = 0.1014
Final *R* indexes [all data]	R_1 = 0.0463, wR_2 = 0.1057
Largest diff. peak/hole / e Å^{-3}	0.324/ -0.241

Name	5-Me-saltach **[9b]**
Identification code	phw1118
Empirical formula	$C_{30}H_{39}N_3O_3$
Formula weight	489.64
Temperature / K	110.0
Crystal system	trigonal
Space group	*P*31c
a / Å, b / Å, c / Å	14.2781(7), 14.2781(7), 7.8801(4)
α / °, β / °, γ / °	90.00, 90.00, 120.00
Volume / Å^3	1391.26(12)
Z	2
ρ_{calc} / mg mm^{-3}	1.169
μ / mm^{-1}	0.076
F(000)	528
Crystal size / mm^3	0.3155 × 0.1659 × 0.1467
2θ range for data collection / °	5.7 to 64.32°
Index ranges	$-18 \leq h \leq 8$, $-20 \leq k \leq 19$, $-11 \leq l \leq 9$
Reflections collected	4801
Independent reflections	2325 [R_{int} = 0.0314]
Data / restraints / parameters	2325/1/118
Goodness-of-fit on F^2	1.089
Final *R* indexes [$I > 2\sigma(I)$]	R_1 = 0.0622, wR_2 = 0.1793
Final *R* indexes [all data]	R_1 = 0.0739, wR_2 = 0.1929
Largest diff. peak/hole / e Å^{-3}	0.405/ -0.208

Name	4-NMe_2-tachimben **[11a]·EtOH**
Identification code	phw1301
Empirical formula	$C_{35}H_{48}N_6O$
Formula weight	568.79
Temperature / K	110.00(10)
Crystal system	monoclinic
Space group	$P2_1/n$
a / Å, b / Å, c / Å	11.6014(5), 9.7929(4), 29.2781(12)
α / °, β / °, γ / °	90.00, 90.850(4), 90.00
Volume / $Å^3$	3326.0(2)
Z	4
ρ_{calc} / mg mm^{-3}	1.136
μ / mm^{-1}	0.070
F(000)	1232.0
Crystal size / mm^3	0.2369 × 0.1651 × 0.0437
2θ range for data collection / °	5.6 to 56°
Index ranges	$-15 \leq h \leq 15$ $-10 \leq k \leq 12$ $-38 \leq l \leq 23$
Reflections collected	12634
Independent reflections	6771 [R_{int} = 0.0346]
Data / restraints / parameters	6771/4/410
Goodness-of-fit on F^2	1.049
Final *R* indexes [$I > 2\sigma(I)$]	R_1 = 0.0598, wR_2 = 0.1260
Final *R* indexes [all data]	R_1 = 0.0888, wR_2 = 0.1413
Largest diff. peak/hole / e $Å^{-3}$	0.21/-0.24

Name	4-CF_3-tachimben **[15a]**
Identification code	phw1308
Empirical formula	$C_{30}H_{24}F_9N_3$
Formula weight	597.52
Temperature / K	110.05(10)
Crystal system	orthorhombic
Space group	*P*bca
a / Å, b / Å, c / Å	19.0875(3), 12.10177(17), 24.0122(3)
α / °, β / °, γ / °	90.00 , 90.00, 90.00
Volume / $Å^3$	5546.65(15)
Z	8
ρ_{calc} / mg mm^{-3}	1.431
μ / mm^{-1}	0.127
F(000)	2448.0
Crystal size / mm^3	0.2777 × 0.1474 × 0.0697
2θ range for data collection / °	6.4 to 56.06°
Index ranges	$-24 \leq h \leq 13$ $-15 \leq k \leq 10$ $-31 \leq l \leq 18$
Reflections collected	14716
Independent reflections	5708 [R_{int} = 0.0213]
Data / restraints / parameters	5708/37/406
Goodness-of-fit on F^2	1.059
Final *R* indexes [$I > 2\sigma(I)$]	R_1 = 0.0445, wR_2 = 0.0958
Final *R* indexes [all data]	R_1 = 0.0601, wR_2 = 0.1041
Largest diff. peak/hole / e $Å^{-3}$	0.23/-0.43

Name	[Co(II)-tachimpyr]Cl_2 **[18]Cl_2·2.5EtOH**
Identification code	phw1103
Empirical formula	$C_{29}H_{39}N_6Cl_2CoO_{2.5}$
Formula weight	641.49
Temperature / K	110.0
Crystal system	monoclinic
Space group	$P2_1/n$
a / Å, b / Å, c / Å	11.3868(9), 14.0237(11), 19.2597(15)
α / °, β / °, γ / °	90.00, 99.711(9), 90.00
Volume / $Å^3$	3031.4(4)
Z	4
ρ_{calc} / mg mm^{-3}	1.406
μ / mm^{-1}	0.782
F(000)	1344
Crystal size / mm^3	0.3941 × 0.1767 × 0.0965
2θ range for data collection / °	5.82 to 55.9°
Index ranges	$-14 \leq h \leq 14$, $-17 \leq k \leq 12$, $-24 \leq l \leq 21$
Reflections collected	12340
Independent reflections	6108 [R_{int} = 0.0218]
Data / restraints / parameters	6108/6/382
Goodness-of-fit on F^2	1.043
Final *R* indexes [$I > 2\sigma(I)$]	R_1 = 0.0497, wR_2 = 0.1215
Final *R* indexes [all data]	R_1 = 0.0589, wR_2 = 0.1284
Largest diff. peak/hole / e $Å^{-3}$	1.412/ -0.735

Name	[Co(II)-tachpyr]$CoCl_4$ **[19]$CoCl_4$**
Identification code	phw1106_twin1_hklf4
Empirical formula	$C_{24}H_{30}N_6Cl_4Co_2$
Formula weight	662.20
Temperature / K	110.0
Crystal system	monoclinic
Space group	$P2_1$
a / Å, b / Å, c / Å	9.6223(3), 14.7571(3), 10.6813(3)
α / °, β / °, γ / °	90.00, 115.949(4), 90.00
Volume / $Å^3$	1363.82(7)
Z	2
ρ_{calc} / mg mm^{-3}	1.613
μ / mm^{-1}	1.634
F(000)	676
Crystal size / mm^3	0.06 × 0.04 × 0.04
2θ range for data collection / °	6.96 to 58.22°
Index ranges	$-12 \leq h \leq 12$, $-20 \leq k \leq 19$, $-14 \leq l \leq 14$
Reflections collected	13897
Independent reflections	5903 [R_{int} = 0.0319]
Data / restraints / parameters	5903/1/334
Goodness-of-fit on F^2	1.040
Final *R* indexes [$I > 2\sigma(I)$]	R_1 = 0.0349, wR_2 = 0.0835
Final *R* indexes [all data]	R_1 = 0.0417, wR_2 = 0.0854
Largest diff. peak/hole / e $Å^{-3}$	0.472/ -0.694

Name	Ru(II)-dimers
Identification code	phw1120
Empirical formula	$C_{13}H_{44.5}Cl_{1.5}O_{10.5}Ru_2S_6$
Formula weight	816.02
Temperature / K	110.00
Crystal system	monoclinic
Space group	$P2_1/n$
a / Å, b / Å, c / Å	15.5134(6), 10.8600(4), 18.0560(12)
α / °, β / °, γ / °	90.00, 106.470(6), 90.00
Volume / Å^3	2917.2(3)
Z	4
ρ_{calc} / mg mm^{-3}	1.858
μ / mm^{-1}	1.643
F(000)	1663.0
Crystal size / mm^3	0.2844 × 0.1058 × 0.0886
2θ range for data collection / °	6.02 to 60.3°
Index ranges	$-20 \leq h \leq 21$ $-14 \leq k \leq 14$ $-24 \leq l \leq 25$
Reflections collected	21935
Independent reflections	7625 [R_{int} = 0.0379]
Data / restraints / parameters	7625/1/355
Goodness-of-fit on F^2	1.181
Final *R* indexes [$I > 2\sigma(I)$]	R_1 = 0.0420, wR_2 = 0.0705
Final *R* indexes [all data]	R_1 = 0.0593, *wR2* = 0.0767
Largest diff. peak/hole / e Å^{-3}	0.83/-0.90

Name	[Ru(II)-tachpyr]Cl_2 **[20]Cl_2**
Identification code	phw1202
Empirical formula	$C_{24}H_{26.5}Cl_2N_6Ru$
Formula weight	570.98
Temperature / K	110.00(10)
Crystal system	triclinic
Space group	*P*-1
a / Å, b / Å, c / Å	10.5125(7), 12.8761(8), 13.0224(9)
α / °, β / °, γ / °	102.955(6), 110.920(6), 107.384(6)
Volume / $Å^3$	1459.07(16)
Z	2
ρ_{calc} / mg mm^{-3}	1.300
μ / mm^{-1}	0.741
F(000)	581.0
Crystal size / mm^3	0.2465 × 0.1333 × 0.0709
2θ range for data collection / °	5.94 to 64.28°
Index ranges	$-9 \leq h \leq 15$ $-18 \leq k \leq 14$ $-18 \leq l \leq 16$
Reflections collected	15679
Independent reflections	9142 [R_{int} = 0.0248]
Data / restraints / parameters	9142/0/308
Goodness-of-fit on F^2	1.032
Final *R* indexes [$I > 2\sigma(I)$]	R_1 = 0.0491, wR_2 = 0.1266
Final *R* indexes [all data]	R_1 = 0.0592, wR_2 = 0.1330
Largest diff. peak/hole / e $Å^{-3}$	1.43/-1.23

Appendix II. Fe experiments – complete IC_{50} tables

A549 human adenocarcinoma cells

[Fe]	Ref to positive control	Ref to positive control + Fe
377 µM	5.40 ± 0.10 µM	5.49 ± 0.10 µM
189 µM	5.02 ± 0.09 µM	5.01 ± 0.11 µM
94 µM	4.90 ± 0.17 µM	4.90 ± 0.17 µM
47 µM	4.81 ± 0.06 µM	4.78 ± 0.06 µM

Table II.1: Addition of Fe on day 1. Partial loss of viability due to the Fe was observed.

[Fe]	Ref to positive control	Ref to positive control + Fe
377 µM	-	-
189 µM	6.03 ± 0.15 µM	6.11 ± 0.08 µM
94 µM	5.70 ± 0.10 µM	5.78 ± 0.08 µM
47 µM	5.64 ± 0.13 µM	5.75 ± 0.09 µM

Table II.2: Addition of Fe on day 2, Fe first followed by tachpyr.

[Fe]	Ref to positive control	Ref to positive control + Fe
377 µM	7.27 ± 0.34 µM	7.88 ± 0.14 µM
189 µM	6.46 ± 0.15 µM	6.58 ± 0.13 µM
94 µM	5.28 ± 0.14 µM	5.44 ± 0.07 µM
47 µM	5.59 ± 0.15 µM	5.72 ± 0.09 µM

Table II.3: Addition of Fe on day 2, Fe and tachpyr mixed together.

[Fe]	Ref to positive control	Ref to positive control + Fe
377 µM	-	-
189 µM	5.27 ± 0.16 µM	5.39 ± 0.14 µM
94 µM	4.97 ± 0.13 µM	5.03 ± 0.12 µM
47 µM	4.89 ± 0.14 µM	4.94 ± 0.13 µM

Table II.4: Addition of Fe on day 2, 8 h after addition of tachpyr.

[Fe]	Ref to positive control	Ref to positive control + Fe
200 µM	5.39 ± 0.09 µM	5.49 ± 0.01 µM

Table II.5: Fe removed after 24 h.

A2780 human ovarian cancer cells

[Fe]	Ref to positive control	Ref to positive control + Fe
377 µM	3.60 ± 0.35 µM	3.69 ± 0.22 µM
189 µM	2.98 ± 0.07 µM	2.98 ± 0.06 µM
94 µM	2.91 ± 0.03 µM	2.91 ± 0.03 µM
47 µM	3.03 ± 0.03 µM	3.03 ± 0.02 µM

Table II.6: Addition of Fe on day 1. Partial loss of viability due to the Fe was observed.

[Fe]	Ref to positive control	Ref to positive control + Fe
377 µM	-	-
189 µM	4.35 ± 0.08 µM	4.43 ± 0.02 µM
94 µM	4.47 ± 0.06 µM	4.51 ± 0.03 µM
47 µM	4.10 ± 0.11 µM	4.24 ± 0.05 µM

Table II.7: Addition of Fe on day 2, Fe first followed by tachpyr.

[Fe]	Ref to positive control	Ref to positive control + Fe
377 µM	5.26 ± 0.14 µM	5.51 ± 0.03 µM
189 µM	4.50 ± 0.02 µM	4.49 ± 0.01 µM
94 µM	4.18 ± 0.12 µM	4.37 ± 0.07 µM
47 µM	4.40 ± 0.02 µM	4.46 ± 0.02 µM

Table II.8: Addition of Fe on day 2, Fe and tachpyr mixed together.

[Fe]	Ref to positive control	Ref to positive control + Fe
377 µM	-	-
189 µM	2.03 ± 0.17 µM	< 2 µM
94 µM	< 2 µM	< 2 µM
47 µM	< 2 µM	< 2 µM

Table II. 9: Addition of Fe on day 2, 8 h after addition of tachpyr.

[Fe]	Ref to positive control	Ref to positive control + Fe
200 µM	3.01 ± 0.07 µM	3.10 ± 0.07 µM

Table II.10: Fe removed after 24 h.

Abbreviations

°	degrees
°C	degrees Celsius
^{13}C	carbon
^{1}H	proton
Å	Angstroms
A	Amperes
AAS	atomic absorption spectroscopy
ap	apparent
Ar	aromatic
b	broad
Boc	*t*-butoxycarbonyl
Bu	butyl
CD	circular dichroism
cm	centimetres
cm^{-1}	wavenumber
COSY	correlation spectroscopy
ct	calf thymus
d	doublet
DCM	dichloromethane
dd	doublet of doublets
DEPT	distortionless enhancement by polarisation transfer
DMEM	Dulbecco modified Eagle medium
DMSO	dimethylsulfoxide
DNA	deoxyribonucleic acid
DPPA	diphenylphosphorylazide
EDTA	ethylendiaminetetraacetic acid
eq. or equiv.	equivalents
ER	estrogen receptor
ESI	electrospray ionisation
Et	ethyl
Et_2O	diethyl ether

EtOH	ethanol
FBS	foetal bovine serum
g	grams
h	hour(s)
HEPES	4-(2-hydroxyethyl)-1-piperazineethanesulfonic acid
HMBC	heteronuclear multiple bond correlation
HPLC	high performance (pressure) liquid chromatography
HSQC	heteronuclear single quantum correlation
Hz	Hertz
IC_{50}	inhibiting concentration 50, concentration of drug able to inhibit 50% of cell growth
J	coupling constant
K	Kelvin
LD	linear dichroism
M	molar
m	multiplet
m/z	mass/charge
mDa	milliDalton
Me	methyl
MeOH	methanol
mg	milligrams
MHz	mega Hertz
min	minutes
mL	millilitres
mmol	millimoles
MMP	matrix metalloproteinase
mol	moles
MPD	2-methyl-2,4-pentan-diol
MS	mass spectrometry
MTT	3-(4,5-dimethyltriazol-2-yl)-2,5-diphenyltetrazolium bromide
ng	nanograms
nm	nanometres

NMR	nuclear magnetic resonance
ORTEP	Oak Ridge thermal-ellipsoid plot
p	pseudo
PEG	polyethylene glycol
PBS	phosphate buffer saline
Ph	phenyl
ppm	parts per million
RH	relative humidity
rpm	rotations per minute
RPMI	Roswell Park memorial institute medium
SARs	structure-activity relationships
SDS	sodium dodecyl sulfate
s	singlet
t	triplet
td	triplet of doublets
TFA	trifluoroacetic acid
THF	tetrahydrofuran
TOF	time of flight
TRIS	2-amino-2-(hydroxymethyl)-1,3-propanediol
tt	triplet of triplets
UV	ultraviolet
V	Volts
Vis	visible
WL	wavelength
δ	chemical shift
λ	wavelength
µg	micrograms
µL	microlitres
µM	micromolar
µmol	micromoles

References

1. Cancer Research UK, http://www.cancerresearchuk.org/cancer-info/cancerstats/world/the-global-picture/cancer-overall-world, Accessed 20th September, 2013.
2. World Health Organisation, http://www.who.int/mediacentre/factsheets/fs297/en/, Accessed 20th September, 2013.
3. Cancer Research UK, http://publications.cancerresearchuk.org/downloads/Product/CS_REPORT_INCIDENCE.pdf, Accessed 20th September, 2013.
4. R. Siegel, D. Naishadham and A. Jemal, *CA - Cancer J. Clin.*, 2013, **63**, 11-30.
5. G. L. Patrick, in *An introduction to medicinal chemistry*, 3rd Ed., Oxford University Press, Oxford ; New York, 2005, pp. 489-557.
6. B. Ames, in *The Biological Revolution*, Springer US, 1979, pp. 117-148.
7. E. C. Miller and J. A. Miller, *Cancer*, 1981, **47**, 2327-2345.
8. R. E. Shore, *Cancer*, 1988, **62**, 1747-1754.
9. H. N. Ananthaswamy and W. E. Pierceall, *Photochem. Photobiol.*, 1990, **52**, 1119-1136.
10. J. W. Drake, B. Charlesworth, D. Charlesworth and J. F. Crow, *Genetics*, 1998, **148**, 1667-1686.
11. B. Alberts, A. Johnson, J. Lewis, M. Raff, K. Roberts and P. Walter, in *Molecular biology of the cell*, 5th Ed., Garland Science, New York, 2008, pp. 1205-1267.
12. L. A. Loeb, K. R. Loeb and J. P. Anderson, *Proc. Natl. Acad. Sci.*, 2003, **100**, 776-781.
13. D. Hanahan and Robert A. Weinberg, *Cell*, 2011, **144**, 646-674.
14. L. A. Loeb, C. F. Springgate and N. Battula, *Cancer Res.*, 1974, **34**, 2311-2321.
15. K. R. Loeb and L. A. Loeb, *Carcinogenesis*, 2000, **21**, 379-385.
16. X. Feng, Y. Hara and K. Riabowol, *Trends Cell Biol.*, 2002, **12**, 532-538.

17. H. F. Lodish, A. Berk, C. A. Kaiser, M. Krieger, M. P. Scott, A. Bretscher, H. Ploegh and P. Matsudaira, in *Molecular cell biology*, 6th Ed., W.H. Freeman, New York, 2008, pp. 1107-1146.
18. N. Rivlin, R. Brosh, M. Oren and V. Rotter, *Genes & Cancer*, 2011, **2**, 466-474.
19. D. Ding, J. Zhou, M. Wang and Y.-S. Cong, *FEBS J.*, 2013, **280**, 3205-3211.
20. N. Kim, M. Piatyszek, K. Prowse, C. Harley, M. West, P. Ho, G. Coviello, W. Wright, S. Weinrich and J. Shay, *Science*, 1994, **266**, 2011-2015.
21. J. Folkman, *Cancer Res.*, 1986, **46**, 467-473.
22. R. H. Thomlinson and L. H. Gray, *Br. J. Cancer*, 1955, **9**, 539-549.
23. M. Höckel and P. Vaupel, *J. Natl. Cancer Inst.*, 2001, **93**, 266-276.
24. J. M. Brown and W. R. Wilson, *Nat. Rev. Cancer*, 2004, **4**, 437-447.
25. M. Greaves and C. C. Maley, *Nature*, 2012, **481**, 306-313.
26. P. Nowell, *Science*, 1976, **194**, 23-28.
27. M. M. Gottesman, *Annu. Rev. Med.*, 2002, **53**, 615-627.
28. M. Kartalou and J. M. Essigmann, *Mutat. Res. - Fund. Mol. M.*, 2001, **478**, 23-43.
29. B. C. Baguley, *Mol. Biotechnol.*, 2010, **46**, 308-316.
30. Cancer Research UK, http://scienceblog.cancerresearchuk.org/2011/06/29/near-doubling-of-uk-cancer-research-funding-in-less-than-10-years/, Accessed 26th September, 2013.
31. E. Chu, J. C. Drake, D. Boarman, J. Baram and C. J. Allegra, *J. Biol. Chem.*, 1990, **265**, 8470-8478.
32. J. Borsa and G. F. Whitmore, *Cancer Res.*, 1969, **29**, 737-744.
33. D. V. Santi, C. S. McHenry and H. Sommer, *Biochemistry*, 1974, **13**, 471-481.
34. M. J. Osborn, M. Freeman and F. M. Huennekens, *Proc. Soc. Exp. Biol. Med.*, 1958, **97**, 429-431.
35. C. Oefner, A. D'Arcy and F. K. Winkler, *Eur. J. Biochem.*, 1988, **174**, 377-385.
36. V. Cody, J. R. Luft, E. Ciszak, T. I. Kalman and J. H. Freisheim, *Anti-Cancer Drug Des.*, 1992, **7**, 483-491.

37. R. C. Reynolds, S. R. Campbell, R. G. Fairchild, R. L. Kisliuk, P. L. Micca, S. F. Queener, J. M. Riordan, W. D. Sedwick, W. R. Waud, Leung, R. W. Dixon, W. J. Suling and D. W. Borhani, *J. Med. Chem.*, 2007, **50**, 3283-3289.
38. Y. Takemura, H. Kobayashi and H. Miyachi, *Hum. Cell*, 2001, **14**, 185-202.
39. A. M. Brzozowski, A. C. Pike, Z. Dauter, R. E. Hubbard, T. Bonn, O. Engstrom, L. Ohman, G. L. Greene, J. A. Gustafsson and M. Carlquist, *Nature*, 1997, **389**, 753-758.
40. R. L. Eckert and B. S. Katzenellenbogen, *J. Biol. Chem.*, 1982, **257**, 8840-8846.
41. M. S. Christodoulou, N. Fokialakis, D. Passarella, A. N. Garcia-Argaez, O. M. Gia, I. Pongratz, V. L. Dalla and S. A. Haroutounian, *Bioorg. Med. Chem.*, 2013, **21**, 4120-4131.
42. K. R. A. Abdellatif, A. Belal and H. A. Omar, *Bioorg. Med. Chem. Lett.*, 2013, **23**, 4960-4963.
43. D. J. Needleman, M. A. Ojeda-Lopez, U. Raviv, K. Ewert, H. P. Miller, L. Wilson and C. R. Safinya, *Biophys. J.*, 2005, **89**, 3410-3423.
44. A. J. Barker, K. H. Gibson, W. Grundy, A. A. Godfrey, J. J. Barlow, M. P. Healy, J. R. Woodburn, S. E. Ashton, B. J. Curry, L. Scarlett, L. Henthorn and L. Richards, *Bioorg. Med. Chem. Lett.*, 2001, **11**, 1911-1914.
45. J. Dancey and E. A. Sausville, *Nat. Rev. Drug Discov.*, 2003, **2**, 296-313.
46. Y. Hu, M. J. Turner, J. Shields, M. S. Gale, E. Hutto, B. L. Roberts, W. M. Siders and J. M. Kaplan, *Immunology*, 2009, **128**, 260-270.
47. G. P. Warwick, *Cancer Res.*, 1963, **23**, 1315-1333.
48. G. P. Wheeler, *Cancer Res.*, 1962, **22**, 651-688.
49. P. D. Lawley and P. Brookes, *Nature*, 1965, **206**, 480-483.
50. L. F. Povirk and D. E. Shuker, *Mutat. Res.-Rev. Genet.*, 1994, **318**, 205-226.
51. R. Saffhill, G. P. Margison and P. J. O'Connor, *Biochim. Biophys. Acta, Rev. Cancer*, 1985, **823**, 111-145.
52. A. Gilman, *Am. J. Sur.*, 1963, **105**, 574-578.
53. P. Brookes and P. D. Lawley, *Biochem J*, 1961, **80**, 496-503.
54. S. M. Rink, M. S. Solomon, M. J. Taylor, S. B. Rajur, L. W. McLaughlin and P. B. Hopkins, *J. Am. Chem. Soc.*, 1993, **115**, 2551-2557.

55. H. F. Gram, C. W. Mosher and B. R. Baker, *J. Am. Chem. Soc.*, 1959, **81**, 3103-3108.
56. D. A. Lyttle and H. G. Petering, *J. Am. Chem. Soc.*, 1958, **80**, 6459-6460.
57. N. Brock and H. J. Hohorst, *Cancer*, 1967, **20**, 900-904.
58. T. K. H. Chang, G. F. Weber, C. L. Crespi and D. J. Waxman, *Cancer Res.*, 1993, **53**, 5629-5637.
59. P. J. Cox, *Biochem. Pharmacol.*, 1979, **28**, 2045-2049.
60. L. C. Erickson, M. O. Bradley, J. M. Ducore, R. A. Ewig and K. W. Kohn, *Proc. Natl. Acad. Sci.*, 1980, **77**, 467-471.
61. B. Boëns, M. Azouz, T.-S. Ouk and R. Zerrouki, *Nucleos. Nucleot. Nucl.*, 2013, **32**, 69-80.
62. Q.-Z. Zheng, F. Zhang, K. Cheng, Y. Yang, Y. Chen, Y. Qian, H.-J. Zhang, H.-Q. Li, C.-F. Zhou, S.-Q. An, Q.-C. Jiao and H.-L. Zhu, *Bioorg. Med. Chem.*, 2010, **18**, 880-886.
63. S. Li, X. Wang, Y. He, M. Zhao, Y. Chen, J. Xu, M. Feng, J. Chang, H. Ning and C. Qi, *Eur. J. Med. Chem.*, 2013, **67**, 293-301.
64. L. S. Lerman, *J. Mol. Biol.*, 1961, **3**, 18-30.
65. W. E. Ross and M. O. Bradley, *Biochim. Biophys. Acta, Nucleic Acids Protein Synth.*, 1981, **654**, 129-134.
66. W. E. Ross, D. Glaubiger and K. W. Kohn, *Biochim. Biophys. Acta, Nucleic Acids Protein Synth.*, 1979, **562**, 41-50.
67. X. Liu, L. Ouyang, X. Cai, Y. Huang, X. Feng, Q. Fan and W. Huang, *Biosens. Bioelectron.*, 2013, **41**, 218-224.
68. B. Rama Raju, S. Naik, P. J. G. Coutinho and M. S. T. Gonçalves, *Dyes Pigments*, 2013, **99**, 220-227.
69. W. Zhang, Q.-M. Chen, X. Cheng, N. Wu, G.-B. Yi, D. Li, J.-H. Tan, Z.-S. Huang, L.-Q. Gu and L.-K. An, *Dyes Pigments*, 2013, **99**, 82-89.
70. G. Wang, H. Wu, D. Wang, C. Yan and Y. Lu, *Spectrochim. Acta, Part A*, 2013, **104**, 492-496.
71. M. J. Waring, *J. Mol. Biol.*, 1965, **13**, 269-282.
72. G. N. Hortobágyi, *Drugs*, 1997, **54**, 1-7.

73. B. Zhang, D. Qian, H. H. Ma, R. Jin, P. X. Yang, M. Y. Cai, Y. H. Liu, Y. J. Liao, H. X. Deng, S. J. Mai, H. Zhang, Y. X. Zeng, M. C. Lin, H. F. Kung, D. Xie and J. J. Huang, *Oncogene*, 2012, **31**, 1-12.
74. D. Gewirtz, *Biochem. Pharmacol.*, 1999, **57**, 727-741.
75. B. Pang, X. Qiao, L. Janssen, A. Velds, T. Groothuis, R. Kerkhoven, M. Nieuwland, H. Ovaa, S. Rottenberg, T. O. van, J. Janssen, P. Huijgens, W. Zwart and J. Neefjes, *Nat. Commun.*, 2013, **4**, ncomms2921, 2913 pp.
76. A. Di Marco, F. Arcamone and F. Zunino, in *Mechanism of Action of Antimicrobial and Antitumor Agents*, Springer Berlin Heidelberg, 1975, pp. 101-128.
77. L. Stryer, in *Biochemistry*, 4th Ed., W.H. Freeman, New York, 1995, pp. 75-94 and 787-793.
78. N. Osheroff, *Pharmacol. Therapeut.*, 1989, **41**, 223-241.
79. J. M. Berger, *Curr. Opin. Struc. Biol.*, 1998, **8**, 26-32.
80. A. Di Marco, R. Silvestrini, S. Di Marco and T. Dasdia, *J. Cell Biol.*, 1965, **27**, 545-550.
81. F. Zunino, R. Gambetta and A. Di Marco, *Biochem. Pharmacol.*, 1975, **24**, 309-311.
82. O. Cuvillier, V. E. Nava, S. K. Murthy, L. C. Edsall, T. Levade, S. Milstien and S. Spiegel, *Cell Death Differ.*, 2001, **8**, 162-171.
83. E. Lorenzo, C. Ruiz-Ruiz, A. J. Quesada, G. Hernández, A. Rodríguez, A. López-Rivas and J. M. Redondo, *J. Biol. Chem.*, 2002, **277**, 10883-10892.
84. B. S. Chhikara, D. Mandal and K. Parang, *J. Med. Chem.*, 2012, **55**, 1500-1510.
85. H. Ehrhardt, D. Schrembs, C. Moritz, F. Wachter, S. Haldar, U. Graubner, M. Nathrath and I. Jeremias, *Blood*, 2011, **118**, 6123-6131.
86. E. Sanchez, M. Li, C. Wang, C. M. Nichols, J. Li, H. Chen and J. R. Berenson, *Clin. Cancer Res.*, 2012, **18**, 3856-3867.
87. G. Takemura and H. Fujiwara, *Prog. Cardiovasc. Dis.*, 2007, **49**, 330-352.
88. P. K. Singal, C. M. R. Deally and L. E. Weinberg, *J. Mol. Cell. Cardiol.*, 1987, **19**, 817-828.

89. S. Ayla, I. Seckin, G. Tanriverdi, M. Cengiz, M. Eser, B. C. Soner and G. Oktem, *Int. J. Cell Biol.*, 2011, **2011**, Article ID 390238.
90. P. G. Baraldi, A. Bovero, F. Fruttarolo, D. Preti, M. A. Tabrizi, M. G. Pavani and R. Romagnoli, *Med. Res. Rev.*, 2004, **24**, 475-528.
91. G. S. Khan, A. Shah, R. Zia ur and D. Barker, *J. Photochem. Photobiol. B: Biology*, 2012, **115**, 105-118.
92. X. Cai, P. J. Gray Jr and D. D. Von Hoff, *Cancer Treat. Rev.*, 2009, **35**, 437-450.
93. V. N. Iyer and W. Szybalski, *Proc. Natl. Acad. Sci.*, 1963, **50**, 355-361.
94. L. H. Hurley and D. R. Needham-VanDevanter, *Acc. Chem. Res.*, 1986, **19**, 230-237.
95. J. W. Lown and A. V. Joshua, *Biochem. Pharmacol.*, 1979, **28**, 2017-2026.
96. S. Kumar, R. Lipman and M. Tomasz, *Biochemistry*, 1992, **31**, 1399-1407.
97. H. Borowy-Borowski, R. Lipman and M. Tomasz, *Biochemistry*, 1990, **29**, 2999-3006.
98. M. Tomasz and R. Lipman, *Biochemistry*, 1981, **20**, 5056-5061.
99. C. Cargill, E. Bachmann and G. Zbinden, *J. Natl. Cancer Inst.*, 1974, **53**, 481-486.
100. F. M. Arcamone, F. Animati, B. Barbieri, E. Configliacchi, R. D'Alessio, C. Geroni, F. C. Giuliani, E. Lazzari and M. Menozzi, *J. Med. Chem.*, 1989, **32**, 774-778.
101. A. Abu-Daya and K. R. Fox, *Nucleic Acids Res.*, 1997, **25**, 4962-1969.
102. M. L. Kopka, C. Yoon, D. Goodsell, P. Pjura and R. E. Dickerson, *Proc. Natl. Acad. Sci.*, 1985, **82**, 1376-1380.
103. J. G. Pelton and D. E. Wemmer, *J. Am. Chem. Soc.*, 1990, **112**, 1393-1399.
104. M. Coll, C. A. Frederick, A. H. Wang and A. Rich, *Proc. Natl. Acad. Sci.*, 1987, **84**, 8385-8389.
105. J. Viallet, D. Stewart, F. Shepherd, J. Ayoub, Y. Cormier, N. DiPietro and W. Steward, *Lung Cancer*, 1996, **15**, 367-373.
106. M. Broggini, H. M. Coley, N. Mongelli, E. Pesenti, M. D. Wyatt, J. A. Hartley and M. Dlncaici, *Nucleic Acids Res.*, 1995, **23**, 81-87.

107. T. Yamori, A. Matsunaga, S. Sato, K. Yamazaki, A. Komi, K. Ishizu, I. Mita, H. Edatsugi, Y. Matsuba, K. Takezawa, O. Nakanishi, H. Kohno, Y. Nakajima, H. Komatsu, T. Andoh and T. Tsuruo, *Cancer Res.*, 1999, **59**, 4042-4049.

108. M. H. Helal, Z. A. Al-Mudaris, M. H. Al-Douh, H. Osman, H. A. Wahab, B. O. Alnajjar, H. H. Abdallah and M. A. M. S. Abdul, *Int. J. Oncol.*, 2012, **41**, 504-510.

109. Y.-H. Yang, M.-S. Cheng, Q.-H. Wang, H. Nie, N. Liao, J. Wang and H. Chen, *Eur. J. Med. Chem.*, 2009, **44**, 1808-1812.

110. F. Yang, N. G. Nickols, B. C. Li, G. K. Marinov, J. W. Said and P. B. Dervan, *Proc. Natl. Acad. Sci.*, 2013, **110**, 1863-1868.

111. A. Vidal, C. Muñoz, M.-J. Guillén, J. Moretó, S. Puertas, M. Martínez-Iniesta, A. Figueras, L. Padullés, F. J. García-Rodriguez, M. Berdiel-Acer, M. A. Pujana, R. Salazar, M. Gil-Martin, L. Martí, J. Ponce, D. G. Molleví, G. Capella, E. Condom, F. Viñals, D. Huertas, C. Cuevas, M. Esteller, P. Avilés and A. Villanueva, *Clin. Cancer Res.*, 2012, **18**, 5399-5411.

112. Y. Pommier, P. Pourquier, Y. Fan and D. Strumberg, *Biochim. Biophys. Acta, Gene Struct. Expr.*, 1998, **1400**, 83-106.

113. R. P. Hertzberg, M. J. Caranfa and S. M. Hecht, *Biochemistry*, 1989, **28**, 4629-4638.

114. Y. H. Hsiang, R. Hertzberg, S. Hecht and L. F. Liu, *J. Biol. Chem.*, 1985, **260**, 14873-14878.

115. B. L. Staker, K. Hjerrild, M. D. Feese, C. A. Behnke, A. B. Burgin and L. Stewart, *Proc. Natl. Acad. Sci.*, 2002, **99**, 15387-15392.

116. D. F. S. Kehrer, O. Soepenberg, W. J. Loos, J. Verweij and A. Sparreboom, *Anti-Cancer Drugs*, 2001, **12**, 89-105.

117. L.-X. Yang, X. Pan and H.-J. Wang, *Bioorg. Med. Chem. Lett.*, 2002, **12**, 1241-1244.

118. D. Ormrod and C. M. Spencer, *Drugs*, 1999, **58**, 533-551.

119. R. M. Goldberg, D. J. Sargent, R. F. Morton, C. S. Fuchs, R. K. Ramanathan, S. K. Williamson, B. P. Findlay, H. C. Pitot and S. R. Alberts, *J. Clin. Oncol.*, 2004, **22**, 23-30.

120. H. B. Taussig, *Pediatrics*, 1962, **30**, 654-659.

121. W. Lenz, *Teratology*, 1988, **38**, 203-215.
122. S. Timmermans and V. Leiter, *Soc. Stud. Sci.*, 2000, **30**, 41-71.
123. S. K. Teo, K. E. Resztak, M. A. Scheffler, K. A. Kook, J. B. Zeldis, D. I. Stirling and S. D. Thomas, *Microbes Infect.*, 2002, **4**, 1193-1202.
124. R. J. D'Amato, M. S. Loughnan, E. Flynn and J. Folkman, *Proc. Natl. Acad. Sci.*, 1994, **91**, 4082-4085.
125. M. Cavo, E. Zamagni, P. Tosi, C. Cellini, D. Cangini, P. Tacchetti, N. Testoni, M. Tonelli, A. de Vivo, G. Palareti, S. Tura and M. Baccarani, *Haematologica*, 2004, **89**, 826-831.
126. F. L. Urbach, J. E. Sarneski, L. J. Turner and D. H. Busch, *Inorg. Chem.*, 1968, **7**, 2169-2171.
127. R. A. D. Wentworth and J. J. Felten, *J. Amer. Chem. Soc.*, 1968, **90**, 621-626.
128. L. Cronin, S. P. Foxon, P. J. Lusby and P. H. Walton, *J. Biol. Inorg. Chem.*, 2001, **6**, 367-377.
129. L. Cronin and P. H. Walton, *Chem. Commun.*, 2003, 1572-1573.
130. B. Greener, S. P. Foxon and P. H. Walton, *New J. Chem.*, 2000, **24**, 269-273.
131. A. J. Gamble, J. M. Lynam, R. J. Thatcher, P. H. Walton and A. C. Whitwood, *Inorg. Chem.*, 2013, **52**, 4517-4527.
132. A. J. Gamble, PhD Thesis, University of York, 2012.
133. S. V. Torti, F. M. Torti, S. P. Whitman, M. W. Brechbiel, G. Park and R. P. Planalp, *Blood*, 1998, **92**, 1384-1389.
134. R. Zhao, R. P. Planalp, R. Ma, B. T. Greene, B. T. Jones, M. W. Brechbiel, F. M. Torti and S. V. Torti, *Biochem. Pharmacol.*, 2004, **67**, 1677-1688.
135. G. Park, F. H. Lu, N. Ye, M. W. Brechbiel, S. V. Torti, F. M. Torti and R. P. Planalp, *J. Biol. Inorg. Chem.*, 1998, **3**, 449-457.
136. A. M. Samuni, M. C. Krishna, W. DeGraff, A. Russo, R. P. Planalp, M. W. Brechbiel and J. B. Mitchell, *Biochim. Biophys. Acta - Gen. Subjects*, 2002, **1571**, 211-218.
137. G. Park, A. M. Przyborowska, N. Ye, N. M. Tsoupas, C. B. Bauer, G. A. Broker, R. D. Rogers, M. W. Brechbiel and R. P. Planalp, *Dalton Trans.*, 2003, 318-324.

138. B. T. Greene, J. Thorburn, M. C. Willingham, A. Thorburn, R. P. Planalp, M. W. Brechbiel, J. Jennings-Gee, J. Wilkinson, F. M. Torti and S. V. Torti, *J. Biol. Chem.*, 2002, **277**, 25568-25575.

139. N. Ye, G. Park, A. M. Przyborowska, P. E. Sloan, T. Clifford, C. B. Bauer, G. A. Broker, R. D. Rogers, R. Ma, S. V. Torti, M. W. Brechbiel and R. P. Planalp, *Dalton Trans.*, 2004, 1304-1311.

140. M. L. Childers, F. Su, A. M. Przyborowska, B. Bishwokarma, G. Park, M. W. Brechbiel, S. V. Torti, F. M. Torti, G. Broker, J. S. Alexander, R. D. Rogers, K. Ruhlandt-Senge and R. P. Planalp, *Eur. J. Inorg. Chem.*, 2005, 3971-3982.

141. S. V. Torti, R. Ma, V. J. Venditto, F. M. Torti, R. P. Planalp and M. W. Brechbiel, *Bioorg. Med. Chem.*, 2005, **13**, 5961-5967.

142. D. P. Kennedy, A. G. DiPasquale, A. L. Rheingold and R. P. Planalp, *Polyhedron*, 2007, **26**, 197-203.

143. C. M. da Silva, D. L. da Silva, L. V. Modolo, R. B. Alves, M. A. de Resende, C. V. B. Martins and Â. de Fátima, *J. Adv. Res.*, 2011, **2**, 1-8.

144. S. Shukla, R. S. Srivastava, S. K. Shrivastava, A. Sodhi and P. Kumar, *Med. Chem. Res.*, 2013, **22**, 1604-1617.

145. K. Sztanke, A. Maziarka, A. Osinka and M. Sztanke, *Bioorg. Med. Chem.*, 2013, **21**, 3648-3666.

146. M. M. Ghorab, M. A. Shaaban, H. M. Refaat, H. I. Heiba and S. S. Ibrahim, *Eur. J. Med. Chem.*, 2012, **53**, 403-407.

147. M. Hranjec, K. Starčević, S. K. Pavelić, P. Lučin, K. Pavelić and G. Karminski Zamola, *Eur. J. Med. Chem.*, 2011, **46**, 2274-2279.

148. K. Cheng, Q.-Z. Zheng, J. Hou, Y. Zhou, C.-H. Liu, J. Zhao and H.-L. Zhu, *Bioorg. Med. Chem.*, 2010, **18**, 2447-2455.

149. G. Kumari and R. Singh, *Med. Chem. Res.*, 2013, **22**, 927-933.

150. A. M. Asiri, S. A. Khan, H. M. Marwani and K. Sharma, *J. Photochem. Photobiol. B: Biology*, 2013, **120**, 82-89.

151. P. Vicini, A. Geronikaki, M. Incerti, B. Busonera, G. Poni, C. A. Cabras and P. La Colla, *Bioorg. Med. Chem.*, 2003, **11**, 4785-4789.

152. N. A. Al-Masoudi, N. M. Aziz and A. T. Mohammed, *Phosphorus, Sulfur Silicon Relat. Elem.*, 2009, **184**, 2891-2901.

153. S. Sondhi, S. Arya, R. Rani, N. Kumar and P. Roy, *Med. Chem. Res.*, 2012, **21**, 3620-3628.
154. M. S. Alam, J.-H. Choi and D.-U. Lee, *Bioorg. Med. Chem.*, 2012, **20**, 4103-4108.
155. N. Bharti, Shailendra, M. T. Gonzalez Garza, D. E. Cruz-Vega, J. Castro-Garza, K. Saleem, F. Naqvi, M. R. Maurya and A. Azam, *Bioorg. Med. Chem. Lett.*, 2002, **12**, 869-871.
156. G. Grivani and A. Akherati, *Inorg. Chem. Commun.*, 2013, **28**, 90-93.
157. M. Asadi, N. Savaripoor, Z. Asadi, M. H. Ghatee, F. Moosavi, R. Yousefi and M. Jamshidi, *Spectrochim. Acta, Part A*, 2013, **101**, 394-399.
158. L. G. Wade, in *Organic chemistry*, 6th Ed., Pearson Prentice Hall, Upper Saddle River, N.J., 2006, pp. 840-843.
159. P. Purushottamachar, A. Khandelwal, T. S. Vasaitis, R. D. Bruno, L. K. Gediya and V. C. O. Njar, *Bioorg. Med. Chem.*, 2008, **16**, 3519-3529.
160. L. Blackburn and R. J. K. Taylor, *Org. Lett.*, 2001, **3**, 1637-1639.
161. T. Bowen, R. P. Planalp and M. W. Brechbiel, *Bioorg. Med. Chem. Lett.*, 1996, **6**, 807-810.
162. H. Günther, *NMR spectroscopy: basic principles, concepts, and applications in chemistry*, Wiley, Chichester ; New York, 1995.
163. G. Park, J. Shao, F. H. Lu, R. D. Rogers, N. D. Chasteen, M. W. Brechbiel and R. P. Planalp, *Inorg. Chem.*, 2001, **40**, 4167-4175.
164. L. Farrugia, *J. Appl. Crystallogr.*, 2012, **45**, 849-854.
165. G. R. Desiraju and T. Steiner, in *The weak hydrogen bond: in structural chemistry and biology*, Oxford University Press, Oxford, 1999, pp. 1-28.
166. E. A. Lewis, PhD Thesis, University of York, 2002.
167. E. A. Lewis, J. R. Lindsay Smith, P. H. Walton, S. J. Archibald, S. P. Foxon and G. M. P. Giblin, *J. Chem. Soc., Dalton Trans.*, 2001, 1159-1161.
168. J. Vicente, M. T. Chicote, A. J. Martinez-Martinez, D. Bautista and P. G. Jones, *Org. Biomol. Chem*, 2011, **9**, 2279-2285.
169. S. Mahmood, M. A. Malik, M. Motevalli, P. B. Nunn and P. O'Brien, *Tetrahedron*, 1998, **54**, 5721-5730.

170. H. Kargar, R. Kia, A. Adabi Ardakani and M. N. Tahir, *Acta Crystallogr. Sect. E*, 2012, **68**, o2348.
171. H. Yu, Y.-B. Jin, Y.-K. Chang and K.-W. Lei, *Acta Crystallogr. Sect. E*, 2012, **68**, o2401.
172. B. Greener, L. Cronin, G. D. Wilson and P. H. Walton, *J. Chem. Soc., Dalton Trans.*, 1996, 401-403.
173. B. Greener, PhD Thesis, University of York, 1997.
174. P. Ebrahimpour, M. Cushion, M. F. Haddow, A. J. Hallett and D. F. Wass, *Dalton Trans.*, 2010, **39**, 10910-10919.
175. H. H. Jaffé, *Chem. Rev.*, 1953, **53**, 191-261.
176. H.-O. Kalinowski, S. Berger and S. Braun, Wiley, Chichester, New York, 1988, pp. 576-585.
177. D. H. Williams and I. Fleming, *Spectroscopic methods in organic chemistry*, McGraw-Hill, London, 1995.
178. S. J. Archibald, A. K. Nairn, P. Timmins and P. H. Walton, *Tetrahedron Lett.*, 2005, **46**, 6441-6443.
179. T. W. Greene and P. G. M. Wuts, in *Protective groups in organic synthesis*, 2nd Ed., Wiley, New York, 1991, pp. 327-330.
180. I. Schiffers, T. Rantanen, F. Schmidt, W. Bergmans, L. Zani and C. Bolm, *J. Org. Chem.*, 2006, **71**, 2320-2331.
181. S. Chandrudu, P. Simerska and I. Toth, *Molecules*, 2013, **18**, 4373-4388.
182. B. Rosenberg, L. Van Camp and T. Krigas, *Nature*, 1965, **205**, 698-699.
183. N. J. Wheate, S. Walker, G. E. Craig and R. Oun, *Dalton Trans.*, 2010, **39**, 8113-8127.
184. P. Köpf-Maier, *Eur. J. Clin. Pharmacol.*, 1994, **47**, 1-16.
185. L. H. Einhorn, *Proc. Natl. Acad. Sci.*, 2002, **99**, 4592-4595.
186. L. Kelland, *Nat. Rev. Cancer*, 2007, **7**, 573-584.
187. B. Köberle, K. A. Grimaldi, A. Sunters, J. A. Hartley, L. R. Kelland and J. R. W. Masters, *Int. J. Cancer*, 1997, **70**, 551-555.
188. R. J. Parker, A. Eastman, F. Bostick-Bruton and E. Reed, *J. Clin. Invest.*, 1991, **87**, 772-777.
189. T. Ishikawa and F. Ali-Osman, *J. Biol. Chem.*, 1993, **268**, 20116-20125.

190. C. Meijer, N. H. Mulder, H. Timmer-Bosscha, W. J. Sluiter, G. J. Meersma and E. G. E. de Vries, *Cancer Res.*, 1992, **52**, 6885-6889.
191. A. Fajao, J. Da Silva, J.-C. Ahomadegbe, J.-G. Rateau, J.-F. Bernaudin, G. Riou and J. Bénard, *Int. J. Cancer*, 1996, **68**, 67-74.
192. P. M. Takahara, A. C. Rosenzweig, C. A. Frederick and S. J. Lippard, *Nature*, 1995, **377**, 649-652.
193. C. J. Van Garderen and L. P. A. Van Houte, *Eur. J. Biochem.*, 1994, **225**, 1169-1179.
194. F. Coste, J.-M. Malinge, L. Serre, M. Leng, C. Zelwer, W. Shepard and M. Roth, *Nucleic Acids Res.*, 1999, **27**, 1837-1846.
195. R. C. Todd and S. J. Lippard, *Metallomics*, 2009, **1**, 280-291.
196. A. M. J. Fichtinger-Schepman, J. L. Van der Veer, J. H. J. Den Hartog, P. H. M. Lohman and J. Reedijk, *Biochemistry*, 1985, **24**, 707-713.
197. R. J. Knox, F. Friedlos, D. A. Lydall and J. J. Roberts, *Cancer Res.*, 1986, **46**, 1972-1979.
198. J. Graham, M. Muhsin and P. Kirkpatrick, *Nat. Rev. Drug Discov.*, 2004, **3**, 11-12.
199. G. Sava, A. Bergamo and P. J. Dyson, *Dalton Trans.*, 2011, **40**, 9069-9075.
200. T. Gianferrara, I. Bratsos and E. Alessio, *Dalton Trans.*, 2009, 7588-7598.
201. P. Pigeon, S. Top, A. Vessières, M. Huché, E. A. Hillard, E. Salomon and G. Jaouen, *J. Med. Chem.*, 2005, **48**, 2814-2821.
202. D. S. Williams, G. E. Atilla, H. Bregman, A. Arzoumanian, P. S. Klein and E. Meggers, *Angew. Chem. Int. Ed.*, 2005, **44**, 1984-1987.
203. K. S. M. Smalley, R. Contractor, N. K. Haass, A. N. Kulp, G. E. Atilla-Gokcumen, D. S. Williams, H. Bregman, K. T. Flaherty, M. S. Soengas, E. Meggers and M. Herlyn, *Cancer Res.*, 2007, **67**, 209-217.
204. P. Köpf-Maier, *J. Struct. Biol.*, 1990, **105**, 35-45.
205. M. Guo, Z. Guo and P. Sadler, *J. Biol. Inorg. Chem.*, 2001, **6**, 698-707.
206. A. L. Beauchamp, D. Cozak and A. Mardhy, *Inorg. Chim. Acta*, 1984, **92**, 191-197.
207. M. Guo, H. Sun, H. J. McArdle, L. Gambling and P. J. Sadler, *Biochemistry*, 2000, **39**, 10023-10033.

208. A. D. Tinoco, E. V. Eames and A. M. Valentine, *J. Am. Chem. Soc.*, 2008, **130**, 2262-2270.
209. G. Lümmen, H. Sperling, H. Luboldt, T. Otto and H. Rübben, *Cancer Chemother. Pharmacol.*, 1998, **42**, 415-417.
210. O. R. Allen, A. L. Gott, J. A. Hartley, J. M. Hartley, R. J. Knox and P. C. McGowan, *Dalton Trans.*, 2007, 5082-5090.
211. O. R. Allen, L. Croll, A. L. Gott, R. J. Knox and P. C. McGowan, *Organometallics*, 2003, **23**, 288-292.
212. G. N. Kaluđerović, V. Tayurskaya, R. Paschke, S. Prashar, M. Fajardo and S. Gómez-Ruiz, *Appl. Organomet. Chem.*, 2010, **24**, 656-662.
213. J. Zagermann, A. Deally, N. Metzler-Nolte, H. Müller-Bunz, D. Wallis and M. Tacke, *Polyhedron*, 2011, **30**, 2387-2390.
214. J. Claffey, H. Müller-Bunz and M. Tacke, *J. Organomet. Chem.*, 2010, **695**, 2105-2117.
215. J. B. J. Milbank, R. J. Stevenson, D. C. Ware, J. Y. C. Chang, M. Tercel, G. O. Ahn, W. R. Wilson and W. A. Denny, *J. Med. Chem.*, 2009, **52**, 6822-6834.
216. P. J. Blower, J. R. Dilworth, R. I. Maurer, G. D. Mullen, C. A. Reynolds and Y. Zheng, *J. Inorg. Biochem.*, 2001, **85**, 15-22.
217. T. W. Failes, C. Cullinane, C. I. Diakos, N. Yamamoto, J. G. Lyons and T. W. Hambley, *Chem. Eur. J.*, 2007, **13**, 2974-2982.
218. A. Bergamo, C. Gaiddon, J. H. M. Schellens, J. H. Beijnen and G. Sava, *J. Inorg. Biochem.*, 2012, **106**, 90-99.
219. C. Turro, *Proc. Natl. Acad. Sci.*, 2011, **108**, 17573-17574.
220. E. Antonarakis and A. Emadi, *Cancer Chemother. Pharmacol.*, 2010, **66**, 1-9.
221. C. G. Hartinger, M. A. Jakupec, S. Zorbas-Seifried, M. Groessl, A. Egger, W. Berger, H. Zorbas, P. J. Dyson and B. K. Keppler, *Chem. Biodivers.*, 2008, **5**, 2140-2155.
222. A. Bergamo, R. Gagliardi, V. Scarcia, A. Furlani, E. Alessio, G. Mestroni and G. Sava, *J. Pharmacol. Exp. Ther.*, 1999, **289**, 559-564.
223. S. Zorzet, A. Bergamo, M. Cocchietto, A. Sorc, B. Gava, E. Alessio, E. Iengo and G. Sava, *J. Pharmacol. Exp. Ther.*, 2000, **295**, 927-933.

224. S. Kapitza, M. Pongratz, M. A. Jakupec, P. Heffeter, W. Berger, L. Lackinger, B. K. Keppler and B. Marian, *J. Cancer Res. Clin.*, 2005, **131**, 101-110.
225. C. Scolaro, A. Bergamo, L. Brescacin, R. Delfino, M. Cocchietto, G. Laurenczy, T. J. Geldbach, G. Sava and P. J. Dyson, *J. Med. Chem.*, 2005, **48**, 4161-4171.
226. C. A. Vock, C. Scolaro, A. D. Phillips, R. Scopelliti, G. Sava and P. J. Dyson, *J. Med. Chem.*, 2006, **49**, 5552-5561.
227. R. E. Morris, R. E. Aird, P. del Socorro Murdoch, H. Chen, J. Cummings, N. D. Hughes, S. Parsons, A. Parkin, G. Boyd, D. I. Jodrell and P. J. Sadler, *J. Med. Chem.*, 2001, **44**, 3616-3621.
228. H. Chen, J. A. Parkinson, R. E. Morris and P. J. Sadler, *J. Am. Chem. Soc.*, 2002, **125**, 173-186.
229. C. Scolaro, A. B. Chaplin, C. G. Hartinger, A. Bergamo, M. Cocchietto, B. K. Keppler, G. Sava and P. J. Dyson, *Dalton Trans.*, 2007, 5065-5072.
230. C. Scolaro, T. J. Geldbach, S. Rochat, A. Dorcier, C. Gossens, A. Bergamo, M. Cocchietto, I. Tavernelli, G. Sava, U. Rothlisberger and P. J. Dyson, *Organometallics*, 2005, **25**, 756-765.
231. R. A. D. Wentworth, P. S. Dahl, C. J. Huffman, W. O. Gillum, W. E. Streib and J. C. Huffman, *Inorg. Chem.*, 1982, **21**, 3060-3063.
232. K. A. Hilfiker, M. W. Brechbiel, R. D. Rogers and R. P. Planalp, *Inorg. Chem.*, 1997, **36**, 4600-4603.
233. W. O. Gillum, J. C. Huffman, W. E. Streib and R. A. D. Wentworth, *J. Chem. Soc., Chem. Commun.*, 1969, 843-844.
234. E. B. Fleischer, A. E. Gebala, D. R. Swift and P. A. Tasker, *Inorg. Chem.*, 1972, **11**, 2775-2784.
235. G. Park, N. Ye, R. D. Rogers, M. W. Brechbiel and R. P. Planalp, *Polyhedron*, 2000, **19**, 1155-1161.
236. G. Park, E. Dadachova, A. Przyborowska, S.-j. Lai, D. Ma, G. Broker, R. D. Rogers, R. P. Planalp and M. W. Brechbiel, *Polyhedron*, 2001, **20**, 3155-3163.
237. R. D. Shannon and C. T. Prewitt, *Acta Crystallogr. Sect. B*, 1969, **25**, 925-946.
238. R. Shannon, *Acta Crystallogr. Sect. A*, 1976, **32**, 751-767.

239. J.-X. Dai, F.-H. Wu, W.-R. Yao and Q.-F. Zhang, *Z. Naturforsch., B: Chem. Sci.*, 2007, **62**, 491-494.
240. A. K. Ghosh, D. Ghoshal, J. Ribas, G. Mostafa and N. R. Chaudhuri, *Crystal Growth & Design*, 2005, **6**, 36-39.
241. T. D. Kim, T. J. McNeese and A. L. Rheingold, *Inorg. Chem.*, 1988, **27**, 2554-2555.
242. E. M. Nagy, C. Nardon, L. Giovagnini, L. Marchio, A. Trevisan and D. Fregona, *Dalton Trans.*, 2011, **40**, 11885-11895.
243. L. Giovagnini, S. Sitran, I. Castagliuolo, P. Brun, M. Corsini, P. Zanello, A. Zoleo, A. Maniero, B. Biondi and D. Fregona, *Dalton Trans.*, 2008, 6699-6708.
244. A.-F. Ibao, M. Gras, B. Therrien, G. Suess-Fink, O. Zava and P. J. Dyson, *Eur. J. Inorg. Chem.*, 2012, **2012**, 1531-1535.
245. J. Carmichael, J. B. Mitchell, W. G. DeGraff, J. Gamson, A. F. Gazdar, B. E. Johnson, E. Glatstein and J. D. Minna, *Br. J. Cancer*, 1988, **57**, 540-547.
246. J. Meerloo, G. L. Kaspers and J. Cloos, in *Cancer Cell Culture*, Humana Press, 2011, pp. 237-245.
247. T. Mosmann, *J. Immunol. Methods*, 1983, **65**, 55-63.
248. L. Lyons, in *A practical guide to data analysis for physical science students*, Cambridge University Press, Cambridge, 1991, pp. 31-33.
249. H. F. Lodish, A. Berk, C. A. Kaiser, M. Krieger, M. P. Scott, A. Bretscher, H. Ploegh and P. Matsudaira, in *Molecular cell biology*, 6th Ed., W.H. Freeman, New York, 2008, p. 115.
250. M. Schade, J. Behlke, K. Lowenhaupt, A. Herbert, A. Rich and H. Oschkinat, *FEBS Lett.*, 1999, **458**, 27-31.
251. J. Zhao, A. Bacolla, G. Wang and K. Vasquez, *Cell. Mol. Life Sci.*, 2010, **67**, 43-62.
252. Z. Yu and H. Mao, *The Chemical Record*, 2013, **13**, 102-116.
253. G. P. Schroth and P. S. Ho, *Nucleic Acids Res.*, 1995, **23**, 1977-1983.
254. M. J. Hannon, *Chem. Soc. Rev.*, 2007, **36**, 280-295.
255. B. Nordén and T. Kurucsev, *J. Mol. Rec.*, 1994, **7**, 141-155.

256. K. E. Van Holde, W. C. Johnson and P. S. Ho, in *Principles of physical biochemistry*, 2nd Ed., Pearson/Prentice Hall, Upper Saddle River, N.J., 2006, pp. 465-500.
257. J. Rajesh, M. Rajasekaran, G. Rajagopal and P. Athappan, *Spectrochim. Acta, Part A*, 2012, **97**, 223-230.
258. S. Agarwal, D. K. Jangir and R. Mehrotra, *J. Photochem. Photobiol. B: Biology*, 2013, **120**, 177-182.
259. Y.-M. Chang, C. K. M. Chen and M.-H. Hou, *Int. J. Mol. Sci.*, 2012, **13**, 3394-3413.
260. F. M. Pohl and T. M. Jovin, *J. Mol. Biol.*, 1972, **67**, 375-396.
261. R. Solimani, *Int. J. Biol. Macromol.*, 1996, **18**, 287-295.
262. A. Terenzi, C. Ducani, L. Male, G. Barone and M. J. Hannon, *Dalton Trans.*, 2013, **42**, 11220-11226.
263. D. R. G. Pitter, J. Wigenius, A. S. Brown, J. D. Baker, F. Westerlund and J. N. Wilson, *Org. Lett.*, 2013, **15**, 1330-1333.
264. B. Nordén, M. Kubista and T. Kurucsev, *Q. Rev. Biophys.*, 1992, **25**, 51-170.
265. K. Omidfar, S. Kia, S. Kashanian, M. Paknejad, A. Besharatie, S. Kashanian and B. Larijani, *Appl. Biochem. Biotechnol.*, 2010, **160**, 843-855.
266. G. P. Holmes-Hampton, N. D. Jhurry, S. P. McCormick and P. A. Lindahl, *Biochemistry*, 2012, **52**, 105-114.
267. D. R. Lide, *CRC Handbook of chemistry and physics*, Chapman and Hall/CRCnetBASE, Boca Raton, FL, 2008-9.
268. H. M. Wallace, *The polyamines: small molecules in the 'omics' era*, Portland Press, 2009.
269. A. Kabir, M. Hossain and G. S. Kumar, *J. Chem. Thermodyn.*, 2013, **57**, 445-453.
270. N. Seiler and F. Raul, *J. Cell. Mol. Med.*, 2005, **9**, 623-642.
271. R. G. Schipper, L. C. Penning and A. A. J. Verhofstad, *Semin. Cancer Biol.*, 2000, **10**, 55-68.
272. F. Cañizares, J. Salinas, M. d. las Heras, J. Diaz, I. Tovar, P. Martinez and R. Peñafiel, *Clin. Cancer Res.*, 1999, **5**, 2035-2041.

273. N. Shah, T. Thomas, A. Shirahata, L. H. Sigal and T. J. Thomas, *Biochemistry*, 1999, **38**, 14763-14774.

274. N. E. Davidson, H. A. Hahm, D. E. McCloskey, P. M. Woster and R. A. Casero, *Endocrine-Related Cancer*, 1999, **6**, 69-73.

275. N. H. Saab, E. E. West, N. C. Bieszk, C. V. Preuss, A. R. Mank, R. A. Casero and P. M. Woster, *J. Med. Chem.*, 1993, **36**, 2998-3004.

276. Y. Huang, E. R. Hager, D. L. Phillips, V. R. Dunn, A. Hacker, B. Frydman, J. A. Kink, A. L. Valasinas, V. K. Reddy, L. J. Marton, R. A. Casero and N. E. Davidson, *Clin. Cancer Res.*, 2003, **9**, 2769-2777.

277. A. Rodger, S. Taylor, G. Adlam, I. S. Blagbrough and I. S. Haworth, *Bioorg. Med. Chem.*, 1995, **3**, 861-872.

278. G.-Y. Li, K.-J. Du, J.-Q. Wang, J.-W. Liang, J.-F. Kou, X.-J. Hou, L.-N. Ji and H. Chao, *J. Inorg. Biochem.*, 2013, **119**, 43-53.

279. R. E. McKnight, E. Reisenauer, M. V. Pintado, S. R. Polasani and D. W. Dixon, *Bioorg. Med. Chem. Lett.*, 2011, **21**, 4288-4291.

280. J. Olmsted, III and D. R. Kearns, *Biochemistry*, 1977, **16**, 3647-3654.

281. A. R. Morgan, J. S. Lee, D. E. Pulleyblank, N. L. Murray and D. H. Evans, *Nucleic Acids Res.*, 1979, **7**, 547-565.

282. B. Nordén and F. Tjerneld, *Biopolymers*, 1982, **21**, 1713-1734.

283. G. L. Patrick, in *An introduction to medicinal chemistry*, 3rd Ed., Oxford University Press, Oxford ; New York, 2005, pp. 134-162.

284. K. Brzezinski, A. Brzuszkiewicz, M. Dauter, M. Kubicki, M. Jaskolski and Z. Dauter, *Nucleic Acids Res.*, 2011, **39**, 6238-6248.

285. H. Ohishi, Y. Tozuka, Z. Da-Yang, T. Ishida and K. Nakatani, *Biochem. Biophys. Res. Commun.*, 2007, **358**, 24-28.

286. S. E. Ealick, *Curr. Opin. Chem. Biol.*, 2000, **4**, 495-499.

287. A. Vagin and A. Teplyakov, *J. Appl. Crystallogr.*, 1997, **30**, 1022-1025.

288. G. N. Murshudov, A. A. Vagin and E. J. Dodson, *Acta Crystallogr. Sect. D*, 1997, **53**, 240-255.

289. P. Emsley, B. Lohkamp, W. G. Scott and K. Cowtan, *Acta Crystallogr. Sect. D*, 2010, **66**, 486-501.

290. S. McNicholas, E. Potterton, K. S. Wilson and M. E. M. Noble, *Acta Crystallogr. Sect. D*, 2011, **67**, 386-394.
291. C. Ban and M. Sundaralingam, *Biophys. J.*, 1996, **71**, 1222-1227.
292. S. Thiyagarajan and N. Gautham, *Crystallogr. Rev.*, 2005, **11**, 337-355.
293. S. Jain, G. Zon and M. Sundaralingam, *J. Mol. Biol.*, 1987, **197**, 141-145.
294. F. Quadrifoglio, G. Manzini and N. Yathindra, *J. Mol. Biol.*, 1984, **175**, 419-423.
295. H. Ohishi, N. Terasoma, I. Nakanishi, G. van der Marel, J. H. Van Boom, A. Rich, A. H. J. Wang, T. Hakoshima and K.-i. Tomita, *FEBS Lett.*, 1996, **398**, 291-296.
296. B. Pan, C. Ban, M. C. Wahl and M. Sundaralingam, *Biophys. J.*, 1997, **73**, 1553-1561.
297. C. Ban, B. Ramakrishnan and M. Sundaralingam, *Biophys. J.*, 1996, **71**, 1215-1221.
298. R. B. DuBridge, P. Tang, H. C. Hsia, P. M. Leong, J. H. Miller and M. P. Calos, *Mol. Cell. Biol.*, 1987, **7**, 379-387.
299. X. Wang, X. Du, H. Li, D. S.-B. Chan and H. Sun, *Angew. Chem. Int. Ed.*, 2011, **50**, 2706-2711.
300. O. V. Dolomanov, L. J. Bourhis, R. J. Gildea, J. A. K. Howard and H. Puschmann, *J. Appl. Crystallogr.*, 2009, **42**, 339-341.
301. L. Palatinus and G. Chapuis, *J. Appl. Crystallogr.*, 2007, **40**, 786-790.
302. G. Sheldrick, *Acta Crystallogr. Sect. A*, 2008, **64**, 112-122.
303. W. Kabsch, *Acta Crystallogr. Sect. D*, 2010, **66**, 125-132.
304. G. Winter, *J. Appl. Crystallogr.*, 2010, **43**, 186-190.
305. P. Evans, *Acta Crystallogr. Sect. D*, 2006, **62**, 72-82.